

# **Vacuum Gas Carburizing – Fate of Hydrocarbons**

zur Erlangung des akademischen Grades eines  
DOKTORS DER INGENIEURWISSENSCHAFTEN (Dr.-Ing.)

der Fakultät für Chemieingenieurwesen und Verfahrenstechnik der  
Universität Fridericiana Karlsruhe (TH)  
genehmigte

DISSERTATION

von

**M.Sc. Rafi Ullah Khan**

aus Pakistan

Tag des Kolloquiums: 29.07.2008

Referent: Prof. Dr.-Ing. Rainer Reimert

Korreferent: Prof. Dr. Olaf Deutschmann

## Acknowledgements

I am highly indebted to Professor Rainer Reimert, my supervisor, for his many suggestions and constant support during this research. Without his guidance this work would not have been possible. I am also highly obliged to Professor Olaf Deutschmann, my co-supervisor, for his useful advices and providing me the DETCHEM software as well as the preprints of his joint work with Koyo Norinaga. Special thanks to Professor George Shaub for his suggestions from time to time which helped me to improve my work. I am also obliged to Professor Jürgen Warnatz and Professor Ulrich Maas for providing software HOMREA for my research work.

I am thankful to Siegfried Bajohr and Frank Graf for the guidance, discussions and providing the experimental data. I would also like to thank Walter Swady for useful CFD tips during the start of my research work. I am also thankful to Agnes von Garnier for helping me in official procedures and to explain many technical terms from German language. I am also thankful to Dominic Buchholz for useful discussions and translating the summary of my work to German language. Many thanks to Vinod M. Janardhanan, Steffan Tischer and Kyo Norinaga for their support to run the DETCHEM software.

I highly appreciate the help and support of Ms. Sabine Hecht throughout my stay at the Engler-Bunte-Institut. I am thankful to the colleagues at the Engler-Bunte-Institut, who are impossible to mention in this short paragraph, created a pleasant working environment.

I must acknowledge the financial support of Higher Education Commission of Pakistan (HEC) for my Ph.D. studies. I should also mention the German Academic Exchange Service (DAAD) who provided financial support for German language courses, administered my studies as well as arranged educational, social and recreational activities throughout my stay in Germany.

I am grateful to my family and friends in Pakistan for their moral support and encouragement during my stay abroad.

## Abstract

Carburizing is the case-hardening process in which carbon is added to the surface of low-carbon steels at temperatures generally between 850 and 1050 °C. In the conventional gas carburizing at atmospheric pressure, the carbon potential is controlled by adjusting the flow rate of the carburizing gas. Carbon potential of the furnace atmosphere can be related to partial pressure of CO<sub>2</sub> or O<sub>2</sub> or vapour pressure of water by equilibrium relationships and a sensor can be used to measure it. This method of carbon-potential control cannot be used for vacuum gas carburizing due to the absence of thermodynamic equilibrium which is one of the main difficulties of the vacuum carburizing process. The formation of soot during carburization is also undesirable and the process parameters should be selected such that the formation of soot is minimized. The amount of carbon available for carburizing the steel depends on the partial pressure of the carburizing gas, carbon content in the carburizing gas and the pyrolysis reactions of the carburizing gas. The pyrolysis reactions of the carburizing gas are also affected by the contacting pattern or how the gas flows through and contacts with the steel parts being carburized.

This work focuses on gaseous reactive flows in ideal and non-ideal reactors. The objective of this research is the development of models for the numerical simulation of homogeneous reactive flows under vacuum carburizing conditions of steel with propane and acetylene. These models can be used for further investigations of heterogeneous reactions during vacuum carburizing of steel to predict the carbon flux on the complex shaped steel parts to understand and, eventually, optimize the behavior of the whole reactor.

Two different approaches have been used to model the pyrolysis of propane and acetylene under vacuum carburizing conditions of steel. One approach is based on formal or global kinetic mechanisms together with the computational fluid dynamics (CFD) tool. The other approach is based on detailed chemistry with simplified or ideal flow models. Two global mechanisms developed at the Engler-Bunte-Institut for pyrolysis of propane and acetylene respectively were used in this work. One detailed mechanism developed at the Institute of Chemical Technology by the research group of Professor Deutschmann was used for modeling the pyrolysis of both the propane and acetylene. Experimental data from investigations on vacuum carburizing conducted at the Engler-Bunte-Institut were used to validate the modeling results.

# Table of Contents

<b>Table of Contents</b>	<b>i</b>
<b>1 Introduction</b>	<b>1</b>
1.1 An Overview of the Carburizing Process . . . . .	1
1.1.1 Gas Carburizing . . . . .	2
1.1.2 Vacuum or Low Pressure Carburizing . . . . .	6
1.2 Objective . . . . .	7
1.3 Structure of thesis . . . . .	8
<b>2 Pyrolysis of Carburizing Gas</b>	<b>9</b>
2.1 Pyrolysis of Propane . . . . .	9
2.2 Pyrolysis of Acetylene . . . . .	11
2.2.1 Formation of Polycyclic Aromatic Hydrocarbons (PAHs) and Soot . . . . .	13
<b>3 Reactive Flow Modeling</b>	<b>16</b>
3.1 Governing equations . . . . .	16
3.1.1 Governing equations for mass, momentum and species . . . . .	16
3.1.2 Heat transfer . . . . .	18
3.1.3 Transport properties . . . . .	18
3.1.4 Thermodynamic properties . . . . .	19
3.2 Modeling Chemical Reactions . . . . .	20
3.2.1 Temperature Dependence of Rate Coefficients . . . . .	22
3.2.2 Pressure Dependence of Rate Coefficients . . . . .	22
<b>4 Computational Tools</b>	<b>25</b>
4.1 Introduction . . . . .	25
4.2 DETCHEM . . . . .	26
4.2.1 DETCHEM Structure . . . . .	26
4.2.2 DETCHEM Models . . . . .	26
4.3 HOMREA . . . . .	30
4.3.1 Sensitivity Analysis . . . . .	31
4.3.2 Reaction Flow Analysis . . . . .	32
4.4 FLUENT . . . . .	32
4.4.1 FLUENT structure . . . . .	33
4.4.2 Species transport and reaction model . . . . .	34
4.4.3 Solution Convergence in Reacting Flows . . . . .	34

<b>5</b>	<b>Experimental Data</b>	<b>36</b>
5.1	Tubular Flow Reactor . . . . .	36
5.1.1	Operating conditions . . . . .	37
5.2	Thermogravimetric Reactor . . . . .	39
5.2.1	Operating conditions . . . . .	42
5.3	Vacuum Reactor . . . . .	44
5.3.1	Operating Conditions . . . . .	45
<b>6</b>	<b>Modeling of Propane Pyrolysis</b>	<b>46</b>
6.1	Tubular Flow Reactor . . . . .	46
6.1.1	Computational Fluid Dynamics (CFD) model . . . . .	46
6.1.2	Comparison of simulation and experimental results . . . . .	49
6.1.3	Detailed chemistry model . . . . .	49
6.1.4	Kinetic mechanism analysis . . . . .	50
6.1.5	Comparison of simulation and experimental results . . . . .	56
6.2	Thermogravimetric Reactor . . . . .	60
6.3	Vacuum Reactor . . . . .	66
<b>7</b>	<b>Modeling of Acetylene Pyrolysis</b>	<b>68</b>
7.1	Computational Fluid Dynamics Modeling . . . . .	68
7.1.1	Tubular flow reactor . . . . .	68
7.1.2	Thermogravimetric reactor . . . . .	77
7.1.3	Vacuum reactor . . . . .	82
7.2	Modeling with Detailed Chemistry . . . . .	88
7.2.1	Tubular flow reactor . . . . .	89
7.2.2	Effect of Acetone . . . . .	95
7.2.3	Thermogravimetric reactor . . . . .	98
7.2.4	Vacuum reactor . . . . .	98
<b>8</b>	<b>Summary and Outlook</b>	<b>102</b>
<b>A</b>	<b>FLUENT UDFs</b>	<b>124</b>
A.1	FLUENT UDF for the global mechanism . . . . .	124
A.2	FLUENT UDFs used for Temperature Profiles . . . . .	130
A.2.1	Temperature profiles in Thermogravimetric Reactor . . . . .	131
A.2.2	Temperature profiles in Vacuum Reactor . . . . .	134
<b>B</b>	<b>Pyrolysis of propane</b>	<b>138</b>
<b>C</b>	<b>List of Species and Detailed Reaction Mechanism</b>	<b>140</b>

# Chapter 1

## Introduction

This chapter briefly introduces the carburizing process of steel. Objectives of the present work are also discussed. Finally the structure of the thesis is explained.

### 1.1 An Overview of the Carburizing Process

Carburizing is the case-hardening process in which carbon is added to the surface of low-carbon steels at temperatures generally between 850 and 1050°C, at which austenite, with its high solubility for carbon, is the stable crystal structure. Hardening is accomplished when the high-carbon surface layer is quenched to form martensite so that a high-carbon martensitic case with good wear and fatigue resistance is superimposed on a tough, low-carbon steel core. Carburizing can be done in different ways:

- Gas Carburizing
- Vacuum Carburizing
- Plasma Carburizing
- Salt Bath Carburizing
- Pack Carburizing

The vast majority of parts are carburized by gas carburizing. Vacuum carburizing and plasma carburizing are being applied at commercial level due to their usefulness. Salt bath and pack carburizing are not feasible for products with high demands on quality and reproducibility and done occasionally at commercial level.

### 1.1.1 Gas Carburizing

The carburizing process of steel can be divided into five parallel physical and chemical subprocesses as shown in Figure 1.1. The flow conditions (1) in the reactor affect the pyrolysis (2) and the transport(3) of the hydrocarbon species considerably. The pyrolysis and transport processes are followed by the carbon release at the steel surface (4). The last subprocess is the diffusion of carbon into the steel (5) which changes the carbon concentration at the steel surface.

Gas carburizing can be run as a batch or as a continuous process. Furnace atmosphere for gas carburizing usually consists of a carrier gas and an enriching gas. The carrier gas is supplied at a high enough flow rate to maintain a positive furnace pressure thereby minimizing the air entry into the furnace. The enriching gas, the source of the carbon for carburizing, is supplied at a rate sufficient to satisfy the carbon demand of the charge [1].

Carburizing atmosphere can be categorized as an uncontrolled carbon potential or controlled carbon potential. In the gas carburizing under uncontrolled carbon potential, gaseous hydrocarbons or nitrogen-hydrocarbon blends free of oxygen are used. However, most gas carburizing is done under conditions in which the carbon potential of the atmosphere is controlled rather than uncontrolled. In controlled carbon potential atmosphere, usually a CO-rich gas called an endothermic gas (Endogas) derived from air and a hydrocarbon gas such as natural gas, propane or butane is used. The derived endothermic gas is a mixture consisting of carbon monoxide, carbon dioxide, methane, nitrogen, hydrogen and water vapor. The composition of this gas depends on the type of hydrocarbon gas used for generating the endothermic gas, the processing temperature, and the amount of gas added during the process. The carbon transfer takes place by the reverse Boudouard reaction 1.1 shown below.



The carbon potential in the gas phase determines the carbon concentration at the surface of the steel parts being carburized. In practice, control of carbon potential is achieved by controlling one of the following:

- carbon dioxide concentration
- water vapour concentration
- oxygen partial pressure

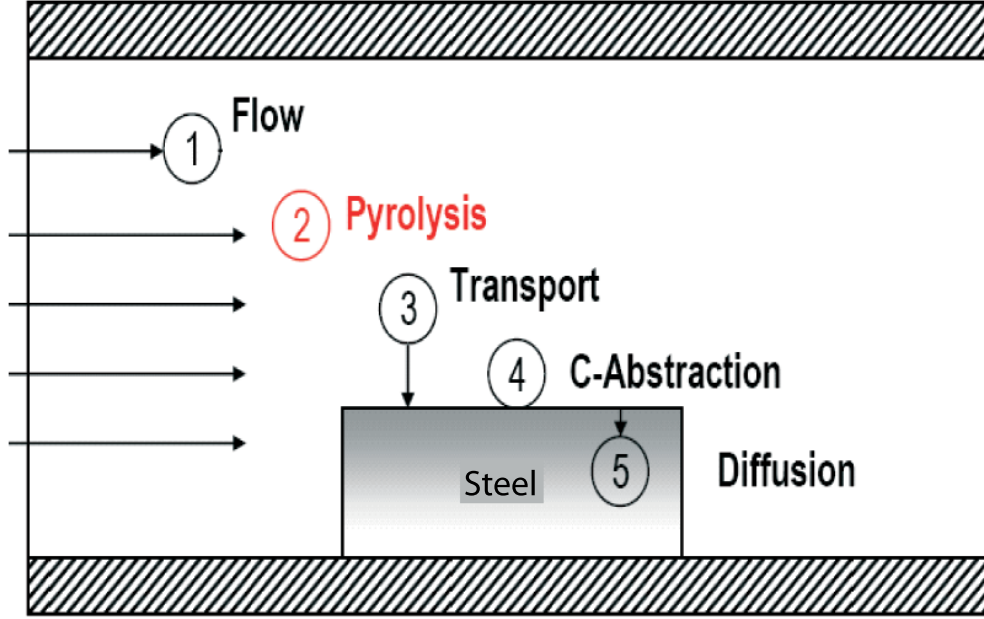


Figure 1.1: Schematic diagram of carburizing process [2]

The principle of carbon-potential control based on carbon dioxide concentration can be shown by the equilibrium reaction 1.1 for which the equilibrium constant  $K_1$  is given by the following relationship:

$$K_1 = \frac{a_c p_{CO_2}}{p_{CO}^2} \quad (1.2)$$

The equation (1.2) can be rearranged as follows:

$$a_c = \frac{K_1 p_{CO}^2}{p_{CO_2}} \quad (1.3)$$

where  $a_c$  is the activity of carbon and  $p_{CO_2}$  and  $p_{CO}$  are the partial pressures of  $CO_2$  and  $CO$  respectively. The quantity  $a_c$  is related to the carbon potential by the equilibrium relationship.  $K_1$  is temperature dependent only and  $p_{CO}$  being in large excess remains essentially constant, the carbon potential may be controlled by varying the  $p_{CO_2}$ . The concentration of  $CO_2$  can be measured by infrared gas analysis. Similar relationships exist which demonstrate the principle of control of carbon potential by control of water vapour by dew point measurement or partial pressure of oxygen using a zirconia oxygen sensor[3]. The partial pressure of water is related to the partial pressure of carbon dioxide under equilibrium conditions. The water-gas reaction can be used to show this relationship as under:





The equilibrium constant for the above reaction can be written as:

$$K_2 = \frac{p_{H_2O} p_{CO}}{p_{H_2} p_{CO_2}} \quad (1.5)$$

The above relationship can be rearranged as:

$$p_{CO_2} = \frac{p_{H_2O} p_{CO}}{K_2 p_{H_2}} \quad (1.6)$$

Substituting the right side of equation 1.6 in equation 1.3:

$$a_c = K_1 K_2 \frac{p_{CO} p_{H_2}}{p_{H_2O}} \quad (1.7)$$

Since  $p_{CO}$  and  $p_{H_2}$  remain constant in the carburizing atmosphere and  $K_1$  and  $K_2$  are temperature dependent, the carbon potential can be controlled by controlling the vapour pressure of  $H_2O$  (dew point).

Partial pressure of oxygen can in principle be also used to control the carbon potential. Under equilibrium the partial pressure of oxygen is related to the partial pressure of carbon dioxide.



The equilibrium constant  $K_3$  for the above reaction can be written as:

$$K_3 = \frac{p_{CO_2}}{p_{CO} p_{O_2}^{\frac{1}{2}}} \quad (1.9)$$

From equation 1.9, expression for  $p_{CO_2}$  can be derived as under:

$$p_{CO_2} = K_3 p_{CO} p_{O_2}^{\frac{1}{2}} \quad (1.10)$$

Substituting the equation 1.10 for  $p_{CO_2}$  in equation 1.3 gives:

$$a_c = \frac{K_1 p_{CO}}{K_3 p_{O_2}^{\frac{1}{2}}} \quad (1.11)$$

$K_1$  and  $K_3$  are temperature dependent and  $p_{CO}$  remains constant in the carburizing atmosphere so the carbon potential can be controlled by monitoring the partial pressure of oxygen.

### Diffusion of Carbon

Many researcher have studied the diffusion process of carbon during gas carburizing of steel [4–10]. At the steel/gas phase interface the carburization reaction depends on the difference between the carbon activity in the atmosphere and at the steel surface. Carbon will diffuse from the gas atmosphere to the steel surface when the activity of the carbon in the gas atmosphere is higher than the activity of carbon on the steel surface which depends on furnace temperature and the initial carbon concentration in the steel. Typical profiles of carbon in steel during carburization are shown in the Fig. 1.2.

The rate of carbon transport to the steel surface can be described by means of

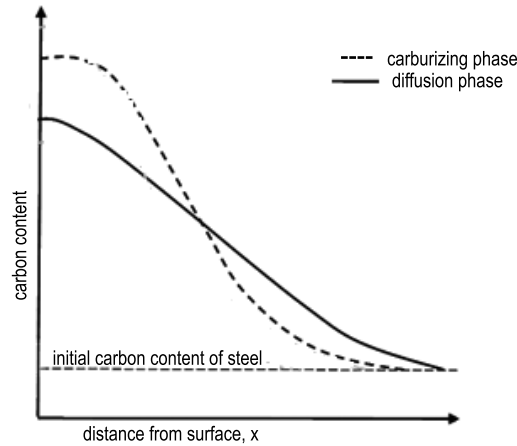


Figure 1.2: Typical carbon profile for a carburized steel

Fick's law of diffusion:

$$J_i = -D_i \frac{\partial C_i}{\partial x} \quad (1.12)$$

In this equation,  $J_i$  is the flux of species  $i$  which in this case will be carbon, i.e. the amount of species  $i$  passing through unit area of reference plane per unit of time,  $C_i$  represents the concentration of species  $i$  and  $x$  is the cartesian coordinate.  $D_i$  represents the diffusion coefficient (diffusivity) of species  $i$  in the medium in which it is diffusing and has units of area/time. The value of  $D_i$  will depend strongly on the process temperature. The transport of carbon from the surface of the steel towards the centre can also be described by Fick's law of diffusion by equation 1.13:

$$\frac{\partial C_i}{\partial t} = D_i \frac{\partial^2 C_i}{\partial x^2} \quad (1.13)$$

Following results can be obtained for the carbon concentration as a function of distance and time,  $C(x, t)$ , during carburisation of steel:

$$C(x, t) - C_0 = C_1 - C_0 \left[ 1 - \operatorname{erf} \left( \frac{x}{2\sqrt{D_C^\gamma t}} \right) \right] \quad (1.14)$$

where  $x = 0$  is defined as the surface of the steel in contact with the carburizing atmosphere,  $C(x,t)$  is the carbon concentration at a depth  $x$  below the surface,  $C_0$  is the basic carbon content of the steel at time  $t=0$ ,  $C_1$  is the carbon content at the surface of the steel at any time  $t$ ,  $x$  is the depth below the surface,  $D_C^\gamma$  is the diffusion coefficient of carbon in austenite depending on temperature according to equation 1.15,  $t$  is the time and erf is the error function.

$$D_C^\gamma = (D_0)_C^\gamma \exp \left[ -\frac{Q_C^\gamma}{RT} \right] \quad (1.15)$$

In the above equation, the pre-exponential term  $(D_0)_C^\gamma$  is called the frequency factor and has units of  $\text{m}^2 \text{s}^{-1}$  and  $Q_C^\gamma$  is called the activation energy for diffusion which has units of  $\text{J mol}^{-1}$ . Both these properties are material specific properties i.e. material of the diffusing solute which in this particular case is carbon and the material of the matrix which in this case is steel (austenite). In this equation,  $R$  is the gas constant ( $8.314 \text{ J K}^{-1} \text{ mol}^{-1}$ ) and  $T$  is the absolute temperature at which carburization is performed.

### 1.1.2 Vacuum or Low Pressure Carburizing

The vacuum carburizing or low pressure carburizing of steel with subsequent high pressure gas quenching is a modern process for the case hardening of steel parts such as cog wheels, gearbox parts or shafts that need a wear resistant, hard surface with a co-requisite ductile core. The process, as its name implies, is carried out in a vac-

uum furnace at pressures below normal atmospheric pressure. Vacuum carburizing using methane ( $\text{CH}_4$ ) as the carburizing gas was introduced in the 1960s but this process requires higher temperatures and pressures up to 500 mbar. The problems experienced with this process were the uniformity and repeatability required to meet the quality specifications for precision parts. Other drawbacks include the formation of soot and higher hydrocarbons which can settle on furnace walls requiring higher maintenance time and cost. To overcome these problems, propane ( $\text{C}_3\text{H}_8$ ), ethylene ( $\text{C}_2\text{H}_4$ ) or acetylene ( $\text{C}_2\text{H}_2$ ) are being used for carburizing at pressures below 20 mbar. The steel parts are exposed to the carburizing gas at temperatures between 900-1050 °C and total pressures between 2-20 mbar. Under the high temperature the carburizing gases are pyrolyzed and form atomic carbon on the steel surface. The carbon diffuses into the steel and locally increases the carbon concentration. At the surface the concentration of carbon is about 1 mass- % and then decreases to the core concentration of typically 0.2 mass-% depending on the steel type [11–24]. The vacuum carburizing process has some advantages as compared to gas carburizing e.g.

- High temperature carburizing resulting in shorter carburizing time or increased productivity
- Creation of a surface free of oxides
- Carburization of complex shapes such as blind holes
- Reproducible and uniform results
- Environment friendliness

## 1.2 Objective

In the conventional gas carburizing at atmospheric pressure, the carbon potential is controlled by adjusting the flow rate of the carburizing gas. Carbon potential of the furnace atmosphere can be related to partial pressure of  $\text{CO}_2$  or  $\text{O}_2$  or vapour pressure of water by equilibrium relationships as discussed in the previous section and a sensor can be used to measure it. This method of carbon-potential control cannot be used for vacuum gas carburizing due to the absence of thermodynamic equilibrium which is one of the main difficulties of the vacuum carburizing process. The formation of soot during carburization is also undesirable and the process parameters should be selected such that the formation of soot is minimized. The amount of carbon available for carburizing the steel depends on the partial pressure of the

carburizing gas, carbon content in the carburizing gas and the pyrolysis reactions of the carburizing gas. The pyrolysis reactions of the carburizing gas are also affected by the contacting pattern or how the gas flows through and contacts with the steel parts being carburized.

In the current work, investigations are carried out to achieve a better understanding of the reaction mechanisms of propane and acetylene pyrolysis under the vacuum carburizing condition of steel. It focuses on gaseous reactive flows in ideal and non-ideal reactors. The objective of this research is the development of models for the numerical simulation of homogeneous reactive flows under vacuum carburizing conditions of steel with propane and acetylene. The developed models can predict the gas compositions resulting from the homogeneous gas phase reactions of propane and acetylene pyrolysis. These models can be used for further investigations of heterogeneous reactions during vacuum carburizing of steel to predict the carbon flux on the complex shaped steel parts to understand and, eventually, optimize the behavior of the whole reactor.

### **1.3 Structure of thesis**

Chapter 2 will review the literature on the pyrolysis mechanisms of propane and acetylene. Chapters 3 and 4 will describe the concept for modeling the reactive flows and the computational tools for the numerical simulations. In Chapter 5, the experimental data available for validating the modeling results will be described. In Chapters 6 and 7, the modeling concepts and computational tools discussed in Chapter 3 and 4 will be applied. Also the modeling results will be validated with the experimental data described in Chapter 5. Chapter 8 will provide an outlook and summary of the work.

# Chapter 2

## Pyrolysis of Carburizing Gas

Propane and acetylene are commonly used as a source of carbon during vacuum carburizing of steel. This chapter presents a literature review on the pyrolysis of propane and acetylene. The products and the mechanisms of pyrolysis are discussed.

### 2.1 Pyrolysis of Propane

Propane is a widely used feedstock in the petrochemical industry and hence much effort has been devoted to investigate the kinetics of its pyrolysis at varying conditions. These studies include at plant level, shock-tube [25–29], tubular flow reactors [30–36] and static systems. Pyrolysis of propane like that of many other hydrocarbons leads to hundreds of species and reactions. Sugiyama et al [13] suggested that most of the propane during the vacuum carburizing is cracked without coming into contact with the steel surface and such reaction products result in sooting. Following reaction sequence of furnishing carbon on the heated steel surface was suggested during vacuum carburizing with propane:



The first stage in the pyrolysis of propane can be designated as the primary reactions wherein the propane is decomposed through free radical chain mechanism into the principal primary products such as  $CH_4$ ,  $C_2H_4$ ,  $C_3H_6$ ,  $H_2$  and other minor primary products. The second stage encompasses secondary reactions involving

further pyrolysis of olefins produced by primary reactions, hydrogenation and dehydrogenation reactions of the olefins and condensation reactions wherein two or more smaller fragments combine to produce large stable structures such as cyclodiolefins and aromatics [37, 38].

The rate of propane pyrolysis has been reported in early studies to be first order but most of the studies after 1965 show that the overall rate is not well described by first order or simple order equations. The propane pyrolysis involves complicated series of consecutive and simultaneous free radical steps. At conversions less than 20%, the overall reaction may be presented as: [39, 40]



Two possibilities of initiation reaction of propane pyrolysis by breaking of C-C or C-H bond have been discussed in literature [37, 41]. On the basis of the comparison of bond dissociation energies, C-C rupture is most favourable. The initiation step and following propagation steps are as follows:



The evaluated and estimated data on the kinetics of reactions involving propane as well as thermodynamic and transport properties data have been published by Tsang [42]. Kaminski and Sobkowski [43] studied the pyrolysis of propane in the presence of hydrogen, deuterium and argon in the temperature range of 890-1019 K. They observed an increase in the yields of methane, ethane and ethylene in the presence of hydrogen and deuterium while the yields of hydrogen and propylene decrease. However the reaction was not effected by the dilution of propane with argon.

Keeping in view the fact that reactor wall may play an active role in a gas phase reaction, studies to investigate the effect of surface on the pyrolysis of propane have been conducted [30, 31, 40, 44, 45]. Perrin and Martin [40] studied the pyrolysis of propane between 743 and 803 K and reported that propane pyrolysis is strongly inhibited by the walls of reactors packed with stainless steel, zirconium or palladium foils. The rates of product formation increase in the presence of hydrogen. The

inhibiting effects of metallic walls on propane pyrolysis have been interpreted by the heterogeneous termination of chains carried by hydrogen atoms. The course of a chain reaction is not effected by metallic walls when chains are not carried by hydrogen atoms. The heterogeneous reaction occurring can be represented as:



Kunugi et al [46] observed that quartz surface has no significant effect on the decomposition rate of propane pyrolysis. Ziegler [47] studied the influence of surface on chemical kinetics of pyrocarbon deposition obtained by propane pyrolysis. The increase of surface to volume ratio (S/V) effects the products of pyrolysis by decreasing the concentration of the gas species and more decrease is observed for unsaturated species. Bajohr [48] studied the pyrolysis of propane under the conditions of vacuum carburizing of steel and has suggested a formal kinetic mechanism which consists of 9 species and 10 chemical reactions.

## 2.2 Pyrolysis of Acetylene

Acetylene is an unsaturated hydrocarbon gas having one triple bond (H-C≡C-H) with a heat of formation value of -226.7 kJ/mole [15]. According to Sugiyama et al [13], acetylene rapidly dissociates into carbon and hydrogen when it comes into contact with hot steel resulting in the diffusion of carbon into the steel. The following reactions rapidly occur when acetylene gas is introduced into a vacuum carburizing furnace:



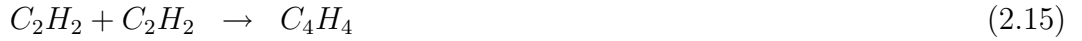
The above reactions are not the only reactions which occur during vacuum carburizing of steel. The thermal decomposition of acetylene has been studied by many researchers in static systems[49, 50], in flow systems [51–55], in shock tubes [56–65] and in flames [66, 67]. The temperature range covered in these studies is about 625 K to 4650 K. A radical chain mechanism was proposed in 1970s [68, 57, 69] with the assumption of following initiation reaction:





According to Kiefer et al [70] acetylene pyrolysis can be divided into three different temperature regimes:

- (i)  $T < 1100$  K where the homogeneous reaction is a molecular polymerization.
- (ii)  $1100 < T < 1800$  K where the process is still dominated by a molecular polymerization, but a fragment radical chain is clearly involved.
- (iii)  $T > 1800$ , where a fragment chain carried by  $C_2H$  and  $H$  drives a polymerization to polyacetylene. The core mechanism of acetylene pyrolysis has been reported as follows:



Frenklach and coworkers [61] identified two isomers  $n-C_4H_3$  and  $i-C_4H_3$  and proposed that the reaction (2.19) shown below is the initiation reaction.



Wu et al[62] proposed that  $i-C_4H_3$  is the product after noting the discrepancy between endothermicity of the reaction (2.19) and the observed activation energy. Duran et al [71] suggested that acetylene polymerizes by isomerization to vinylidene which is further converted to vinylacetylene by the following mechanism:



Colket et al [72] proposed a detailed radical chain mechanism for acetylene pyrolysis suggesting reaction (2.14) inconsistent with thermochemistry and acetone as a source

of initiation reaction. The initiation by acetone is described as follows:



Kruse and Roth [65] studied the pyrolysis of acetylene at high temperature in shock tube and proposed a detailed mechanism for high temperature pyrolysis of acetylene. The initiation reaction consists of successive abstraction of H atoms as below:



Krestinin [73] studied the kinetics of heterogeneous pyrolysis of acetylene to explain the carbon film formation on a hot cylinder surface. The work of Callear and Smith [74] who investigated the addition of hydrogen to acetylene provides the evidence of radical chain mechanism.

The effect of acetone on the pyrolysis of acetylene has been also studied by Dimitrijevic et al [53] at 914-1039 K and 6-47 kPa. The presence of acetone was found to accelerate the formation of vinyl acetylene and benzene.

Recently Norinaga and Deutschmann [75] studied the pyrolysis of acetylene at 900 °C for chemical vapour deposition of carbon and developed a detailed mechanism comprising of 227 species and 827 reactions. Acetylene is consumed by dimerization to  $C_4H_4$  (68 %),  $C_4H_2$  (17 %) and formation of benzene by the combination of  $C_4H_4$  and  $C_2H_2$ (7%).

Graf [2] studied the pyrolysis of acetylene in a tubular flow reactor and proposed a reaction mechanism consisting of 7 species and 9 chemical reactions.

## 2.2.1 Formation of Polycyclic Aromatic Hydrocarbons (PAHs) and Soot

Formation of soot during carburizing of steel is not only an environmental problem but is an operational problem too. So efforts are made to avoid the formation of soot during carburizing of steel. In the previous studies, the primary and secondary products resulting from the pyrolysis of acetylene have been distinguished [50, 76]. In the lower temperature region below 1200 K vinyl acetylene ( $C_4H_4$ ) is the initial product while in the high temperature region diacetylene ( $C_4H_2$ ) is the primary

molecular product. Hydrogen, methane, ethylene, butadiene and benzene are also formed in varying amounts depending on the temperature and conversion. In the early works of Bertholot, the formation of benzene via direct polymerization of acetylene was suggested. Colket [63] concluded that in case of acetylene pyrolysis below 1500 K, formation of benzene follows the following path:



At higher temperatures above 1500 K, phenyl is formed as:



Frenklach and Warnatz [66] suggested four pathways for the formation of first aromatic ring based on the cyclization of unsaturated aliphatic radicals:



The formation of the first aromatic ring, formation of PAHs, soot inception and its growth are believed to be the important steps of soot formation [77].

The growth of smaller molecules such as benzene to polycyclic aromatic hydrocarbons (PAHs) involve smaller molecules among which acetylene is important. The molecular precursors of soot particles are thought to be PAHs with molecular weight 500-1000 amu [61, 79, 80]. The particles grow by surface growth which follows a sequential two step process of H-abstraction- $C_2H_2$ -addition (HACA) as shown in figures 2.1 and by coagulation [78, 81] as shown in 2.2.



# Chapter 3

## Reactive Flow Modeling

### 3.1 Governing equations

In chemical reacting flows, pressure, temperature, density, velocity of the flow and concentration of species can change in time and space. These properties change as a result of fluid flow (convective transport), molecular transport, radiation and chemical reaction. Properties such as mass, momentum and energy are conserved in reacting flows. Equations governing the conserved properties can be derived by considering either a given quantity of matter or *control mass* and its extensive properties, such as mass, momentum, and energy. This approach is used to study the dynamics of solid bodies where the control mass is identified easily. In case of fluid flows, the flow within a certain spatial region called *control volume* is considered as a system. This approach is called control-volume approach and is more convenient for flow problems. The governing equations are based on conservation principles for an extensive property. By transformation of these laws into a control volume form, the fundamental variables will be intensive properties which are independent of the amount of mass considered. Density  $\rho$  (mass per unit volume) and velocity  $\vec{u}$  (momentum per unit mass) are examples of intensive properties. [82, 83, 81, 84, 85].

#### 3.1.1 Governing equations for mass, momentum and species

The law of mass conservation leads to the mass continuity equation as shown below:

$$\frac{\partial \rho}{\partial t} + \frac{\partial(\rho u_j)}{\partial x_j} = 0 \tag{3.1}$$

where  $x_j$  ( $j = x, y, z$ ) are the Cartesian coordinates and  $u_j$  or  $(u_x, u_y, u_z)$  are the Cartesian components of the velocity vector  $\vec{u}$ . Although in classical chemistry mass can neither be created nor destroyed, a source term is introduced in the above equation when this is applied for modeling the continuous fluid phase of a reactor. Mass can be added to that phase or removed from that phase for example vaporization of liquid droplets or mass deposition in chemical vapour deposition. In such cases, the above equation can be used to treat the flow across the boundaries of the system using a source term and can be written as :

$$\frac{\partial \rho}{\partial t} + \frac{\partial(\rho u_j)}{\partial x_j} = S_m \quad (3.2)$$

The momentum balance for Newtonian fluids leads to the following equation:

$$\frac{\partial}{\partial t}(\rho u_i) + \frac{\partial}{\partial x_j}(\rho u_j u_i) + \frac{\partial}{\partial x_i} p - \frac{\partial}{\partial x_j}(\tau_{ij}) = \rho g_i \quad (3.3)$$

where  $p$  is the static pressure,  $\tau_{ij}$  is the stress tensor, and the  $\rho \vec{g}$  denote the gravitational body force. The only body force,  $\rho \vec{g}$ , taken into account in the above equation can often be neglected when modeling chemical reactions.

$$\tau_{ij} = \mu \left( \frac{\partial}{\partial x_j} u_i + \frac{\partial}{\partial x_i} u_j - \frac{2}{3} \frac{\partial}{\partial x_k} u_k \delta_{i,j} \right) \quad (3.4)$$

Here  $\delta_{i,j}$  is Kronecker symbol ( $\delta_{i,j} = 1$  if  $i = j$  and  $\delta_{i,j} = 0$  otherwise). The coupled mass continuity and momentum equations have to be solved for the description of the flow field. In case of multicomponent mixtures, mixing of chemical species and reactions among them are also possible which need additional partial differential equations. The mass balance  $m_i$  of each species  $i$  in the reactor lead to the following set of equations:

$$\frac{\partial}{\partial t}(\rho Y_i) + \frac{\partial}{\partial x_j}(\rho u_j Y_i) + \frac{\partial}{\partial x_j}(j_{i,j}) = R_i^{hom} \quad (i = 1, \dots, k_g) \quad (3.5)$$

Here,  $Y_i$  is mass fraction of species  $i$  in the mixture,  $k_g$  is the number of gas phase species,  $j_{i,j}$  is component  $j$  of the diffusion mass flux of the species  $i$  and  $R_i^{hom}$  is the net rate of production of species  $i$  due to homogeneous chemical reactions. These additional  $k_g$  equation are coupled with Eqs. (3.1) and (3.3).

### 3.1.2 Heat transfer

Heat released by chemical reactions and its transport will lead to temperature distribution in the reactor and can be predicted by the law of energy conservation. For a multicomponent fluid flow, the governing equation can be written in the following form:

$$\frac{\partial}{\partial t}(\rho h) + \frac{\partial}{\partial x_i}(\rho h u_i) = \frac{\partial}{\partial t}p + u_i \frac{\partial}{\partial x_i}p - \frac{\partial}{\partial x_i}q_i - \tau_{ij} \frac{\partial}{\partial x_j}u_i \quad (3.6)$$

where  $h$  is the specific enthalpy,  $q_i$  is the heat flux which mainly result from the heat conduction and mass diffusion.

### 3.1.3 Transport properties

The viscosity of a pure species is given by the kinetic theory as under:

$$\mu_i = \frac{5}{6} \frac{\sqrt{\pi M_i k_B T / N_A}}{\pi \sigma_i \Omega^{(2,2)*} T_i^*} \quad (3.7)$$

The transport coefficients for multi-component mixtures are usually derived from the transport coefficients of the individual species and the mixture composition applying empirical approximations. The viscosity of the mixture  $\mu$  can be calculated from the viscosity of species  $\mu_i$  by the following relationship:

$$\mu = \frac{1}{2} \left[ \sum_i^{k_g} X_i \mu_i + \left( \sum_i^{k_g} \frac{X_i}{\mu_i} \right)^{-1} \right] \quad (3.8)$$

Heat conduction and viscosity in gases are caused by transfer of energy and momentum, respectively. Therefore, they are related to each other. The individual species conductivities are composed of translational, rotational, and vibrational contributions and can be calculated as explained by Warnatz [86].

The thermal conductivity of the mixture  $\lambda$  can be calculate from the species thermal conductivity  $\lambda_i$

$$\lambda = \frac{1}{2} \left[ \sum_i^{k_g} X_i \lambda_i + \left( \sum_i^{k_g} \frac{X_i}{\lambda_i} \right)^{-1} \right] \quad (3.9)$$

The binary diffusion coefficient can be expressed as a function of temperature  $T$  and  $p$  :

$$D_{ij} = \frac{3}{16} \frac{\sqrt{2\pi N_A k_B^3 T^3 / M_{ij}}}{p\pi\sigma_{ij}^2 \Omega_{ij}^{(1,1)*}(T_{ij}^*)} \quad (3.10)$$

The effective mass diffusion coefficients  $D^M$  can be estimated [83] as:

$$D_i^M = \frac{1 - Y_i}{\sum_{j \neq i}^{k_g} \frac{X_j}{D_{ij}}} \quad (3.11)$$

The approximation (3.11) violates mass conservation, therefore the diffusion fluxes have to be corrected by

$$\vec{j}_{corr} = - \sum_i^{k_g} \vec{j}_i \quad (3.12)$$

### 3.1.4 Thermodynamic properties

The thermodynamic properties of species  $i$  can be described by a polynomial fit of fourth order to the specific heat at constant pressure:

$$c_{p,i}(T) = \frac{R}{M_i} \sum_{n=1}^5 a_{ni} T^{n-1} = \frac{R}{M_i} (a_{1i} + a_{2i}T + a_{3i}T^2 + a_{4i}T^3 + a_{5i}T^4) \quad (3.13)$$

The temperature dependence of the species heat capacities is often described by polynomials when used in computations e.g. by a polynomial of fourth order according to the NASA computer programs. The other thermodynamic properties can be calculated from the specific heat. The standard state enthalpy and standard state entropy are calculated as follows:

$$h_i(T) = h_i(T_{ref}) + \int_{T_{ref}}^T c_{p,i}(T') dT' \quad (3.14)$$



The specific standard enthalpy of formation  $\Delta h_{f,298,i}^0$  can be used as integration constant  $h_i(T_{ref}=298.15 \text{ K}, p^0=1 \text{ bar})$

$$s_i(T) = s_i(T_{ref}) + \int_{T_{ref}}^T \frac{c_{p,i}(T')}{T'} dT' \quad (3.15)$$

In the above equation, the specific standard entropy  $s_{298,i}^0$  can be used as integration constant  $s_i(T_{ref}=298.15 \text{ K}, p^0=1 \text{ bar})$ . The entropies are needed for the calculation of the equilibrium constants. Chemical reaction mechanism works with a thermodynamic database and a transport property database for the chemical species involved. These databases usually organize the thermodynamic and transport data in terms of polynomials as functions of temperature: for example, NASA database.

## 3.2 Modeling Chemical Reactions

In general, a chemical reaction can be written in the following form

$$\sum_{i=1}^{k_g} \nu'_i A_i = \sum_{i=1}^{k_g} \nu''_i A_i \quad (3.16)$$

where  $A_i$  is  $i$ -th species symbol and  $\nu'_i$ ,  $\nu''_i$  are the stoichiometric coefficients of the reactants and products respectively. The forward reaction rate for species  $i$  can be written as:

$$\dot{\omega}_{i,f} = \nu_i k_f \prod_{i=1}^{k_g} c_i^{a'_i} \quad (3.17)$$

where

$$\nu_i = \nu''_i - \nu'_i \quad (3.18)$$

$a'_i$  is the reaction order with respect to the species  $i$ . The reaction orders of elementary reactions are always integers and equal the molecularity of the reaction. Global reactions can have complex rate laws where the reaction orders are not necessarily

integers. For the reverse reaction:



The rate law can be written as:

$$\dot{\omega}_{i,b} = \nu_i k_b \prod_i^{k_g} c_i^{a_i''} \quad (3.20)$$

The net rate of creation/destruction of species  $i$  can be written as:

$$\dot{\omega}_i = \dot{\omega}_{i,f} - \dot{\omega}_{i,b} \quad (3.21)$$

At chemical equilibrium the forward and reverse reaction rate are equal:

$$\nu_i k_f \prod_i^{k_g} c_i^{a_i'} = \nu_i k_b \prod_i^{k_g} c_i^{a_i''} \quad (3.22)$$

and the ratio

$$\frac{k_f}{k_b} = \prod_i^{k_g} c_i^{a_i'' - a_i'} \quad (3.23)$$

is the equilibrium constant  $K_c$  which can be calculated from the thermodynamic data and  $k_r$  can be calculated as:

$$k_b = \frac{k_f}{K_c} \quad (3.24)$$

For elementary reactions, the equation 3.23 can be written as:

$$\frac{k_f}{k_b} = \prod_i^{k_g} c_i^{\nu_i} \quad (3.25)$$

### 3.2.1 Temperature Dependence of Rate Coefficients

In general, the rate coefficients of chemical reactions depend strongly on temperature in a nonlinear way. According to Arrhenius law, this temperature dependence can be described by an exponential function. An additional small temperature dependence is introduced into the model based on more accurate measurements which lead to the following modified Arrhenius expression:

$$k = A T^b \cdot \exp\left(-\frac{E_a}{RT}\right) \quad (3.26)$$

where  $A$  and  $E_a$  are called the pre-exponential factor and activation energy respectively. When the concept of global reactions is used, rate coefficients are fitting parameters and have no physical meanings. But when the concept of elementary reactions is applied, these parameters have physical meanings. Then the activation energy  $E_a$  is considered a barrier which has to be overcome during the reaction. The maximum value of  $E_a$  corresponds to bond energies in the molecules but it can also be much smaller or zero if new bonds are formed with breaking of old bonds during the reaction. The pre-exponential factor can be connected to a mean lifetime of an activated molecule and a collision rate, for unimolecular and bimolecular reactions, respectively [83, 81].

### 3.2.2 Pressure Dependence of Rate Coefficients

In many cases, the rate coefficients of dissociation and recombination reactions have also pressure dependence in addition to temperature dependence. This fact indicates that these reactions are not elementary and are a sequence of reactions. In these reactions another collision partner has to be present during the reaction to provide or absorb energy. Therefore, the rate coefficients of these reactions depend on the number of collisions, that means on the pressure. The pressure dependence can be understood using the Lindemann Model. According to this model, a unimolecular decomposition is only possible, if the energy in the molecule is sufficient to break the bond. So prior to the decomposition reaction energy must be added to the molecule by collision with molecules  $M$  called third bodies. Because the different chemical species, called third bodies, differ in their efficiency for providing and absorbing energy in a collision, the rate coefficient also depends on the kind of that partner, i.e., a single dissociation or recombination reaction has to be expressed by a large number of elementary reactions. Such reactions are normally written in the following

form:



where M indicates the third body. The different collision efficiencies of the third bodies are then taken into account by defining their efficiency coefficients with respect to different reactions. The pressure dependence of the rate coefficients could be described by setting up a separate kinetic scheme for each pressure value under consideration. This procedure is not very handy, therefore, more complex expressions for the rate coefficients are commonly used. The Troe formalism has found widespread application. According to Lindemann theory, one can observe a direct proportionality in the low-pressure limit while saturation is achieved in high pressure limit [83, 81]. In Arrhenius form, the parameters are given for the low pressure limit and the high pressure limit as follows:

$$k_0 = A_0 T^{b_0} e^{-\frac{E_{a0}}{RT}} \quad (3.28)$$

$$k_\infty = A_\infty T^{b_\infty} e^{-\frac{E_{a\infty}}{RT}} \quad (3.29)$$

According to the Lindemann theory the rate coefficients at any pressure is taken to be:

$$k = k_\infty \left( \frac{p_r}{1 + p_r} F \right) \quad (3.30)$$

where  $p_r$  is the reduced pressure given by :

$$p_r = \frac{k_0[M]}{k_\infty} \quad (3.31)$$

and  $[M]$  is the concentration of the mixture which can include third-body efficiencies.  $F$  is called the pressure fall-off blending function. For the simple case when  $F=1$  in equation 3.30,  $k \rightarrow k_0[M]$  in the low pressure limit i.e. when  $[M] \rightarrow 0$ . In the high-pressure limit,  $[M] \rightarrow \infty$  and  $k \rightarrow k_\infty$  i.e. a constant value.

In DETCHEM, the Troe formalism has been implemented to model this function as

under:

$$\log_{10} F = \left[ 1 + \left( \frac{\log_{10} p_r + c}{n - d(\log_{10} p_r + c)} \right)^2 \right]^{-1} \log_{10} F_{cent} \quad (3.32)$$

where

$$c = -0.4 - 0.67 \log_{10} F_{cent} \quad (3.33)$$

$$n = 0.75 - 1.27 \log_{10} F_{cent} \quad (3.34)$$

$$d = 0.14 \quad (3.35)$$

and

$$F_{cent} = (1 - \alpha)e^{-T/T^{***}} + \alpha e^{-T/T^*} + e^{-T^{**}/T} \quad (3.36)$$

The parameters  $\alpha$ ,  $T^{***}$ ,  $T^*$  and  $T^{**}$  are called the Troe parameters and are used to fit the experimental data.

# Chapter 4

## Computational Tools

This chapter introduces the computational tools for reactive flow modeling used in the present work.

### 4.1 Introduction

Reactive flow processes are often characterized by a complex interaction of transport and chemical kinetics. The chemistry may include gas phase as well as surface reactions and flow may be complex. The numerical simulation of reactive flows including detailed schemes for surface and gas phase chemistry is receiving considerable attention due to the availability of faster computers, the development of new numerical algorithms, and the establishment of elementary reaction mechanisms. A key problem is the stiffness of the governing equations because of different time scales introduced by chemical reactions including adsorption and desorption. Therefore, simulations of chemical reactors frequently use a simplified model, either of the flow field or chemistry. This simplification can be risky if there is a strong interaction between flow and chemistry. While the currently available commercial CFD codes are able to simulate even very complex flow configurations including turbulence and multi-component transport, the use of complex models for the chemical processes is still very limited to the number of species and reactions [83]. Computational tools used in the present work include DETCHEM, HOMREA and FLUENT which are discussed in the next sections of this chapter.

## 4.2 DETCHEM

The DETCHEM (DETAiled CHEMistry) software package applies detailed models for the description of chemical reactions and transport processes. It has been designed for a better understanding of the interactions between transport and chemistry. The chemistry may include gas phase as well as surface reactions. It can assist in reactor development and process optimization [87, 88]. DETCHEM can also be coupled to commercial CFD codes such as FLUENT [89, 90].

### 4.2.1 DETCHEM Structure

DETCHEM is a library of FORTRAN routines, which have been developed and applied for the simulation of chemically reacting gaseous flows focusing on the implementation of complex models for the description of heterogeneous chemical reactions. The structure of DETCHEM is shown in Fig. 4.1.

### 4.2.2 DETCHEM Models

#### One dimensional model

DETCHEM<sup>PLUG</sup> is a computational tool that simulates one dimensional reacting flows with and without mass and heat transfer. Plug-flow equations enormously reduce the computational cost by simplifying the balance equations for mass, species and energy. These equations are derived based on the assumptions of (a) negligible axial diffusion and (b) infinite mixing in the radial direction. Assumption (b) means that there is no variation in the transverse direction. Furthermore, DETCHEM<sup>PLUG</sup> is a steady-state model. Hence, the 1-D partial differential conservation equations become ordinary differential equations with the axial coordinate as time-like variable. Schematic diagram of the plug flow is shown in Fig. 4.2.

With these assumptions, the system of differential-algebraic equations (DAE) consist of the continuity equation (governing equations in general form already discussed in section 3.1.1)

$$A_c \frac{d(\rho u)}{dz} = A_s \sum_{k=1}^{k_g} \dot{s}_k M_k \quad (4.1)$$

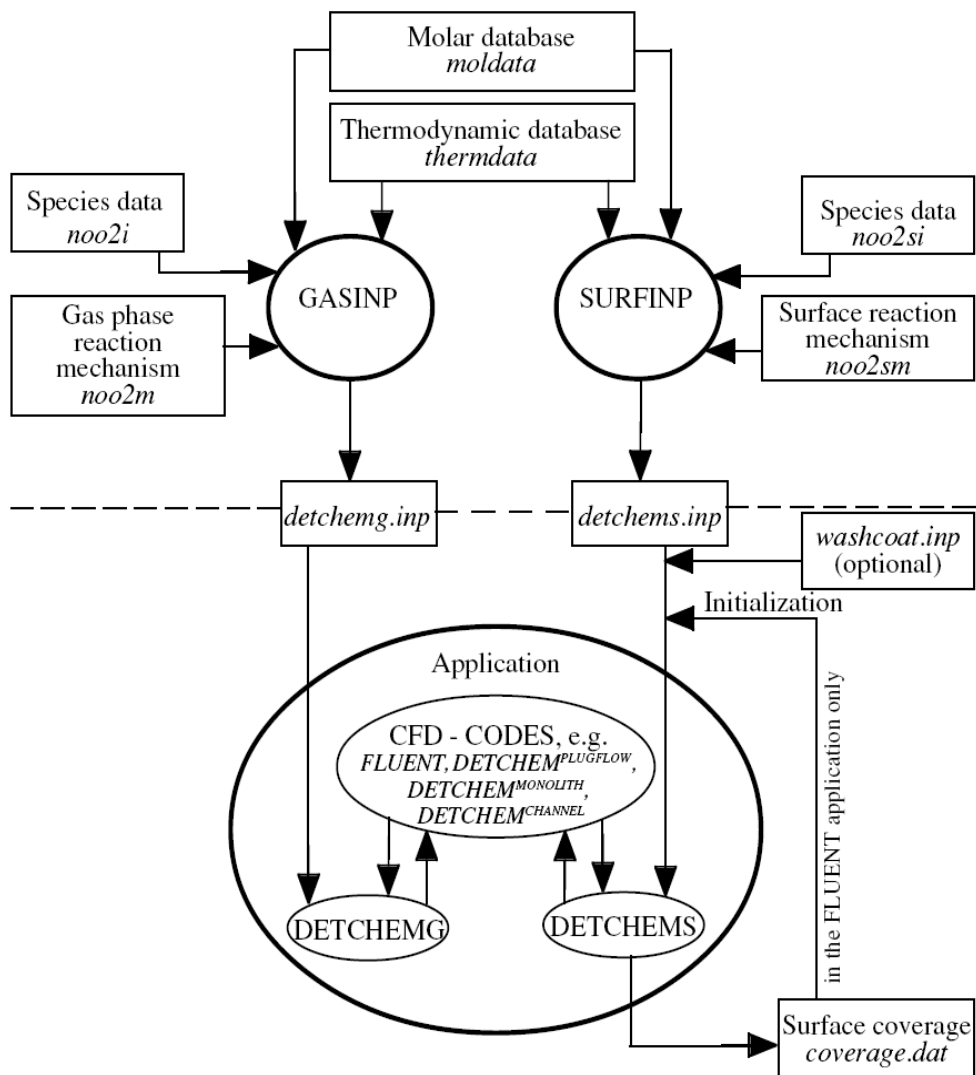


Figure 4.1: Structure of DETCHEM [83]

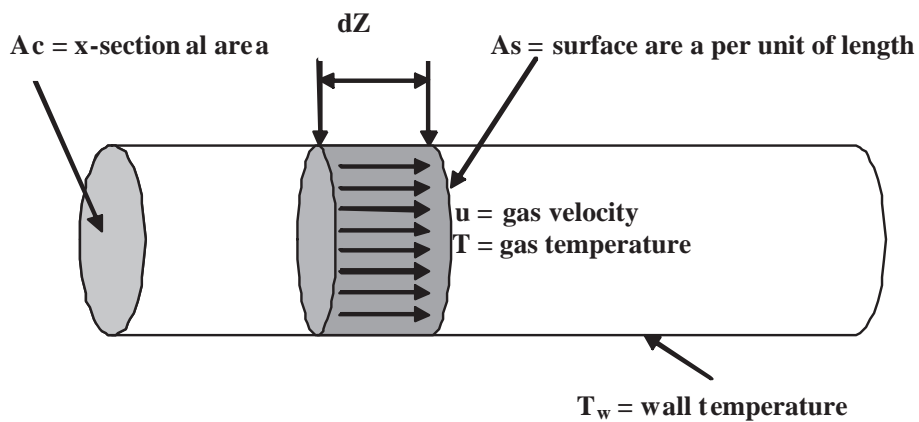


Figure 4.2: Schematic diagram of the plug flow



the equation for conservation of the  $k$ -th species ( $k = 1, \dots, k_g$ )

$$A_c \frac{d(\rho u Y_k)}{dz} = M_k (A_s \dot{s}_k + A_c \dot{\omega}_k) \quad (4.2)$$

the energy equation

$$\rho u A_c \frac{d(c_p T)}{dz} + \sum_{k=1}^{k_g} \dot{\omega}_k h_k M_k A_c + \sum_{k=1}^{k_g} \dot{s}_k h_k M_k A_s = U A_s (T_w - T) \quad (4.3)$$

and the ideal gas law is assumed as equation of state

$$p \bar{M} = \rho R T \quad (4.4)$$

In the absence of surface reactions, the term  $\dot{s}_k$  becomes zero and equations 4.1, 4.2 and 4.3 can be written as:

$$A_c \frac{d(\rho u)}{dz} = 0 \quad (4.5)$$

$$A_c \frac{d(\rho u Y_k)}{dz} = M_k A_c \dot{\omega}_k \quad (4.6)$$

$$\rho u A_c \frac{d(c_p T)}{dz} + \sum_{k=1}^{k_g} \dot{\omega}_k h_k M_k A_c = U A_s (T_w - T) \quad (4.7)$$

In these equations  $\rho$  is the density,  $u$  is the velocity,  $A_c$  is the area of cross section,  $A_s$  is the surface area per unit length,  $k_g$  is the number of gas phase species,  $\dot{s}_k$  is the molar rate of production of species  $k$  by surface reactions,  $\dot{\omega}_k$  is the molar rate of production of species  $k$  by gas-phase reactions,  $M_k$  is the molecular mass of the species  $k$ ,  $Y_k$  is the mass fraction of species  $k$ ,  $c_p$  is the specific heat capacity,  $h_k$  is the specific enthalpy of the species  $k$ ,  $U$  is the overall heat transfer coefficient,  $T$  is the gas temperature,  $T_w$  is the wall temperature,  $p$  is the pressure, and  $\bar{M}$  is the average molecular weight. All the terms containing  $\dot{s}_k$  vanish in the absence of surface

reactions. The DAE system is integrated using the solver LIMEX. The input consists of kinetic parameters for reactions in the Arrhenius format and thermodynamic data as polynomial fits in temperature.

## Two-dimensional model

DETCHEM<sup>CHANNEL</sup> is a computational tool that solves a parabolic system of differential-algebraic equations, which are obtained by simplifying the Navier-Stokes equations using the same assumptions as in the boundary-layer approximation. That is, since there is a preferred direction of transport due to convection along the axis of a channel, the diffusive transport in axial direction is neglected. However, in radial direction the diffusive transport is dominating and radial pressure gradients vanish.

The CHANNEL model solves the following steady-state equations in cylinder symmetric form:

Continuity equation

$$\frac{\partial \rho u}{\partial z} + \frac{1}{r} \frac{\partial (r \rho v)}{\partial r} = 0 \quad , \quad (4.8)$$

conservation of axial momentum

$$\rho u \frac{\partial u}{\partial z} + \rho v \frac{\partial u}{\partial r} = -\frac{\partial p}{\partial z} + \frac{1}{r} \frac{\partial}{\partial r} \left( \mu r \frac{\partial u}{\partial r} \right) \quad , \quad (4.9)$$

conservation of radial momentum (radial pressure gradients vanish)

$$0 = \frac{\partial p}{\partial r} \quad , \quad (4.10)$$

conservation of species  $k$  ( $k = 1, \dots, k_g$ )

$$\rho u \frac{\partial Y_k}{\partial z} + \rho v \frac{\partial Y_k}{\partial r} = -\frac{1}{r} \frac{\partial (r j_{k,r})}{\partial r} + \dot{\omega}_k M_k \quad , \quad (4.11)$$

and conservation of thermal energy

$$\rho c_p \left( u \frac{\partial T}{\partial z} + v \frac{\partial T}{\partial r} \right) = \frac{1}{r} \frac{\partial}{\partial r} \left( r \lambda \frac{\partial T}{\partial r} \right) - \sum_{k=1}^{k_g} c_{pk} j_{k,r} \frac{\partial T}{\partial r} - \sum_{k=1}^{k_g} h_k \dot{\omega}_k M_k \quad . \quad (4.12)$$

Here, in addition  $r$  is the radial coordinate,  $v$  is the radial velocity,  $\mu$  is the viscosity,  $\lambda$  is the thermal conductivity, and  $j_{k,r}$  is the radial component of the mass flux vector.

Again, ideal gas law (Eq. 4.4) is used as equation of state. The boundary conditions for a steady state at the catalytic wall require that the gas-phase species mass flux produced by heterogeneous chemical reactions must be balanced by the diffusive and convective flux of that species in the gas in radial direction:

$$\dot{s}_k M_k = -(j_{k,r} + \rho Y_k v_{stef}) \quad (k = 1, \dots, k_g) \quad (4.13)$$

with the Stefan velocity

$$v_{stef} = -\frac{1}{\rho} \sum_{k=1}^{k_g} \dot{s}_k M_k \quad . \quad (4.14)$$

The above model equations are semi-discretized in the radial direction  $r$  by the method of lines with non-uniform grid discretization leading to a structured system of differential-algebraic equations. The DAEs are solved by an implicit method, based on the backward differentiation formulas (BDF), with variable order, variable step size control methods and an efficient modified Newton method for the solution of the nonlinear equations arising from the BDF discretization [91]

### 4.3 HOMREA

As reported [92], HOMREA is a software package for computing time dependent homogeneous reaction systems under various operational assumptions. Included are systems at constant pressure, constant volume, constant temperature or adiabatic conditions. Furthermore, it is possible to simulate systems with user-specified time-dependent profiles for pressure, volume, or temperature. The program has the following features:

- Calculation of ignition delay time
- Calculation of time-varying concentration of species, temperature and pressure
- Computation of sensitivity coefficients
- Determination of chemical flows

The governing equations are derived from the Navier-Stokes equations with the following assumptions (1) The ideal gas is valid, and (2) the heat flux caused by radiation of gases is negligible [93].

### 4.3.1 Sensitivity Analysis

Sensitivity analysis of a reaction mechanism is performed to identify the rate limiting reaction steps in the mechanism. It indicates the change in solution of the system with respect to the change in system parameters. For a reaction mechanism with  $k_g$  species and  $R$  reactions, rate laws can be written in the following form:

$$\dot{\omega}_i = F_i(C_1, \dots, C_{k_g}; k_1, \dots, k_R) \quad (i = 1, \dots, k_g) \quad (4.15)$$

$$C_i(t = t_0) = C_i^0 \quad (4.16)$$

Here the time  $t$  is independent variable, the concentrations  $C_i$  of species  $i$  are dependent variables,  $k_r = k_1, \dots, k_R$  are the parameters of the system and  $C_i^0$  denote the initial conditions at time  $t_0$ .

The solution of the differential equation system i.e. the values of concentration at time  $t$ , depend on initial conditions and on the parameters  $k_r$  (rate coefficients) of reactions in the mechanism. The change in the parameter values will change the solution. Comparatively the change in some of these parameters or rate coefficients largely effect the solution of the system. So these reactions are rate-determining or rate-limiting steps and their rate coefficients need to be determined accurately.

The dependence of the solution  $C_i$  (concentrations of species) on the parameters  $k_r$  (rate coefficients) is called the sensitivity. Absolute and relative sensitivities are defined as:

$$E_{i,r} = \frac{\partial C_i}{\partial k_r} \quad (4.17)$$

$$E_{i,r}^{rel} = \frac{k_r}{C_i} \frac{\partial C_i}{\partial k_r} = \frac{\partial \ln C_i}{\partial \ln k_r} \quad (4.18)$$

where  $E_{i,r}$  and  $E_{i,r}^{rel}$  are absolute and relative sensitivity coefficients respectively.

### 4.3.2 Reaction Flow Analysis

Reaction flow analysis is performed to identify the important reactions in the mechanism based on their contribution to the formation or consumption of species in the mechanism. A reaction can be regarded as unimportant if its contribution to the formation or consumption of all species is below a certain limit e.g. 1%. Two types of reaction flow analysis can be performed with HOMREA.

- (1) Integral reaction flow analysis which considers the formation and consumption of species during the whole reaction time
- (2) Local reaction flow analysis which considers the formation and consumption of species at specific times [81].

## 4.4 FLUENT

FLUENT is a commercially available computational fluid dynamics (CFD) computer program for modeling fluid flow and heat transfer in complex geometries. It is reported [94] that FLUENT provides mesh flexibility, including the ability to solve problems using unstructured meshes that can be generated about complex geometries. Different mesh types that can be used with this program include 2D triangular/quadrilateral, 3D tetrahedral/hexahedral/pyramid/wedge, and mixed (hybrid) meshes. The program also allows to refine or coarsen the grid based on the flow solution. Since it is written in the C computer programming language, dynamic memory allocation, efficient data structures, and flexible solver control are all possible. In addition, it uses a client/server architecture, which allows it to run as separate simultaneous processes on client desktop workstations and powerful compute servers. This architecture allows for efficient execution, interactive control, and complete flexibility between different types of machines or operating systems. All functions required to compute a solution and display the results are accessible through an interactive, menu-driven user interface.

Following are the basic procedural steps to solve a problem using this program:

- Define the modeling goals.
- Create the model geometry and grid.
- Set up the solver and physical models.
- Compute and monitor the solution.
- Examine and save the results.

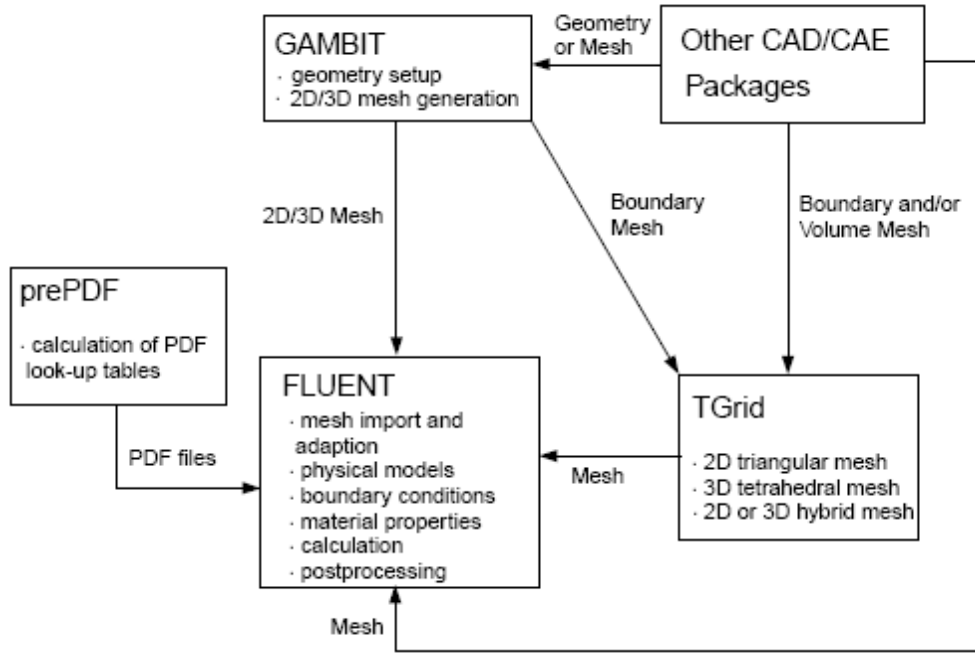


Figure 4.3: Structure of FLUENT [94]

- Consider revisions to the numerical or physical model parameters, if necessary.

#### 4.4.1 FLUENT structure

The program structure is shown in the Fig. 4.3. The package includes (i) FLUENT, the solver (ii) GAMBIT, the preprocessor for geometry modeling and mesh generation (iii) TGrid, an additional preprocessor that can generate volume meshes from existing boundary meshes. (iv) Filters (translators) for import of surface and volume meshes from CAD/CAE packages. In the present work GAMBIT will be used to generate the mesh for the FLUENT solver. FLUENT also uses a utility called cortex that manages the user interface and basic graphical functions. The FLUENT serial solver manages file input and output, data storage, and flow field calculations using a single solver process on a single computer. FLUENT's parallel solver allows to compute a solution using multiple processes that may be executing on the same computer, or on different computers in a network. Parallel processing in FLUENT involves an interaction between FLUENT, a host process, and a set of compute-node processes. FLUENT interacts with the host process and the collection of compute nodes using the cortex user interface utility. Table 4.1 provides a comparison of main features of computational tools DETCHEM, HOMREA and FLUENT.

## 4.4.2 Species transport and reaction model

FLUENT can model the mixing and transport of chemical species by solving conservation equations describing convection, diffusion, and reaction sources for each component species. Multiple simultaneous chemical reactions can be modeled, with reactions occurring in the bulk phase (volumetric reactions) and/or on wall or particle surfaces, and in the porous region. Species transport modeling both with and without reactions is possible. To solve conservation equations for chemical species, FLUENT predicts the local mass fraction of each species,  $Y_i$ , through the solution of a convection-diffusion equation (3.5) already discussed in Section 3.1 for the  $i$ th species. A source term is also added to account for any addition by the dispersed phase or user defined sources. Since the mass fractions of the species must sum to unity, the mass fraction of the last species is determined as one minus the sum of the all other solved mass fractions. To minimize numerical error, the last species should be selected as that species with the overall largest mass fraction.

## 4.4.3 Solution Convergence in Reacting Flows

Obtaining a converged solution in a reacting flow can be difficult for a number of reasons. First, the impact of the chemical reaction on the basic flow pattern may be strong, leading to a model in which there is strong coupling between the mass/momentum balances and the species transport equations. This is especially true in combustion, where the reactions lead to a large heat release and subsequent density changes and large accelerations in the flow. All reacting systems have some degree of coupling, however, when the flow properties depend on the species concentrations. These coupling issues are best addressed by the use of a two-step solution process. In this process, the flow, energy, and species equations are solved with reactions disabled (cold-flow or unreacting flow). When the basic flow pattern has thus been established, the reactions are reenabled and calculations are continued. The cold-flow solution provides a good starting solution.

A second convergence issue in reacting flows involves the magnitude of the reaction source term. When the FLUENT model involves very rapid reaction rates (reaction time scales are much faster than convection and diffusion time scales), the solution of the species transport equations becomes numerically difficult. Such systems are termed stiff systems and can be solved using either the segregated solver with the Stiff Chemistry Solver option enabled, or the Coupled Solver in FLUENT.

Table 4.1: Comparison of Reactive Flow Modeling Tools

<b>DETCHEM</b>	<b>HOMREA</b>	<b>FLUENT</b>
Detailed reaction mechanism can be used in 1D or 2D to simulate the reactive flows	Detailed Reaction mechanism can be used in 0D to simulate the reactive flows	Reaction mechanism upto 50 species can be used in 2D or 3D to simulate the reactive flows
Ideal flows e.g. parabolic flow in a channel, Plug flow or CSTR can be simulated	Computes time dependent reaction system	Ideal or non-ideal flows can be simulated
Requires no other software for grid construction. Reactor dimensions and grid size is defined in the form of a text input file.	Requires no other software for grid construction. Residence time in the reactor should be provided as input.	Requires GAMBIT or other softwares for grid construction. The grid should be imported to simulate the reactor.
Provides no graphical user interface(GUI). All the input should be provided as formatted text files.	Provides no graphical user interface(GUI). All the input should be provided as formatted text files.	Provides graphical user interface(GUI). No formatted text files required for input.
Sensitivity or reaction flow analysis can not be performed for the current version 2.0 but will be possible with the coming versions in near future	Sensitivity analysis as well as reaction flow analysis can be performed	Sensitivity analysis or reaction flow analysis can not be performed
Homogeneous and surface reactions can be used in the reaction mechanism	Only homogeneous reactions can be used in the reaction mechanism	Homogeneous and surface reactions can be used in the reaction mechanism
No built in post processing tool. The post processing can be performed by a third party spreadsheet software or Tecplot	Can plot the results as output. The post processing can be performed by a third party spreadsheet software.	Has built in post processor which can plot the results. Also the contours and animation of results possible with the built in post processor. The results can be exported and processed with a third party spreadsheet or many other CFD post processing tools.
Can be obtained for academic or research purposes (non-commercial) at a nominal cost	Can be obtained for academic or research purposes(non-commercial)	Commercial software. Licence fee payable even for academic or research purposes



# Chapter 5

## Experimental Data

This chapter summarizes the available experimental data and briefly explains the experimental setups, reactor dimensions and operating conditions for the pyrolysis of propane and acetylene. The vacuum carburizing of steel with propane or acetylene is performed normally under these operating conditions on industrial scale.

### 5.1 Tubular Flow Reactor

The laboratory scale apparatus used for the experiments consists of the gas feed system, the reactor and the product gas analysis as shown in Fig.5.1. The gas feed system consists of 5 mass flow controllers(Brooks Model 5850) for the hydrocarbon gas (propane or acetylene),  $N_2$ ,  $H_2$ ,  $O_2$  and iso-butane ( $i-C_4H_{10}$ ). Nitrogen is used as an inert carrier gas,  $O_2$  for burning the deposited carbon from pyrolysis and iso-butane as internal standard for gas chromatography as it is only formed in negligible amounts during the propane or acetylene pyrolysis under the investigated reaction conditions. There is also a facility to bypass the reactor and analyze the inlet gas composition for calibration purposes. The reactor shown in Fig.5.2 consists of a ceramic pipe with an inner diameter of 20 mm, outer diameter of 25 mm and a length of 600 mm. A ceramic filter is placed at the outlet of the reactor to separate any possibly formed solid carbon from the gas stream. The gaseous products of pyrolysis are measured by a gas chromatograph (Hewlett-Packard GC Type 5890 with a 30 m column). Detected products include  $C_3H_8$ ,  $CH_4$ ,  $C_2H_2$ ,  $C_2H_4$ ,  $C_2H_6$  and  $C_3H_6$ . The higher hydrocarbons are measured by a second gas chromatograph (Hewlett-Packard GC Type 5890 with a 50 m column) which can separate hydrocarbons containing up to 30 carbon atoms. Hydrogen, not measured in the pyrolysis product stream,

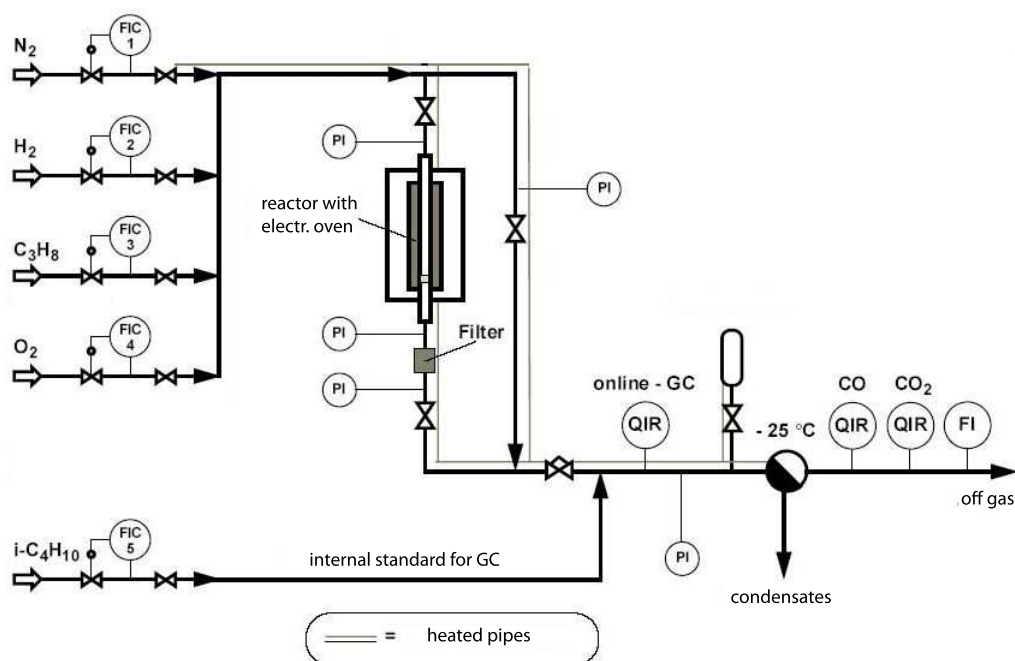


Figure 5.1: Simple flow sheet of the lab scale apparatus used for the experimental investigations [48]

is calculated by a hydrogen mass balance not taking into account any traces of  $H_2$  eventually bound in the deposited carbon. The carbon deposited is burned with a mixture of 5 vol. %  $O_2$  in  $N_2$ . Both  $CO$  and  $CO_2$  formed by burning the deposited carbon are analysed by an infra red analyser and are used for the carbon balancing. The temperature profile is measured at the center of the reactor as shown in Fig.5.2.

### 5.1.1 Operating conditions

#### Propane pyrolysis

Operating parameters for the pyrolysis of propane are summarized in table 5.1. The flow rate of propane is 150 lit/hr(NTP) and the concentration is 0.5 mol% (8 mbar partial pressure) in all experiments. The total pressure is 1.6 bar. The temperature is varied from 640 to 1010 °C. These temperatures are not isothermal reactor temperatures but there is a temperature profile for each of these equivalent temperature values shown in the table 5.1.

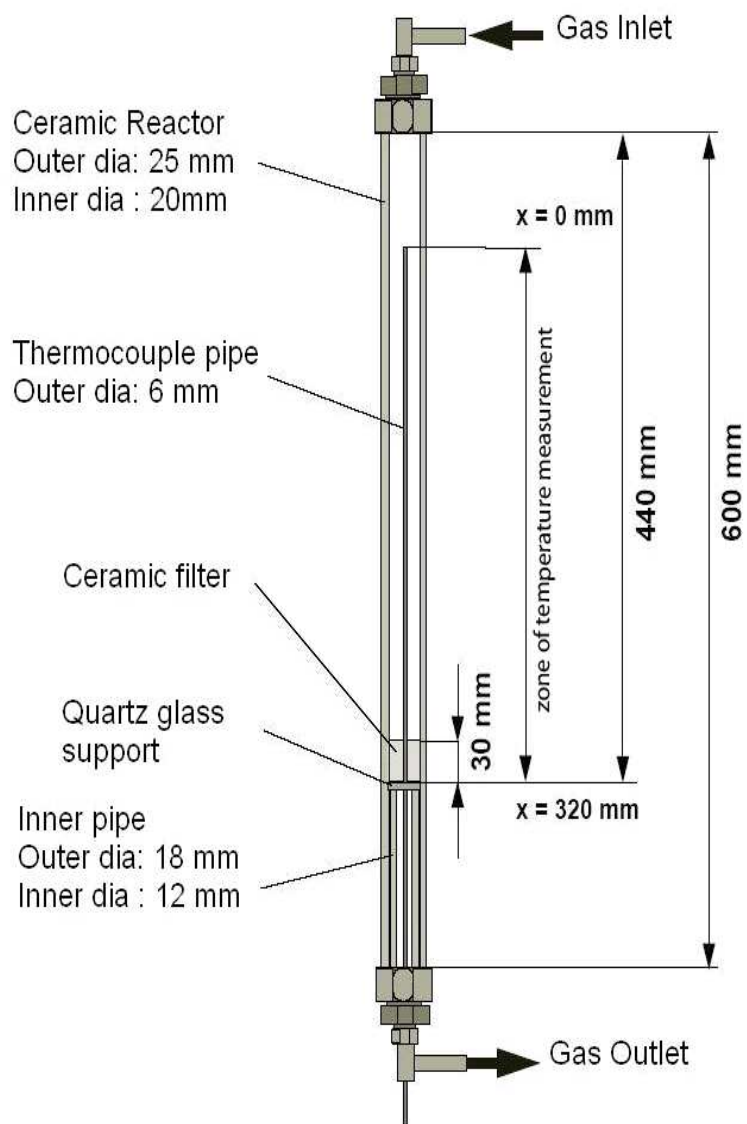


Figure 5.2: Sketch of the reactor used for the experimental investigations [48]

Table 5.1: Operating conditions for propane pyrolysis measurements in Tubular Flow Reactor

Flow Rate l/h	Total Pressure bar	Concentration propane mol%	Equivalent Temperature °C
150	1.6	0.5	640
			690
			730
			780
			830
			870
			920
			960
			1010

Table 5.2: Operating conditions for acetylene pyrolysis measurements in Tubular Flow Reactor

Flow Rate l/h	Total Pressure bar	Concentration acetylene mol%	Controller Temperature $T_R$ in °C
150	1.6	0.625	500
			550
			600
			650
			700
			750
		and  1.25	800
			850
			900
			950
			1000
			1050

### Acetylene pyrolysis

Operating parameters for the pyrolysis of acetylene are summarized in table 5.2. The flow rate of acetylene is 150 l/h (NTP) and the concentration is 0.625 mol% and 1.25 mol%(10 and 20 mbar partial pressure) respectively in all experiments. The total pressure is 1.6 bar. The temperature is varied from 650 to 1050 °C. These temperatures are temperature controller values rather than reactor isothermal temperature values. There is an axial temperature profile for each of these temperature values shown in the table 5.2.

## 5.2 Thermogravimetric Reactor

The flow sheet of the thermogravimetric apparatus is shown in Fig. 5.4. The apparatus consists of the thermobalance (type NETZSCH STA-409 CD) connected with the gas feed system and with the gas analysis system. In the gas feed system, the flow rates can be regulated and mixed by maximally six different gases by means of mass flow controllers (MFC) (type Bronkhorst EL-FLOW). Over three-way Valves they can be directed either to a calibration system or in a common line into the reactor of the thermo balance. The weighing mechanism is not separated from the reaction space of the thermobalance, therefore the balancing system must be protected from damage caused by the entrance of particles, corrosive or reactive gases. The weighing mechanism is also thoroughly flushed with an inert gas (argon). The flow rate of the cleaning gas is measured by a mass flow controller in a pulse box. With this pulse box two sample gas streams with a specified volume can be fed into

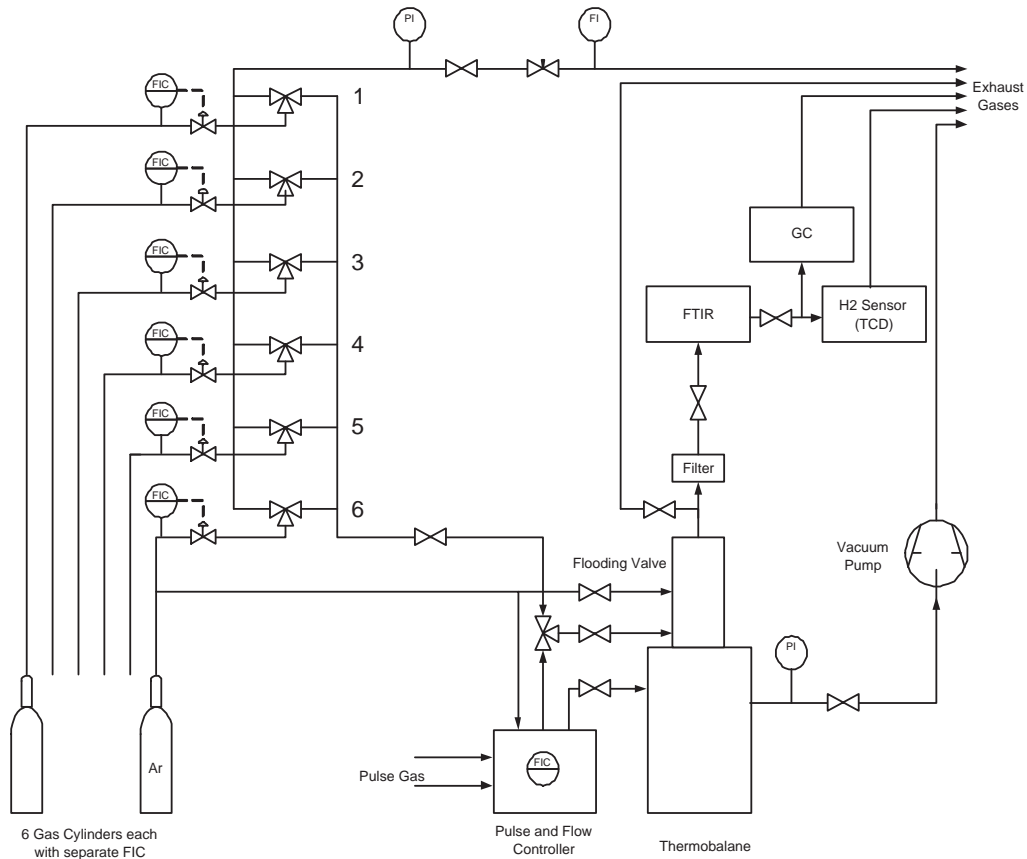


Figure 5.3: Simple Process Flow diagram of the Thermogravimetric apparatus

the thermo balance (TGA). Over a valve the reactor can be flooded also directly with inert gas. The maximum flow rate (NTP) should not exceed 9 l/h, since otherwise the sample carrier begins to swing and the weighing accuracy is strongly affected from the incident flow. Under the low flow rates, the Bodenstein No. values are approximately smaller than 20. From the reactor exit, the product or exhaust gases flow through a bypass to the outlet or through a 200 °C heated line to a Fourier transform infrared spectrometer (type Bruker Tensor 27). In order to protect the following analytic devices against tar-like hydrocarbons and soot particles, a heated fine filter made of sinter metal with a pore diameter of 15  $\mu\text{m}$  is used upstream. After going through the IR gas measuring cell, the hydrogen content of the exhaust gas is measured in a heat conductivity detector (type ABB Caldos 17). In addition, part of the exhaust gas passes through a Micro Gas Chromatograph (type Varian CP 4900). After leaving the analyzers, the exhaust gases are led to the outlet. An oil-free vacuum pump (BOC Edward XDS5-S) is attached to the thermo balance, with which the equipment including the gas measuring cell of the FTIR can be evacuated. The maximum positive pressure in the apparatus should not exceed 0.1 bar.

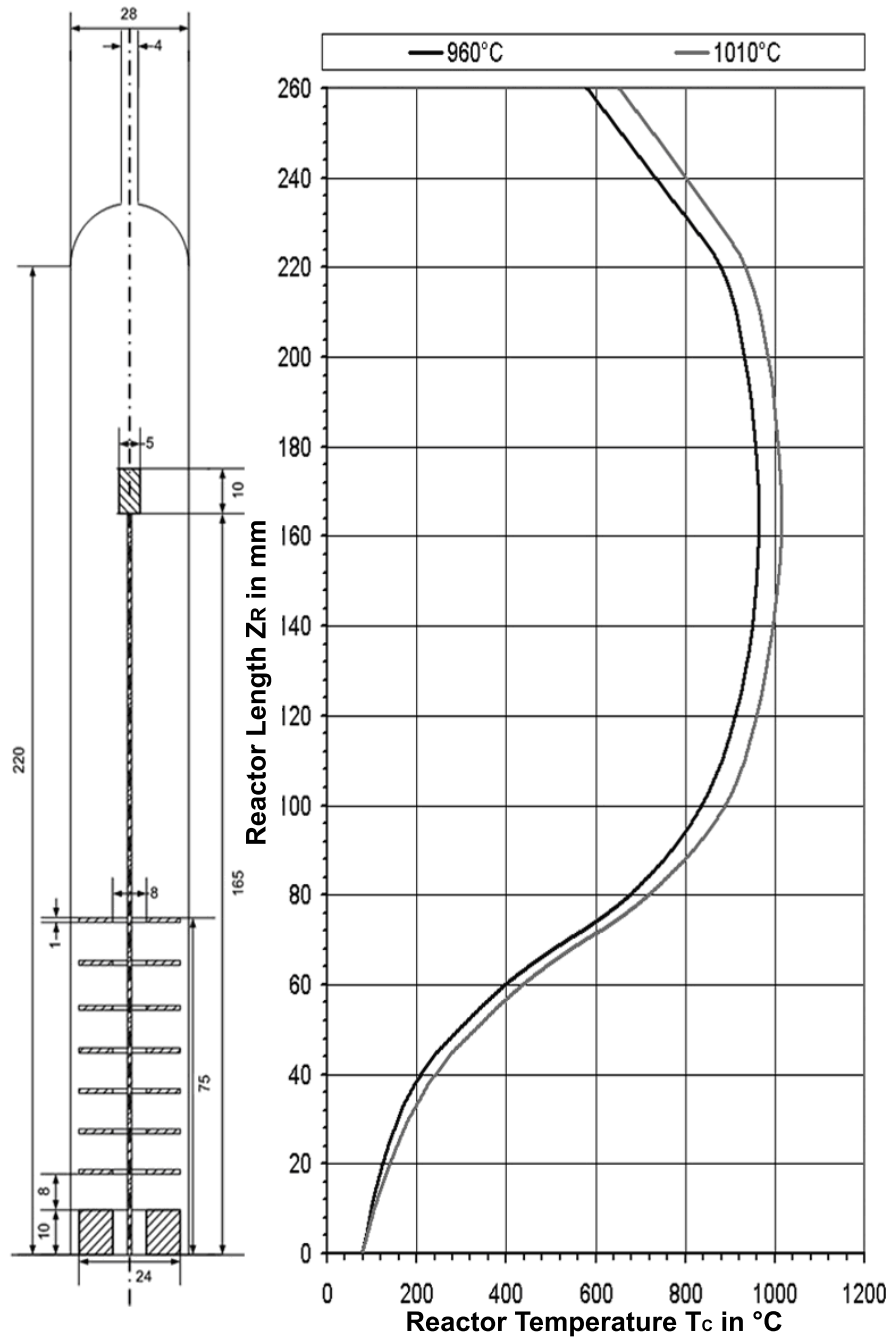


Figure 5.4: Sketch of the Thermobalance (NETZSCH STA-409 CD) with typical temperature profiles [2]

Table 5.3: Operating conditions for propane pyrolysis measurements in Thermogravimetric Reactor

Controller Temp. $T_R$ in °C	Vol. Flow Rate (l/h)	Inlet Propane( $C_3H_8$ ) Conc. vol%	Total Pressure atm
900	6	1.08	1
1000			

Fig. 5.4 shows the sketch of the thermo balance used for experimental investigations. The thermo balance has a measuring range from 0 to 18 gram and a measuring accuracy of  $\pm 5 \mu\text{g}$ . A sample carrier rod holds a ceramic crucible containing the test sample. Two axial temperature profiles for temperature controller values of 950 and 1000 °C are shown in Fig. 5.4. The reactor, the sample carrier and the protection shields in the heating zone are all made of  $\text{Al}_2\text{O}_3$  and are appropriate for temperatures up to 1600 °C. At the upper end of the sample carrier a thermocouple (type S) measures the temperature in the sample. The reactor is heated from the outside with an electrical resistance heating. The furnace temperature is regulated by the temperature measurement at the sample carrier. The reaction gas passes through an annular ring from downside of the reactor and after passing through the protection shields flows toward the sample. The highest temperature is reached at the end of the sample carrier. By the interior pipe at the reactor entrance, the cleaning gas flows through the balancing system into the reactor. In order to exclude the possibility that carburizing is disturbed by nitriding of the steel sample with nitrogen ( $\text{N}_2$ ), argon (Ar) is used as a carrier gas. Cylinders with different dimensions made from 16MnCr5 steel are used as samples for studying the carburizing process.

## 5.2.1 Operating conditions

### Propane pyrolysis

Operating conditions for the pyrolysis of propane are summarized in table 5.3. Pyrolysis of propane at two different temperature values 900 and 1000 °C has been performed. These temperatures are temperature controller values rather than the reactor isothermal temperatures. There is an axial temperature profile for these temperature values. Total flow rate is 6 l/h (NTP), the inlet propane ( $\text{C}_3\text{H}_8$ ) concentration is 1.08 vol% whereas rest of the mixture consist of argon(Ar). The total presuure is 1 atm.

Table 5.4: Operating conditions for pyrolysis measurements in Thermogravimetric Reactor

Controller Temp. $T_R$ in °C	Vol. Flow Rate (l/h)	Inlet acetylene ( $C_2H_2$ ) Conc. vol%	Total Pressure atm
900	6	1.62	1
950	3	0.25	
		0.5	
		1	
		1.62	
	6	0.25	
		0.5	
		1	
		1.62	
	9	0.25	
		0.5	
		1	
		1.62	
1000	3	0.25	
		0.5	
		1	
		1.62	
	6	0.25	
		0.5	
		1	
		1.62	
	9	0.25	
		0.5	
		1	
		1.62	

### Acetylene pyrolysis

Operating parameters for the pyrolysis of acetylene are summarized in table 5.4 for the Thermogravimetric Reactor. Pyrolysis of acetylene at three different temperature values 900, 950 and 1000 °C has been performed. These temperatures are temperature controller values rather than the reactor isothermal temperatures as in the case of propane pyrolysis discussed above. The flow rate of acetylene is 3, 6 and 9 l/h (NTP) and the concentrations are 0.25, 0.5, 1, 1.62 vol% . Argon (Ar) is used as a dilution gas. The total pressure is 1 atm.



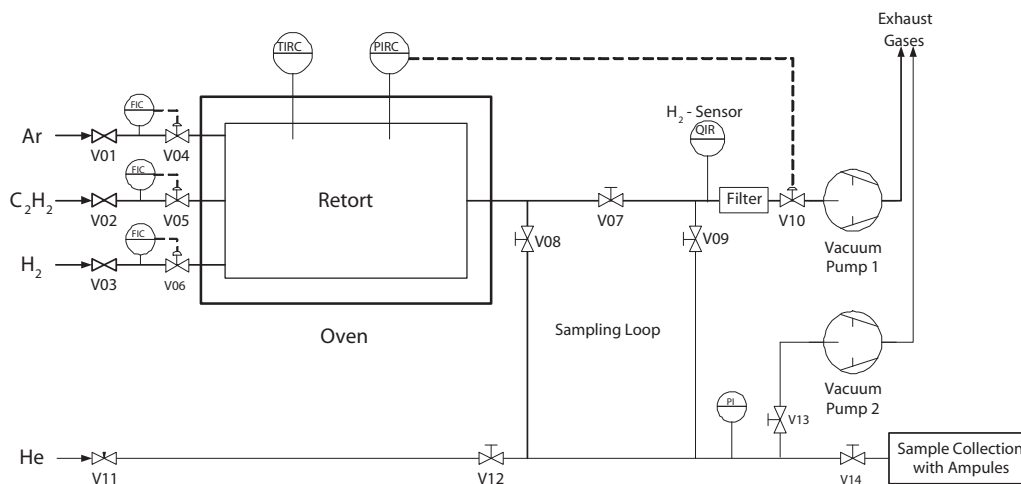


Figure 5.5: Flow diagram of Vacuum Reactor [2]

### 5.3 Vacuum Reactor

The flow diagram of the system is shown in the Fig.5.5. The apparatus consists of an oven (Xerion XRetort 1150/80) with electric heating for temperatures up to 1150 °C. There are also temperature, pressure and flow controllers (Eurotherm 2408) simultaneously for three gas streams. After passing through the reactor, the gas flows into an analysis unit, with which different analyses of the exhaust gases can be performed at reduced pressure and at ambient pressure.

The required pressures are achieved with an oil-free Scroll pump (BOC Edward GVSP30). The unlubricated operating pump is required since with a conventional lubricated rotary vane pump oil diffuses towards the furnace and is found in the gas analysis. Gas analysis is continuously performed in the vacuum range with a H<sub>2</sub>-Sensor (WLD detector), a carbon -FID to measure the carbon content of the exhaust gas and a gas sample system for glass ampoules, developed at the Institute. With this sample system gas samples can be collected at the intervals of 2-minutes. The representative gas samples collected in the glass ampoules are analyzed with an external gas chromatograph for hydrocarbons by means of GC-FID. Apart from this quasi-continuous measurement of the pyrolysis product gases, the carbon content of the carburized steel samples is measured gravimetrically after completion of the experiment.

The reactor is made of a high temperature nickel alloy (Nicrofer HT 6025) and is heated in a horizontal furnace over a length of 400 mm by an electric resistance heating. Before the start of experiments, the reactor is sufficiently carburized to avoid any loss of carbon resulting from the carburization of the reactor itself. As shown in the Fig. 5.5, there are three inlets for the feed gases (V01 - V03) and a

Table 5.5: Operating conditions for acetylene pyrolysis in Vacuum Reactor

Feed gas	Controller Temp. $T_R$ in °C	Flow rate (l/h)	Total Pressure (mbar)
Propane	1000	10	10
Acetylene	980	6.3	10
		9	
		12	
	1050	6.3	
		9	
		12	

discharge opening for the exhaust or product gases (V08). There is also a connection for the pressure and for the temperature measurement (V06, V07). In order to protect the seal of the flange connection against thermal damage, the front part of the reactor is cooled by a cooling jacket with a glycol/water mixture (V04, V05). The reactor has an inside diameter of 135 mm and a length of 680 mm with a wall thickness of 3 mm. Radiation protection shields are located in the front as well as in the end part of the reactor. The piping consists of 3/4 inch high-grade steel and is heated to approximately 200 °C, in order to prevent the condensing of higher hydrocarbons. For taking gas samples via glass ampoules a defined gas volume can be locked with pneumatic driven ball valves.

### 5.3.1 Operating Conditions

Operating parameters for the pyrolysis of propane and acetylene in the Vacuum Reactor are summarized in table 5.5. Pyrolysis of propane has been performed at 1000 °C and pyrolysis of acetylene has been performed at two different temperature values of 980 and 1050 °C . These temperatures are temperature controller values rather than reactor isothermal temperatures. There is an axial temperature profile measured at the centre of reactor for these temperature values. The flow rate of propane is 10 lit/hr while that of acetylene has different values of 6.3, 9 and 12 lit/hr (NTP) and the total pressure is 10 mbar i.e the reactor is operated under vacuum without any dilution with inert gas.

# Chapter 6

## Modeling of Propane Pyrolysis

### 6.1 Tubular Flow Reactor

The geometry and the experimental conditions are already discussed in chapter 5. The conditions given in table 5.1 were used to simulate the reactor behaviour. The diameter of the reactor is small and the Bodenstein No. is approximately 43 [48] so the diffusion in the axial direction may be negligible.

#### 6.1.1 Computational Fluid Dynamics (CFD) model

Computational Fluid Dynamics (CFD) modeling tool FLUENT discussed in chapter 5 was used to model the pyrolysis of propane. Gambit software was used to generate a three dimensional (3-D) grid according to the reactor dimensions. The grid was imported into FLUENT and scaled to actual dimensions of the reactor. For the reactive flow modeling of pyrolysis of propane, a kinetic mechanism is required. Although the pyrolysis of propane follow a complex scheme of reactions, there are limitations on the use of detailed mechanisms in CFD codes. So a simple mechanism consisting of 9 species and 10 reactions was selected from the previous work of Bajohr [48]. The mechanism consists of 9 species which include carbon  $C_{(s)}$ ,  $H_2$  and hydrocarbons consisting of  $CH_4$ ,  $C_2H_2$ ,  $C_2H_4$ ,  $C_2H_6$ ,  $C_3H_6$ ,  $C_3H_8$ ,  $C_6H_6$ . The overall mechanism consists of 10 reactions shown in table 6.1. These are the major products of propane pyrolysis at the investigated operating conditions. The species  $C_{(s)}$  represents the carbon content of soot or hydrocarbons higher than benzene ( $C_6H_6$ ). Since the reactor is not operated isothermally, the measured temperature profile in the form of the polynomial fit (6.1) as shown below was used in the simulations for

Table 6.1: Operational kinetic mechanism of propane pyrolysis [48]

rate constant $k_f = Ae^{-E_a/RT}$			
Nr	Reaction	$A(\text{mol}, \text{m}^3, \text{s})$	$E_a(\text{kJ/mol})$
1	$\text{C}_3\text{H}_8 \rightarrow \text{CH}_4 + \text{C}_2\text{H}_4$	$5.1 \cdot 10^6$	144.0
2	$\text{C}_3\text{H}_8 \rightarrow \text{C}_3\text{H}_6 + \text{H}_2$	$6.2 \cdot 10^{10}$	228.0
3	$\text{C}_3\text{H}_8 + \text{C}_2\text{H}_4 \rightarrow \text{C}_2\text{H}_6 + \text{C}_3\text{H}_6$	$8.5 \cdot 10^7$	143.0
4	$2 \text{C}_3\text{H}_6 \rightarrow 3 \text{C}_2\text{H}_4$	$1.2 \cdot 10^{11}$	181.0
5	$\text{C}_3\text{H}_6 \rightarrow \text{C}_2\text{H}_2 + \text{CH}_4$	$2.2 \cdot 10^{10}$	212.0
6	$\text{C}_2\text{H}_6 \rightarrow \text{C}_2\text{H}_4 + \text{H}_2$	$6.0 \cdot 10^6$	140.0
7	$\text{C}_2\text{H}_4 \rightarrow \text{C}_2\text{H}_2 + \text{H}_2$	$9.0 \cdot 10^8$	216.0
8	$3 \text{C}_2\text{H}_2 \rightarrow \text{C}_6\text{H}_6$	$8.0 \cdot 10^{-8}$	-223
9	$2 \text{CH}_4 \rightarrow \text{C}_2\text{H}_6 + \text{H}_2$	$5.5 \cdot 10^{13}$	329.0
10	$\text{C}_6\text{H}_6 \rightarrow 6 \text{C}_{(s)} + 3 \text{H}_2$	237	46.4

the description of the temperature field.

$$T(T_e, z) = (a \cdot z^2 + b \cdot z + c) \cdot T_e + d \cdot z^2 + e \cdot z + f \quad (6.1)$$

$T(T_e, z)$  represents the temperature as a function of the position  $z$  along the reactor length, whereas  $T_e$  represents an equivalent temperature and  $a, b, c, d, e, f$  are the polynomial coefficients with values of  $-0.00223 \text{ /cm}^2$ ,  $0.066 \text{ /cm}$ ,  $0.65$ ,  $0.37 \text{ }^\circ\text{C/cm}^2$ ,  $-3.20 \text{ }^\circ\text{C/cm}$ ,  $-110 \text{ }^\circ\text{C}$  respectively. So the measured temperatures can be computed from the above single equation by substituting the values of given polynomial coefficients and equivalent temperature  $T_e$  at any position  $z$  in centimeters. The conversion of propane is related by the following relationship [48]:

$$f_{\text{C}_3\text{H}_8}(T_e) = \frac{1}{L_R} \int_{z=0}^{L_R} f_{\text{C}_3\text{H}_8}(T(T_e, z)) dz \quad (6.2)$$

The temperature profile was implemented by using the polynomial (6.1) through the user defined functions (UDFs) in FLUENT. These functions are written in a C programming language and need to be compiled before they can be used. The species transport and reaction model was used to implement the mechanism with parameters shown in table (6.1). The other options activated for the FLUENT solver include segregated, steady state, implicit and laminar. The solution was converged to species residuals of  $10^{-6}$  and the data was processed by the FLUENT built in postprocessor. Also the mole fractions were exported to spreadsheet software Microsoft Excel for further processing and plotting the results.

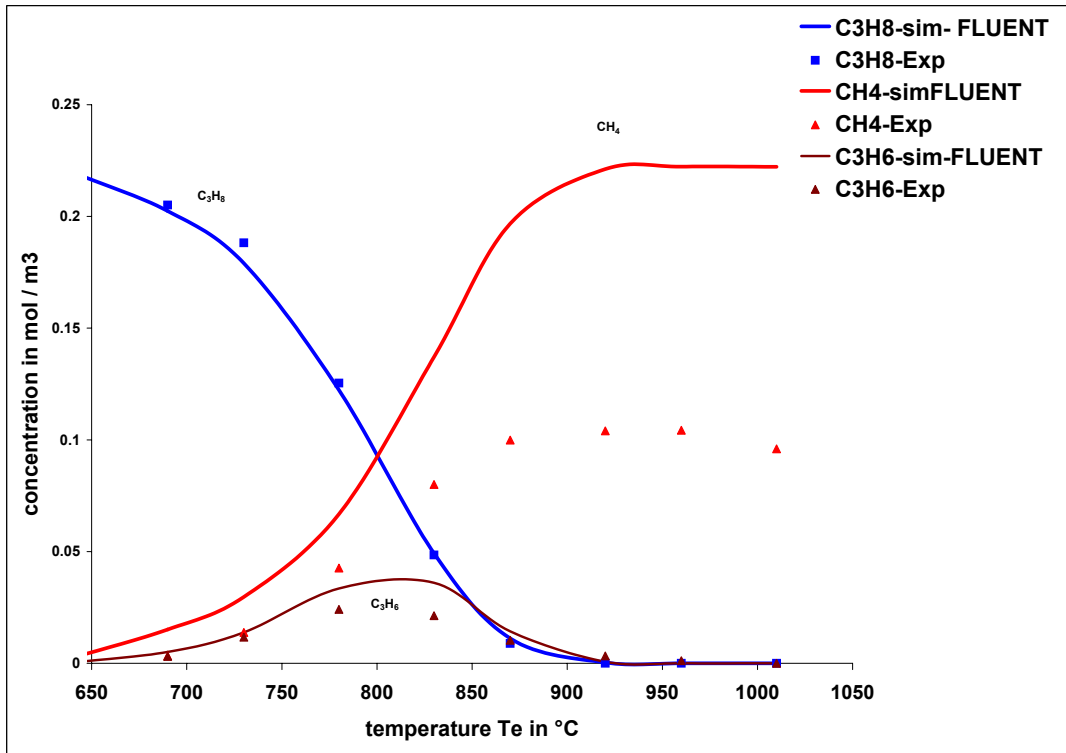


Figure 6.1: Comparison of CFD simulations and experimental results for pyrolysis of propane in a lab scale tubular flow reactor.

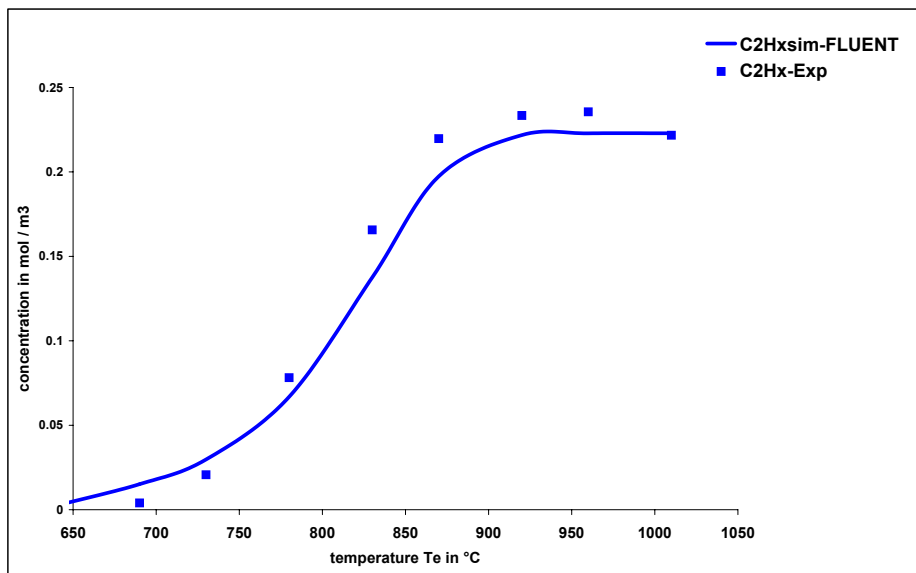


Figure 6.2: Comparison of CFD simulations and experimental results for pyrolysis of propane in a lab scale tubular flow reactor.

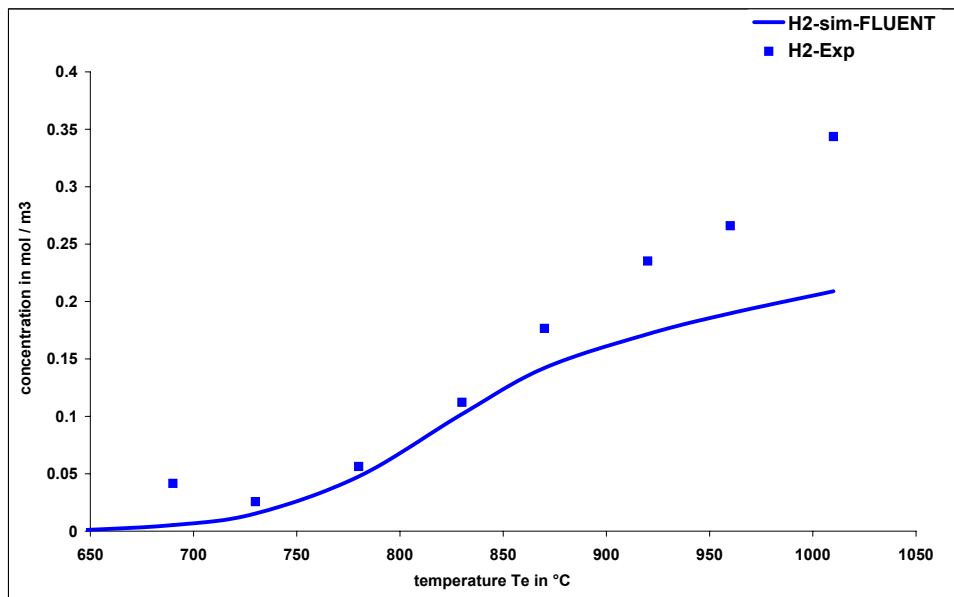


Figure 6.3: Comparison of CFD simulations and experimental results for pyrolysis of propane in a lab scale tubular flow reactor

### 6.1.2 Comparison of simulation and experimental results

The results of CFD simulations are compared with the experimental results in Fig. 6.1 to 6.3. The species  $C_2H_x$  represents the sum of  $C_2H_2$ ,  $C_2H_4$  and  $C_2H_6$ . The comparison of simulation and experimental results reveals that the model can predict well the concentrations of propane, propylene and  $C_2H_x$ . However the model overpredicts the concentration of  $CH_4$  and underpredicts  $H_2$  above 850 °C. The model was unable to predict benzene and soot because these were formed in negligible amounts as compared to experimental data so the comparison is not shown.

### 6.1.3 Detailed chemistry model

Simulations were carried out by using PLUG and CHANNEL modules of DETCHEM 2.0 discussed in chapter 4. A detailed kinetic mechanism[75] was used which consists of 227 species and 827 reactions. The mechanism was developed for the pyrolysis of light hydrocarbons. The measured temperature profile in the form of the polynomial (6.1) as shown above was used in the simulations for the description of the temperature field.

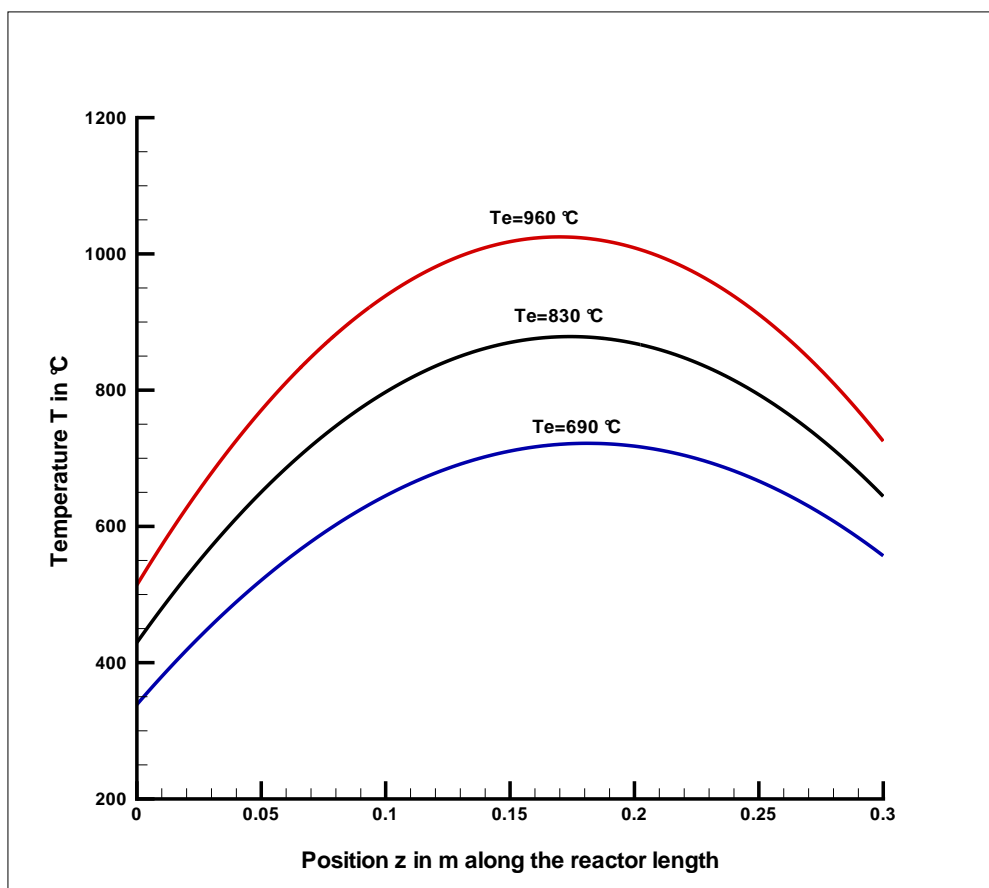


Figure 6.4: Temperature profiles in the lab scale tubular flow reactor for different typical values of equivalent temperature  $T_e$

Typical plots of the temperature profiles for different equivalent temperature values are shown in Fig. 6.4.

In 2-D simulations, the temperature profile was not implemented by the polynomial (6.1) because it requires wall temperature  $T_w$  as well as gas temperature  $T$ . So the measured inlet gas temperature  $T$  was specified only at the inlet of the reactor while  $T_w$  takes the values according to the measured temperature profile. The temperature profile was divided into small pieces and a piecewise linear temperature profile was implemented by providing two pairs of values of position  $z$  and  $T_w$ .

Table 6.2 summarizes the products distribution obtained from the propane pyrolysis at various temperatures.

#### 6.1.4 Kinetic mechanism analysis

The detailed reaction mechanism consists of 227 species and 827 elementary reactions most of which are reversible. The mechanism was developed for modeling pyrolysis of light hydrocarbons at temperatures of approximately 900 °C. The mechanism

Table 6.2: Product distribution in %C based on feed carbon (C1) at various temperatures (experimental)

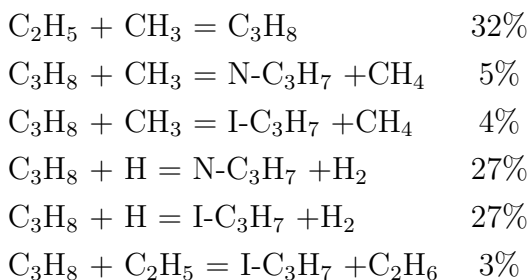
$T_e$ in $^{\circ}C$	$T_e$ in K	$C_3H_8$	$CH_4$	$C_2H_2$	$C_2H_4$	$C_2H_6$	$C_3H_6$	$C_5+$	Soot & Pyr. C
640	913	99.46	0.00	0.00	0.00	0.00	0.27	0.27	0
690	963	94.35	1.70	0.00	0.00	0.00	3.14	0.81	0
730	1003	84.35	2.06	0.00	5.41	0.78	5.24	2.15	0
780	1053	56.20	6.36	0.3	19.75	3.32	10.80	3.14	0.13
830	1103	21.74	11.95	3.11	40.70	5.71	9.55	6.63	0.62
870	1143	3.99	14.93	10.16	50.92	4.57	4.62	8.61	2.22
920	1193	0.00	15.54	19.72	47.96	2.06	1.48	9.41	3.83
960	1233	0.00	15.58	26.29	40.16	0.51	0.54	12.19	4.73
1010	1283	0.00	14.34	38.19	28.06	0.00	0.00	12.28	7.13

and the thermodynamic data for all the species has already been published [75]. The mechanism does not describe the deposition of solid carbon from the gas phase.

The reaction flow analysis and sensitivity analysis was performed by HOMREA software package at 870  $^{\circ}C$  for 0.8 sec residence time. The reactions and their contribution to the consumption or formation of the species of interest are discussed below.

### Consumption and formation of propane

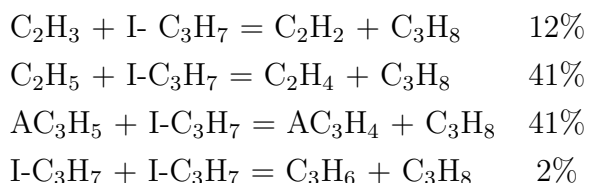
The consumption of propane occurs by six different reactions as shown below:



Species symbols and the reaction's parameters can be found in the appendix C. The relative importance of these reactions varies with temperature. At the flow reactor and shock tube temperatures these reactions are important with the unimolecular decomposition dominating [34, 95]. The sensitivity analysis with respect to propane is shown in Fig.6.5 which reveals the importance of decomposition step of propane resulting in the formation of  $C_2H_5$  and  $CH_3$  radicals. The first stage in the pyrolysis of propane can be designated as the primary reactions wherein the propane is decomposed through free radical chain mechanism into the principal primary products such as  $CH_4$ ,  $C_2H_4$ ,  $C_3H_6$ ,  $H_2$  and other minor primary products.



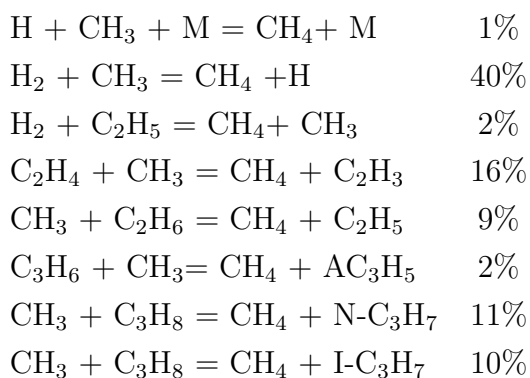
The reactions responsible for the formation of propane under the assumed conditions along with their contributions are given below:



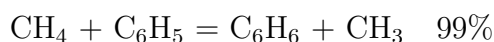
Most of the propane is formed from the I- C<sub>3</sub>H<sub>7</sub> radical when it reacts with other radicals such as C<sub>2</sub>H<sub>5</sub> and AC<sub>3</sub>H<sub>5</sub>.

### Formation and consumption of methane

Methane is formed mainly by the CH<sub>3</sub> radical which reacts with hydrogen, ethylene, ethane and propane.

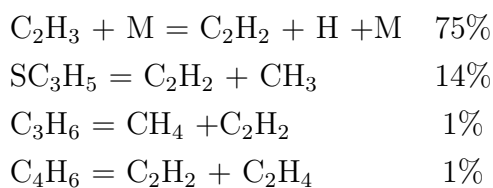


The consumption of methane takes place by its reaction with C<sub>6</sub>H<sub>5</sub> radical producing benzene and CH<sub>3</sub> radical. Although this reaction consumes most of the methane, relative contribution to the overall formation of benzene is not significant under the assumed operating conditions.

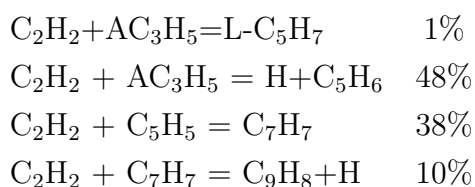


### Formation and consumption of acetylene

Acetylene is formed mainly by the decomposition of C<sub>2</sub>H<sub>3</sub> and SC<sub>3</sub>H<sub>5</sub> radicals according to the reactions shown below.

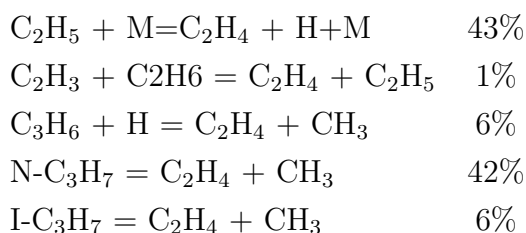


Acetylene plays an important role in the formation and growth of higher hydrocarbons.

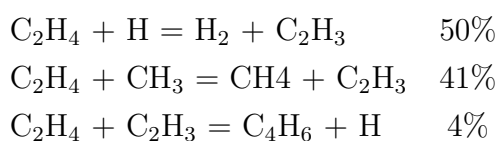


### Formation and consumption of ethylene

Formation of ethylene results mainly by the decomposition of  $\text{C}_2\text{H}_5$  and  $\text{N-C}_3\text{H}_7$  radical. The decomposition of  $\text{C}_2\text{H}_5$  is also a source for H radicals which react with propane to produce  $\text{N-C}_3\text{H}_7$  and  $\text{I-C}_3\text{H}_7$  radicals.

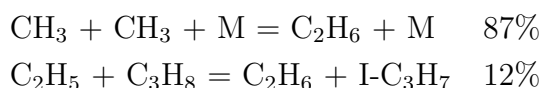


Ethylene is consumed mainly by its reactions with H and  $\text{CH}_3$  radicals by the following reactions.

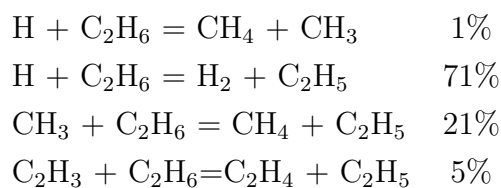


### Formation and consumption of ethane

Ethane is formed mainly (87%) by the recombination of  $\text{CH}_3$  radicals. The reaction of  $\text{C}_2\text{H}_5$  radical with propane also produces propylene as shown below.

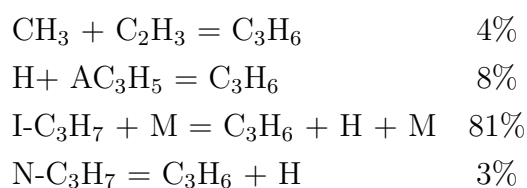


Ethane is mainly consumed by its reactions with H and  $\text{CH}_3$  radicals.

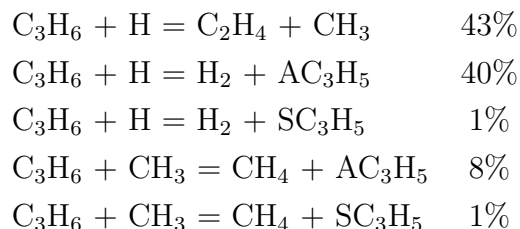


### Formation and consumption of propylene

The formation of propylene takes place mainly by the dissociation of the i-C<sub>3</sub>H<sub>7</sub> radical while the dissociation of n-C<sub>3</sub>H<sub>7</sub> produces comparatively small amounts of propylene. The other reactions which form the propylene include the recombination of radical AC<sub>3</sub>H<sub>5</sub> with H radical and CH<sub>3</sub> radical with C<sub>2</sub>H<sub>3</sub> radical.

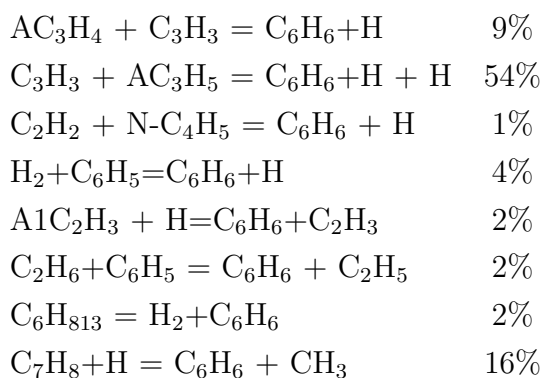


The consumption of propylene takes place by the attack of H and CH<sub>3</sub> radicals on propylene resulting in the formation of smaller molecules CH<sub>4</sub> and C<sub>2</sub>H<sub>4</sub> as well as other radicals as shown below.

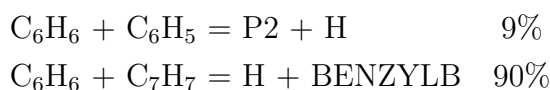


### Formation and consumption of benzene

The propargyl radical, C<sub>3</sub>H<sub>3</sub>, plays an important role in the formation of benzene. Benzene is formed mainly by the recombination of C<sub>3</sub>H<sub>3</sub> with AC<sub>3</sub>H<sub>4</sub> and AC<sub>3</sub>H<sub>5</sub>. The radical H attacks on toluene is also responsible for the formation of significant amount of benzene as shown in the following reactions.

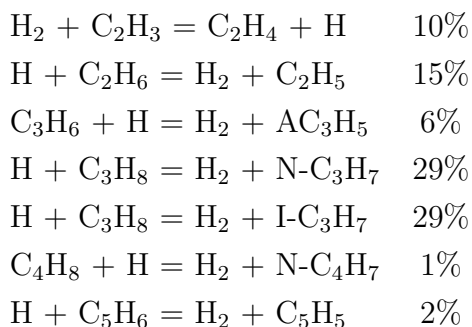


Consumption of benzene leads to the formation of higher molecular weight hydrocarbons. Most of the benzene is consumed by its reaction with benzyl radical to form benzylbenzene. Biphenyl is also produced by the reaction of benzene with phenyl radical.

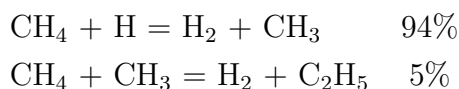


### Formation and consumption of Hydrogen

The dissociation of propane molecules results in the formation of  $C_2H_5$  and  $CH_3$  radicals as discussed above. Dissociation of  $C_2H_5$  results in the formation of H radicals which react with  $C_3H_8$ ,  $C_3H_6$ ,  $C_2H_6$  and  $C_2H_4$  to produce most of the hydrogen by the following reactions.



The consumption of hydrogen is mainly caused by its reactions with  $CH_3$  and  $C_2H_5$  radicals to produce the methane.



The second stage encompasses secondary reactions involving further pyrolysis of olefins produced by primary reactions, hydrogenation and dehydrogenation reactions of the olefins and condensation reactions wherein two or more smaller fragments com-

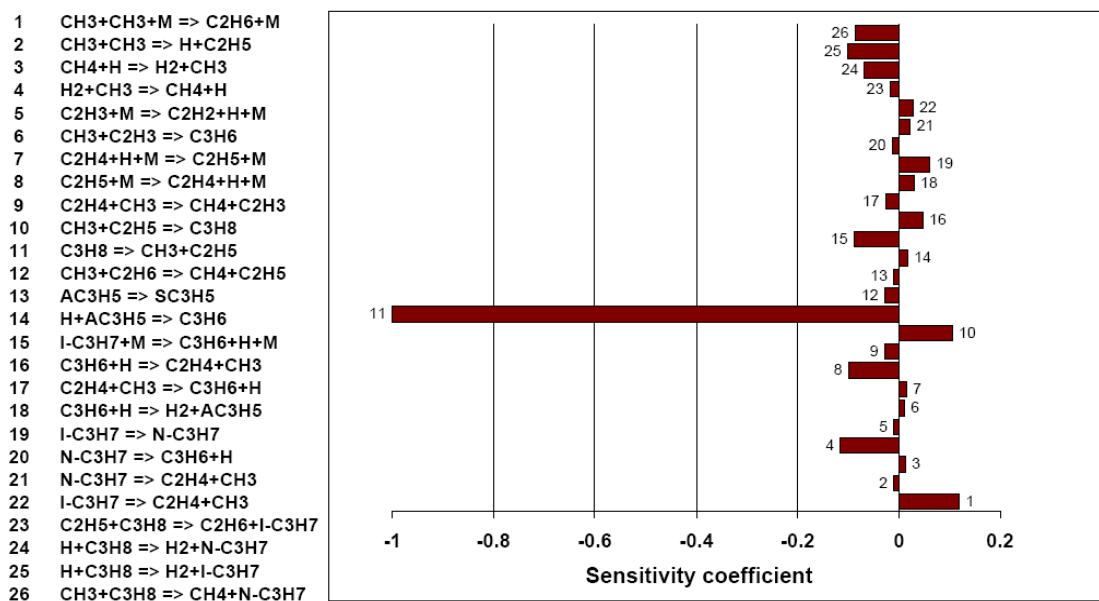


Figure 6.5: Sensitivity analysis with respect to propane at 870 °C performed by HOMREA software

bine to produce large stable structures such as cyclodiolefins and aromatics [37, 38].

### 6.1.5 Comparison of simulation and experimental results

The comparisons of the 1-D, 2-D simulation and experimental results are shown in Fig. 6.6 to 6.10 at various temperatures [96]. In general the agreement between simulation and experimental results is good for 2-D and satisfactory for 1-D simulations (Figures 6.6 – 6.9). The conversions of propane predicted by the 1-D model are slightly higher than the experimental measurements. The deviations can be explained by the differences in the treatment of radial transport limitations of the 1-D and 2-D models. While the 2-D model does not need additional assumptions about the radial transport, the 1-D simulation requires empirical models for heat and mass transfer coefficients. Therefore, the conversion of propane is slightly higher than in experiments. Moreover, the comparison indicates that the reaction mechanism used is suitable to simulate the pyrolysis of propane properly under the given conditions.

A typical parabolic mole fraction profile of propane in 2-D is shown in Fig. 6.11. The hydrocarbons measured as  $\text{C}_5+$  are compared to the simulation results of  $\text{C}_6\text{H}_6$  as shown in Fig. 6.10. The difference between simulation and experimental results in this case is most probably due to the amount of hydrocarbons other than the  $\text{C}_6\text{H}_6$  present in the gas phase leading to soot or solid carbon.

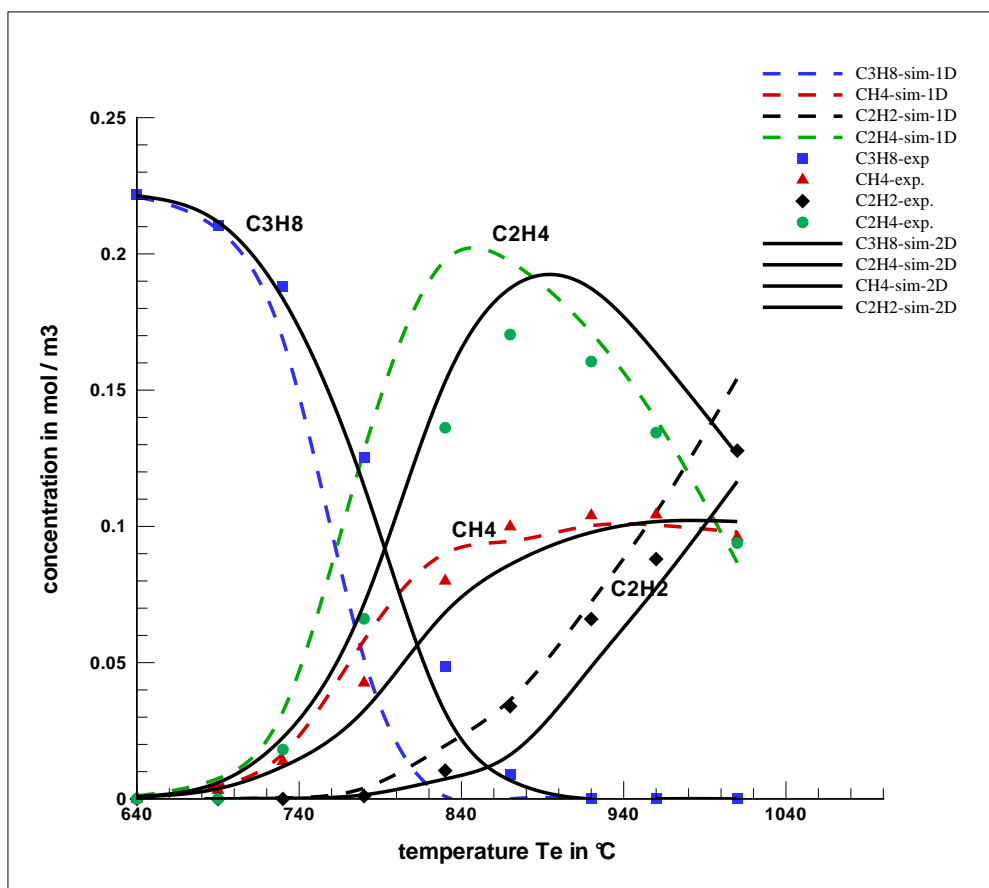


Figure 6.6: Comparison of 1-D, 2-D simulation and experimental results for the lab scale tubular flow reactor – exit concentrations of smaller hydrocarbons

The 2-D simulations are more time consuming than 1-D simulations and the accuracy of the latter is sufficient for our further discussions, therefore the axial profiles of the 1-D simulations only are compared for several temperatures.

Figure 6.12 shows the 1-D model results for propane at selected temperatures. The decomposition of propane gradually increases with increase of temperature and complete conversion can be achieved only at a fraction of the reactor length at higher temperatures.

Figure 6.13 shows 1-D model results for  $\text{CH}_4$ . The formation of methane is barely affected at temperatures above  $850^\circ\text{C}$  and only a small decrease is observed at temperatures above  $950^\circ\text{C}$  as shown in Fig. 6.6.

Figure 6.14 shows the model predictions for  $\text{C}_2\text{H}_2$ . The selectivity for  $\text{C}_2\text{H}_2$  gradually increases with temperature as shown in Fig. B.1. Yields of species are also shown in Fig. B.2.

Figure 6.15 shows the mole fraction profiles of  $\text{C}_2\text{H}_4$  along the reactor length at various selected temperatures. The maximum amount of  $\text{C}_2\text{H}_4$  formed shifts toward

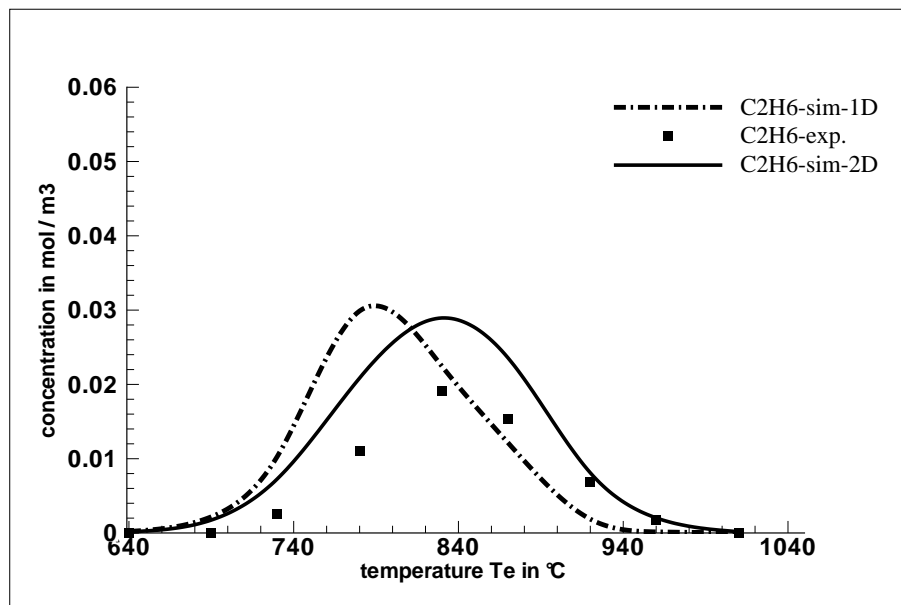


Figure 6.7: Comparison of 1-D, 2-D simulation and experimental results for the lab scale tubular flow reactor – exit concentrations of  $C_2H_6$

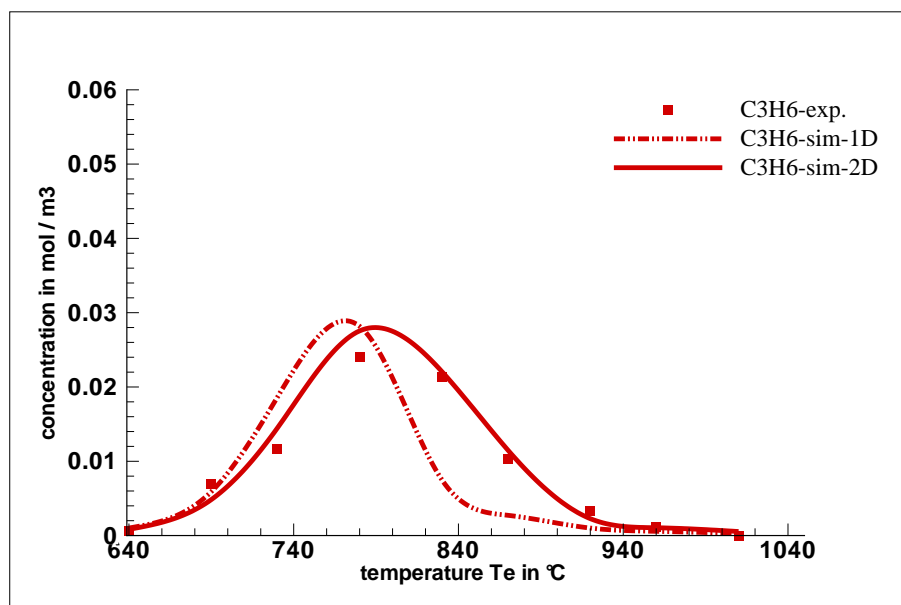


Figure 6.8: Comparison of 1-D, 2-D simulation and experimental results for the lab scale tubular flow reactor – exit concentrations of  $C_3H_6$

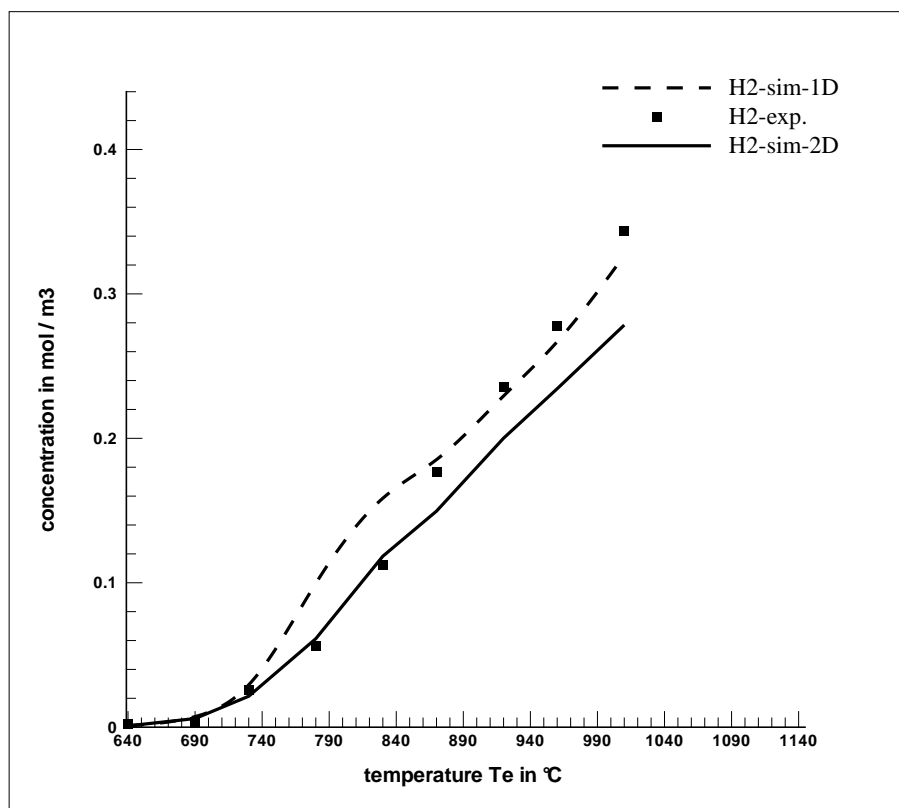


Figure 6.9: Comparison of 1D, 2-D simulation and experimental results for the lab scale tubular flow reactor – exit concentrations of hydrogen

the reactor inlet at higher values of equivalent temperature  $T_e$ . So the selectivity for  $C_2H_4$  increases up to a temperature of about  $900\text{ }^\circ C$  and then decreases.

The formation of further products of pyrolysis  $C_2H_6$  and  $C_3H_6$  is shown in Figures 6.16 and 6.17 respectively. The maximum amount increases up to a temperature of approximately  $800\text{ }^\circ C$  at the reactor outlet and then gradually decreases to very low amounts at higher temperatures.

Figure 6.18 shows the mole fractions of  $H_2$  formed at various temperatures. The amount of  $H_2$  formed increases with the increase of temperature.

Thus, the validated model can now be used to study the homogeneous pyrolysis of propane under the technical operating conditions of vacuum carburizing of steel. Further investigations on the heterogeneous reactions leading to the carburizing of steel are required. The model developed in the present work needs to be extended by including such reactions so that it can be used to control the vacuum carburizing process.



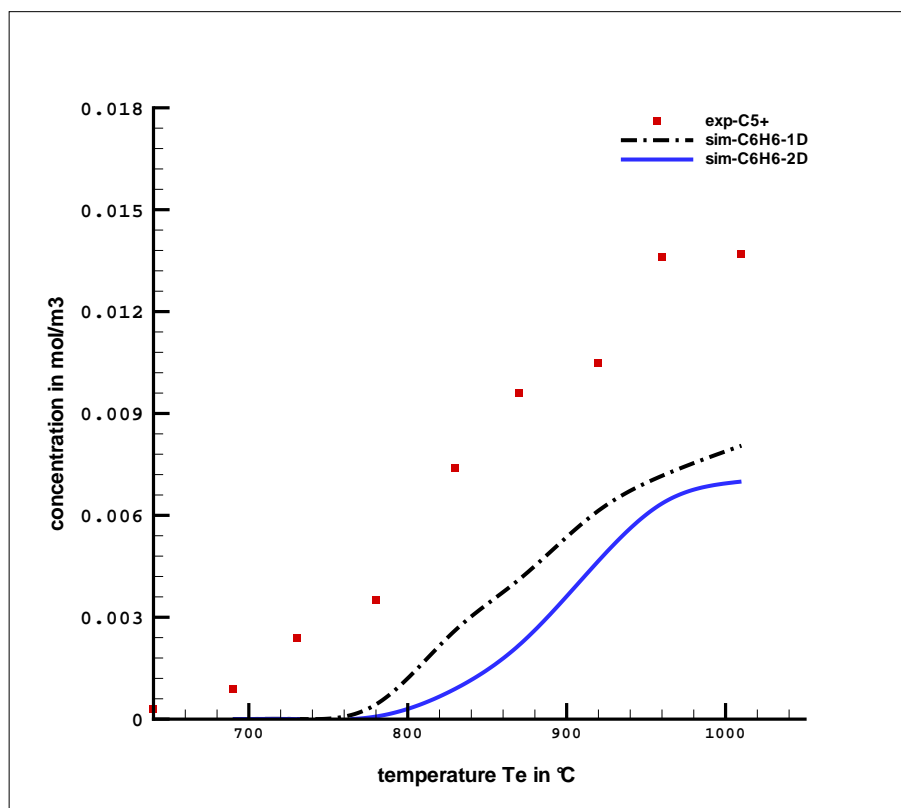


Figure 6.10: Comparison of 1D, 2-D simulation and experimental results for the lab scale tubular flow reactor – exit concentrations of higher hydrocarbons ( $C_{5+}$ )

## 6.2 Thermogravimetric Reactor

To simulate the Thermogravimetric Reactor, PLUG module of DETCHEM 2.0 coupled with the detailed mechanism (discussed in the previous section) was used. The use of computational fluid dynamics (CFD) to model the reacting flows with such detailed mechanism is difficult due to the computational cost and hence the limit of maximum number of species by the modeling software (FLUENT). The convergence of solution for reacting flows with large number of species also becomes a challenge due to the stiffness of the governing equations as discussed in chapter 4. The experimentally measured species include  $H_2$ ,  $CH_4$ ,  $C_2H_2$ ,  $C_2H_4$ ,  $C_4H_4$ ,  $C_4H_2$  and  $C_6H_6$ . The soot has not been measured experimentally but the amount of carbon in the form of soot has been calculated by mass balance with the assumption that rest of the hydrocarbons except the measured species are soot. The reactor was also simulated with the same mechanism using the HOMREA software. The results obtained by using the HOMREA software are also comparable to the DETCHEM results [75]. The measured temperature profile was implemented for simulations with DETCHEM PLUG model. In the case of simulation with HOMREA, the tem-

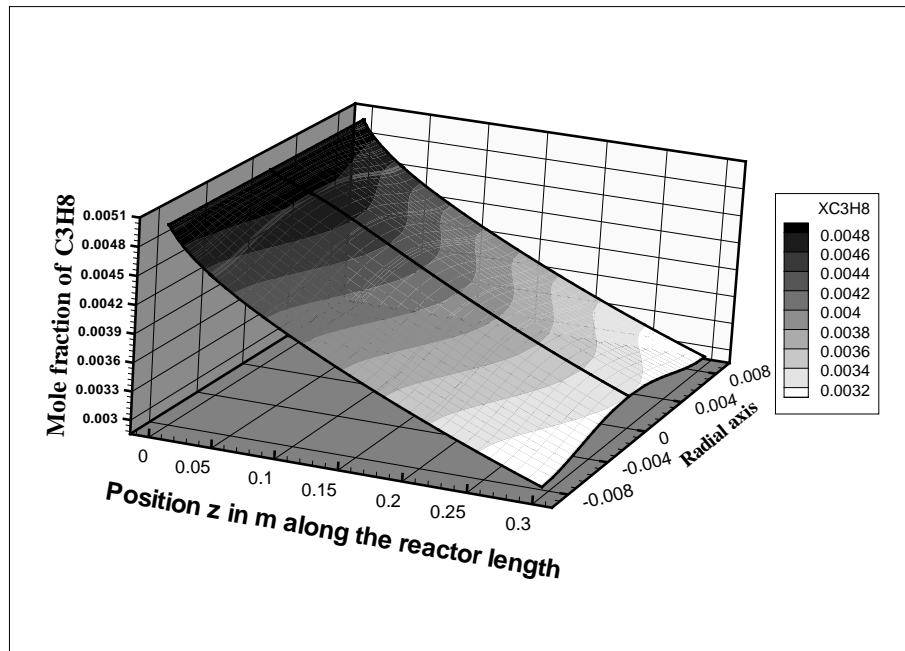


Figure 6.11: Propane mole fractions in 2-D model

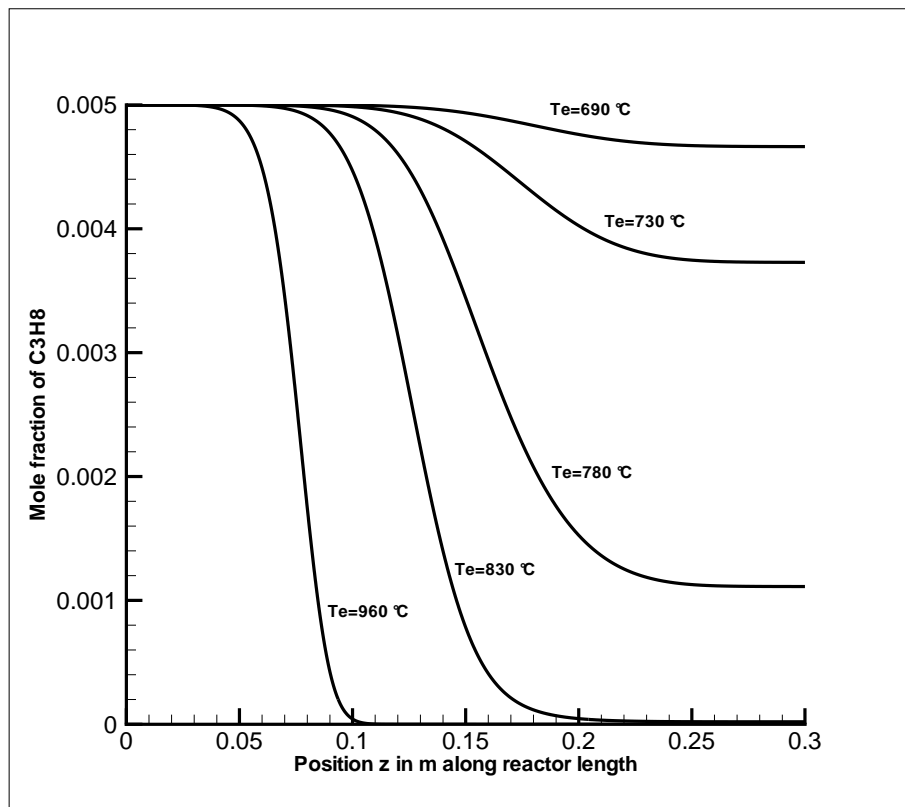


Figure 6.12: C<sub>3</sub>H<sub>8</sub> mole fraction profiles for 1-D model at different values of equivalent temperature  $T_e$  (non-isothermal)

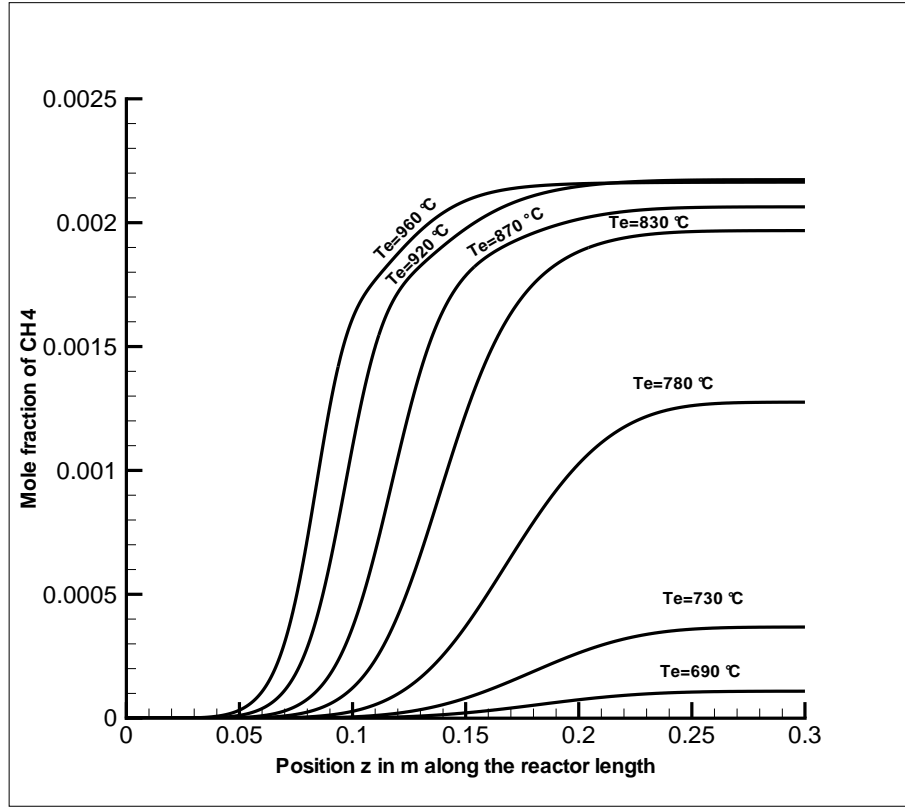


Figure 6.13:  $\text{CH}_4$  mole fraction profiles for 1-D model at different values of equivalent temperature  $T_e$  (non-isothermal)

perature was assumed isothermal which can be justified by the small variation of temperature in the heated section of the reactor. The comparison of the simulation results of both models and experimental results is presented in Fig. 6.19 and Fig. 6.20. For these comparisons, yield of carbon  $\Psi_{i,C}$  was calculated as under:

$$\Psi_{i,C} = \frac{\phi_{i,out} \times N_{C,i}}{\phi_{f,in} \times N_{C,f}} \quad (6.3)$$

In the above equation  $\phi_{i,out}$  is the molar flow rate of species  $i$  at the reactor outlet,  $\phi_{f,in}$  is the molar flow rate of the carburizing gas at the reactor inlet,  $N_{C,i}$  is the number of carbon atoms in species  $i$  molecular formula and  $N_{C,f}$  is the number of carbon atoms in the carburizing gas molecular formula i.e. it is 3 for propane and 2 for acetylene.

The same kinetic parameters were used as in the case of tubular flow reactor. The results show the suitability of the reaction mechanism for predicting the products of pyrolysis of propane even with the ideal flow models used in these simulations.

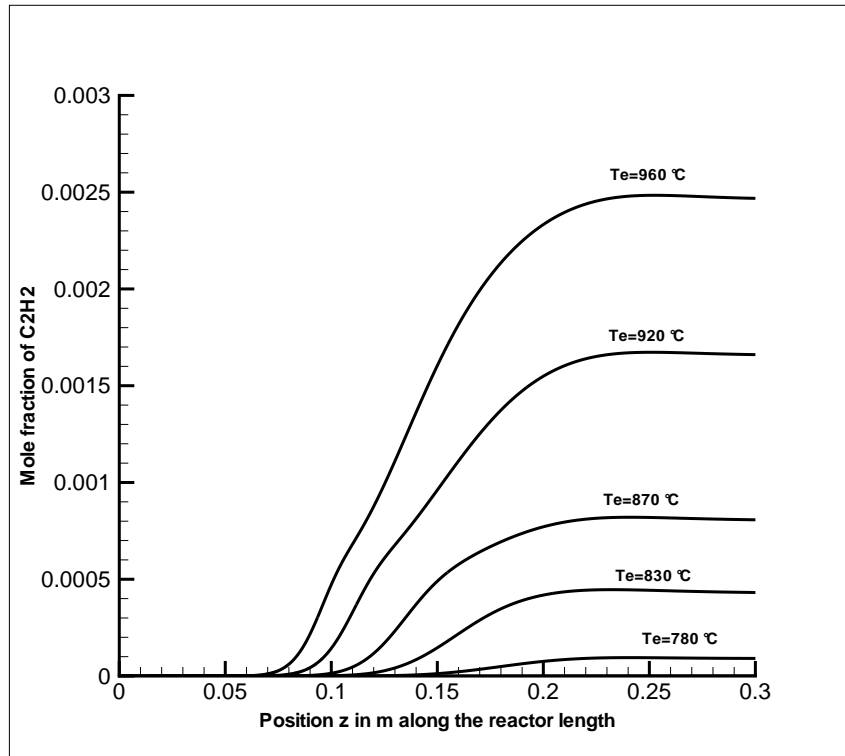


Figure 6.14: C<sub>2</sub>H<sub>2</sub> mole fraction profiles for 1-D model at different values of equivalent temperature  $T_e$  (non-isothermal)

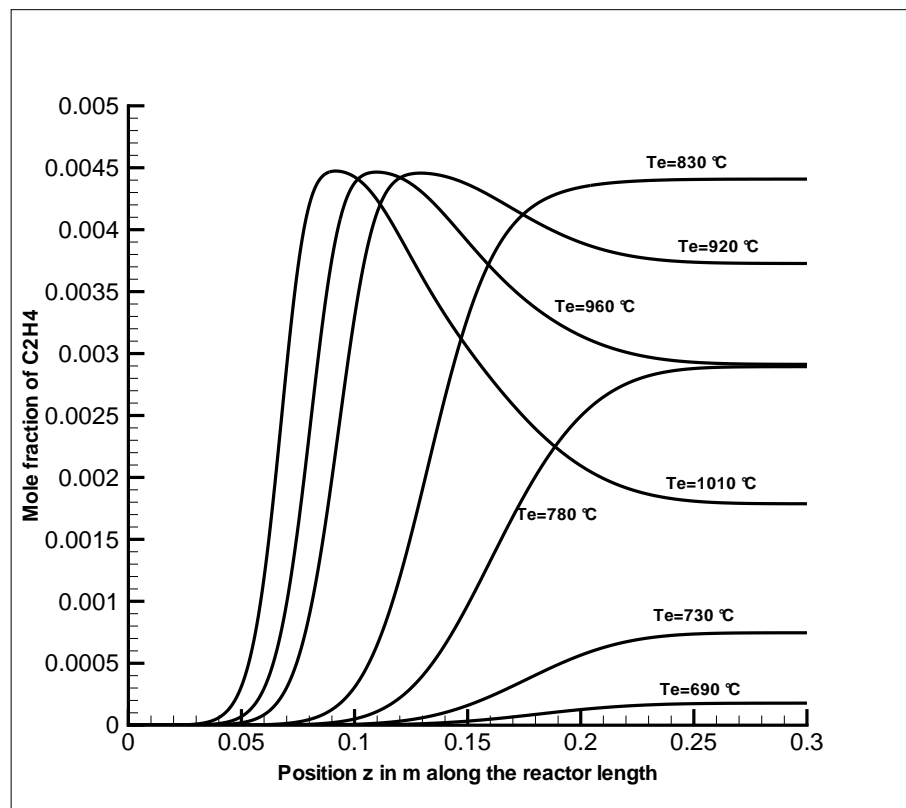


Figure 6.15: C<sub>2</sub>H<sub>4</sub> mole fraction profiles for 1-D model at different values of equivalent temperature  $T_e$  (non-isothermal)

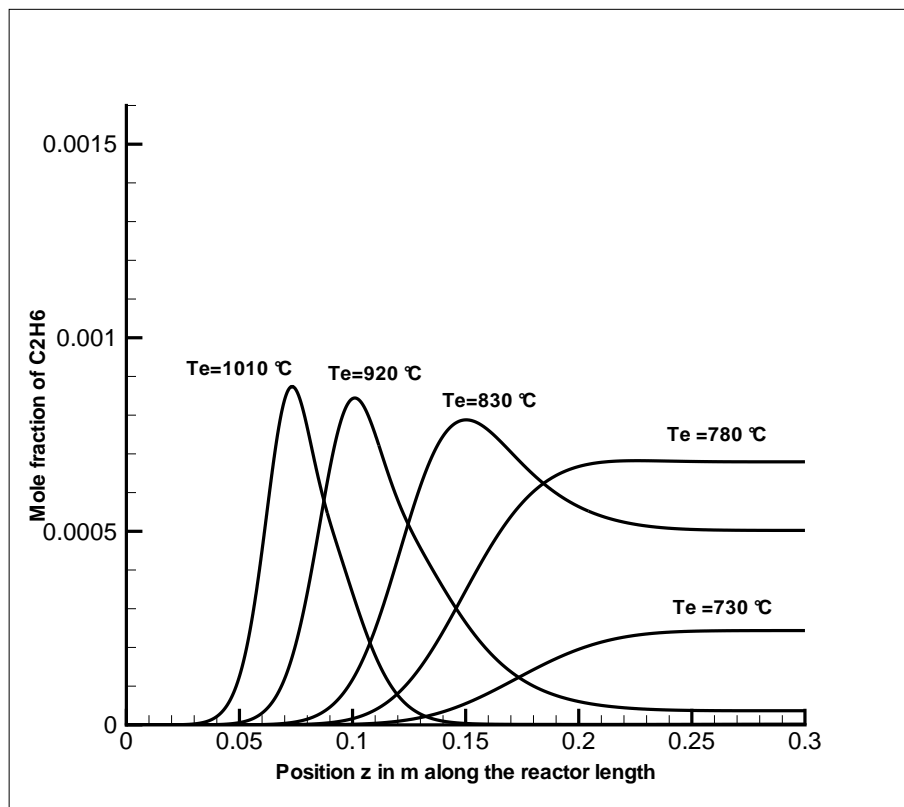


Figure 6.16: C<sub>2</sub>H<sub>6</sub> mole fraction profiles for 1-D model at different values of equivalent temperature  $T_e$  (non-isothermal)

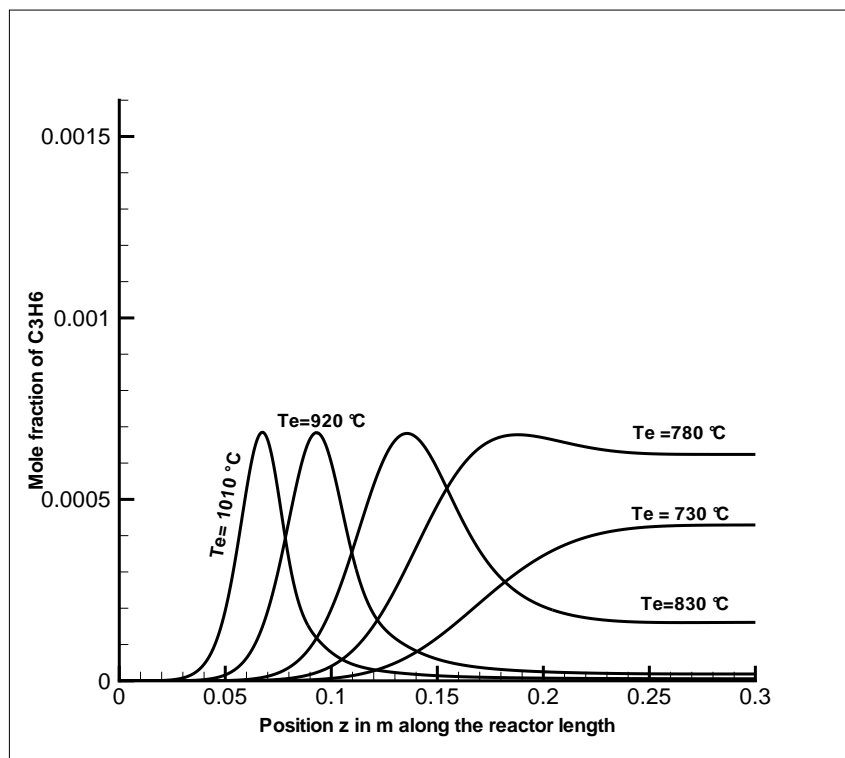


Figure 6.17: C<sub>3</sub>H<sub>6</sub> mole fraction profiles for 1-D model at different values of equivalent temperatures  $T_e$  (non-isothermal)

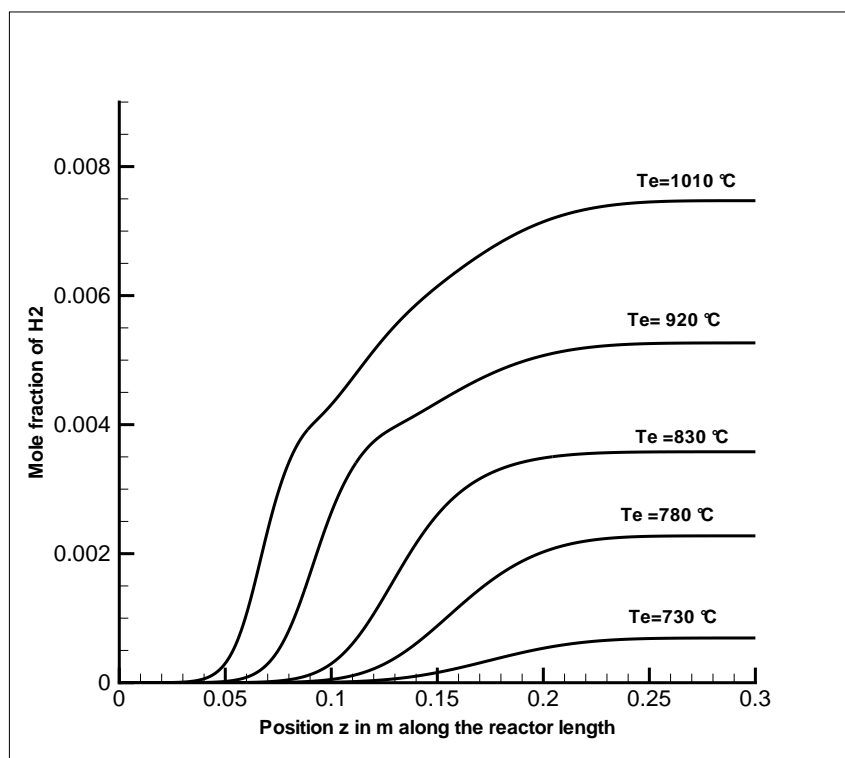


Figure 6.18: H<sub>2</sub> mole fraction profiles for 1-D model at different values of equivalent temperatures  $T_e$  (non-isothermal)

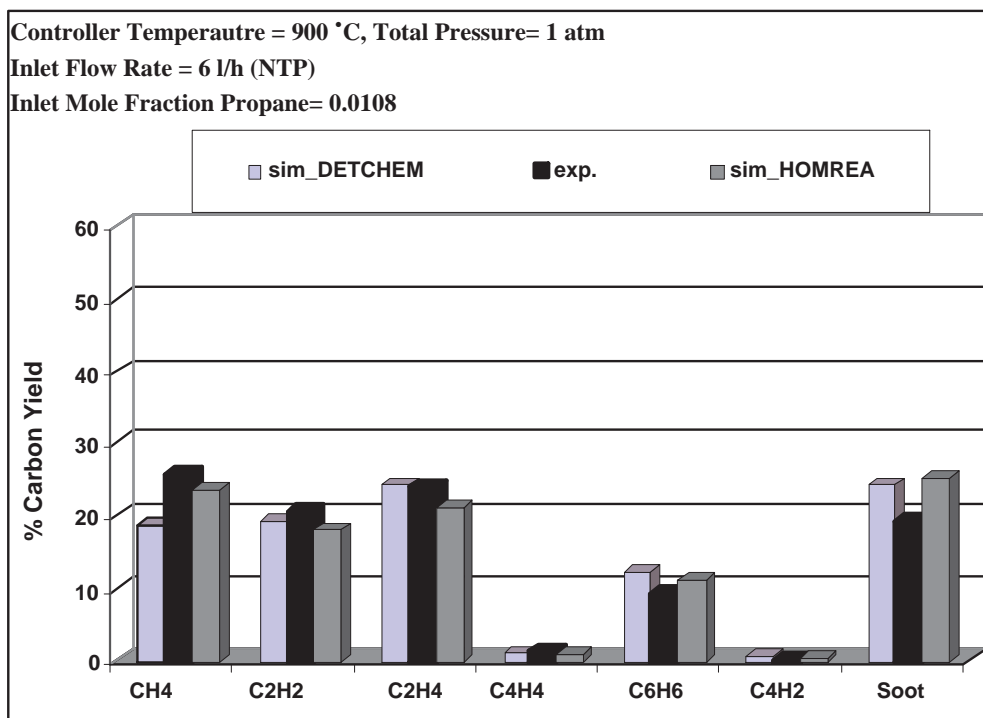


Figure 6.19: Comparison of experimentally observed yields of carbon for different species at the thermogravimetric reactor outlet and those predicted by the models using a detailed reaction mechanism

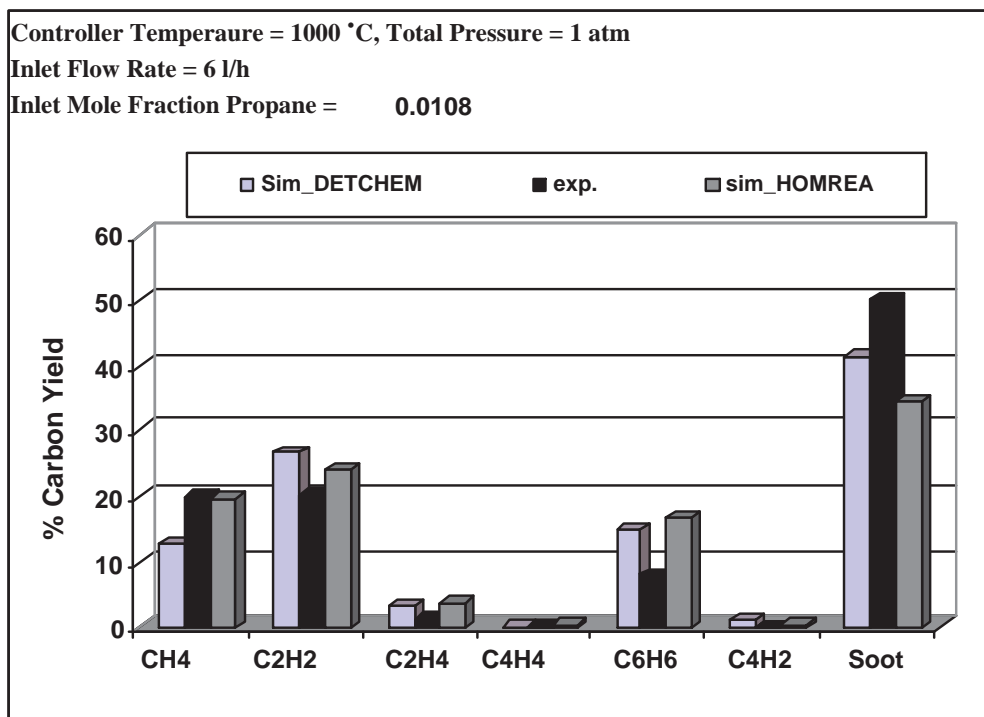


Figure 6.20: Comparison of experimentally observed yields of carbon for different species at the thermogravimetric reactor outlet and those predicted by the models using a detailed reaction mechanism

### 6.3 Vacuum Reactor

The dimensions and the operating conditions of the Vacuum Reactor have been discussed already in chapter 5. So the simulations were carried out at constant temperature of 1000 °C using the HOMREA model coupled with the detailed kinetic mechanism. The main products resulting from the pyrolysis of propane are H<sub>2</sub>, CH<sub>4</sub>, C<sub>2</sub>H<sub>2</sub>, C<sub>2</sub>H<sub>4</sub> and C<sub>6</sub>H<sub>6</sub> under the operating conditions used in experimental measurements. The simulation and experimental results comparison for these products is shown in Fig.6.21. The comparison reveals that the model can predict the composition of resulting gas from the homogeneous pyrolysis of propane in the vacuum reactor.

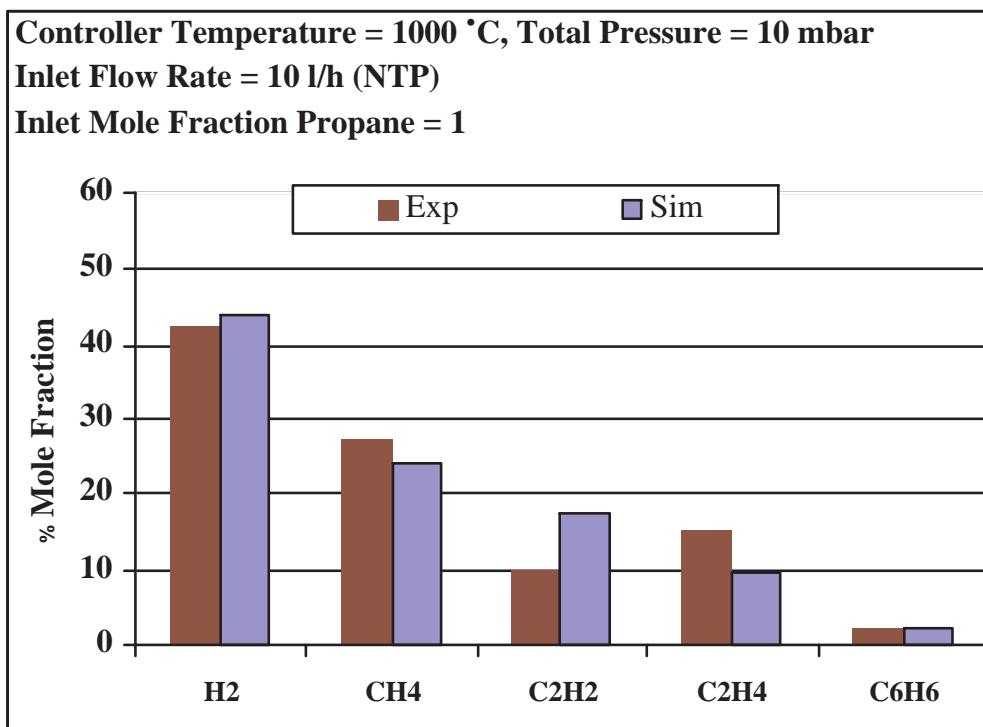


Figure 6.21: Comparison of experimentally observed species mole fractions at the outlet of bench scale reactor operated under vacuum and those predicted by the model using a detailed reaction mechanism



# Chapter 7

## Modeling of Acetylene Pyrolysis

Reactor dimensions and experimental conditions have been already discussed in the chapter 5. Modeling of acetylene pyrolysis with computational fluid dynamics and detailed chemistry will be discussed. Simulations results of both models will be compared to experimental measurements.

### 7.1 Computational Fluid Dynamics Modeling

#### 7.1.1 Tubular flow reactor

A 2-D grid was constructed which consist of 6000 cells to represent a reactor length of 500 mm with diameter of 20 mm. GAMBIT software [97] was used to generate the grid. The species transport and reaction model in Fluent [94] was used to implement the reaction mechanism [2] shown in table 7.1 for modeling the chemistry. The mechanism consists of 7 species which are the major products of acetylene pyrolysis under the vacuum carburizing conditions of steel. These include solid carbon  $C_{(s)}$  and hydrocarbons consisting of  $CH_4$ ,  $C_2H_2$ ,  $C_2H_4$ ,  $C_4H_4$ ,  $C_6H_6$  along with  $H_2$ . The overall mechanism consists of 9 reactions. The estimated Arrhenius parameters, activation energies and proposed reaction rates are also shown in the table 7.1. The mechanism was implemented through a user defined function (UDF) in Fluent. The operating pressure was set equal to 1.6 bar while inlet temperature and velocity boundary conditions were used corresponding to the flow rate of 150 lit/hr. For properties calculation, FLUENT offers different options. For these simulations, default options for these properties were used in the Material panel of the FLUENT. As the reactor is not operated under isothermal conditions, a temperature profile was necessary to model the temperature field. A mathematical fit in the form of a polynomial shown in equation 7.1 below was used for the temperature profile in the

Table 7.1: Operational kinetic mechanism acetylene pyrolysis

rate constant $k_f = Ae^{-E_a/RT}$ , (units of $A$ vary in $mol, m^3, s$ )				
Nr	Reaction	Rate Expression	$A$	$E_a$ (kJ/mol)
1	$C_2H_2 + H_2 \rightarrow C_2H_4$	$r_1 = k_{f1} \cdot c_{C_2H_2} \cdot c_{H_2}^{0.36}$	$4.4 \cdot 10^3$	103.0
2	$C_2H_4 \rightarrow C_2H_2 + H_2$	$r_2 = k_{f2} \cdot c_{C_2H_4}^{0.5}$	$3.8 \cdot 10^7$	200.0
3	$C_2H_2 + 3 H_2 \rightarrow 2 CH_4$	$r_3 = k_{f3} \cdot c_{C_2H_2}^{0.35} \cdot c_{H_2}^{0.22}$	$1.4 \cdot 10^5$	150.0
4	$2 CH_4 \rightarrow C_2H_2 + 3 H_2$	$r_4 = k_{f4} \cdot c_{CH_4}^{0.21}$	$8.6 \cdot 10^6$	195.0
5	$C_2H_2 \rightarrow 2 C_{(s)} + H_2$	$r_5 = k_{f5} \cdot \frac{c_{C_2H_2}^{1.9}}{1+18c_{H_2}}$	$5.5 \cdot 10^6$	165.0
6	$C_2H_2 + C_2H_2 \rightarrow C_4H_4$	$r_6 = k_{f6} \cdot c_{C_2H_2}^{1.6}$	$1.2 \cdot 10^5$	120.7
7	$C_4H_4 \rightarrow C_2H_2 + C_2H_2$	$r_7 = k_{f7} \cdot c_{C_4H_4}^{0.75}$	$1.0 \cdot 10^{15}$	335.2
8	$C_4H_4 + C_2H_2 \rightarrow C_6H_6$	$r_8 = k_{f8} \cdot c_{C_2H_2}^{1.3} \cdot c_{C_4H_4}^{0.6}$	$1.8 \cdot 10^3$	64.5
9	$C_6H_6 \rightarrow 6 C_{(s)} + 3 H_2$	$r_9 = k_{f9} \cdot \frac{c_{C_6H_6}^{0.75}}{1+22c_{H_2}}$	$1.0 \cdot 10^3$	75.0

simulations.

$$T(x) = (a \cdot x^2 + b \cdot x + c) \cdot T_c + d \cdot x^2 + e \cdot x + f \quad (7.1)$$

$T(x)$  represents the temperature as a function of the position  $x$  in relation to the reactor length.  $T_c$  represents controller temperature. This temperature profile was also implemented through a user defined function (UDF) and compiled before loading into Fluent using the default procedures in Fluent. Typical temperature profiles implemented in Fluent are shown in Fig. 7.1. Since the reactor is heated in the middle, the temperature is higher in the centre of the reactor. The contours of velocity predicted by Fluent at 900 °C is shown in Fig. 7.2. The velocity vectors at 900 °C are shown in the Fig. 7.3. Values of Reynold No. predicted by Fluent simulation at 900 °C on different cells of the grid are shown in the Fig.7.4. The flow in the reactor under these experimental conditions is laminar as indicated by the Reynold no. values which are less than 28 as shown in this figure. The solution was converged to species residuals of  $10^{-6}$  or less so that there was no further variation of these residuals. The convergence was fast and achieved in less than 500 iterations.

### Comparison of experimental and simulation results

The measured products of pyrolysis which include solid carbon,  $CH_4$ ,  $C_2H_2$ ,  $C_2H_4$ ,  $C_4H_4$ ,  $C_6H_6$  have been reported as percentage of input feed carbon content at different temperatures. The experimental results are compared with the simulation results of Fluent version 6.2. The amount of hydrogen was calculated by material balance and is also compared with the simulation results. Fig. 7.5 and Fig. 7.7 represent two of the typical contours of mole fractions obtained from simulations

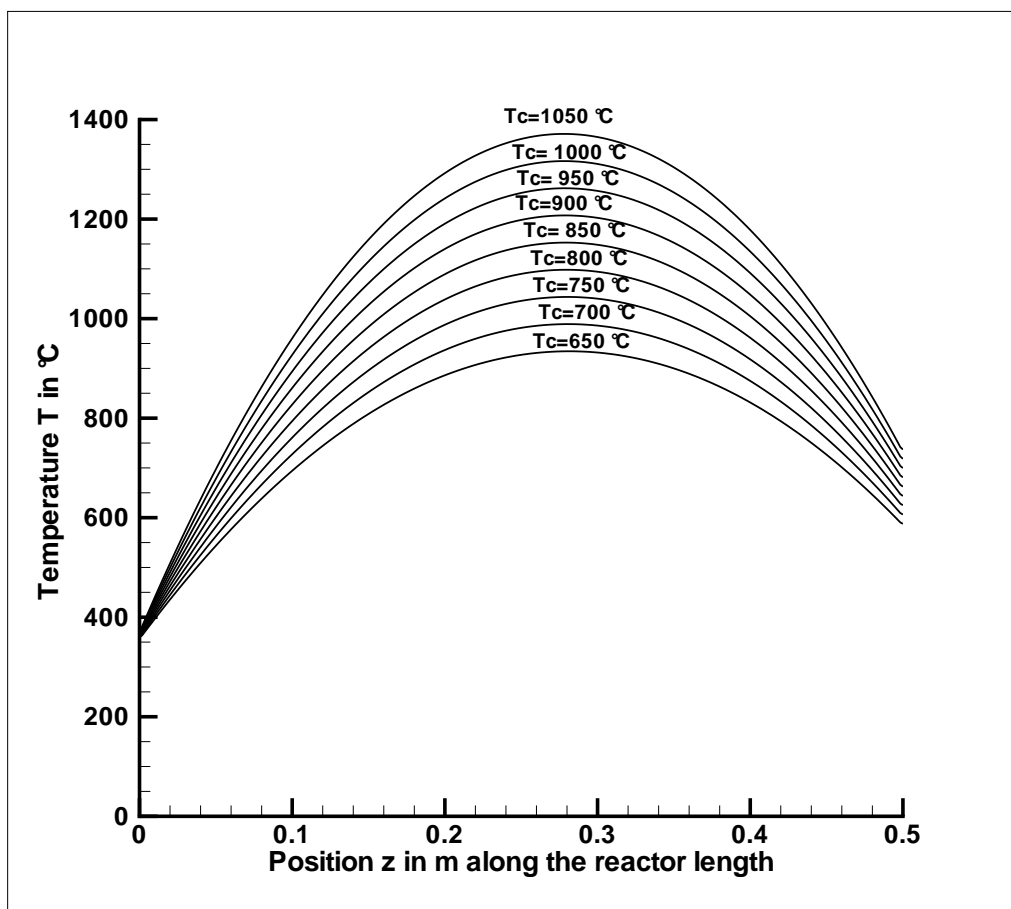


Figure 7.1: Temperature profiles at different controller temperatures  $T_c$  for the lab scale tubular flow reactor

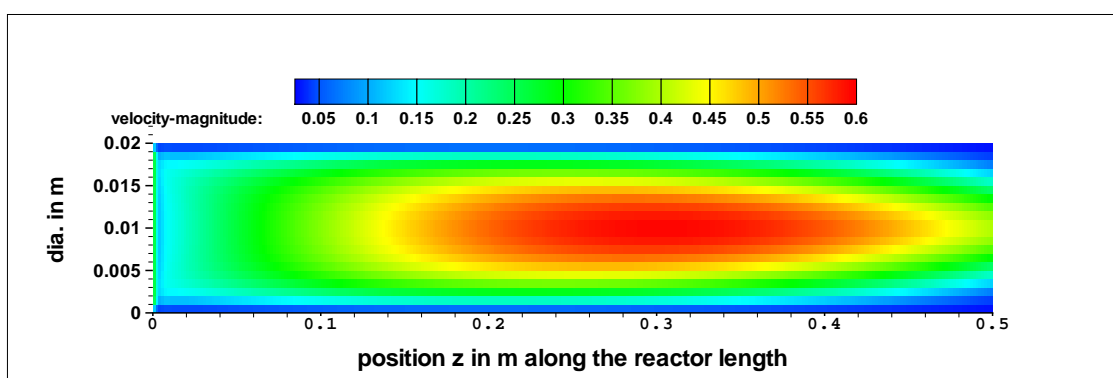


Figure 7.2: Contours of velocity at 900 °C predicted by CFD model for the lab scale tubular flow reactor

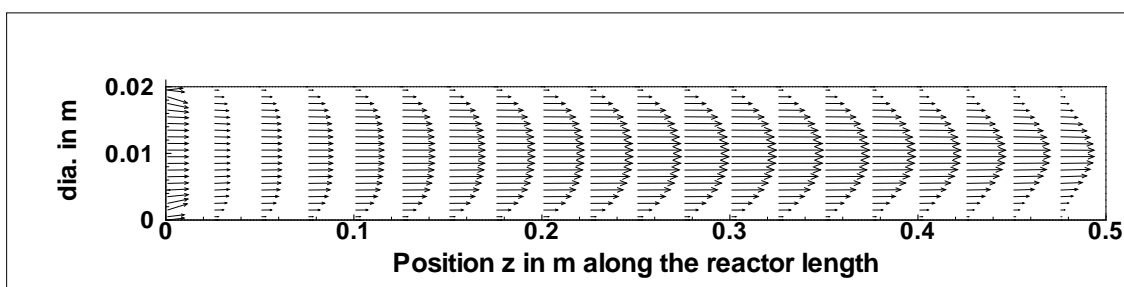


Figure 7.3: Contours of velocity vectors at 900 °C predicted by CFD model for the lab scale tubular flow reactor

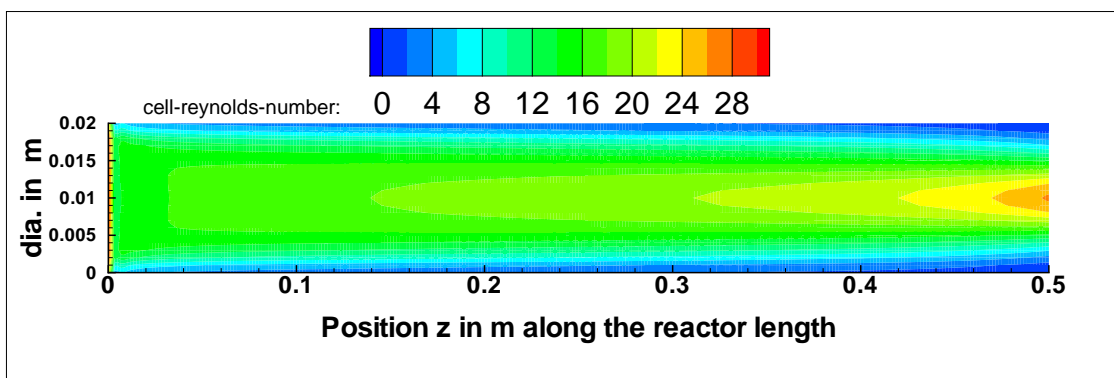


Figure 7.4: Contours of Reynold no. at 900 °C predicted by CFD model for the lab scale tubular flow reactor

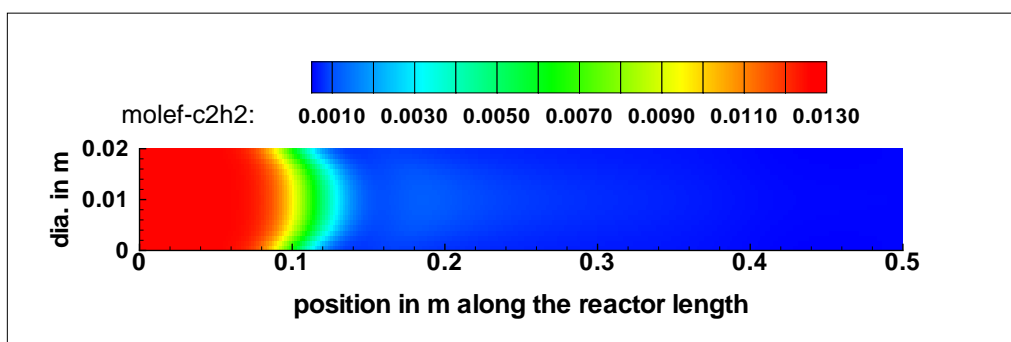


Figure 7.5: Contours of mole fraction of  $C_2H_2$  at 900 °C and 20 mbar partial pressure of acetylene predicted by CFD model for the lab scale tubular flow reactor [98]

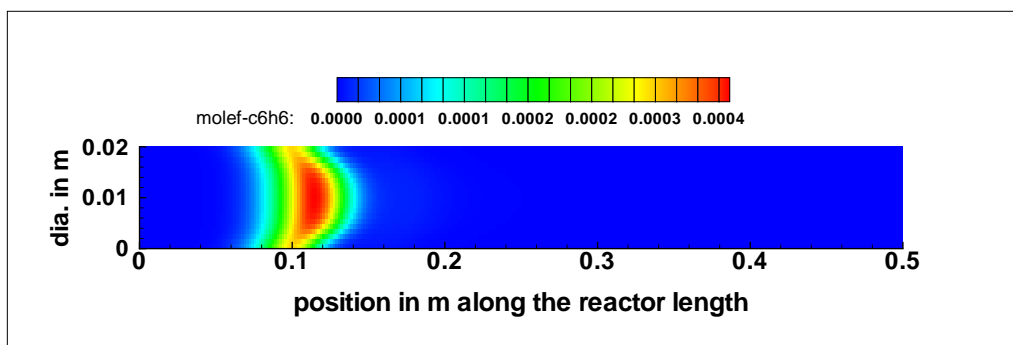


Figure 7.6: Contours of mole fraction of  $C_6H_6$  at 900 °C and 20 mbar partial pressure of acetylene predicted by CFD model for the lab scale tubular flow reactor

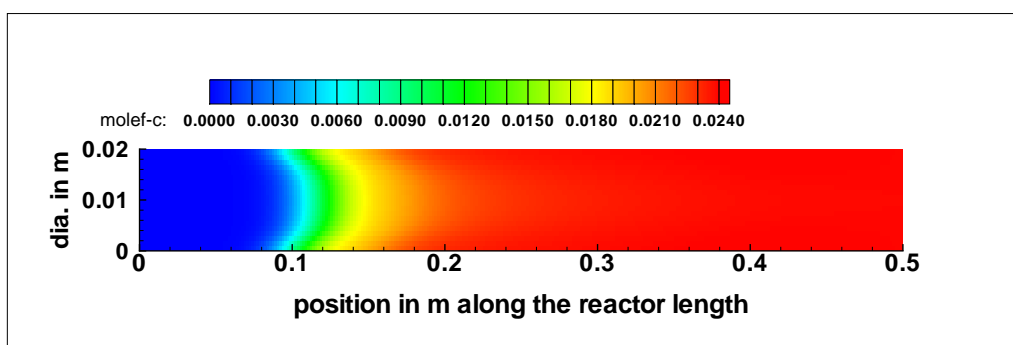


Figure 7.7: Contours of mole fraction of  $C_{(s)}$  at 900 °C and 20 mbar partial pressure of acetylene predicted by CFD model for the lab scale tubular flow reactor

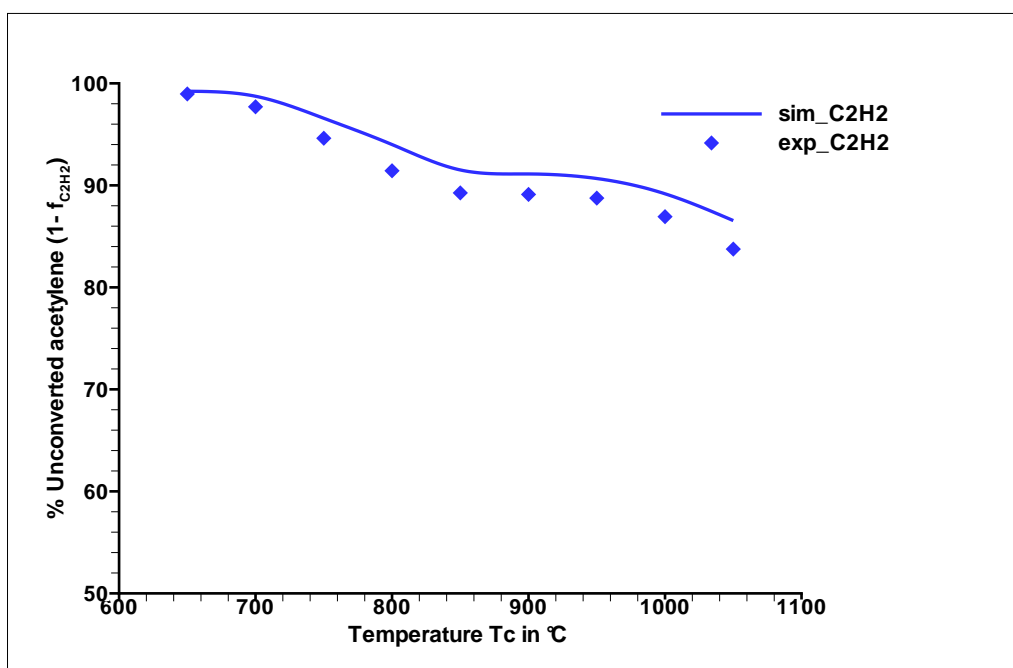


Figure 7.8: Comparison of experimentally observed unconverted percentage of acetylene at the outlet of lab scale tubular flow reactor and CFD model results for pyrolysis of acetylene at 10 mbar acetylene partial pressure

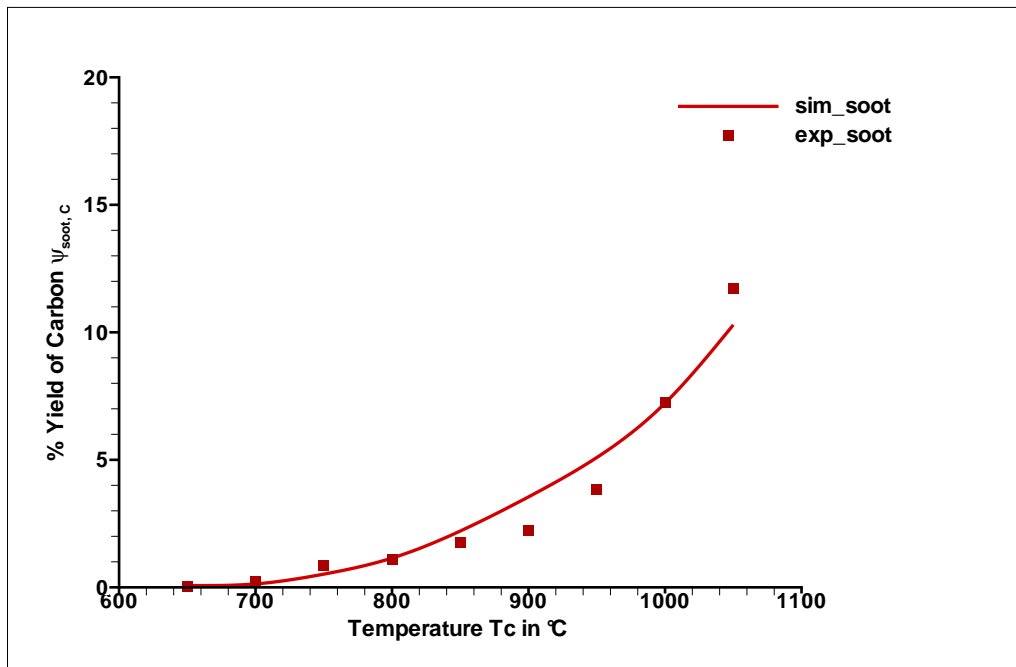


Figure 7.9: Comparison of experimentally observed percentage yield of carbon in the form of soot at the outlet of lab scale tubular flow reactor and CFD model results for pyrolysis of acetylene at 10 mbar acetylene partial pressure

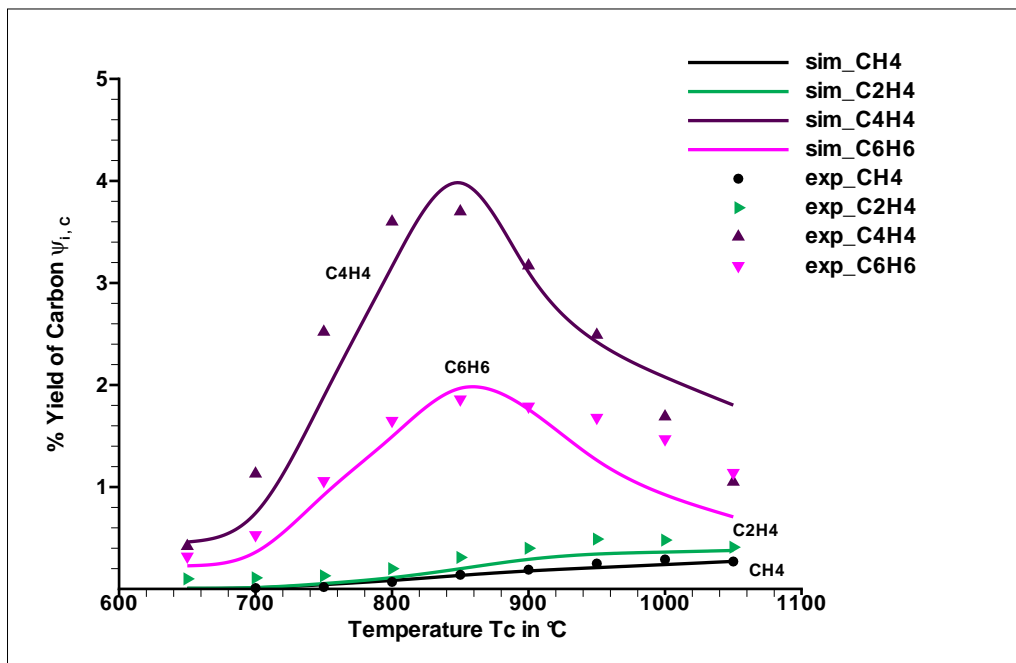


Figure 7.10: Comparison of experimentally observed percentage carbon yields for different species at the outlet of lab scale tubular flow reactor and CFD model results for pyrolysis of acetylene at 10 mbar acetylene partial pressure

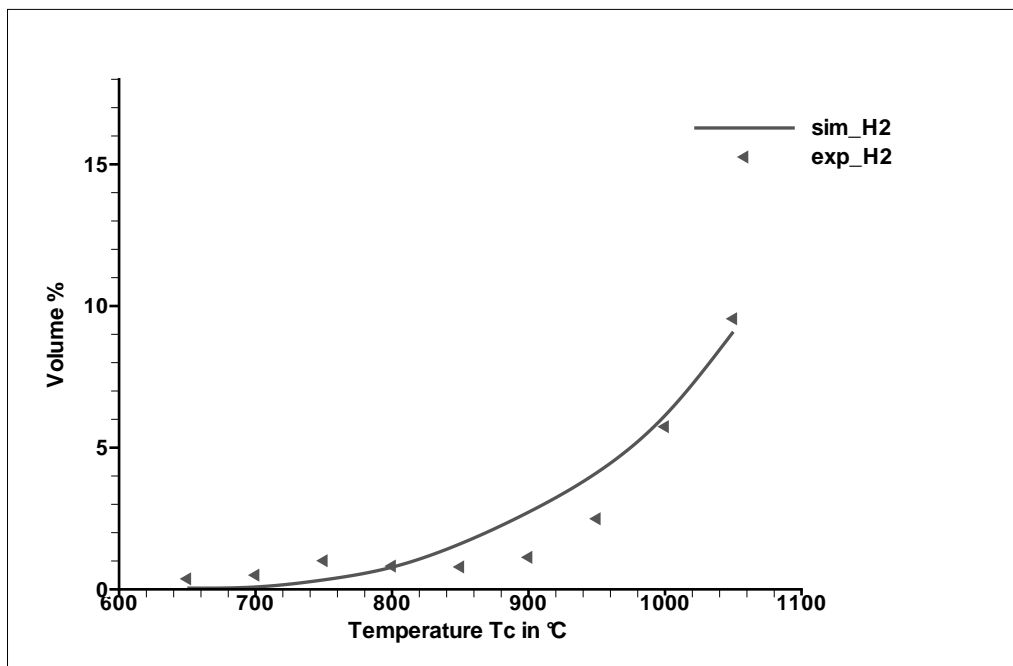


Figure 7.11: Comparison of experimentally observed hydrogen volume percent at the outlet of lab scale tubular flow reactor and CFD model results for pyrolysis of acetylene at 10 mbar acetylene partial pressure

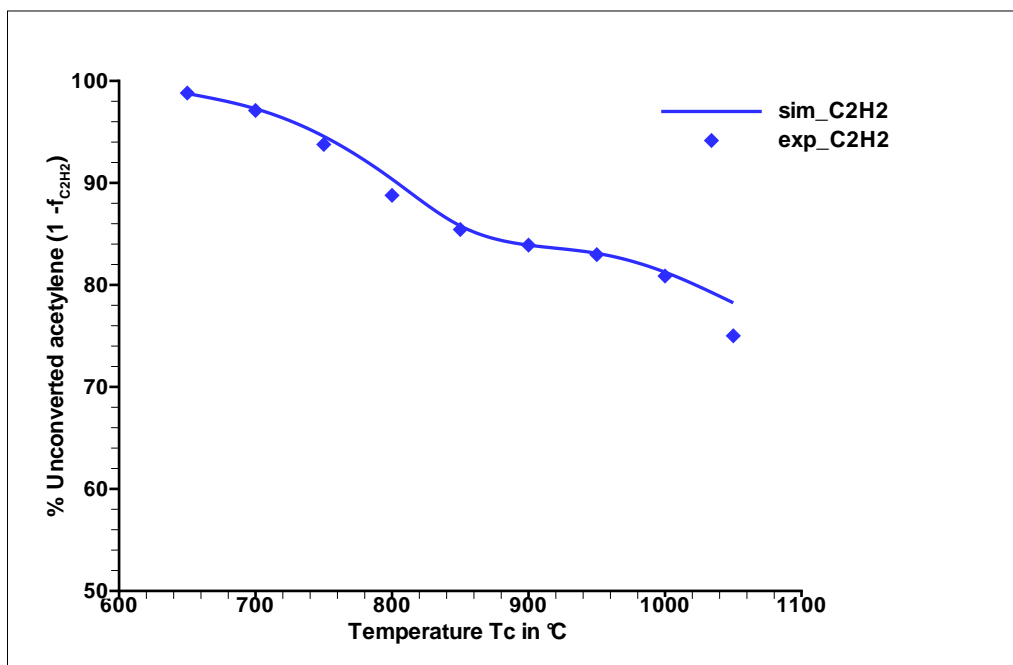


Figure 7.12: Comparison of experimentally observed unconverted percentage of acetylene at the outlet of lab scale tubular flow reactor and CFD model results for pyrolysis of acetylene at 20 mbar acetylene partial pressure

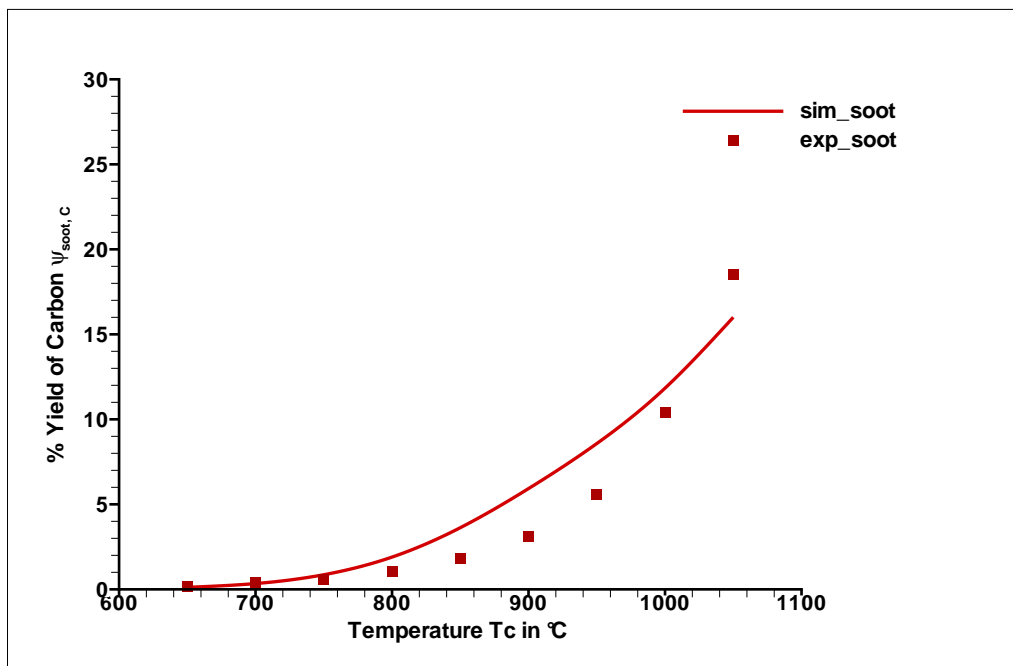


Figure 7.13: Comparison of experimentally observed percentage yield of carbon in the form of soot at the outlet of lab scale tubular flow reactor and CFD model results for pyrolysis of acetylene at 20 mbar acetylene partial pressure

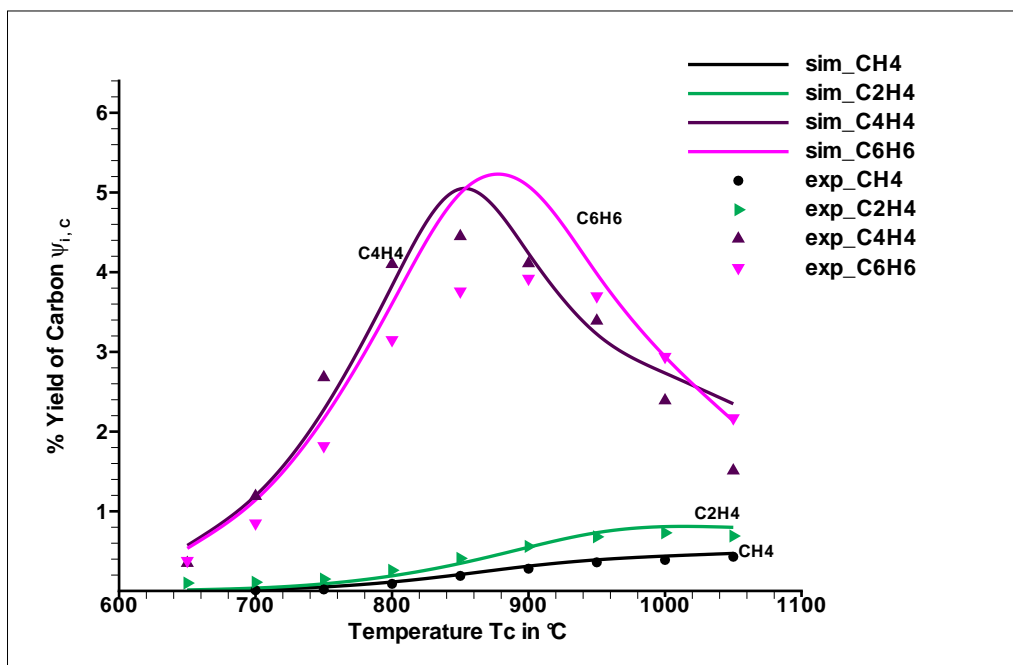


Figure 7.14: Comparison of experimentally observed percentage carbon yields for different species at the outlet of lab scale tubular flow reactor and CFD model results for pyrolysis of acetylene at 20 mbar acetylene partial pressure



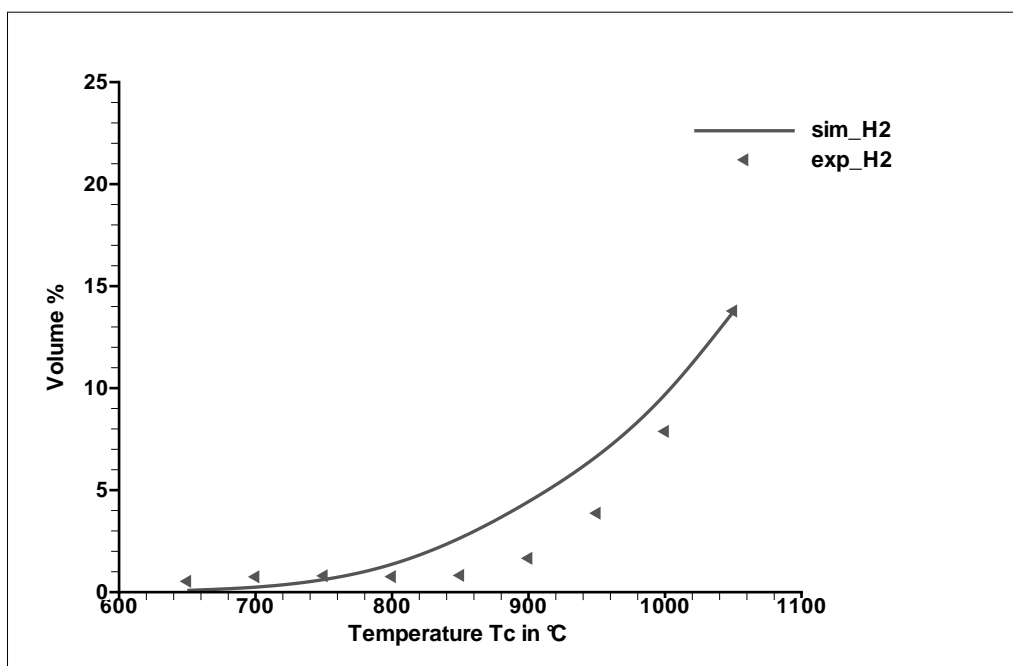


Figure 7.15: Comparison of experimentally observed hydrogen volume percent at the outlet of lab scale tubular flow reactor and CFD model results for pyrolysis of acetylene at 20 mbar acetylene partial pressure

for two important species  $C_2H_2$  and  $C_{(s)}$  at 900 °C and 20 mbar partial pressure of acetylene. Fig. 7.8 shows the comparison of experimental and simulation results for acetylene at 10 mbar partial pressure for a controller temperature variation of 650 °C to 1050 °C. The carbon content carried by unconverted acetylene in the mixture decreases from 99 % at 650 °C to 75 % at 1050 °C for 20 mbar representing a conversion of 25 % of acetylene to other products at the outlet as shown in Fig. 7.12. The second major and important component carrying carbon among the pyrolysis products is the solid carbon for which results are shown for 10 mbar as well as for 20 mbar partial pressure of acetylene. The percentage of solid carbon increases with an increase in temperature. The formation of  $C_4H_4$  and  $C_6H_6$  increases up to a temperature of 900 °C and then gradually decreases at higher temperatures.  $CH_4$  and  $C_2H_4$  are also formed but the carbon content in these compounds is less than 1 % under these experimental conditions [98].

### 7.1.2 Thermogravimetric reactor

A 2-D grid with 7296 cells was constructed to represent a reactor length of 280 mm with diameter of 28 mm as already shown in the sketch of Thermogravimetric Reactor in Chapter 5. For homogeneous pyrolysis simulations, the sample carrier shown in the sketch of the Thermogravimetric Reactor was not included. GAMBIT software was used to generate the grid. The grid was used in FLUENT version 6.2.16 for modeling the reactor behaviour. A segregated implicit 2-D laminar steady-state solver was selected with species transport and reaction model. By default FLUENT solver uses the constant dilute approximation method for the species mass diffusion coefficients i.e. a constant value for  $D_i^M$  where  $D_i^M$  is the mass diffusion coefficient for the species  $i$  in the mixture. So this default method of FLUENT used in these simulations results in a temperature independent mass diffusion coefficients  $D_i^M$ . The reaction mechanism shown in table 7.1 was implemented through user defined function (UDF) in FLUENT. Although the same activation energies values were used, it was necessary to modify some of the the Arrhenius parameters to best fit the data. The UDF used in simulations is included in the appendix. The measured temperature profiles were also implemented through UDF using a polynomial fit. The simulations were carried out till the residuals for species mole fractions were less than  $10^{-6}$  and there was no further variations in the residuals. The solution was converged approximately in less than 1000 iterations. Simulations were carried out for each set of data and results were saved. The FLUENT post processor was used for post processing the results e.g. contours of species mole fractions, temperature profile etc. The results for species mole fractions at the reactor outlet were exported

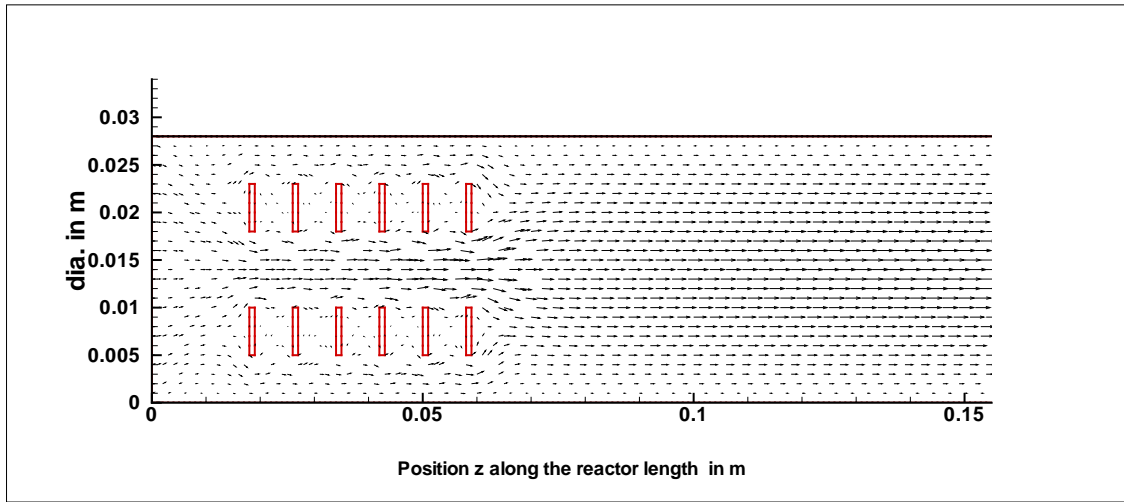


Figure 7.16: Contours of velocity vectors at 900 °C predicted by CFD model for the thermogravimetric reactor

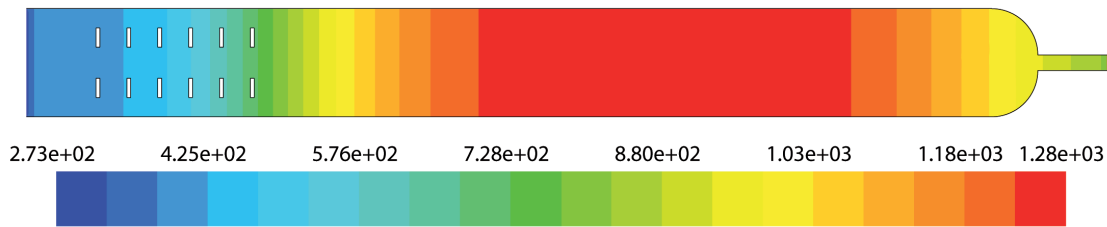


Figure 7.17: Temperature profile for controller temperature  $T_R = 1000$  °C used in CFD model to simulate the thermogravimetric reactor

from FLUENT to spreadsheet program, such as Microsoft Excel, for further processing and comparing with the experimental results. Simulation results for the contours of velocity vectors at 900 °C in Thermogravimetric Reactor are shown in Fig. 7.16. The protection shields at the entrance of the reactor effect the flow field.

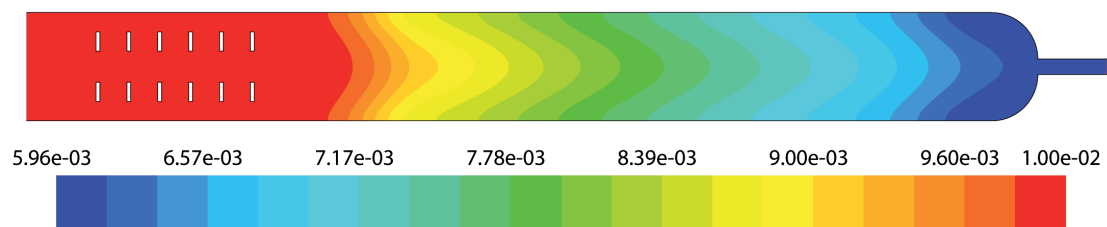


Figure 7.18: Contours of acetylene mole fractions in the thermogravimetric reactor at 1000 °C predicted by CFD model for pyrolysis of acetylene

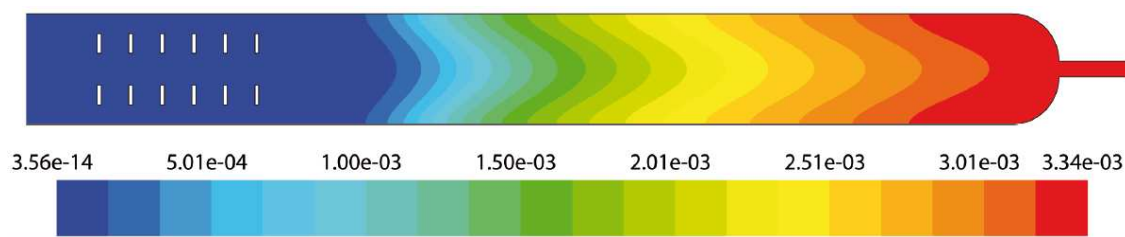


Figure 7.19: Contours of hydrogen mole fractions in the thermogravimetric reactor predicted by CFD model for pyrolysis of acetylene at 1000 °C

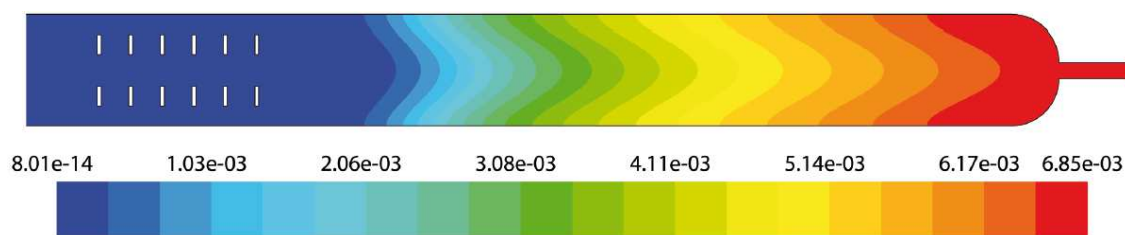


Figure 7.20: Contours of soot mole fractions in the thermogravimetric reactor predicted by CFD model for pyrolysis of acetylene at 1000 °C

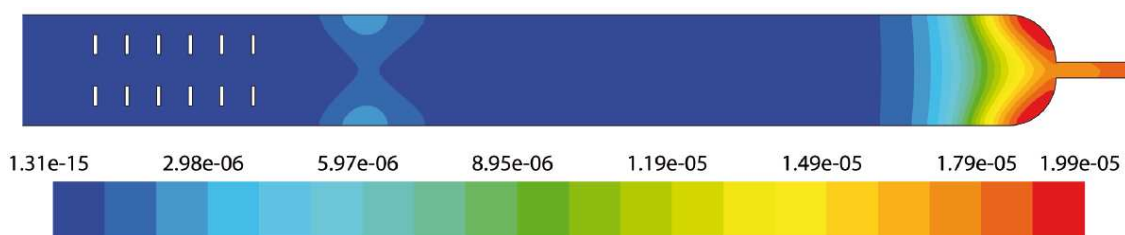


Figure 7.21: Contours of methane mole fractions in the thermogravimetric reactor predicted by CFD model for pyrolysis of acetylene at 1000 °C

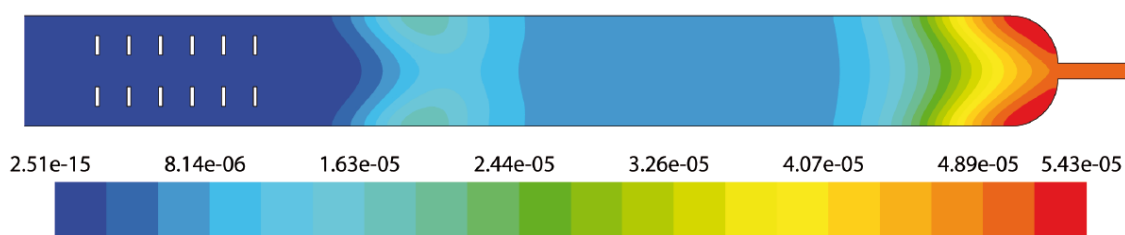


Figure 7.22: Contours of ethylene mole fractions in the thermogravimetric reactor predicted by CFD model for pyrolysis of acetylene at 1000 °C

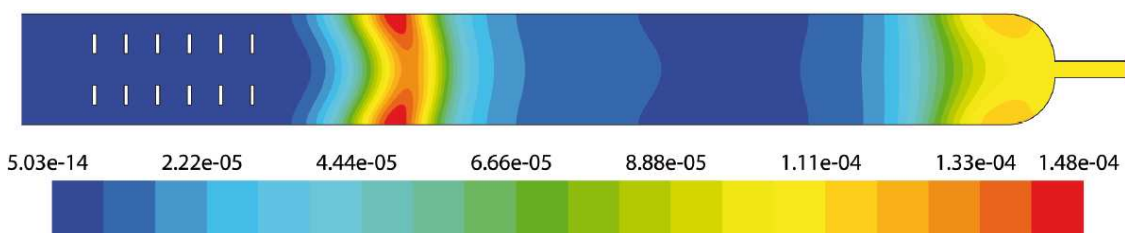


Figure 7.23: Contours of vinyl acetylene mole fractions in the thermogravimetric reactor predicted by CFD model for pyrolysis of acetylene at 1000 °C

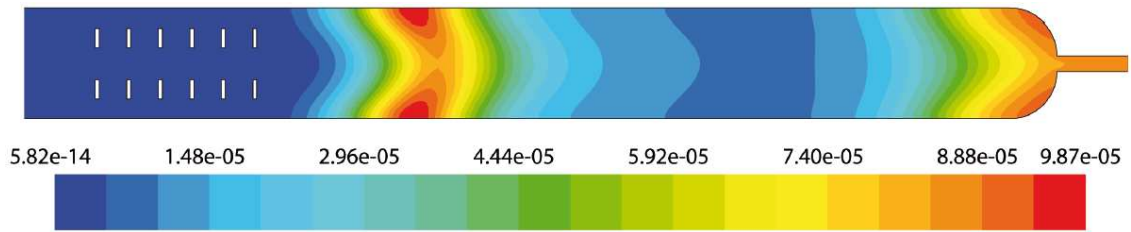


Figure 7.24: Contours of benzene mole fractions in the thermogravimetric reactor predicted by CFD model for pyrolysis of acetylene at 1000 °C

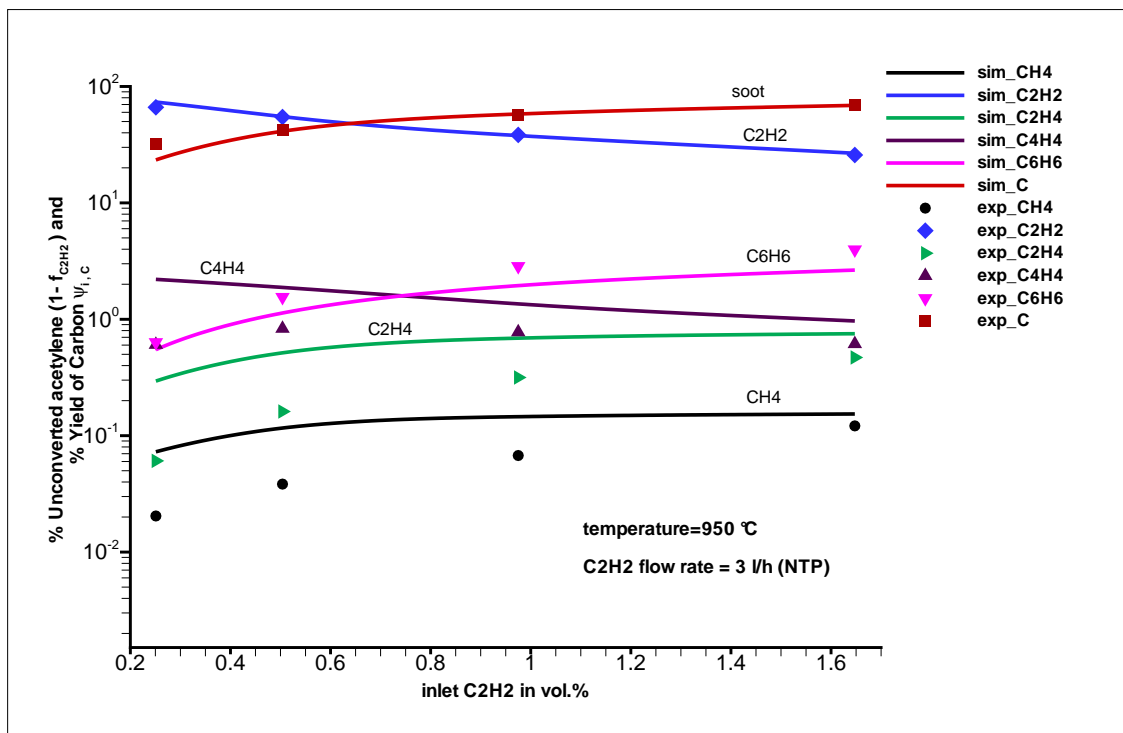


Figure 7.25: Comparison of experimentally observed percentage carbon yields at the outlet of thermogravimetric reactor and CFD model results for pyrolysis of acetylene [99]

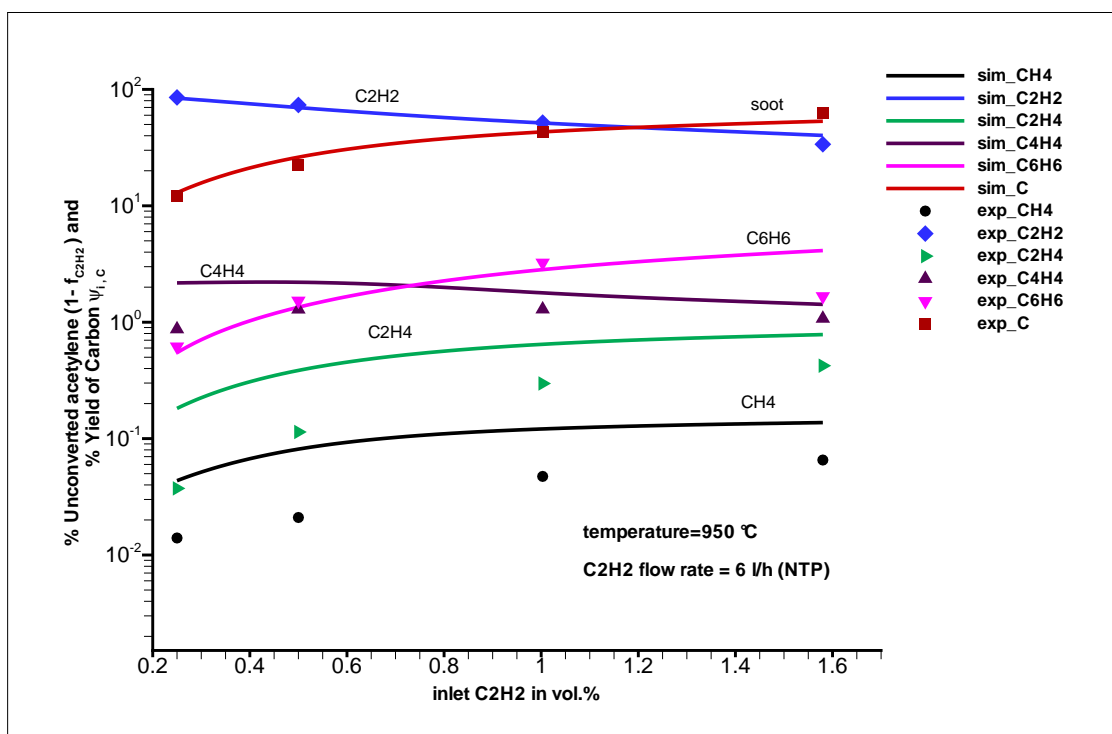


Figure 7.26: Comparison of experimentally observed percentage carbon yields at the outlet of thermogravimetric reactor and CFD model results for pyrolysis of acetylene

### Comparison of experimental and simulation results

The experimentally obtained percentage yield of carbon for different species as a function of acetylene inlet concentration is compared with the results of computational fluid dynamics simulations in Fig. 7.51 to Fig. 7.54.

In Fig. 7.51, comparison is shown for a temperature of 900 °C and a flow rate of 3 lit/hr (NTP) while the inlet concentration is varied. The conversion of acetylene to products increases with increasing the inlet concentration. The hydrocarbons higher than C<sub>6</sub>H<sub>6</sub> are not measured separately and are assumed as soot. The amount of C<sub>6</sub>H<sub>6</sub> and soot formed increases gradually with increasing the conversion of acetylene. The other species CH<sub>4</sub>, C<sub>2</sub>H<sub>4</sub> and C<sub>4</sub>H<sub>4</sub> are formed in low amounts of approximately less than 1%. The decrease in the formation of C<sub>4</sub>H<sub>4</sub> for higher inlet concentrations of C<sub>2</sub>H<sub>2</sub> is most probably due to its conversion to C<sub>6</sub>H<sub>6</sub> by molecular polymerization.

In Fig. 7.26 and Fig. 7.52 the flow rate is 6 lit/hr and 9 lit/hr respectively while the other parameters are same i.e the residence times are shorter. These shorter residence times lower the conversion of acetylene to products and as a result the formation of pyrolysis products is also lowered.

Fig. 7.28 to Fig. 7.54 show the results of acetylene pyrolysis at 1000 °C at two

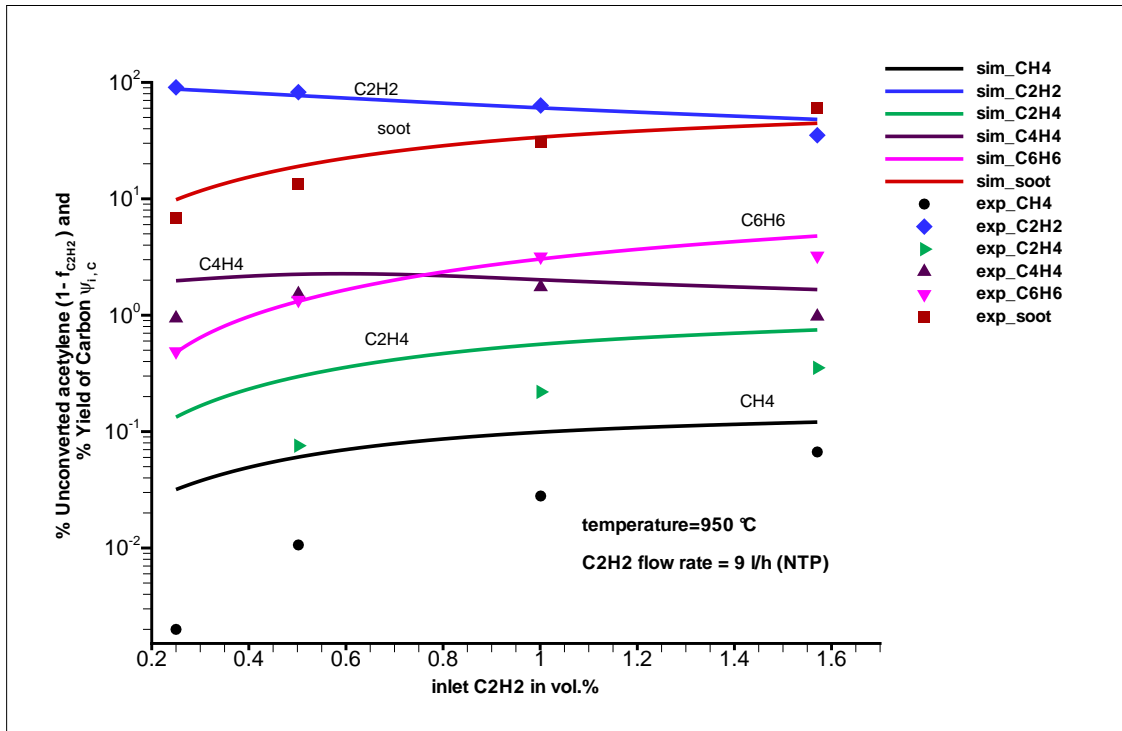


Figure 7.27: Comparison of experimentally observed percentage carbon yields at the outlet of thermogravimetric reactor and CFD model results for pyrolysis of acetylene

different flow rates. For higher temperature the conversion of acetylene increases and the higher amounts of soot are formed compared to previous results at low temperature. The overall comparison of simulation and experimental results is good and show the validity of model under these experimental conditions. So the model can be used to predict the concentration of acetylene and other species discussed above resulting from homogeneous reactions on the steel samples for studying the carburizing process. In the presence of steel samples additional reactions take place on the steel surface which will account for differences in compositions of resulting product gas predicted by the developed model. These reactions may be included to extend the model for predicting the carbon flux on the steel surface.

### 7.1.3 Vacuum reactor

A similar approach as used for the Thermogravimetric Reactor was used to simulate this reactor. A 2-D grid with 23964 cells was constructed to represent a reactor length of 680 mm with diameter of 135 mm. The grid generated by GAMBIT software was used in FLUENT version 6.2.16 for modeling the pyrolysis of acetylene under vacuum. The pressure in the reactor was set to 10 mbar. A segregated implicit 2-D laminar steady-state solver was selected with species transport and re-

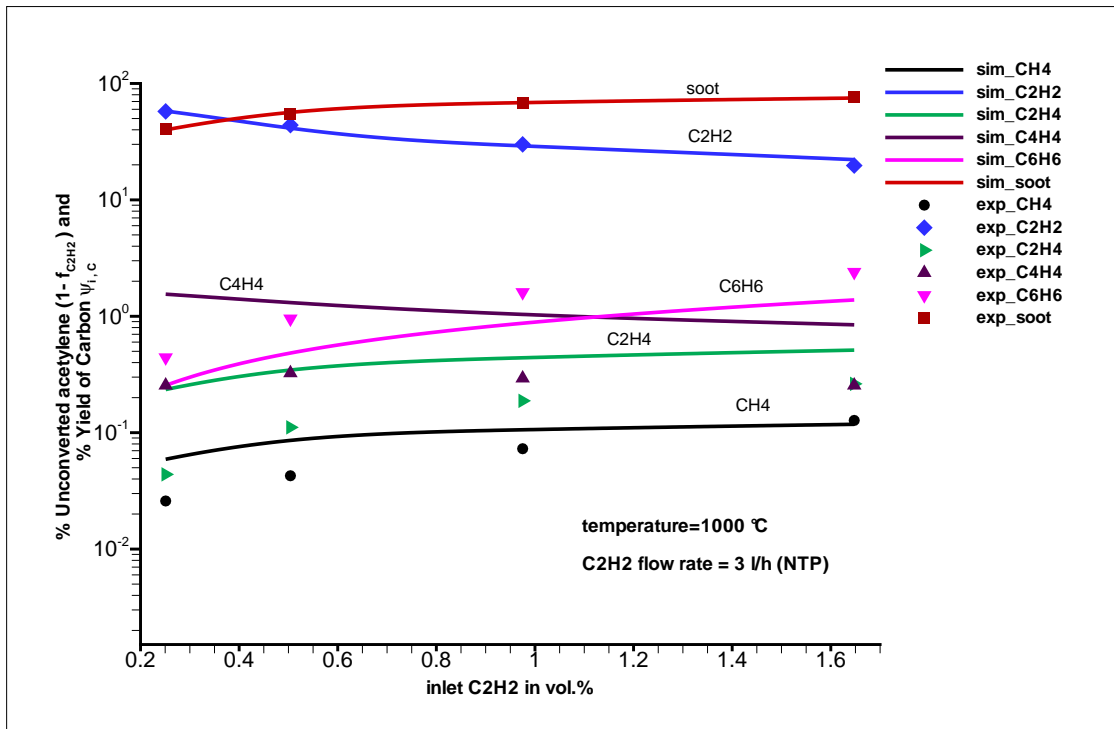


Figure 7.28: Comparison of experimentally observed percentage carbon yields at the outlet of thermogravimetric reactor and CFD model results for pyrolysis of acetylene

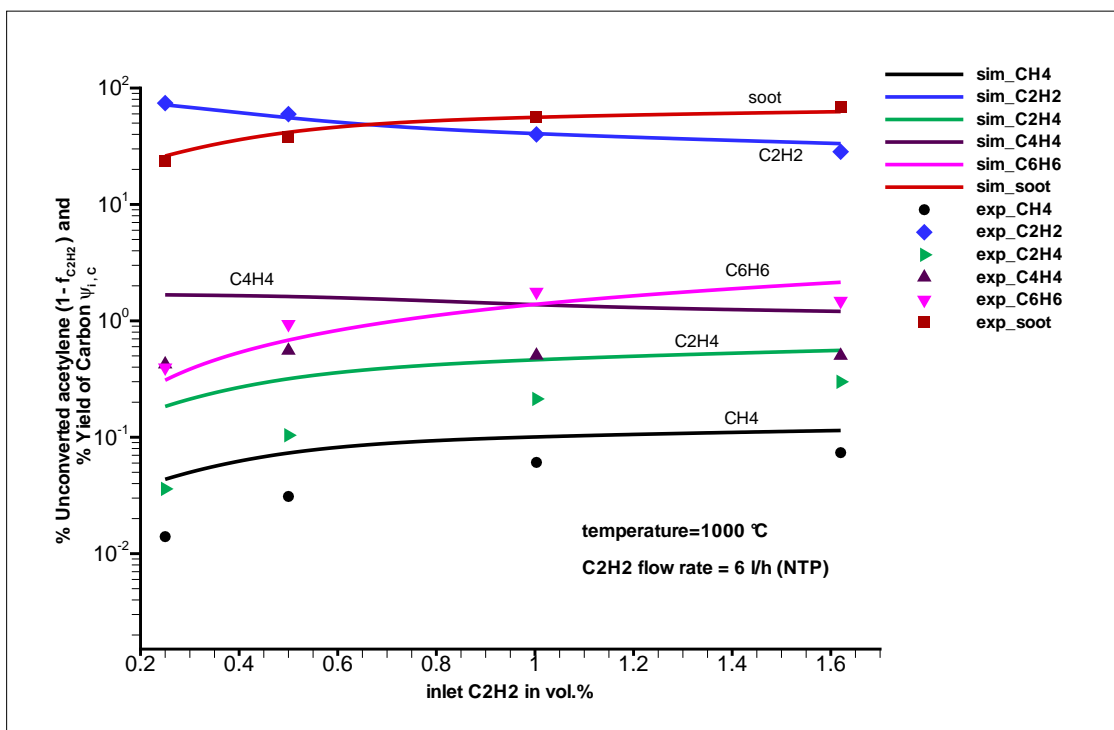


Figure 7.29: Comparison of experimentally observed percentage carbon yields at the outlet of thermogravimetric reactor and CFD model results for pyrolysis of acetylene



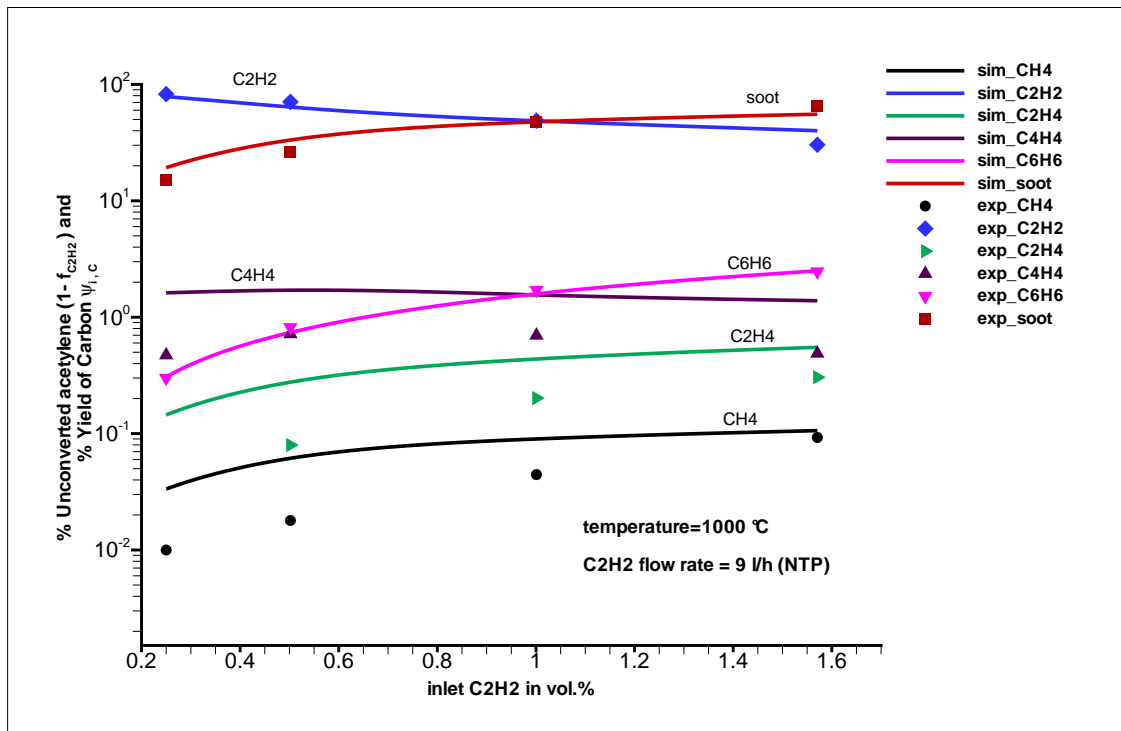


Figure 7.30: Comparison of experimentally observed percentage carbon yields at the outlet of thermogravimetric reactor and CFD model results for pyrolysis of acetylene

action model. The reaction mechanism shown in table 7.1 was implemented through user defined function (UDF) in FLUENT with the same activation energies values and Arrhenius parameters as already optimized for Thermogravimetric Reactor simulations. So the same UDF already used for Thermogravimetric Reactor was used in these simulations. Similarly the measured temperature profiles were also implemented through UDF using a polynomial fit. The simulations were carried out till the residuals for species mole fractions were less than  $10^{-6}$  and there was no further variations in the residuals. The solution was converged approximately in less than 1500 iterations. More time was consumed to get a converged solution compared to previous cases due to the large grid size. The postprocessing of results was carried out by the same way as in previous cases already discussed.

### Comparison of experimental and simulation results

The bench scale vacuum reactor is operated at low pressure of 10 mbar and acetylene is used without any dilution with inert gas. The inlet concentration of acetylene is comparable with the thermogravimetric reactor but the temperature range is higher as already discussed in the previous section. Here the experimentally derived carbon yields as a function of inlet flow rate are compared with the simulation results of computational fluid dynamics model. Fig. 7.40 and Fig. 7.41 show the comparison

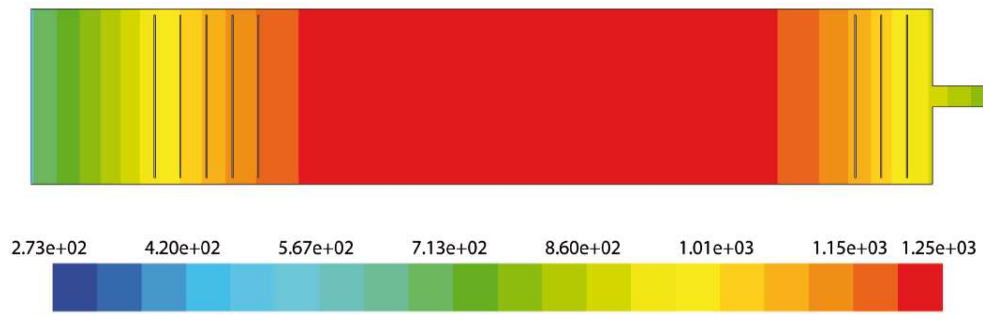


Figure 7.31: Temperature profile for controller temperature  $T_R = 980 \text{ }^\circ\text{C}$  used in CFD model to simulate the bench scale vacuum reactor

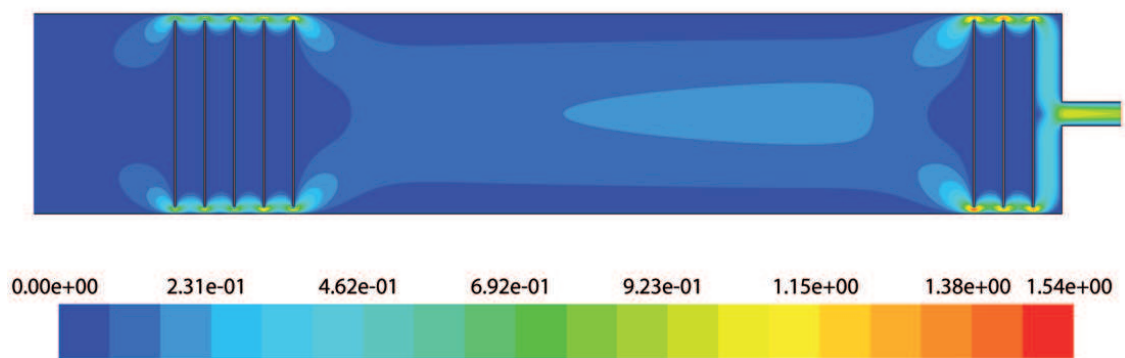


Figure 7.32: Contours of velocity (m/sec) predicted by CFD model in the bench scale vacuum reactor at 980 °C

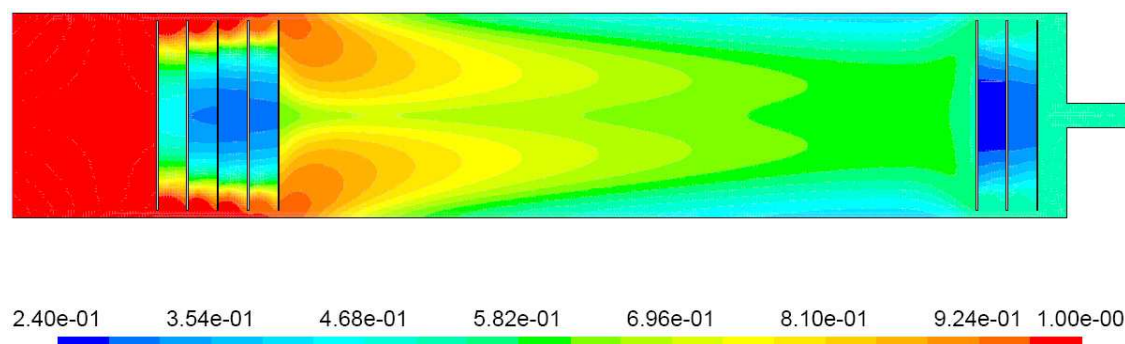


Figure 7.33: Contours of acetylene mole fractions predicted by CFD model in the bench scale vacuum reactor at 980 °C

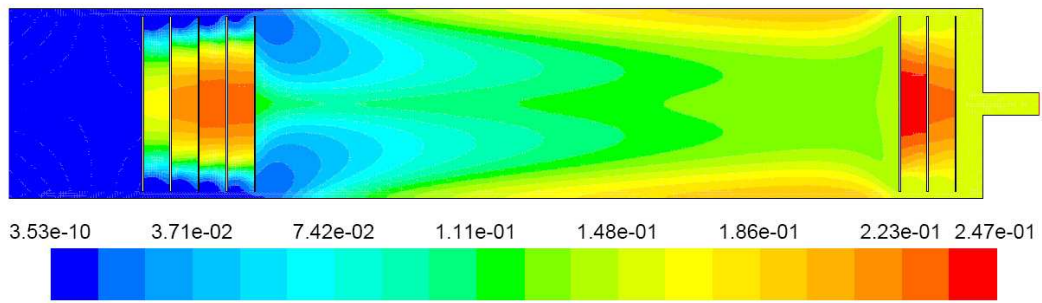


Figure 7.34: Contours of hydrogen mole fractions predicted by CFD model in the bench scale vacuum reactor at 980 °C

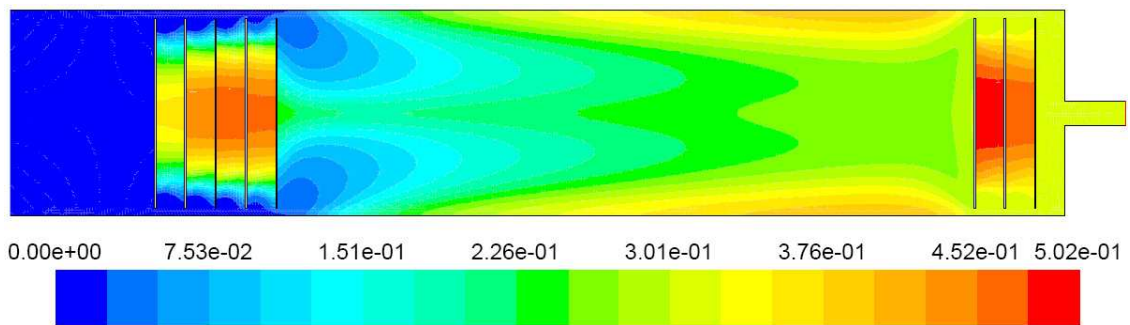


Figure 7.35: Contours of soot mole fractions predicted by CFD model in the bench scale vacuum reactor at 980 °C

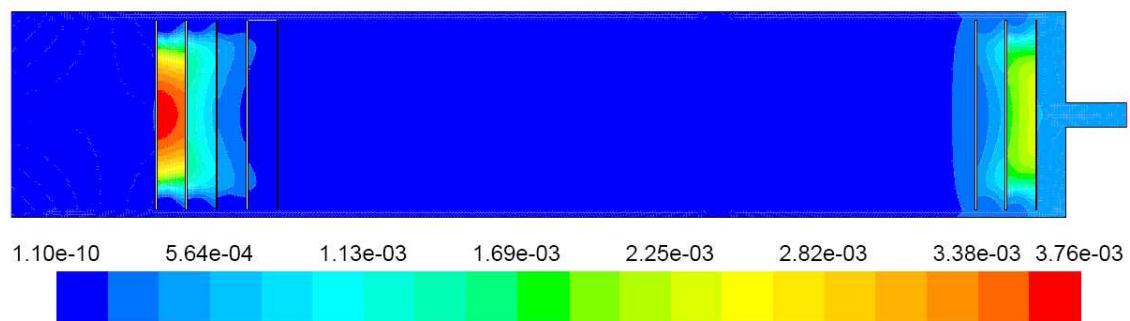


Figure 7.36: Contours of methane mole fractions predicted by CFD model in the bench scale vacuum reactor at 980 °C

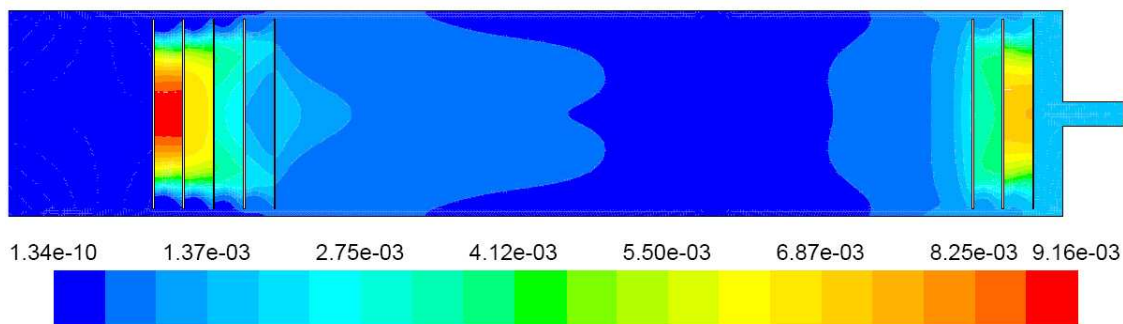


Figure 7.37: Contours of ethylene mole fractions predicted by CFD model in the bench scale vacuum reactor at 980 °C

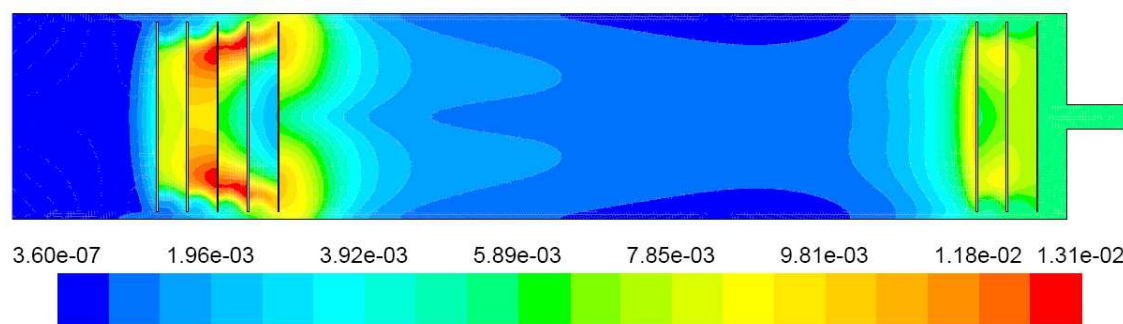


Figure 7.38: Contours of vinyl acetylene mole fractions predicted by CFD model in the bench scale vacuum reactor at 980 °C

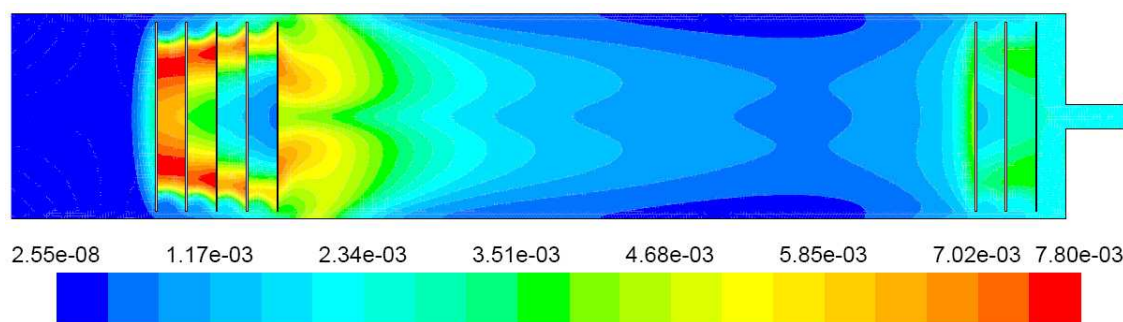


Figure 7.39: Contours of benzene mole fractions predicted by CFD model in the bench scale vacuum reactor at 980 °C

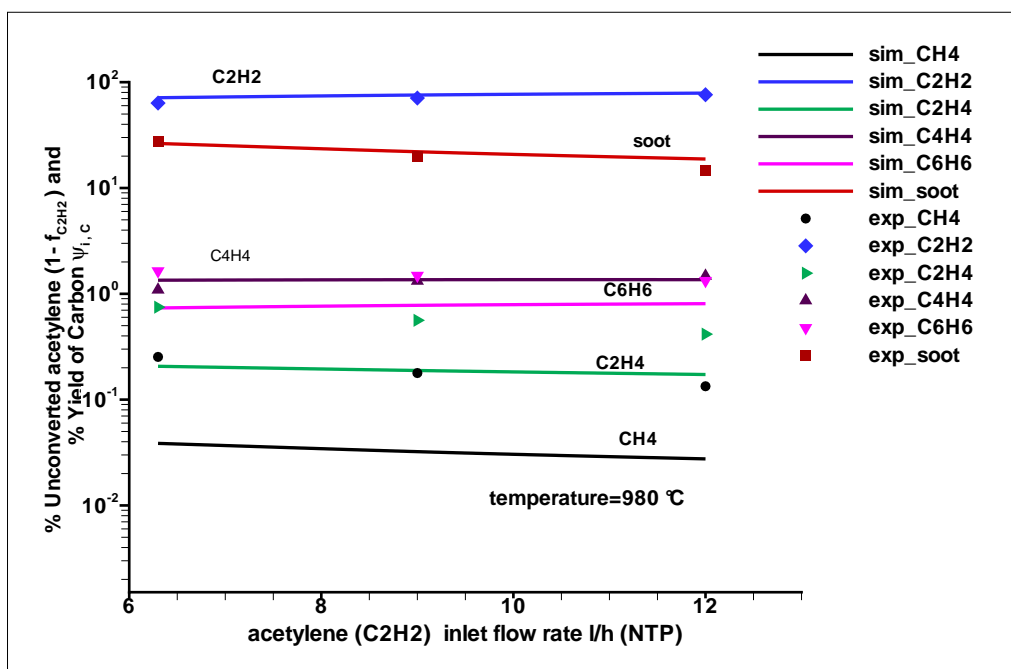


Figure 7.40: Comparison of experimentally observed percentage carbon yields at the outlet of bench scale vacuum reactor and CFD model results for pyrolysis of acetylene at 980 °C

for 980 °C and 1050 °C respectively. The carbon yields at the reactor outlet for species other than soot and unconverted acetylene are less than 1 percent. The experimental results are in good agreement with the model results especially for acetylene, vinyl acetylene and soot.

## 7.2 Modeling with Detailed Chemistry

The operational kinetic or formal kinetic mechanisms have limited applicability because the parameters are determined strictly by fitting to experimental conditions. On the other hand, the use of detailed mechanisms is limited to ideal flow models but they provide more better understanding of the process and provide more accuracy and extensibility. The cylinders, in which acetylene is stored, contain some acetone for safety purposes. The presence of acetone in acetylene also affects the dissociation of acetylene which needs to be considered. The acetone pyrolysis mechanism is available in the detailed mechanism and it can be used to model the reactor behaviour. So the detailed mechanism already used for modeling the propane pyrolysis was used with HOMREA and DETCHEM software packages.

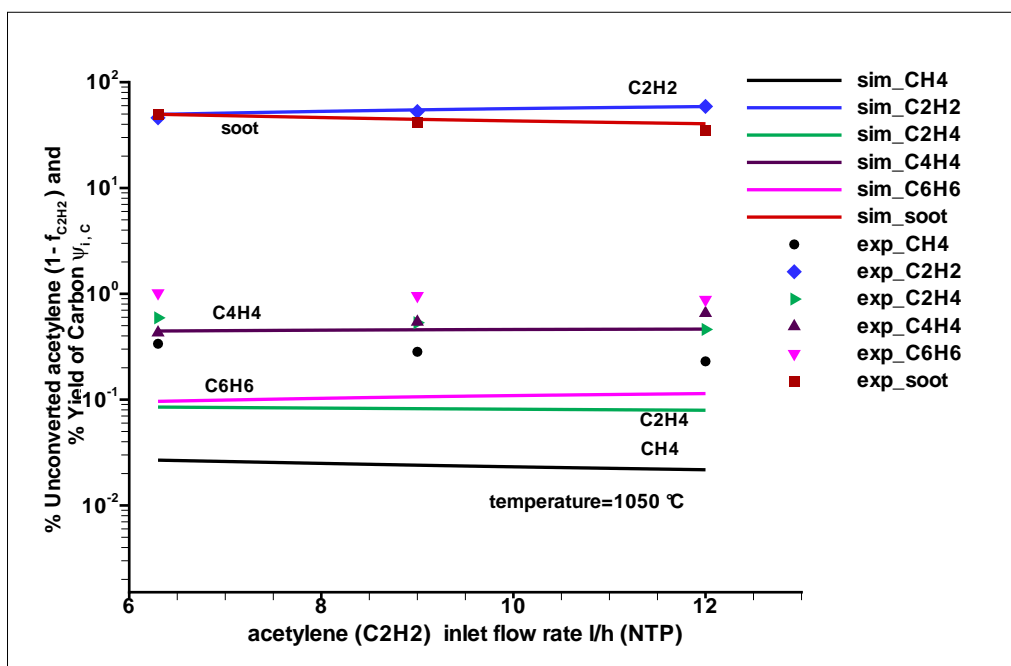


Figure 7.41: Comparison of experimentally observed percentage carbon yields at the outlet of bench scale vacuum reactor and CFD model results for pyrolysis of acetylene at 1050 °C

## 7.2.1 Tubular flow reactor

The reactor was simulated by using the PLUG model of DETCHEM (described in chapter 4) coupled with the detailed mechanism. The measured temperature profile was also implemented by using the polynomial (6.1). The acetylene was assumed to contain 1.5% of acetone. Sensitivity analysis and reaction mechanism analysis were performed with HOMREA software package to identify important reactions and their contribution to the formation and destruction of major species of interest.

### Simulation Results

The simulation results show that consumption of acetylene can be predicted very well as shown in Fig. 7.42. The formation of vinyl acetylene is overpredicted while the formation of benzene is predicted well at higher temperatures but underpredicted at lower temperatures as shown in Fig. 7.43. The main difference between simulation and experimental results was found in case of diacetylene. The model predicts comparatively higher amounts of diacetylene specially above 900 °C as shown in Fig. 7.44. The reaction mechanism analysis shows that following reactions are responsible for the consumption of acetylene.

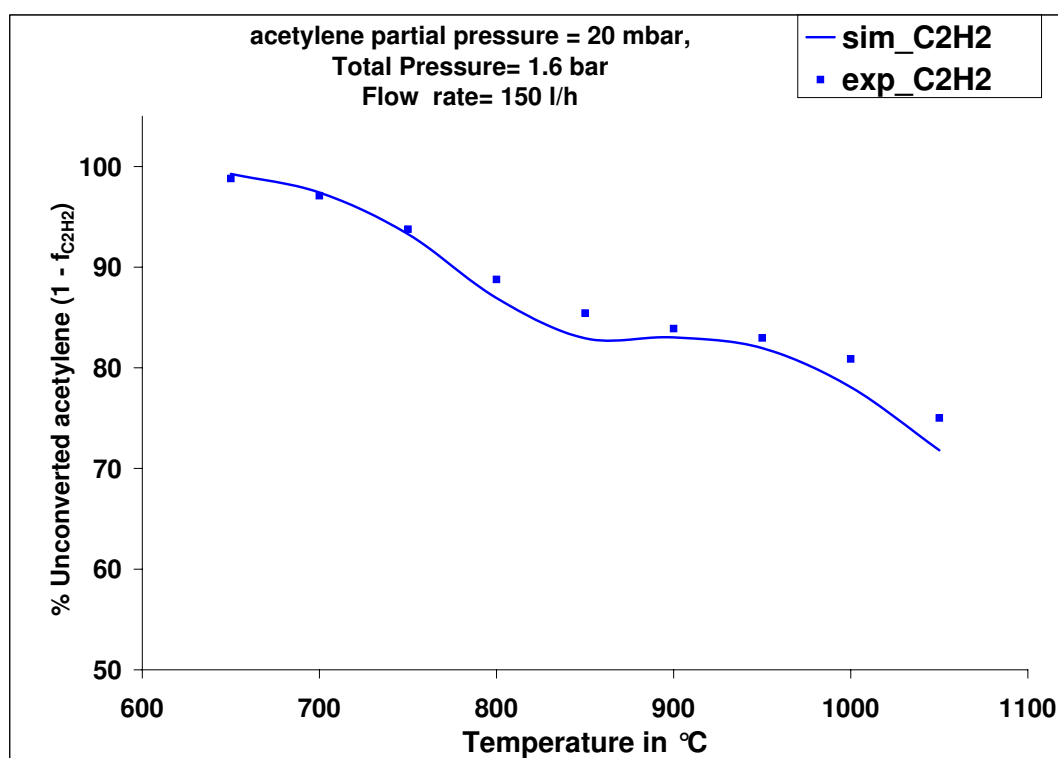
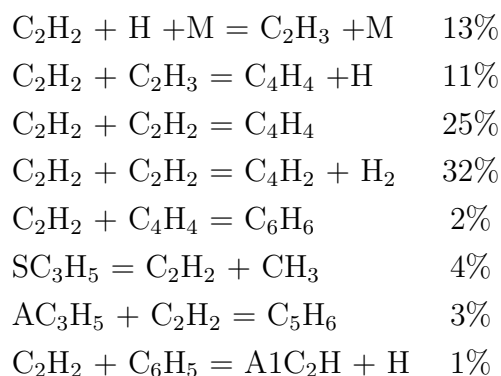


Figure 7.42: Comparison of experimentally observed unconverted percentage of acetylene at the outlet of lab scale tubular flow reactor and simulations with detailed mechanism of Norinaga and Deutschmann coupled with DETCHEM 1D model (PLUG) for pyrolysis of acetylene at various temperatures



Most of the acetylene is consumed by the combination of two acetylene molecules to form diacetylene and hydrogen. The other reactions which consume the acetylene include the formation of vinyl acetylene and formation of benzene. So without assuming the presence of acetone, acetylene is consumed by the molecular mechanism. The results of Norinaga and Deutschmann [75] show that most of the acetylene is converted to vinyl acetylene at a temperature of 900 °C. Vacuum carburizing of steel is accomplished at temperatures higher than 900 °C and has been investigated upto 1080 °C. The model predicts that at temperatures higher than 900 °C most of

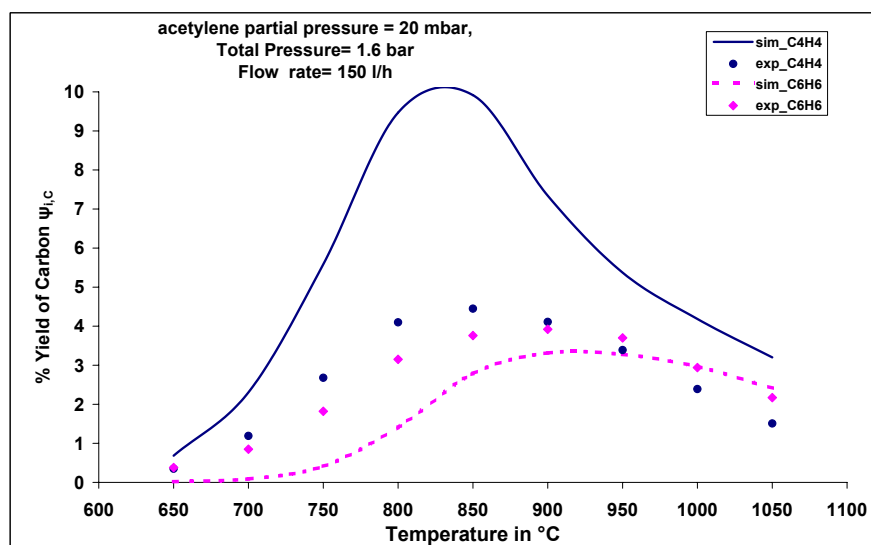
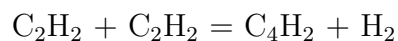


Figure 7.43: Comparison of experimentally observed percentage carbon yields at the outlet of lab scale tubular flow reactor and simulations with detailed mechanism of Norinaga and Deutschmann coupled with DETCHEM 1D model (PLUG) for pyrolysis of acetylene at various temperatures

the acetylene is converted to diacetylene which is against the experimental evidence. So the activation energy of the reaction responsible for the formation of diacetylene should be higher to reduce the amount of diacetylene formed at higher temperature. Also in the literature [70], this reaction has been reported with higher activation energy than used in this mechanism. The kinetic parameters for the following reactions were optimized to better predict the products of pyrolysis.



With the optimized parameters, simulation results are shown in Fig.7.45 to Fig.7.48. The mechanism can predict rather well the major species such as  $\text{C}_2\text{H}_2$ ,  $\text{C}_4\text{H}_4$  and  $\text{C}_6\text{H}_6$  as well as the other species  $\text{C}_2\text{H}_4$ ,  $\text{C}_2\text{H}_6$ ,  $\text{PC}_3\text{H}_4$ ,  $\text{C}_4\text{H}_2$  and  $\text{C}_7\text{H}_8$  present in small amounts. Mechanism analysis for 950 °C and for 0.7 sec of residence time shows that the consumption of acetylene takes place mainly by the following reactions:



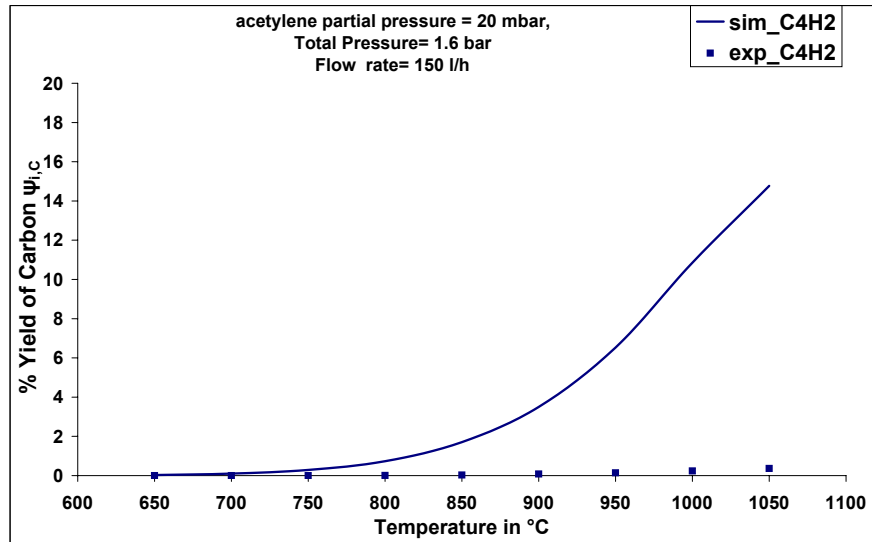
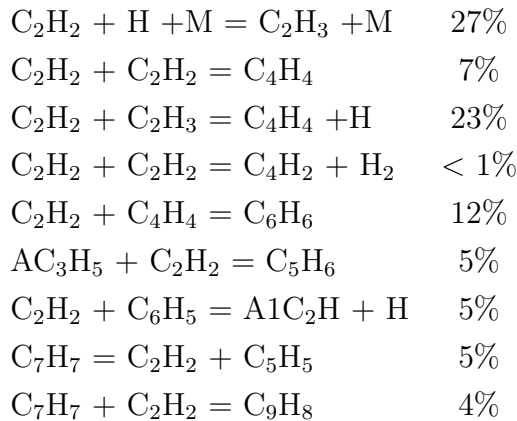


Figure 7.44: Comparison of experimentally observed percentage yields of diacetylene at the outlet of lab scale tubular flow reactor and simulations with detailed mechanism of Norinaga and Deutschmann coupled with DETCHEM 1D model (PLUG) for pyrolysis of acetylene at various temperatures



As shown above, the consumption of acetylene takes place mainly by the formation of vinyl radical ( $C_2H_3$ ), vinyl acetylene and benzene. Vinyl radical reacts with acetylene to produce vinyl acetylene consuming a significant amount of acetylene. Some of the acetylene is consumed for the growth of higher molecular weight hydrocarbons.

The formation of methane takes place mainly by the reactions of methyl radical with other species. The presence of acetone in acetylene also contributes to the formation of methane. The reactions which contribute to the formation of methane

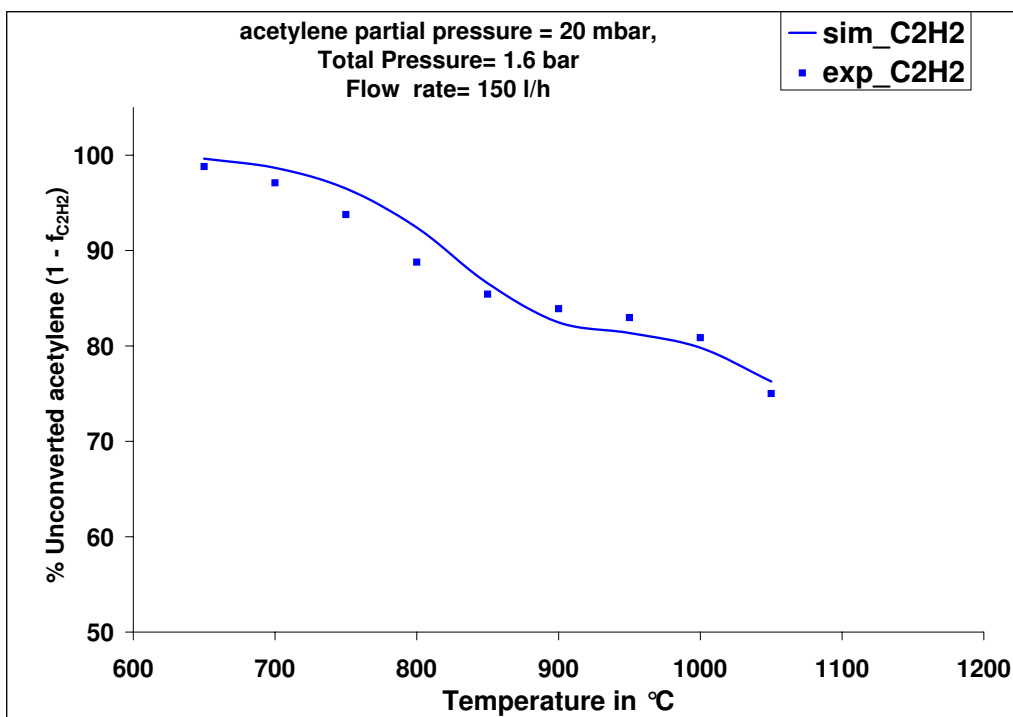


Figure 7.45: Comparison of experimentally observed unconverted percentage of acetylene at the outlet of lab scale tubular flow reactor and simulations with detailed mechanism coupled with DETCHEM 1D model (PLUG) for pyrolysis of acetylene at various temperatures

are summarized below:

$\text{CH}_3 + \text{H} + \text{M} = \text{CH}_4 + \text{M}$	13%
$\text{CH}_3 + \text{C}_2\text{H}_6 = \text{CH}_4 + \text{H}$	38%
$\text{CH}_3 + \text{H}_2 = \text{CH}_4 + \text{C}_2\text{H}_5$	1%
$\text{C}_2\text{H}_4 + \text{CH}_3 = \text{CH}_4 + \text{C}_2\text{H}_3$	2%
$\text{AC}_3\text{H}_4 + \text{CH}_3 = \text{CH}_4 + \text{C}_3\text{H}_3$	4%
$\text{PC}_3\text{H}_4 + \text{CH}_3 = \text{CH}_4 + \text{C}_3\text{H}_3$	9%
$\text{C}_3\text{H}_6 = \text{CH}_4 + \text{C}_2\text{H}_2$	3%
$\text{C}_4\text{H}_4 + \text{CH}_3 = \text{CH}_4 + \text{I-C}_4\text{H}_3$	1%
$\text{C}_5\text{H}_6 + \text{CH}_3 = \text{CH}_4 + \text{C}_5\text{H}_5$	4%
$\text{C}_6\text{H}_6 + \text{CH}_3 = \text{CH}_4 + \text{C}_6\text{H}_5$	1%
$\text{C}_9\text{H}_8 + \text{CH}_3 = \text{CH}_4 + \text{C}_9\text{H}_7$	5%
$\text{CH}_3\text{COCH}_3 + \text{CH}_3 = \text{CH}_4 + \text{CH}_3\text{COCH}_2$	8%

The formation of ethylene takes place mainly by the reactions of vinyl radical with other species. The addition of hydrogen to acetylene also forms significant amount of ethylene. The reactions which contribute to the formation of ethylene are shown

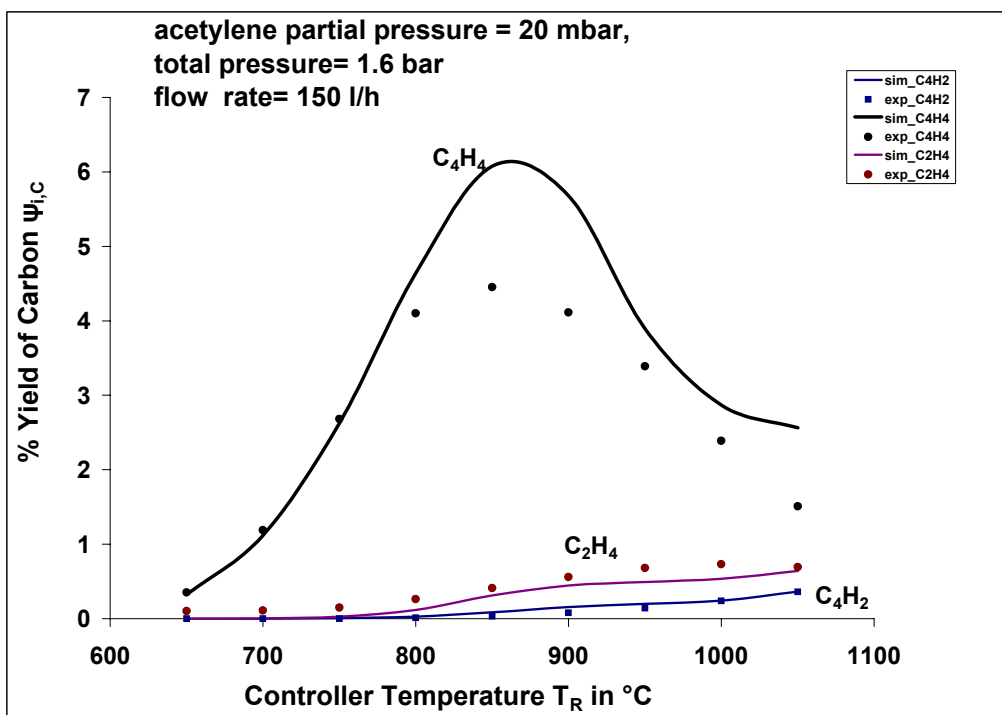
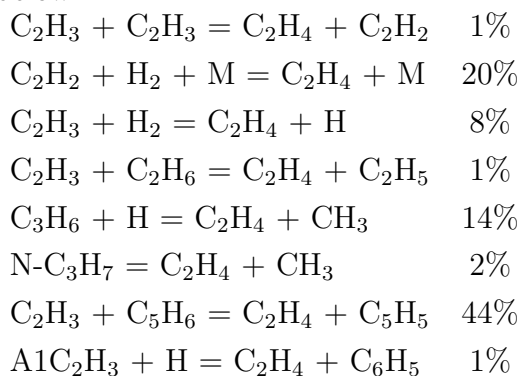
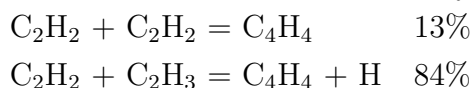


Figure 7.46: Comparison of experimentally observed percentage carbon yields at the outlet of lab scale tubular flow reactor and simulations with the detailed mechanism coupled with DETCHEM 1D model (PLUG) for pyrolysis of acetylene at various temperatures

below:



The formation of vinyl acetylene takes place by the dimerization of two acetylene molecules and the reaction of vinyl radical with acetylene. The following reactions contribute to the formation of vinyl acetylene.



The formation of benzene takes place mainly by the reaction of the acetylene and vinyl acetylene. The other important reaction is the combination of the two propargyl ( $\text{C}_3\text{H}_3$ ) radicals. following reactions:

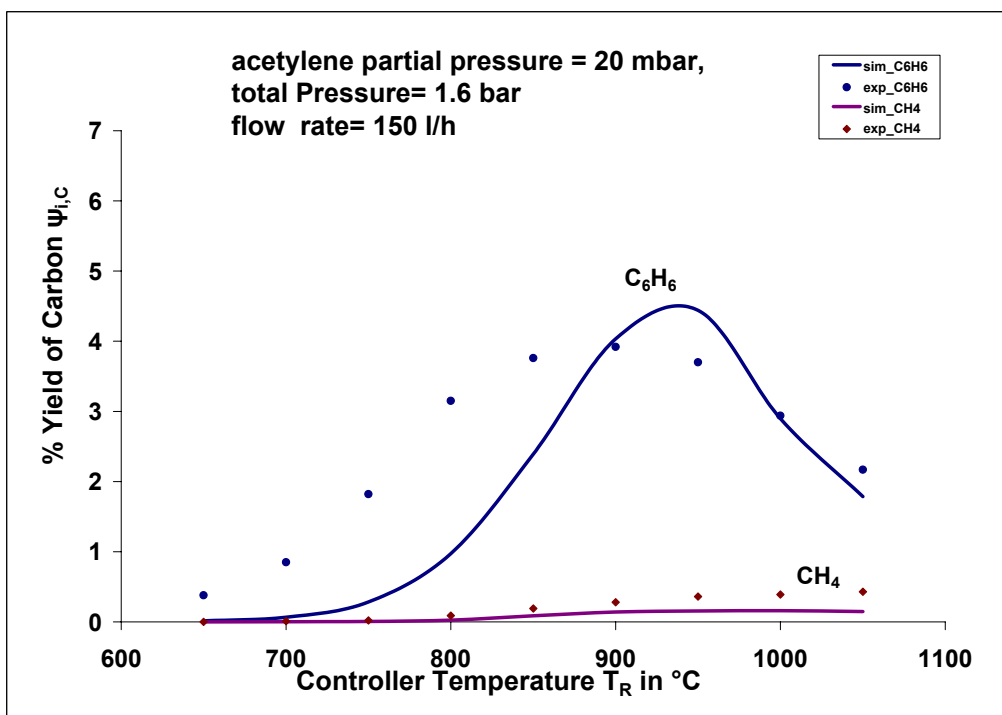
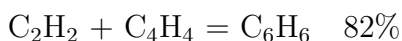
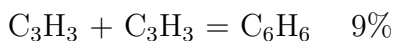


Figure 7.47: Comparison of experimentally observed percentage carbon yields at the outlet of lab scale tubular flow reactor and simulations with the detailed mechanism coupled with DETCHEM 1D model (PLUG) for pyrolysis of acetylene at various temperatures



Sensitivity analysis was also performed at 950 °C and 57 reactions were found to show sensitivity with respect to acetylene. Only 20 selected reactions relatively with higher sensitivities to acetylene are shown in Fig. 7.49

## 7.2.2 Effect of Acetone

The pyrolysis of acetylene in the presence of acetone has not been investigated often so far and specially not for vacuum carburizing conditions of steel. Only few papers were found in the literature which discuss the role of acetone in the pyrolysis of acetylene. The acetone affects the pyrolysis reaction by providing the free radicals even at lower temperatures. In the presence of acetone, the pyrolysis of acetylene is accelerated which is in agreement with the previous experimental studies [53]. As shown in the Fig.7.50, conversion of acetylene is higher in the presence of acetone

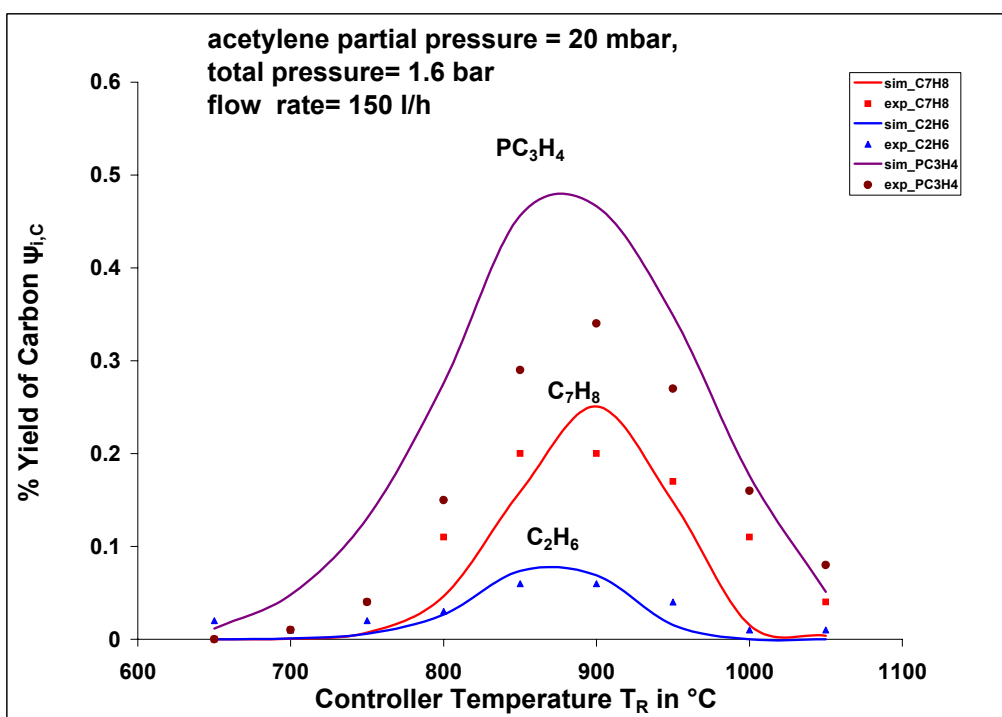


Figure 7.48: Comparison of experimentally observed percentage carbon yields at the outlet of lab scale tubular flow reactor and simulations with the detailed mechanism coupled with DETCHEM 1D model (PLUG) for pyrolysis of acetylene at various temperatures

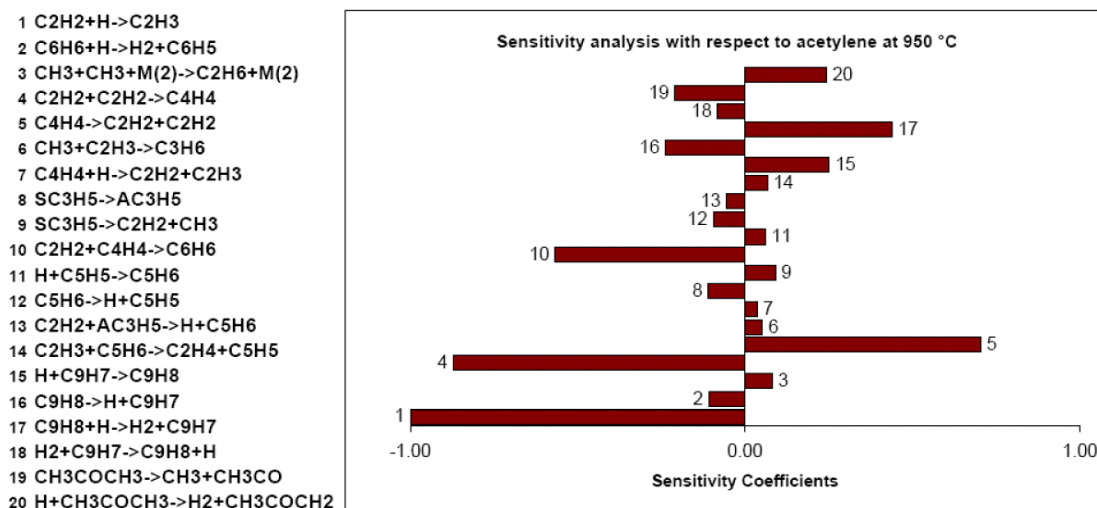


Figure 7.49: Sensitivity analysis at 20 mbar partial pressure of acetylene for 0.7 sec at 950 °C

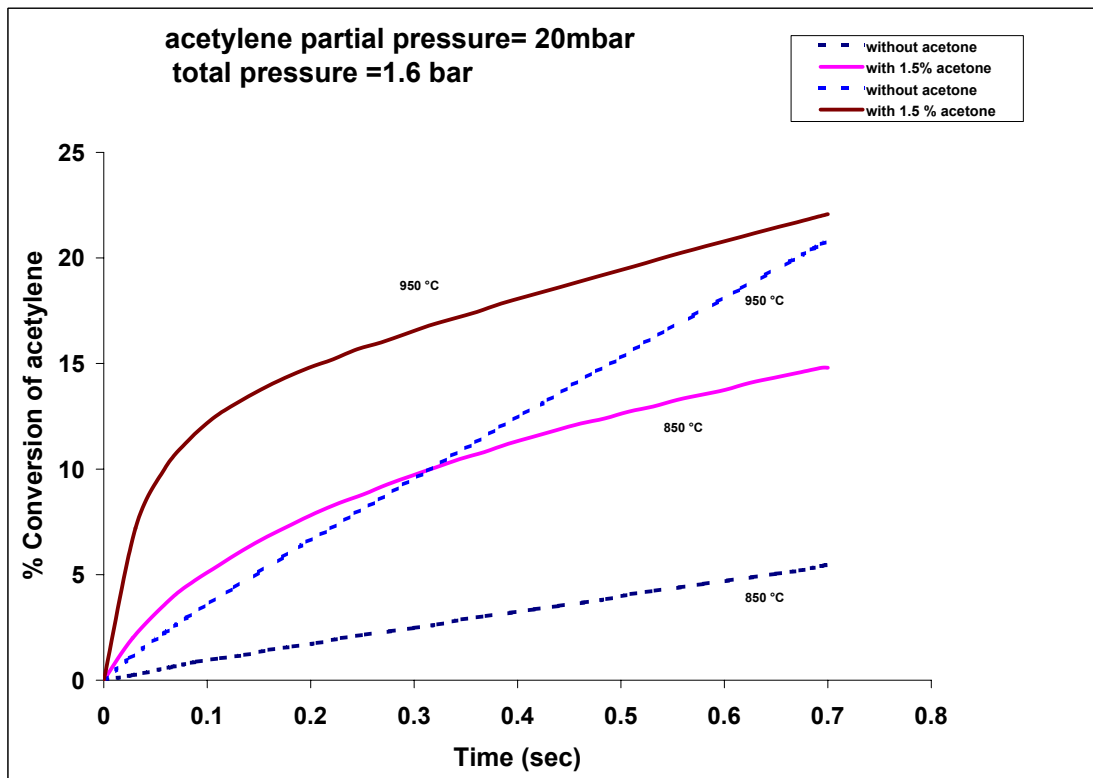
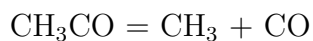
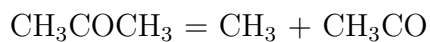


Figure 7.50: Effect of acetone on pyrolysis of acetylene

under the same operating conditions. The effect of acetone on the conversion of acetylene is higher at lower temperature. The sensitivity analysis results shown in Fig. 7.49 reveal that the acetone pyrolysis reaction affects the pyrolysis of acetylene. The dissociation of acetone also leads to the formation of carbon monoxide which is also undesirable for the steel carburizing process. The proposed reactions of formation of carbon monoxide are as follows:



A methyl radical formed by the dissociation of acetone adds to the acetylene to initiate a chain reaction. Further it was found that the prediction of minor species also strongly depend on the presence of acetone. Without assuming small amounts of acetone in acetylene, minor species specially the ethylene and methane are not predicted well.

### 7.2.3 Thermogravimetric reactor

The reactor was numerically simulated using the model of Norinaga and Deutschmann [75]. The model uses the HOMREA[92] software package that performs computational analysis of time-dependent homogeneous reaction systems. The detailed reaction mechanism already discussed in the previous section was used. The HOMREA requires the forward reaction rate parameters and the thermodynamic data for all of the participating species and calculates the backward rate constants for each reversible reaction in the mechanism. The temperature profile in the reactor was not considered. This can be justified to some extent by the fact that temperature in the heated section of the reactor has small variation. Further due to the presence of radiation protection shields at the inlet of the reactor, the temperature is much lower at the inlet section than the middle section and the conversion of acetylene is negligible at these temperatures. So the volume of the reactor simulated for isothermal conditions corresponds to the hot section of the reactor where the variation of the temperature is small allowing to assume it isothermal.

The compounds measured at the exit of the reactor include acetylene, methane, ethylene, vinyl acetylene, diacetylene and benzene. The amount of soot formed was not measured but the hydrocarbons other than the measured were assumed to be converted to soot and carbon yield for these compounds was calculated by material balance. The comparison of experimentally measured yields of carbon and model predictions under vacuum carburizing conditions of steel with acetylene is shown in Figures 7.51 to 7.54. The model predictions are in most cases well in agreement with the experimental measurements.

### 7.2.4 Vacuum reactor

The reactor was numerically simulated using the HOMREA software package as already described in the previous chapter in case of propane pyrolysis using the detailed reaction mechanism. The results of simulations were compared with the experimental results. The simulation and experimental results comparisons are shown in Fig.7.55 to Fig.7.56. The comparison shows that the simulation results are well in agreement with the experimental results.

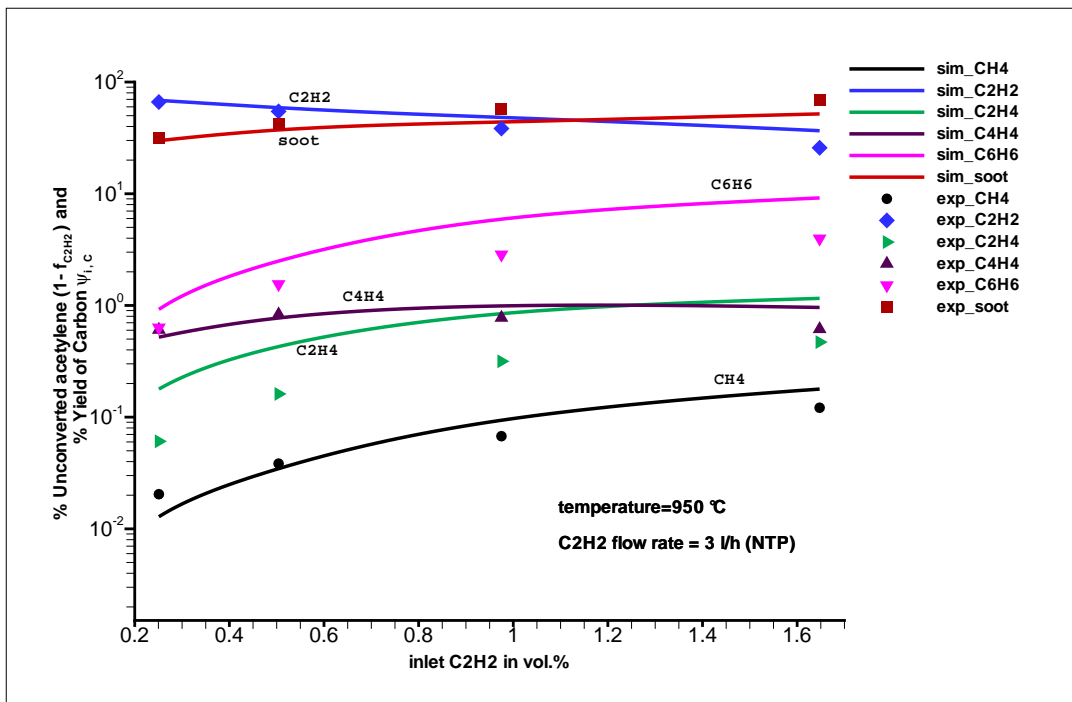


Figure 7.51: Comparison of experimental measurements for percentage carbon yields at the outlet of thermogravimetric reactor and simulations with detailed mechanism

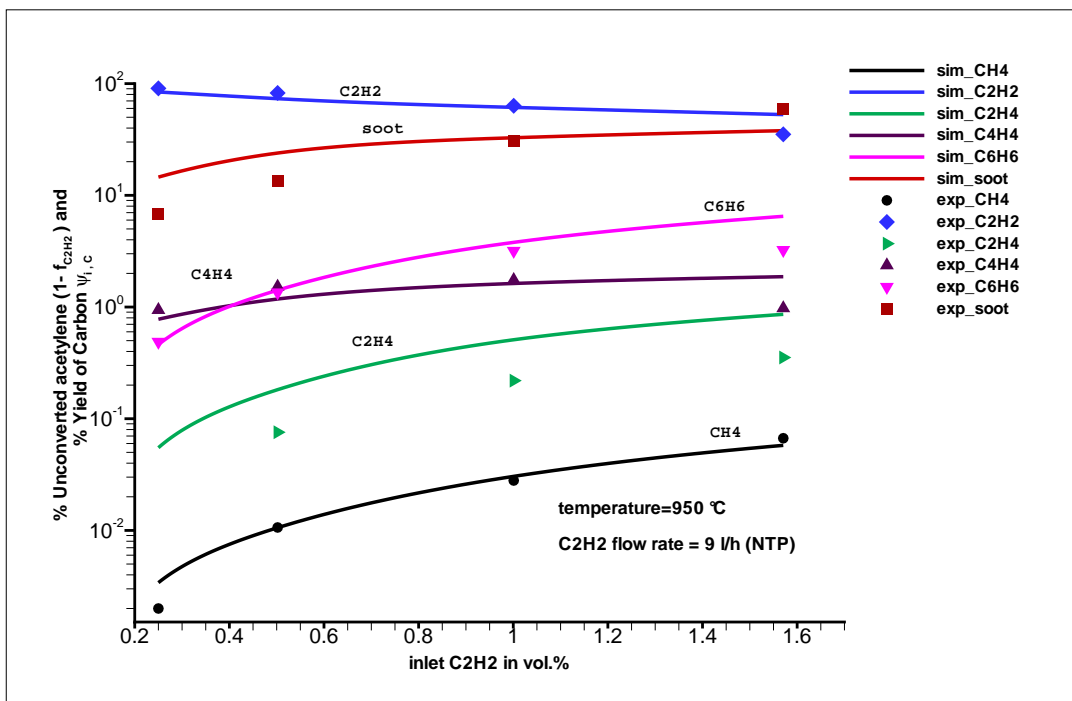


Figure 7.52: Comparison of experimental measurements for percentage carbon yields at the outlet of thermogravimetric reactor and simulations with detailed mechanism



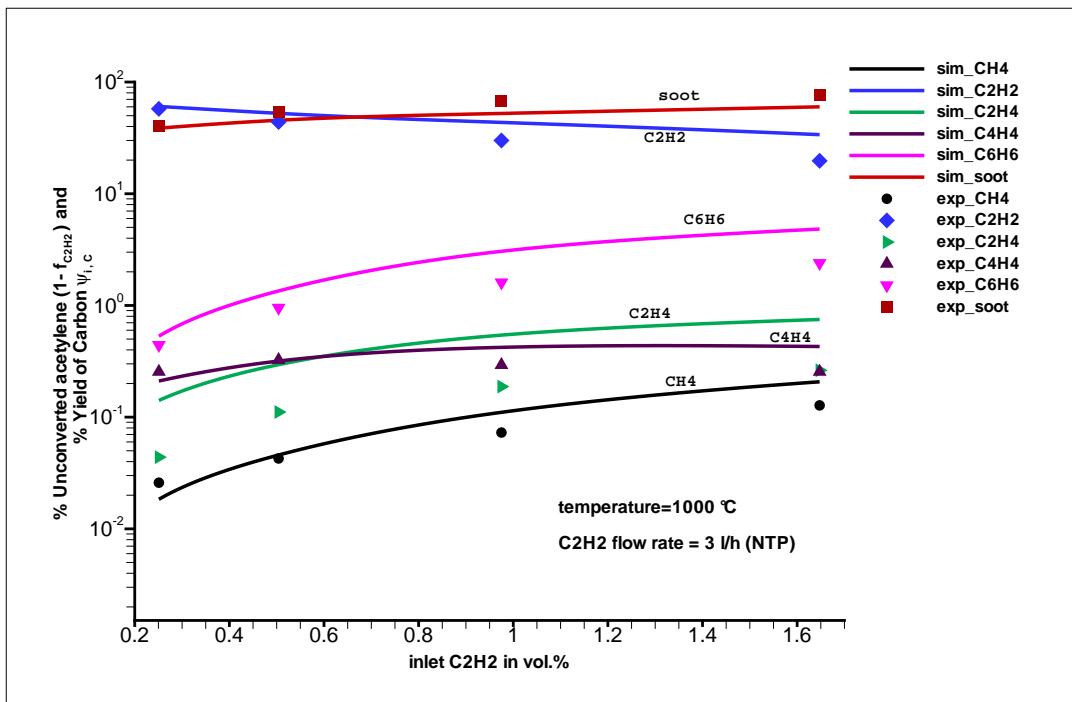


Figure 7.53: Comparison of experimental measurements for percentage carbon yields at the outlet of thermogravimetric reactor and simulations with detailed mechanism

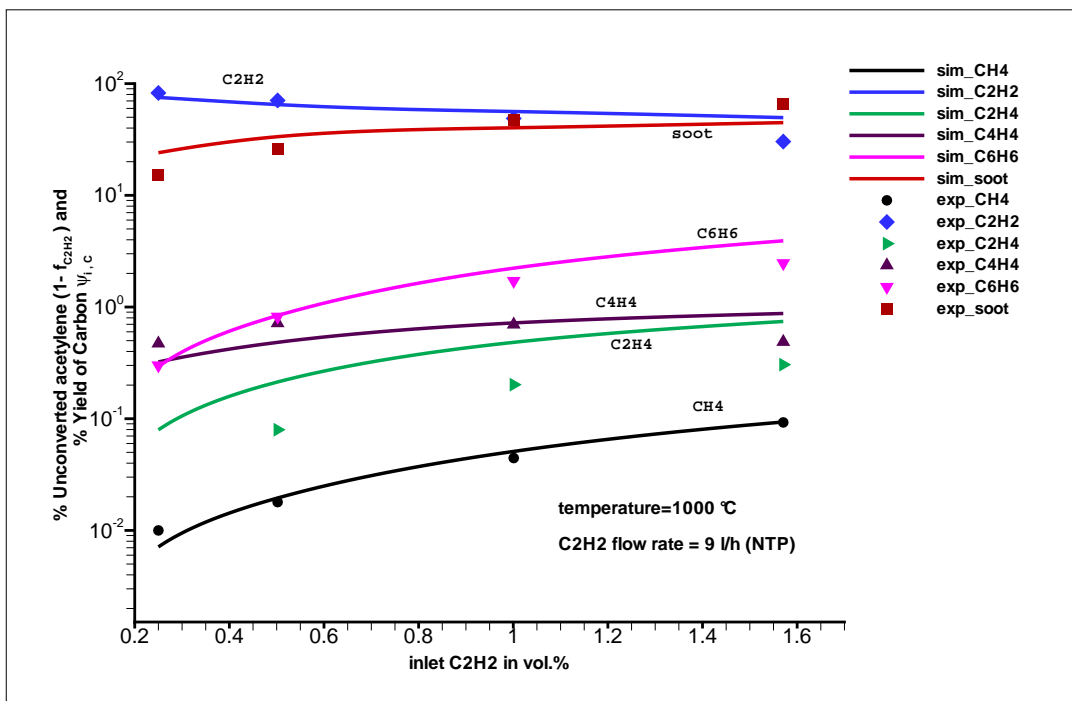


Figure 7.54: Comparison of experimental measurements for percentage carbon yields at the outlet of thermogravimetric reactor and simulations with detailed mechanism

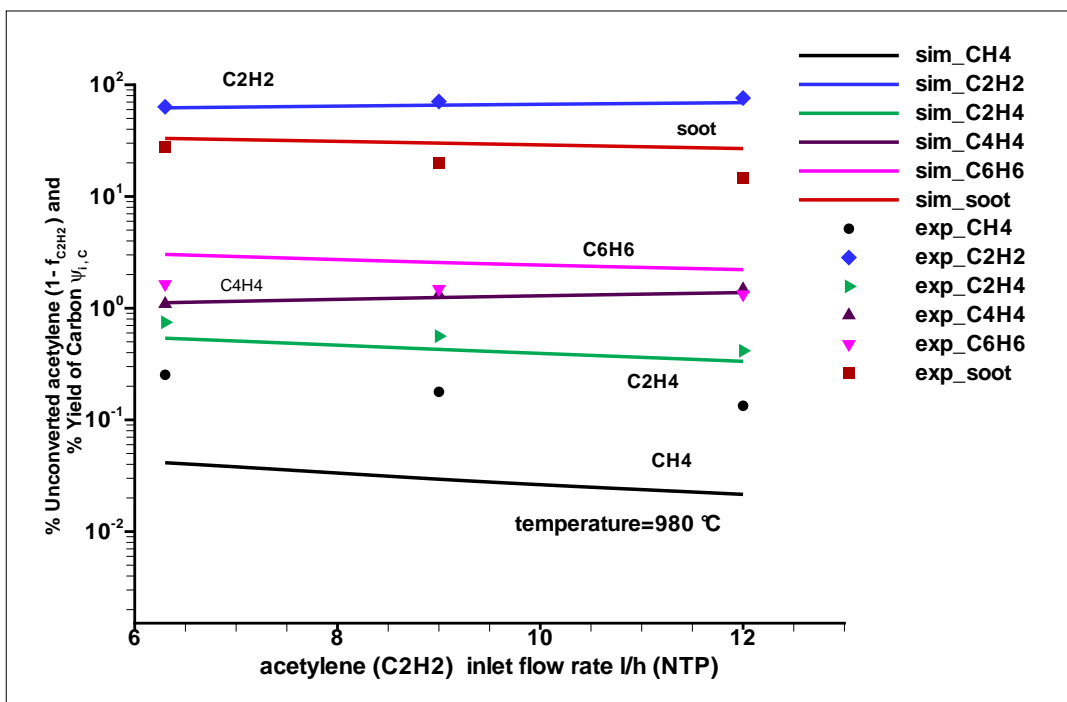


Figure 7.55: Comparison of experimental measurements for percentage carbon yields at the outlet of bench scale vacuum reactor operated at a pressure of 10 mbar and simulations with detailed mechanism for pyrolysis of acetylene at  $980\text{ }^\circ\text{C}$

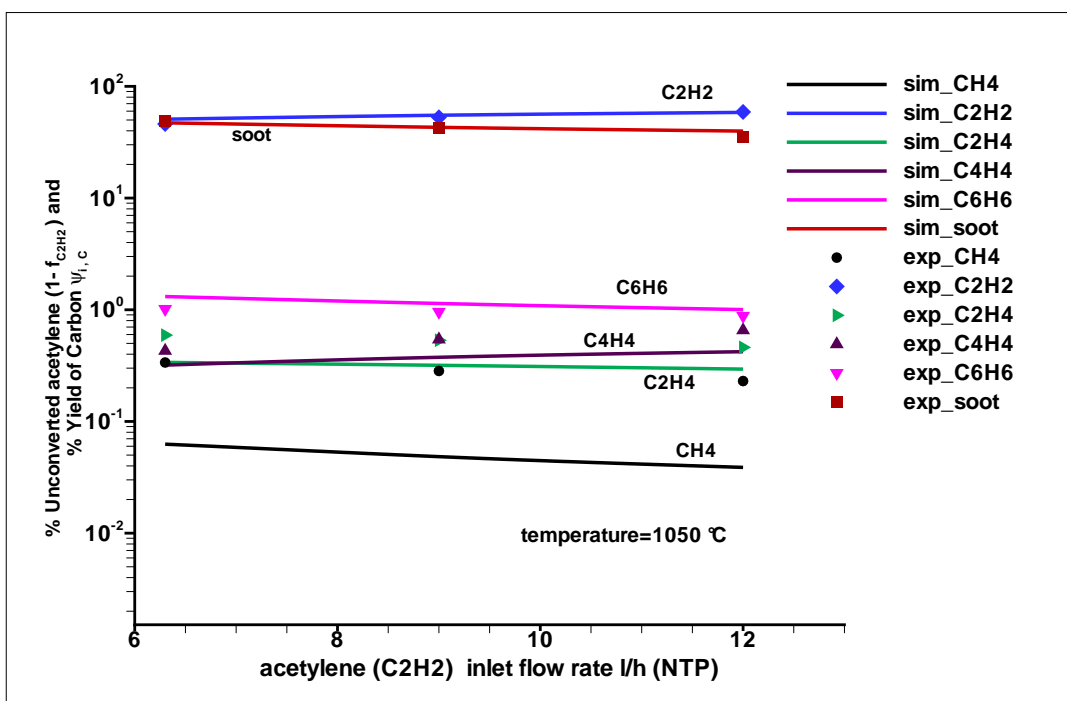


Figure 7.56: Comparison of experimental measurements for percentage carbon yields at the outlet of bench scale vacuum reactor operated at a pressure of 10 mbar and simulations with detailed mechanism for pyrolysis of acetylene at  $1050\text{ }^\circ\text{C}$

# Chapter 8

## Summary and Outlook

Carburizing is the case hardening process of steel by adding carbon to the surface of steel and letting it diffuse into the steel. The conventional process of steel carburizing is carried out at atmospheric pressures. A substantial body of literature can be found on this process. The hardening process can be controlled via the gas phase composition. Supposing a thermodynamic equilibrium between the gas phase and the carbon activity which depends on the carbon content of the steel, sensors can be used to measure the carbon potential in the gas atmosphere, e.g. via the concentration of carbon dioxide, water vapour (dew point) or oxygen. The carbon concentration on the surface of steel indirectly can be determined by the carbon potential in the gas phase. So the process can be regulated by the carbon potential measurement. There exists models for diffusion of carbon within the steel from which one can predict the carbon profile in the steel. The steel hardness is a function of carbon profile so the desired hardness can be achieved in this way.

On the other hand the conventional carburizing process is bound by some limitations. The process is accompanied by the deposition of soot and higher hydrocarbons on the furnace walls. Further the process does not provide the uniformity and repeatability required for precision parts. Blind holes are difficult to carburize. However the vacuum carburizing process of steel does not have these limitations and the formation of soot is also lowered specially when acetylene is used as a carburizing gas. But the control of the process like conventional carburizing is difficult due to the non existence of thermodynamic equilibrium. The pyrolysis of propane or acetylene can produce large number of other hydrocarbon products leading to soot during carburizing of steel. Although there are some efforts to develop sensors to measure the carbon potential of the carburizing atmosphere but there is none available on commercial scale. The investigations on vacuum carburizing process of steel published in the literature are not sufficient to understand the process completely. The process conditions have not been thoroughly investigated. However it is important to inves-

tigate the process conditions in order to understand and optimize the steel vacuum carburizing process. The pyrolysis of carburizing gas e.g. propane or acetylene is a complex process which needs to be addressed as a first step in order to develop further understanding of the carburisation process. Investigations on the pyrolysis of propane and acetylene covering operating parameters in the regime of vacuum carburizing process are not frequently published. It is hard to find computational fluid dynamics models or detailed chemistry models which can describe the pyrolysis of acetylene or propane under the vacuum carburizing conditions of steel.

In the present work two different approaches have been used to model the pyrolysis of propane and acetylene under vacuum carburizing conditions of steel. One approach is based on formal or operational kinetic mechanisms together with CFD computational tools. The other approach is based on detailed chemistry with simplified or ideal flow models. Experimental data from investigations on vacuum carburizing conducted at the Engler-Bunte-Institut were used to validate the modeling results.

Pyrolysis of propane was modeled with operational/formal kinetics as well as with detailed kinetics under the vacuum carburizing conditions of steel. The formal kinetics can be used with the computational fluid dynamics (CFD) codes which solve the Navier Stokes Equation. Since the pyrolysis of propane follows a very complex scheme of reactions in reality, the formal kinetics have limited applicability. It is difficult to fit the kinetic parameters with the reaction network even being limited to only few species and reactions. The models which are based on the operational kinetics are not considered very reliable to predict the data under other operating conditions or even when the residence times are varied considerably under the same operating conditions. The main benefit of the formal kinetics is their low computational time requirement which makes it feasible to couple it with CFD codes so that the complex flow processes can be modeled. The formal kinetic mechanism developed at Engler-Bunte-Institut by Bajohr [48] was coupled to the CFD code Fluent. The measured temperature profile was considered when simulating the reactor. The simulations results were compared with the experimental data and this comparison was not satisfactory for all the species included in the mechanism. The model overpredicts methane and underpredicts hydrogen specially at higher temperatures. Also the model does not describe the formation of benzene and soot ( $C_{(s)}$ ).

The other approach used was based on detailed kinetics. A detailed kinetics mechanism developed by Norinaga and Deutschmann [75] for the pyrolysis of light hydrocarbons such as acetylene, ethylene and propylene was selected. The mechanism

was coupled with 1-D and 2-D models of DETCHEM software and with 0D model of HOMREA software. More computational time was required for 2-D model while 1-D and 0D models computations were relatively very fast. The developed models explain very well the gas composition resulting from the homogeneous pyrolysis of propane over a wide range of temperature. The experimental data of three different reactors including a laboratory scale tubular flow reactor, thermogravimetric reactor and bench scale reactor was described by the developed model. The comparison of simulations and experimental results was found good. The same kinetic parameters were used to simulate three different reactors. The reactions which contribute to the formation and consumption of major species were identified. Sensitivity analysis also reveals the importance of different reactions under the typical selected operating conditions.

On the industrial level, the interest in use of acetylene instead of propane as a carburizing gas is growing due to its ability to carburize complex shapes with uniformity and low soot formation. The mechanism of acetylene pyrolysis at the elementary level as described in literature is controversial among various investigators. To model the pyrolysis of acetylene, a formal kinetic mechanism developed at the Engler-Bunte-Institut by Graf [2] was used with CFD code Fluent. This mechanism consists of only 7 species and 9 reactions. For higher residence times and at higher temperature the species  $\text{CH}_4$ ,  $\text{C}_2\text{H}_4$  and  $\text{C}_4\text{H}_4$  are present in very small amounts (<1%) on the reactor exit. The accurate experimental measurements are also challenging for such minor species when longer residence times are encountered. The developed model can describe the experimental data successfully over the range of parameters used for vacuum carburizing investigations. Acetone can be present in small amounts in acetylene as an impurity. However the model does not describe the effect of acetone presence in acetylene.

The detailed mechanism of Norinaga and Deutschmann was also used for modeling the pyrolysis of acetylene with 1-D model of DETCHEM and 0D model of HOMREA. The comparison of experimental and simulations results were found in agreement except diacetylene ( $\text{C}_4\text{H}_2$ ) at higher temperatures. The model overpredicts the formation of diacetylene. So arrhenius parameters for few reactions were adjusted to reduce the formation of diacetylene. One important thing which was observed was the effect of acetone presence in the acetylene. The mechanism also contains the reactions of acetone pyrolysis. The prediction of minor species was not

possible without assuming the presence of small amounts (1.5%) of acetone in acetylene. The effect of acetone presence on pyrolysis of acetylene was also predicted. The results show that in the presence of acetone the pyrolysis of acetylene is accelerated. The effect of acetone presence in acetylene has not been thoroughly investigated and only few papers can be found in the literature. Further investigations are being carried out at Engler-Bunte-Institut to understand the effect of acetone presence and surface reactions.

The use of such a detailed mechanism with CFD code FLUENT was not possible. The detailed kinetics mechanism should be reduced to certain limit ( e.g 50 species in case of FLUENT software package) due to the available computational hardware limitations and to converge the solution. Although the sensitivity analysis and the reaction flow analysis reveal the important reactions and species in the mechanism it is very laborious to reduce the mechanism manually based on these results. There are some efforts on the development of such software codes which can be used to reduce the detailed mechanisms but still their use is not in common practice. However the approach of using reduced mechanisms with CFD codes will be very useful to advance the research in this field.

Further work is required on experimental as well as on modeling side to include the heterogeneous reactions. After measuring the kinetic parameters for these reactions the developed models can be extended to predict the carbon flux on the surface of steel. However the models describe successfully the homogeneous pyrolysis process under the technical operating conditions of steel.

# Zusammenfassung und Ausblick

Das Aufkohlen ist der Prozessschritt des Einsatzhärtens, bei dem Kohlenstoff der Stahloberfläche hinzugefügt wird. Der herkömmliche Prozess des Stahlaufkohlens wird bei atmosphärischem Druck durchgeführt. Dieser Prozess ist ausführlich erforscht und modelliert worden, und er lässt sich über das Kohlenstoffpotential in der Gasatmosphäre steuern, weil er sich im thermodynamischen Gleichgewicht befindet. Dabei werden die Konzentration des Kohlendioxids, des Wasserdampfs (Taupunkt) oder teilweise auch des Sauerstoffes mit Sensoren gemessen. Die Kohlenstoffkonzentration auf der Oberfläche des Stahls kann dann durch das Kohlenstoffpotential in der Gasphase berechnet werden. Es existieren Modelle für die Diffusion des Kohlenstoffs im Stahl, mit denen das Kohlenstoffprofil im Stahl vorhergesagt werden kann. Die Stahlhärte ist eine Funktion des Kohlenstoffprofils, also kann auf diese Art die gewünschte Härte eingestellt werden.

Der konventionelle Aufkohlungsprozess hat jedoch einige Nachteile, und er unterliegt einigen Beschränkungen, z. B. bilden sich Ruß und höhere Kohlenwasserstoffe auf den Ofenwänden. Des Weiteren liefert der Prozess nicht die Gleichförmigkeit und die Wiederholbarkeit, die für Präzisionsteile erforderlich sind. Sacklöcher sind schwierig aufzukohlen. Der Niederdruckaufkohlungsprozess unterliegt nicht diesen Beschränkungen. Er hat die Fähigkeit, Stahlteile mit Sacklöchern aufzukohlen und liefert die benötigte Gleichförmigkeit und Wiederholbarkeit. Die Ablagerung von Ruß wird speziell im Fall von Ethin als Aufkohlungsgas gesenkt. Aber die Steuerung des Prozesses ist im Vergleich zum konventionellen Gasaufkohlen schwieriger, da sich der Prozess nicht im thermodynamischen Gleichgewicht befindet. Obgleich es Bemühungen gibt, Sensoren zu entwickeln, um das Kohlenstoffpotential der Aufkohlungsatmosphäre zu messen, sind diese Sensoren noch nicht serienreif. Bisher sind in der Literatur zum Niederdruckaufkohlungsprozess sehr wenige Angaben im Vergleich zum konventionellen Gasaufkohlen zu finden. Die Prozessbedingungen sind noch nicht gänzlich erforscht worden. Jedoch ist es wichtig, die Prozessbedingungen zu erforschen, um den Niederdruckstahlaufkohlungsprozess zu verstehen und zu optimieren. Die Pyrolyse der Aufkohlungsgase, wie z.B. Propan

oder Ethin, ist ein komplexer Mechanismus, der in einem ersten Schritt verstanden werden muss, um ein Verständnis über den Prozess zu entwickeln. Obgleich die Pyrolyse von Propan und des Ethin bereits untersucht wurden, sind die Betriebsparameter der vorhergehenden Untersuchungen aus der Literatur selten denen des Niederdruckaufkohlungsprozesses ähnlich. Es ist schwierig, numerische Strömungsmodelle oder detaillierte Kinetikmodelle zu finden, die die Pyrolyse von Ethin oder Propan unter den Bedingungen des Niederdruckaufkohls beschreiben können.

In dieser Arbeit werden zwei Ansätze verfolgt, um die Pyrolyse von Propan und Ethin unter den Bedingungen des Niederdruckaufkohls zu modellieren. Ein Ansatz basiert auf formalen, anwendungsorientierten kinetischen Mechanismen, die mit CFD Berechnungswerkzeugen gekoppelt werden. Der andere Ansatz basiert auf detaillierten kinetischen Ansätzen mit vereinfachten oder idealen Strömungsmodellen. Die experimentellen Daten der vorhergehenden Untersuchungen zum Niederdruckaufkohlen am Engler Bunte Institut wurden verwendet, um die Modellierung zu validieren.

Die Propanpyrolyse wurde mit einer Formalkinetik sowie mit detaillierten kinetischen Ansätzen unter den Bedingungen des Niederdruckaufkohls modelliert. Da die Propanpyrolyse in Realität einem sehr komplexen Reaktionsschema folgt, ist die Anwendbarkeit der formalkinetischen Ansätze begrenzt. Es ist schwierig, die kinetischen Parameter anzupassen, da das Reaktionsnetz auf nur wenige Spezies und Reaktionen begrenzt ist. Modelle, die auf formalkinetischen Ansätzen basieren, eignen sich nicht, um Ergebnisse für andere Betriebsbedingungen vorauszusagen und auch nicht für beträchtlich veränderte Verweilzeiten bei sonst gleichen Betriebsbedingungen. Der Hauptnutzen der formalkinetischen Ansätze ist ihr geringer Berechnungsaufwand, der es möglich macht, sie mit CFD-Modellen zu koppeln und damit komplizierte Strömungsprozesse zu modellieren. Angewendet wurde der am Engler Bunte Institut von Bajohr [48] entwickelte formalkinetische Mechanismus. Für die Simulation des Reaktors wurde ein gemessenes Temperaturprofil vorgegeben. Die Simulationsergebnisse wurden mit den experimentellen Daten verglichen. Dieser Vergleich war nicht für alle Spezies zufriedenstellend, die im Mechanismus berücksichtigt wurden. Das Modell berechnet besonders bei höheren Temperaturen den Methananteil zu hoch und den Wasserstoffanteil zu niedrig. Des Weiteren beschreibt das Modell nicht die Bildung von Benzol und von Ruß.

Als detailliertes Kinetikmodell wurde das von Norinaga und Deutschmann [75] für



die Pyrolyse von leichten Kohlenwasserstoffen wie Ethin, Ethen und Propen ausgewählt. Der Mechanismus wurde mit 1-D und 2-D Modellen der Software DETCHEM und dem 0-D Modell der Software HOMREA verbunden. Für das 2-D Modell wurde viel Rechnerzeit benötigt, während die Berechnung der 1-D und der 0-D Modelle verhältnismäßig schnell war. Das Modell beschreibt die aus der homogenen Pyrolyse von Propan resultierende Gaszusammensetzung über einen weiten Temperaturbereich sehr gut. Die experimentellen Ergebnisse von drei unterschiedlichen Reaktoren (Strömungsrohr im Labormaßstab, Thermowaage und halbtechnischer Reaktor) wurden unter Verwendung stets der gleichen kinetischen Parameter mit guter Übereinstimmung beschrieben. Die Reaktionen, die zur Bildung und zum Verbrauch der Hauptkomponenten beitragen, wurden identifiziert. Durch eine Sensitivitätsanalyse wurde der Einfluss der unterschiedlichen Reaktionen unter den typischen Betriebsbedingungen bestimmt.

In der industriellen Anwendung wächst das Interesse am Gebrauch von Ethin anstelle von Propan als Aufkohlungs gas auf Grund seiner Fähigkeit, komplizierte Geometrien gleichförmig und mit geringerer Rußbildung aufzukohlen. Der Mechanismus der Ethinpyrolyse auf der Basis von Elementarreaktionen ist noch strittig. Zunächst wurde der am Engler Bunte Institut von Graf [2] entwickelte, formalkinetische Ansatz mit einer numerischen Strömungssimulation gekoppelt. Dieser Mechanismus besteht aus nur 7 Spezies und 9 Reaktionen. Für höhere Verweilzeiten und bei höheren Temperaturen sind die Spezies  $\text{CH}_4$ ,  $\text{C}_2\text{H}_4$  und  $\text{C}_4\text{H}_4$  im Reaktorausgang in nur sehr kleinen Anteilen ( $<1\%$ ) zu finden. Die genaue experimentelle Bestimmung dieser Nebenkomponten ist für große Verweilzeiten sehr anspruchsvoll. Das entwickelte Modell kann die experimentellen Daten über einen weiten Parameterbereich der Niederdruckaufkohlungsuntersuchungen erfolgreich beschreiben. Aceton kann in kleinen Mengen in Ethin als Verunreinigung vorhanden sein. Der Effekt der Acetonanwesenheit in Ethin auf die Pyrolyse wird jedoch von diesem Modell noch nicht berücksichtigt.

Der detaillierte Mechanismus von Norinaga und Deutschmann wurde auch für das Modellieren der Pyrolyse von Ethin mit dem 1-D Modell der Software DETCHEM und dem 0-D Modell der Software HOMREA benutzt. Beim Vergleich der experimentellen mit den Simulationsergebnissen wurde eine gute Übereinstimmung mit Ausnahme von Diacetylen ( $\text{C}_4\text{H}_2$ ) bei höheren Temperaturen gefunden. Nach dem Modell wird zu viel Diacetylen gebildet. Deshalb wurden die Arrhenius-Parameter für einige Reaktionen verändert, um die Bildung von Diacetylen zu verringern. Als

große Einflussquelle wurde der Effekt der Acetonanwesenheit in Ethin gefunden. Der Mechanismus enthält auch die Reaktionen der Acetonpyrolyse. Eine Vorhersage der Konzentrationen der Nebenkomponten war ohne das Vorhandensein von etwas Aceton (1,5 %) nicht möglich. Die Ergebnisse zeigen, dass in Anwesenheit von Aceton die Pyrolyse des Ethins beschleunigt wird. Der Effekt der Acetonanwesenheit in Ethin ist noch nicht umfassend erforscht worden, und es konnten darüber nur wenige Beiträge in der Literatur gefunden werden. Weitere Untersuchungen werden Engler Bunte am Institut durchgeführt, um den Effekt der Acetonanwesenheit und der Oberflächenreaktionen zu verstehen.

Der detaillierte Mechanismus konnte mit den vorhandenen Möglichkeiten nicht mit einer detaillierten numerischen Strömungssimulation gekoppelt werden. Der detaillierte Kinetikmechanismus sollte deshalb und um die Konvergenz der Lösung zu gewährleisten, reduziert werden (z.B. 50 Spezies im Falle des Softwarepakets FLUENT). Obgleich die Sensitivitätsanalyse und die Reaktionsflussanalyse die wichtigen Reaktionen und Spezies im Mechanismus aufzeigen, ist es sehr arbeitsintensiv, den Mechanismus manuell auf Basis der Ergebnisse zu vereinfachen. Es gibt zwar Bemühungen, Software-Codes für die Vereinfachung detaillierter Kinetiken zu entwickeln, sie sind aber bisher schlecht verfügbar. Jedoch wäre die Verwendung solcher vereinfachter Mechanismen in Verbindung mit numerischen Strömungssimulationen sehr hilfreich, um die Forschung auf diesem Gebiet voranzubringen.

Weitere Arbeiten sind sowohl auf der experimentellen als auch auf der Modellierungsseite nötig, um die heterogenen Reaktionen einzuschließen. Nach der Messung der kinetischen Parameter für diese Reaktionen können die vorhandenen Modelle erweitert werden, um den Aufkohlungsstrom auf der Stahloberfläche berechnen zu können. Bisher können die Modelle den homogenen Pyrolyseprozess unter den Betriebsbedingungen der technischen Niederdruckstahlaufkohlung erfolgreich beschreiben.

# Bibliography

- [1] C. Stickels. Overview of Carburizing Processes and Modeling. *Carburizing: Processing and Performance*, pages 1–9, 1989.
- [2] F. Graf. *Aufkohlungs- und Pyrolyseverhalten von  $C_2H_2$  bei der Vakuumaufkohlung von Stahl*. PhD thesis, University of Karlsruhe, Faculty of Chemical Engineering, 2007.
- [3] Metals Handbook. vol. 4. *ASM International*, pages 573–574, 1991.
- [4] R. Collin and D. Gunnarson, S.and Thulin. A mathematical model. for predicting carbon concentration profiles of gas-carburized steel. *Iron Steel*, 210:785–789, 1972.
- [5] J.I. Goldstein and A.E. Moren. Diffusion Modeling of the Carburization Process. *Metall. Trans. A*, 9(11):1515–1525, 1978.
- [6] H. Jiménez, MH Staia, and ES Puchi. Mathematical modeling of a carburizing process of a SAE 8620H steel. *Surface & Coatings Technology*, 120:358–365, 1999.
- [7] E. Gianotti. Algorithm for carbon diffusion computation in a vacuum furnace. Experimental methods predict carburizing time. *Heat Treating Progress*, 2(8):27–30, 2002.
- [8] G.S. Gupta, A. Chaudhuri, and PV Kumar. Modelling, simulation, and graphical user interface for industrial gas carburising process. *Materials Science and Technology*, 18(10):1188–1194, 2002.
- [9] P. Jacquet, D.R. Rouse, G. Bernard, and M. Lambertin. A novel technique to monitor carburizing processes. *Materials Chemistry and Physics*, 77(2):542–551, 2003.

- [10] T. Turpin, J. Dulcy, and M. Gantois. Carbon Diffusion and Phase Transformations during Gas Carburizing of High-Alloyed Stainless Steels: Experimental Study and Theoretical Modeling. *Metallurgical and Materials Transactions A*, 36(10):2751–2760, 2005.
- [11] H.W. Westernen. Development of vacuum carburizing. *Metallurgia and Metal Forming*, 39(11):390–393, 1972.
- [12] W.J. Doelker. Vacuum carburizing. *Metal Progress*, 111(5):50–56, 1977.
- [13] M. Sugiyama, K. Ishikawa, and H. Iwata. Vacuum carburizing with acetylene. *Advanced Materials & Processes*, 155(4):29–33, 1999.
- [14] W. Gräfen and B. Edenhofer. Acetylene low-pressure carburising: a novel and superior carburising technology. *Heat Treat. Met*, 4:79, 1999.
- [15] M. Lohrmann, W. Grafen, D. Herring, and J. Greene. Acetylene vacuum carburising(AvaC) as the key to the integration of the case-hardening process into the production line. *Heat Treatment of Metals(UK)*, 29(2):39–43, 2002.
- [16] J. Greene. Clean vacuum carburizing using low-pressure acetylene. In *Surface Engineering: Coatings and Heat Treatments, Proceedings of the 1st ASM International Surface Engineering Congress and the 13th International Federation for Heat Treatment and Surface Engineering Congress, Columbus, OH, United States, Oct. 7-10*, pages 58–62, 2003.
- [17] F.S. Chen and L.D. Liu. Deep-hole carburization in a vacuum furnace by forced-convection gas flow method. *Materials Chemistry and Physics*, 82(3):801–807, 2003.
- [18] Y. Shimosato. Low pressure vacuum carburizing and accelerated gas carburizing. In *Heat Treating and Surface Engineering, Proceedings of the 22nd Heat Treating Society Conference and the 2nd International Surface Engineering Congress, Indianapolis, IN, United States, Sept. 15-17, 2003*, pages 267–270, 2003.
- [19] F. Graf, S. Bajohr, and R. Reimert. Pyrolysis of propane during vacuum carburizing of steel. *HTM, Härtereitechnische Mitteilungen*, 58(1):20–23, 2003.
- [20] H. Iwata. Acetylene vacuum carburizing. *Cailiao Rechuli Xuebao*, 25(5, Pt. 1):370–374, 2004.

- [21] P. Kula, R. Pietrasik, and K. Dybowski. Vacuum carburizing-process optimization. *Journal of Materials Processing Technology*, 164-165:876–881, 2005.
- [22] H. Iwata. Advanced acetylene vacuum carburizing. *IHI Engineering Review*, 38(2):83–88, 2005.
- [23] F.J. Otto and D.H. Herring. Vacuum carburizing of aerospace and automotive components. *Heat Treating Progress*, 5(1):33–37, 2005.
- [24] C.A. Trujillo, F. Graf, S. Bajohr, and R. Reimert. Catalytic treatment of vacuum carburizing off gas. *Chemical Engineering & Technology*, 29(3):390–394, 2006.
- [25] A.M. Benson. Pyrolysis of propane in a shock tube. *AIChE Journal*, 13(5):903–908, 1967.
- [26] J.N. Bradley. Single-pulse shock tube studies of hydrocarbon pyrolysis. part 7. pyrolysis of propane. *Journal of the Chemical Society, Faraday Transactions 1: Physical Chemistry in Condensed Phases*, 75(12):2819–2826, 1979.
- [27] C.C. Chiang and G.B. Skinner. Resonance absorption measurements of atom concentrations in reacting gas mixtures. Pyrolysis of propane and deuteromethane behind shock waves. *Symposium (International) on Combustion, [Proceedings]*, 18th:915–920, 1981.
- [28] M.Z. Al-Alami and J.H. Kiefer. Shock-tube study of propane pyrolysis. rate of initial dissociation from 1400 to 2300 K. *Journal of Physical Chemistry*, 87(3):499–506, 1983.
- [29] E.N. Wami. Pyrolysis of propane at reflected shock-wave temperatures from 1300 to 2700 K. *Chemical Engineering & Technology*, 17(3):195–200, 1994.
- [30] B.L. Crynes and L.F. Albright. Pyrolysis of propane in tubular flow reactors. kinetics and surface effects. *Industrial & Engineering Chemistry Process Design and Development*, 8(1):25–31, 1969.
- [31] J.J. Dunkleman. *Kinetics and surface effects of the pyrolysis of ethane and propane in Vycor, Incoloy, and stainless steel tubular flow reactors from 750 Deg to 900 DegC*. PhD thesis, 1976.
- [32] J.J. Dunkleman and L.F. Albright. Pyrolysis of propane in tubular flow reactors constructed of different materials. *ACS Symposium Series*, 32(Ind. Lab. Pyrolyses.):261–273, 1976.

- [33] M. Koenig, T. Reiher, D. Radeck, and S. Nowak. Modeling of propane pyrolysis. part 1. Formulation of reaction set, implementation and application of propane pyrolysis at  $T < 550$  °C. *Chemische Technik (Leipzig, Germany)*, 32(1):29–33, 1980.
- [34] D.J. Hautman, R.J. Santoro, F.L. Dryer, and I. Glassman. An overall and detailed kinetic study of the pyrolysis of propane. *International Journal of Chemical Kinetics*, 13(2):149–172, 1981.
- [35] G. Bozga, J. Towfighi, and O. Floarea. Optimal temperature profiles for propane pyrolysis in tubular reactors. *Revue Roumaine de Chimie*, 33(1):87–96, 1988.
- [36] F. Billaud. Thermal decomposition of propane: an original method of temperature calibration in a plug flow pyrolysis apparatus. *Journal of Analytical and Applied Pyrolysis*, 21(1-2):15–25, 1991.
- [37] S.K. Layokun and D.H. Slater. Mechanism and kinetics of propane pyrolysis. *Industrial & Engineering Chemistry Process Design and Development*, 18(2):232–236, 1979.
- [38] C. Juste, G. Scacchi, and M. Niclausa. Minor products and initiation rate in the chain pyrolysis of propane. *International Journal of Chemical Kinetics*, 13(9):855–864, 1981.
- [39] A.G. Volkan and G.C. April. Survey of propane pyrolysis literature. *Industrial & Engineering Chemistry Process Design and Development*, 16(4):429–436, 1977.
- [40] D. Perrin and R. Martin. The hetero-homogeneous pyrolysis of propane, in the presence or in the absence of dihydrogen, and the measurement of uptake coefficients of hydrogen atoms. *International Journal of Chemical Kinetics*, 32(6):340–364, 2000.
- [41] G.E. Herriott, R.E. Eckert, and L.F. Albright. Kinetics of propane pyrolysis. *AIChE Journal*, 18(1):84–89, 1972.
- [42] W. Tsang. Chemical Kinetic Data Base for Combustion Chemistry Part 3. Propane. *Journal of Physical and Chemical Reference Data*, 17:887, 1988.
- [43] A.M. Kaminski and J. Sobkowski. Pyrolysis of propane in the presence of hydrogen. *Reaction Kinetics and Catalysis Letters*, 16(2-3):105–109, 1981.

- [44] G. Pratt and D. Rogers. Wall-less reactor studies. part 2. Propane pyrolysis. *Journal of the Chemical Society, Faraday Transactions 1: Physical Chemistry in Condensed Phases*, 75(5):1101–1110, 1979.
- [45] K. Kanan, H. Purnell, and E. Smith. Induced Heterogeneity, a Novel Technique for the Study of Gas-Phase Reactions. Parameters for CC Bond Scission in Propane. *International Journal of Chemical Kinetics*, 15:63–73, 1983.
- [46] T. Kunugi, H. Tominaga, S. Abiko, and A. Namatame. Kinetic study of the pyrolysis of propane in the presence of hydrogen. *International Chemical Engineering*, 7(3):550–556, 1967.
- [47] I. Ziegler, R. Fournet, and P.-M. Marquaire. Influence of surface on chemical kinetic of pyrocarbon deposition obtained by propane pyrolysis. *Journal of Analytical and Applied Pyrolysis*, 73(1):107–115, 2005.
- [48] S. Bajohr. *Untersuchungen zur Propanpyrolyse unter den Bedingungen der Vakuum-/Gasaufohlung von Stahl*. PhD thesis, University of Karlsruhe, Faculty of Chemical Engineering, 2002.
- [49] C.G. Silcocks. The Kinetics of the Thermal Polymerization of Acetylene. *Proceedings of the Royal Society of London. Series A, Mathematical and Physical Sciences*, 242(1231):411–429, 1957.
- [50] C.F. Cullis and N.H. Franklin. The pyrolysis of acetylene at temperatures from 500 to 1000 ° C. *Proc. Roy. Soc. (London)*, 280(Ser. A;1380):139–152, 1964.
- [51] M.S.B. Munson and R. C. Anderson. Vinylacetylene as an intermediate in the formation of acetylenic carbon. *Carbon*, 1:51–54, 1963.
- [52] H.B. Palmer and F.L. Dormish. The Kinetics of Decomposition of Acetylene in the 1500° K Region. *The Journal of Physical Chemistry*, 68(6):1553–1560, 1964.
- [53] S.T. Dimitrijevic, S. Paterson, and P.D. Pacey. Pyrolysis of acetylene during viscous flow at low conversions; influence of acetone. *Journal of Analytical and Applied Pyrolysis*, 53(1):107–122, 2000.
- [54] X. Xu, P.D. Pacey, and S. Matter. Oligomerization and cyclization reactions of acetylene. *Phys. Chem. Chem. Phys.*, 7:326–333, 2005.

- [55] K. Norinaga, O. Deutschmann, and K.J. Hüttinger. Analysis of gas phase compounds in chemical vapor deposition of carbon from light hydrocarbons. *Carbon(New York, NY)*, 44(9):1790–1800, 2006.
- [56] C.F. Aten and E.F. Greene. Rate of formation of carbon from the pyrolysis of acetylene in shock waves. *Discussions of the Faraday Society*, No. 22:162–166, 1956.
- [57] H. Ogura. Pyrolysis of acetylene behind shock waves. *Bulletin of the Chemical Society of Japan*, 50(5):1044–1050, 1977.
- [58] H. Ogura. Effect of hydrogen chloride on the pyrolysis of acetylene as studied with a single-pulse shock tube. *Bulletin of the Chemical Society of Japan*, 53(5):1210–1215, 1980.
- [59] A. Bar-Nun and J.E. Dove. Acetylene pyrolysis and its oxidation by water vapor behind high-temperature shock waves. In *Shock Tubes Waves, Proc. Int. Symp., 12th*, pages 457–464, 1980.
- [60] M. Frenklach, S. Taki, M.B. Durgaprasad, and R.A. Matula. Soot formation in shock-tube pyrolysis of acetylene, allene, and 1,3-butadiene. *Combustion and Flame*, 54(1-3):81–101, 1983.
- [61] M. Frenklach, D.W. Clary, Jr. Gardiner, W.C., and S.E. Stein. Detailed kinetic modeling of soot formation in shock-tube pyrolysis of acetylene. In *the Proceedings of Twentieth International Symposium on Combustion*, pages 887–901, 1984.
- [62] C.H. Wu, H.J. Singh, and R.D. Kern. Pyrolysis of acetylene behind reflected shock waves. *International Journal of Chemical Kinetics*, 19(11):975–996, 1987.
- [63] M.B. Colket III. The pyrolysis of acetylene and vinylacetylene in a single-pulse shock tube. *Symposium (International) on Combustion, [Proceedings]*, 21st.:851–864, 1988.
- [64] Y. Hidaka, K. Hattori, T. Okuno, K. Inami, T. Abe, and T. Koike. Shock-tube and modeling study of acetylene pyrolysis and oxidation. *Combustion and Flame*, 107(4):401–417, 1996.
- [65] T. Kruse and P. Roth. Kinetics of C<sub>2</sub> reactions during high-temperature pyrolysis of acetylene. *Journal of Physical Chemistry A*, 101(11):2138–2146, 1997.



- [66] M. Frenklach and J. Warnatz. Detailed modeling of PAH profiles in a sooting low-pressure acetylene flame. *Combustion science and technology*, 51(4-6):265–283, 1987.
- [67] V.I. Babushok and A.W. Miziolek. Condensation flame of acetylene decomposition. *Combustion and Flame*, 136(1):141–145, 2004.
- [68] M.H. Back. Mechanism of the Pyrolysis of Acetylene. *Canadian Journal of Chemistry*, 49(13):2199–2204, 1971.
- [69] T. Tanzawa and WC Gardiner Jr. Reaction mechanism of the homogeneous thermal decomposition of acetylene. *The Journal of Physical Chemistry*, 84(3):236–239, 1980.
- [70] J.H. Kiefer, W.A. Von Drasek, and W.A. Von Drasek. The mechanism of the homogeneous pyrolysis of acetylene. *International Journal of Chemical Kinetics*, 22(7):747–786, 1990.
- [71] R.P. Duran, V.T. Amorebieta, and A.J. Colussi. Lack of kinetic hydrogen isotope effect in acetylene pyrolysis. *International Journal of Chemical Kinetics*, 21(9):847–858, 1989.
- [72] M.B. Colket III, D.J. Seery, and H.B. Palmer. The pyrolysis of acetylene initiated by acetone. *Combustion and Flame*, 75(3-4):343–366, 1989.
- [73] A.V. Krestinin. On the kinetics of heterogeneous acetylene pyrolysis. *Kinetics and Catalysis (Translation of Kinetika i Kataliz)*, 41(6):729–736, 2000.
- [74] A.B. Callear and G.B. Smith. Recurring chains following addition of atomic hydrogen to acetylene. *The Journal of Physical Chemistry*, 90(14):3229–3237, 1986.
- [75] K. Norinaga and O. Deutschmann. Detailed Kinetic Modeling of Gas-Phase Reactions in the Chemical Vapor Deposition of Carbon from Light Hydrocarbons. *Ind. Eng. Chem. Res*, 46(11):3547–3557, 2007.
- [76] I.D. Gay, G.B. Kistiakowsky, J.V. Michael, and H. Niki. Thermal Decomposition of Acetylene in Shock Waves. *Journal of Chemical Physics*, 43(5):1720–1726, 2004.
- [77] M.S. Skjøth-Rasmussen, P. Glarborg, M. Østberg, T. Johannessen, H. Livbjerg, A. Jensen, and T.S. Christensen. Formation of polycyclic aromatic hydrocarbons and soot in fuel-rich oxidation of methane in a laminar flow reactor. *Combustion and Flame*, 136:91–128, 2004.

- [78] H. Bockhorn. *Soot formation in combustion*. Springer-Verlag Berlin, 1994.
- [79] H. Wang and M. Frenklach. Calculations of Rate Coefficients for the Chemically Activated Reactions of Acetylene with Vinylic and Aromatic Radicals. *The Journal of Physical Chemistry*, 98(44):11465–11489, 1994.
- [80] H. Richter and J.B. Howard. Formation of polycyclic aromatic hydrocarbons and their growth to soot - a review of chemical reaction pathways. *Progress in Energy and Combustion Science*, 26(4):565–608, 2000.
- [81] J. Warnatz, R.W. Dibble, and U. Maas. *Combustion: Physical and Chemical Fundamentals, Modeling and Simulation, Experiments, Pollutant Formation*. Springer, 2001.
- [82] R.B. Bird, W.E. Stewart, and E.N. Lightfoot. *Transport Phenomena*, 1960.
- [83] O. Deutschmann. *Interactions between transport and chemistry in catalytic reactors*. PhD thesis, Heidelberg University, 2001.
- [84] J.H. Ferziger and M. Peric. *Computational methods for fluid dynamics*. Springer New York, 2002.
- [85] S. Tischer. *Simulation Katalytischer Monolithreaktoren unter Verwendung detaillierter Modelle für Chemie und Transport*. PhD thesis, Heidelberg University, 2004.
- [86] J. Warnatz. *Numerical methods in flame propagation*. Wiesbaden: Vieweg and Sohn, 1982.
- [87] O. Deutschmann, C. Correa, S. Tischer, D. Chatterjee, and J. Warnatz. DETCHEM. *User manual, Version 2.0*, 2005.
- [88] <http://www.detchem.com>.
- [89] J.M. Redenius, L.D. Schmidt, and O. Deutschmann. Millisecond catalytic wall reactors: I. Radiant burner. *AIChE Journal*, 47(5):1177–1184, 2001.
- [90] R.P. O’Connor, L.D. Schmidt, and O. Deutschmann. Simulating cyclohexane millisecond oxidation: Coupled chemistry and fluid dynamics. *AIChE Journal*, 48(6):1241–1256, 2002.
- [91] H. D. Minh. *Numerical Methods for Simulation and Optimization of Chemically Reacting Flows in Catalytic Monoliths*. PhD thesis, Faculty of Mathematics and Computer Science, University of Heidelberg, December 2005.

- [92] J. Warnatz. HOMREA User Guide Version 2.5, 2002.
- [93] U. Maas and J. Warnatz. Ignition processes in hydrogen-oxygen mixtures. *Combustion and Flame*, 74(1):53–69, 1988.
- [94] F. Inc. Fluent 6.2 User’s Guide. *Fluent Inc., Lebanon, NH, USA*, 2005.
- [95] T. Koike and W.C. Gardiner Jr. Thermal decomposition of propane. *J. Phys. Chem.*, 84(16):2005–2009, 1980.
- [96] R.U. Khan, S. Bajohr, D. Buchholz, R. Reimert, H.D. Minh, K. Norinaga, V.M. Janardhanan, S. Tischer, and O. Deutschmann. Pyrolysis of propane under vacuum carburizing conditions: An experimental and modeling study. *Journal of Analytical and Applied Pyrolysis*, 81(2):148–156, 2008.
- [97] F. GAMBIT. User Guide, 2001.
- [98] R.U. Khan, S. Bajohr, F. Graf, and R. Reimert. Modeling of Acetylene Pyrolysis under Steel Vacuum Carburizing Conditions in a Tubular Flow Reactor. *Molecules*, 12:290–296, 2007.
- [99] D. Buchholz, R. U. Khan, F. Graf, S. Bajohr, and R. Reimert. Modelling of the acetylene pyrolysis under the conditions of the low pressure carburization of steel. *HTM*, 62(1):5–12, 2007.

# Nomenclature

## Latin Letters

$A$	Arrhenius pre-exponential factor	mol, m <sup>3</sup> , sec
$A_s$	Surface area per unit length	m
$A_0$	Arrhenius pre-exponential factor for the low pressure limit	mol, m <sup>3</sup> , sec
$A_c$	Area of cross section	m <sup>2</sup>
$a_c$	Activity of carbon	-
$A_\infty$	Arrhenius pre-exponential factor for the high pressure limit	mol, m <sup>3</sup> , sec
$a_i''$	Reaction order with respect to product species $i$	-
$a_i'$	Reaction order with respect to reactant species $i$	-
$b$	Temperature exponent in modified Arrhenius expression	-
$b_0$	Temperature exponent in modified Arrhenius expression for the low pressure limit	-
$b_\infty$	Temperature exponent in modified Arrhenius expression for the high pressure limit	-
$c_p$	Specific heat capacity	J kg <sup>-1</sup> K <sup>-1</sup>
$c_{p,i}$	Specific heat capacity of species $i$	J kg <sup>-1</sup> K <sup>-1</sup>
$C_0$	Basic carbon content of steel	g m <sup>-3</sup>
$C_1$	Carbon concentration at the surface of steel	g m <sup>-3</sup>
$C_i$	Concentration of species $i$	mol m <sup>-3</sup>
$C(x, t)$	Carbon concentration at depth $x$ below the surface	g m <sup>-3</sup>

$(D_0)_C^\gamma$	Frequency factor specific to the diffusing solute (carbon) and matrix (austenite)	$m^2 sec^{-1}$
$D_C^\gamma$	Diffusion Coefficient of carbon in austenite at the carburisation temperature	$m^2 sec^{-1}$
$D_{ij}$	Binary diffusion coefficient for species $i$ into species $j$	$m^2 sec^{-1}$
$D_i$	Diffusion Coefficient of species $i$ in the medium into which it is diffusing	$m^2 sec^{-1}$
$D_i^M$	Effective Diffusion Coefficient of species $i$ into the mixture	$m^2 sec^{-1}$
$E_{a0}$	Activation energy for the low pressure limit	$J mol^{-1}$
$E_a$	Activation energy	$J mol^{-1}$
$E_{i,r}$	Absolute sensitivity coefficient for species $i$	
$E_{i,r}^{rel}$	Relative sensitivity coefficients for species $i$	
$E_{a\infty}$	Activation energy for the high pressure limit	$J mol^{-1}$
$f_i$	fractional conversion of species $i$ , $f_i = \frac{n_{i,in} - n_{i,out}}{n_{i,in}}$	-
$F$	Pressure fall-off blending function	-
$F_{cent}$	Troe-Modulation term	-
$g_i$	Gravitational acceleration	$m sec^{-2}$
$h$	Specific enthalpy	$J kg^{-1}$
$h_k$	Specific enthalpy of the species $k$	$J kg^{-1}$
$h_i$	Specific enthalpy of species $i$	$J kg^{-1}$
$\dot{j}_{i,j}$	Component $j$ of diffusion mass flux of the species $i$	$kg m^{-2} sec^{-1}$
$J_i$	Diffusion mass flux of species $i$	$mol m^{-2} sec^{-1}$
$\dot{j}_{k,r}$	Radial component of the mass flux vector	$kg m^{-2} sec^{-1}$
$k_g$	Number of gas phase species	-
$k_r$	Rate coefficient for the reaction $r$	$mol, m^3, sec$
$k_0$	Rate constant for low pressure limit	$mol, m^3, sec$
$K_1$	Equilibrium constant for reaction (1.1)	-
$K_2$	Equilibrium constant for reaction (1.4)	$Pa^{-1}$
$K_3$	Equilibrium constant for reaction (1.8)	$Pa^{-\frac{1}{2}}$

$k_{\infty}$	Rate constant for high pressure limit	mol, m <sup>3</sup> , sec
$k_B$	Boltzmann constant	J K <sup>-1</sup>
$k_b$	Backward rate constant	mol, m <sup>3</sup> , sec
$k_f$	Forward rate constant	mol, m <sup>3</sup> , sec
$L_R$	Reactor Length	m
$\bar{M}$	Average molecular weight	g mol <sup>-1</sup>
$M_i$	Molecular mass of species $i$	g mol <sup>-1</sup>
$m_i$	Mass of species $i$	kg
$M_k$	Molecular mass of the species $k$	g mol <sup>-1</sup>
$N_A$	Avogadro number = $6.022 \cdot 10^{23}$	mol <sup>-1</sup>
$n_i$	Number of moles of species $i$	-
$N_{C,f}$	Number of carbon atoms in the carburizing gas molecular formula	-
$N_{C,i}$	Number of carbon atoms in species $i$ molecular formula	-
$n_{i,in}$	Number of moles of species $i$ at the reactor inlet	-
$n_{i,out}$	Number of moles of species $i$ at the reactor outlet	-
$p$	Pressure	Pa
$p_r$	Reduced pressure	-
$p_{CO}$	Partial pressure of carbon monoxide	Pa
$p_{CO_2}$	Partial pressure of carbon dioxide	Pa
$p_{H_2O}$	Partial pressure of water	Pa
$Q_C^{\gamma}$	Activation energy for diffusion specific to the diffusing solute (carbon) and matrix (austenite)	J mol <sup>-1</sup>
$q_i$	Heat flux	J m <sup>-2</sup> sec <sup>-1</sup>
$R$	Gas constant	8.314 J K <sup>-1</sup> mol <sup>-1</sup>
$r$	Radial coordinate	m
$R_i^{hom}$	Net mass rate of production of species $i$ due to homogeneous chemical reactions	kg m <sup>-3</sup> sec <sup>-1</sup>
$S_{i,j}$	Selectivity of species $i$ with respect to $j$ , $S_{i,j} = \Psi_{i,C} / f_j$	-
$s_i$	Specific entropy of species $i$	J kg <sup>-1</sup> K <sup>-1</sup>
$S_m$	Source term	kg m <sup>-3</sup> sec <sup>-1</sup>

$\dot{s}_k$	Molar rate of production/removal of species $k$ by surface reactions	$\text{mol m}^{-2} \text{sec}^{-1}$
$T$	Temperature	$^{\circ}\text{C}$ or $\text{K}$
$t$	Time	$\text{sec}$
$T_{ij}^*$	Reduced temperature	
$T_R$	Controller Temperature	$^{\circ}\text{C}$ or $\text{K}$
$T^*$	Troe parameter	$\text{K}$
$T^{**}$	Troe parameter	$\text{K}$
$T^{***}$	Troe parameter	$\text{K}$
$T_w$	Wall temperature	$^{\circ}\text{C}$ or $\text{K}$
$U$	Overall heat transfer coefficient	$\text{W m}^{-2} \text{ }^{\circ}\text{C}^{-1}$
$u$	Axial velocity	$\text{m sec}^{-1}$
$u_x$	x components of the velocity vector $\vec{u}$	$\text{m sec}^{-1}$
$u_y$	y components of the velocity vector $\vec{u}$	$\text{m sec}^{-1}$
$u_z$	z components of the velocity vector $\vec{u}$	$\text{m sec}^{-1}$
$v$	Radial velocity	$\text{m sec}^{-1}$
$v_{stef}$	Stefan velocity	$\text{m sec}^{-1}$
$x$	Cartesian coordinate	$\text{m}$
$X_i$	Mole fraction of species $i$	-
$y$	Cartesian coordinate	$\text{m}$
$Y_i$	Mass fraction of species $i$	-
$z$	Cartesian coordinate	$\text{m}$

## Greek Letters

$\alpha$	Troe parameter	-
$\delta_{i,j}$	Kronecker symbol ( $\delta_{i,j} = 1$ if $i = j$ and $\delta_{i,j} = 0$ otherwise)	
$\lambda$	Thermal conductivity of the gas mixture	$\text{W m}^{-1} \text{ }^{\circ}\text{C}^{-1}$
$\lambda_i$	Thermal conductivity of the species $i$	$\text{W m}^{-1} \text{ }^{\circ}\text{C}^{-1}$
$\mu$	Viscosity of the gas mixture	$\text{kg m}^{-1} \text{sec}^{-1}$
$\mu_i$	Viscosity of the species $i$	$\text{kg m}^{-1} \text{sec}^{-1}$
$\nu$	Net stoichiometric coefficient of the species $i$ in a reaction	-
$\nu_i''$	Stoichiometric coefficient of the product species $i$	-

$\nu'_i$	Stoichiometric coefficient of the reactant species $i$	-
$\dot{\omega}_i$	Molar rate of production/removal of species $i$	$\text{mol m}^{-3} \text{sec}^{-1}$
$\dot{\omega}_k$	Molar rate of production/removal of species $k$ by gas-phase reactions	$\text{mol m}^{-3} \text{sec}^{-1}$
$\Omega^{(2,2)*}$	Collision integral for viscosity	-
$\Omega_{ij}^{(1,1)*}$	Collision integral for diffusion	-
$\dot{\omega}_{i,f}$	Forward reaction rate of species $i$	$\text{mol m}^{-3} \text{sec}^{-1}$
$\dot{\omega}_{i,b}$	Backward reaction rate of species $i$	$\text{mol m}^{-3} \text{sec}^{-1}$
$\Psi_{i,C}$	Species $i$ carbon yield	-
$\phi_{f,in}$	Molar flow rate of carburizing gas at the reactor inlet	$\text{mol sec}^{-1}$
$\phi_{i,out}$	Molar flow rate of species $i$ at the reactor outlet	$\text{mol sec}^{-1}$
$\rho$	Density	$\text{kg m}^{-3}$
$\sigma_i$	Lennard-Jones collision diameter	nm
$\tau_{ij}$	Stress tensor	Pa



# Appendix A

## FLUENT UDFs

### A.1 FLUENT UDF for the global mechanism

The following UDF was used for implementing the global kinetic mechanism of acetylene pyrolysis. The kinetic parameters in this UDF are for thermogravimetric reactor and vacuum reactor. For the laboratory scale tubular flow reactor the parameters are shown in table 7.1.

```
/* UDF used for the global kinetic mechanism of pyrolysis of acetylene */
#include "udf.h"

DEFINE_VR_RATE(vol_reac_rate,c,t,r,wk,yk,rate,rr_t)
{
    /*If more than one reaction is defined, it is necessary to distinguish
    between these using the names of the reactions. */
    real ci, prod;
    real c0,c1,c2,c3,c4,c5,c6;
    c0 = C_R(c,t) * yk[0] / wk[0]*1000;
    c1 = C_R(c,t) * yk[1] / wk[1]*1000;
    c2 = C_R(c,t) * yk[2] / wk[2]*1000;
    c3 = C_R(c,t) * yk[3] / wk[3]*1000;
```

```

c4      = C_R(c,t) * yk[4] / wk[4]*1000;
c5      = C_R(c,t) * yk[5] / wk[5]*1000;
c6      = C_R(c,t) * yk[6] / wk[6]*1000;

/* reactions included in the FLUENT speceis transport and reaction model
(1)      C2H2 +H2      =>C2H4
(2)      C2H4          =>C2H2  + H2
(3)      C2H2 +3H2    => 2CH4
(4)      2CH4          => C2H2 + 3H2
(5)      C2H2          => 2C   + H2
(6)      C6H6          => 6C   + 3H2
(7)      2C2H2        => C4H4
(8)      C4H4          => 2C2H2
(9)      C4H4 + C2H2 =>  C6H6

                                          */

if (!strcmp(r->name, "reaction-1"))
{

/* Calculation of reaction rate for Reaction 1 */

prod = 1;

prod  = pow(c2, 1)* pow(c0,0.36);

*rate = 1700 * exp( -103000000 / (8314.47 * C_T(c,t)))* prod/1000;

*rr_t = *rate;

}

/*****/

```

```

        else if (!strcmp(r->name, "reaction-2"))
        {
/* Calculation of reaction rate for Reaction 2 */
        prod = 1;
        prod = pow(c3, 0.5);

        *rate = 38000000 * exp(- 200040000 / (8314.47 * C_T(c,t)))* prod/1000;

        *rr_t = *rate;

        }

/*****/
        else if (!strcmp(r->name, "reaction-3"))
        {
/* Calculation of reaction rate for Reaction 3 */

        prod = 1;

        prod = pow(c2, 0.35) * pow(c0,0.22);
        *rate = 50000 * exp( -150000000 / (8314.47 * C_T(c,t))) * prod/1000;

        *rr_t = *rate;

        }

/*****/

```

```

        else if (!strcmp(r->name, "reaction-4"))
        {
/* Calculation of reaction rate for Reaction 4 */

prod = 1;

        prod = pow(c1, 0.21);
*rate = 8600000 * exp( -195000000 / (8314.47 * C_T(c,t)))* prod/1000;

*rr_t = *rate;

        }

/*****/

        else if (!strcmp(r->name, "reaction-5"))
        {
/* Calculation of reaction rate for Reaction 5 */

prod = 1;

        prod = pow(c2, 2.2)/(1+18*c0);

*rate = 1.3824E-86 *pow(C_T(c,t),30)*exp(-165000000/(8314.47 * C_T(c,t)))
* prod/1000;

```

```

*rr_t = *rate;
    }

/*****

        else if (!strcmp(r->name, "reaction-6"))
        {
/* Calculation of reaction rate for Reaction 6 */

prod = 1;

        prod = pow(c5, 0.75)/(1+22*c0);

*rate = 1000 * exp( -75000000 / (8314.47 * C_T(c,t)))* prod/1000;

*rr_t = *rate;

        }

/*****

        else if (!strcmp(r->name, "reaction-7"))

        {
/* Calculation of reaction rate for Reaction 7 */

prod = 1;

```

```

        prod = pow(c2, 1.6);
*rate =90000 * exp( -120710000 / (8314.47 * C_T(c,t))) * prod/1000;

*rr_t = *rate;

    }

/*****

        else if (!strcmp(r->name, "reaction-8"))
        {
/* Calculation of reaction rate for Reaction 8 */

        prod = 1;

        prod = pow(c4, 0.75);
*rate =pow(10,15) * exp( -335180000 / (8314.47 * C_T(c,t))) * prod/1000;

*rr_t = *rate;

        }

/*****

        else if (!strcmp(r->name, "reaction-9"))
        {
/* Calculation of reaction rate for Reaction 9 */

```

```

prod = 1;

        prod = pow(c2, 1.3)*pow(c4, 0.6);
*rate =2300 * exp( -64490000 / (8314.47 * C_T(c,t))) *prod/1000;

*rr_t = *rate;

    }

/*****/

    else
    {
/*      Message("Unknown Reaction\n"); */
    }

/*      Message("Actual Reaction: %s\n",r->name); */

}

```

## A.2 FLUENT UDFs used for Temperature Profiles

For CFD simulations, the measured temperature profiles were implemented by the FLUENT UDFs. The parameters for the laboratory scale tubular flow reactor used in these UDFs were taken from the equations 6.1 and 7.1 for propane and acetylene pyrolysis respectively. For thermogravimetric reactor and vacuum reactor following UDFs were used:

## A.2.1 Temperature profiles in Thermogravimetric Reactor

```
/* FLUENT UDF used for temperature profile at TR= 900 C
```

```
in the thermogravimetric reactor */
```

```
#include "udf.h"
```

```
DEFINE_PROFILE(wall_T_profil_900, t, i)
```

```
{
```

```
real y[ND_ND];
```

```
real x;
```

```
face_t f;
```

```
real p1, p2, p3, p4, p5 ,p6 ,p7 ,p8 ,p9,p10;
```

```
p1 = 2.8438098e-017 ;
```

```
p2 = -5.2953911e-014 ;
```

```
p3 = 3.9724238e-011 ;
```

```
p4 = -1.5707779e-008 ;
```

```
p5 = 3.5524681e-006 ;
```

```
p6 = -4.6072944e-004 ;
```

```
p7 = 3.1807473e-002 ;
```

```
p8 = -9.4320662e-001 ;
```

```
p9 = 1.1676736e+001 ;
```

```
p10 =7.8635393e+001 ;
```

```
begin_f_loop(f, t)
```

```
{
```

```
F_CENTROID(y,f,t);
```

```
x = y[0]*1000;
```



```

F_PROFILE(f, t, i) = (p1*pow(x,9) + p2*pow(x,8) + p3*pow(x,7)
                    + p4*pow(x,6) + p5*pow(x,5) + p6*pow(x,4)
                    + p7*pow(x,3) + p8*pow(x,2) + p9 *x + p10)
                    +(273)-50;

}

end_f_loop(f, t)
}

```

```

/* FLUENT UDF used for temperature profile at TR= 950 C
in the thermogravimetric reactor */

```

```

#include "udf.h"

```

```

DEFINE_PROFILE(wall_T_profil_950, t, i)
{
real y[ND_ND];
real x;
face_t f;
real p1, p2, p3, p4, p5 ,p6 ,p7 ,p8 ,p9,p10;

p1 = 2.8438098e-017      ;
p2 = -5.2953911e-014    ;
p3 = 3.9724238e-011     ;
p4 = -1.5707779e-008    ;
p5 = 3.5524681e-006     ;
p6 = -4.6072944e-004    ;
p7 = 3.1807473e-002     ;
p8 = -9.4320662e-001    ;

```

```

p9 = 1.1676736e+001      ;
p10 =7.8635393e+001     ;

begin_f_loop(f, t)

{
  F_CENTROID(y,f,t);
  x = y[0]*1000;
  F_PROFILE(f, t, i) = (p1*pow(x,9) + p2*pow(x,8) + p3*pow(x,7)
                        + p4*pow(x,6) + p5*pow(x,5) + p6*pow(x,4)
                        + p7*pow(x,3) + p8*pow(x,2) + p9 *x + p10)+(273);

}

end_f_loop(f, t)
}

/* FLUENT UDF used for temperature profile at TR=1000 °C in the
thermogravimetric reactor */
#include "udf.h"

DEFINE_PROFILE(wall_T_profil_1000, t, i)
{
  real y[ND_ND];
  real x;
  face_t f;
  real p1, p2, p3, p4, p5, p6, p7, p8, p9, p10;

```

```

p1 = 4.0546E-17      ;
p2 = -6.7952E-14    ;
p3 = 4.74255E-11    ;
p4 = -1.78292E-08   ;
p5 = 3.89145E-06    ;
p6 = -0.00049246    ;
p7 = 0.033502       ;
p8 = -0.99628       ;
p9 = 13.22012       ;
p10 =78.5           ;

begin_f_loop(f, t)

{
  F_CENTROID(y,f,t);
  x = y[0]*1000;
  F_PROFILE(f, t, i) = (p1*pow(x,9) + p2*pow(x,8) + p3*pow(x,7)
+ p4*pow(x,6) + p5*pow(x,5) + p6*pow(x,4) + p7*pow(x,3)
+ p8*pow(x,2) + p9 *x + p10)+(273);

}

end_f_loop(f, t)
}

```

## A.2.2 Temperature profiles in Vacuum Reactor

```

/* FLUENT UDF used for temperature profile at TR = 980 C
   in the vacuum reactor */

```

```

#include "udf.h"

DEFINE_PROFILE(wall_T_profil_980, t, i)
{
    real y[ND_ND];
    real x;
    face_t f;
    real p1, p2, p3, p4, p5, p6, p7, p8, p9, p10;

    p1 = 7.9135713e+006      ;
    p2 = -2.5861517e+007   ;
    p3 = 3.5456470e+007    ;
    p4 = -2.6156006e+007   ;
    p5 = 1.0950872e+007    ;
    p6 = -2.4658451e+006   ;
    p7 = 2.3420008e+005    ;
    p8 = -3.3075014e+003   ;
    p9 = 2.5783665e+003    ;
    p10 = 3.8837052e+002   ;

    begin_f_loop(f, t)
    {
        F_CENTROID(y,f,t);

        x = y[0];

        F_PROFILE(f, t, i) = (p1*pow(x,9) + p2*pow(x,8) + p3*pow(x,7) +

```

```

p4*pow(x,6) + p5*pow(x,5) + p6*pow(x,4) + p7*pow(x,3) + p8*pow(x,2) +

p9 *x + p10)+(273);

}

end_f_loop(f, t)
}

/* FLUENT UDF used for temperature profile at TR = 1050 C
   in the vacuum reactor */
#include "udf.h"

DEFINE_PROFILE(wall_T_profil_1050, t, i)
{
real y[ND_ND];
real x;
face_t f;
real p1, p2, p3, p4, p5, p6,p7,p8, p9, p10;

p1 = 7.9135713e+006      ;
p2 = -2.5861517e+007    ;
p3 = 3.5456470e+007     ;
p4 = -2.6156006e+007    ;
p5 = 1.0950872e+007     ;
p6 = -2.4658451e+006    ;
p7 = 2.3420008e+005     ;
p8 = -3.3075014e+003    ;
p9 = 2.5783665e+003     ;

```

```

p10 = 4.5837052e+002      ;

begin_f_loop(f, t)

{
  F_CENTROID(y,f,t);
  x = y[0];
  F_PROFILE(f, t, i) = (p1*pow(x,9) + p2*pow(x,8) + p3*pow(x,7) +
  p4*pow(x,6) + p5*pow(x,5) + p6*pow(x,4) + p7*pow(x,3) + p8*pow(x,2) +
  p9 *x + p10)+(273);

}

end_f_loop(f, t)
}

```

# Appendix B

## Pyrolysis of propane

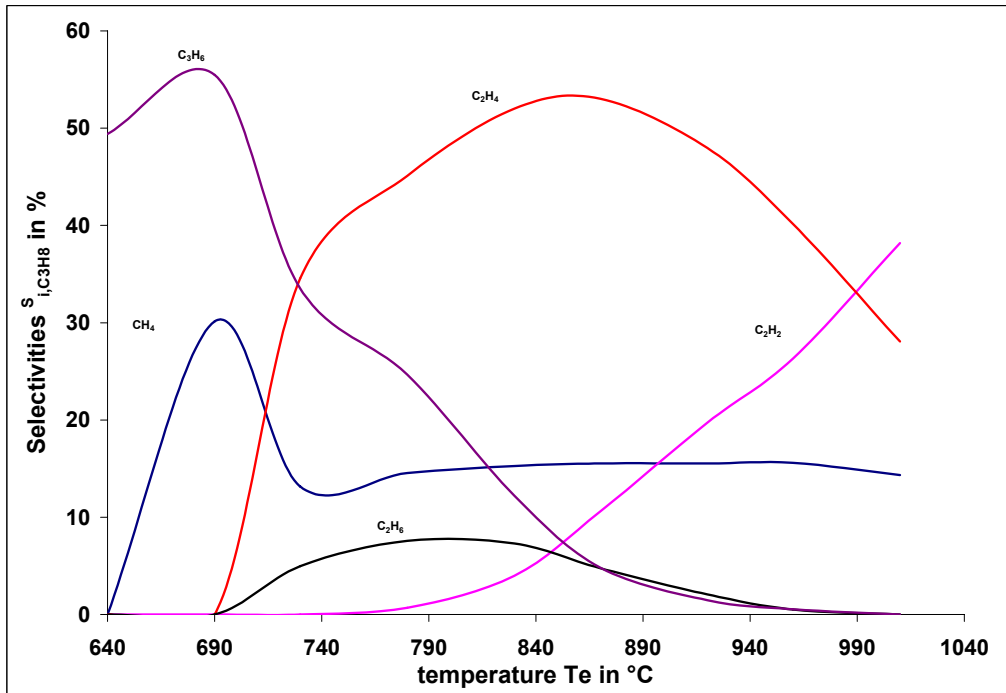


Figure B.1: Selectivities of different species as a function of temperature for pyrolysis of propane in the tubular flow reactor

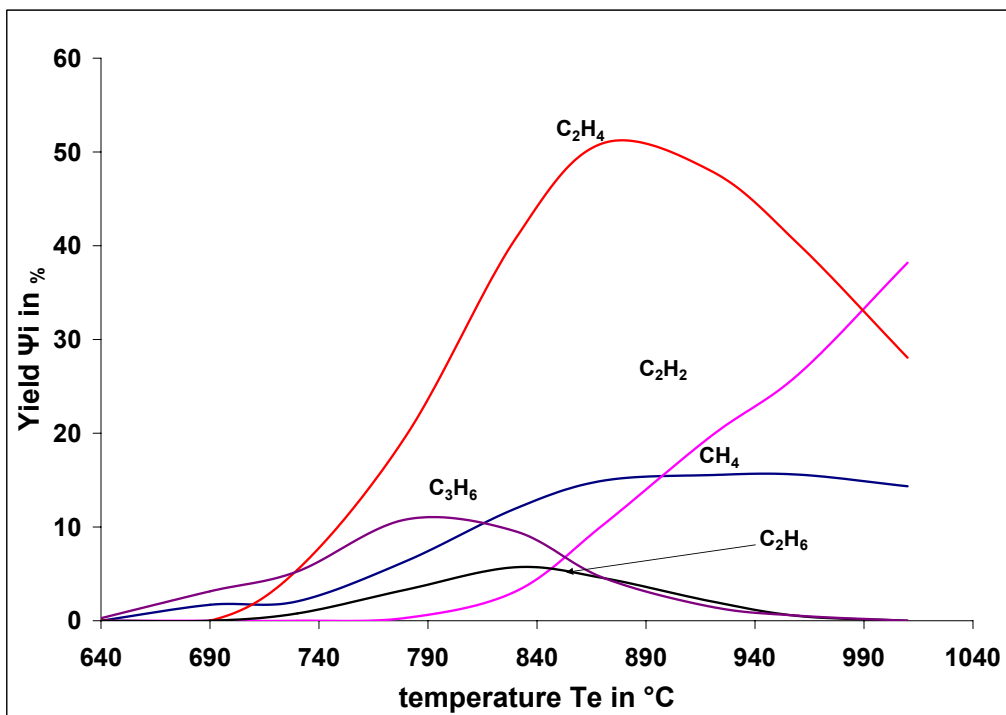


Figure B.2: Yields of carbon for different species as a function of temperature for pyrolysis of propane in the tubular flow reactor



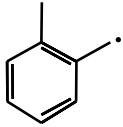
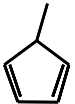
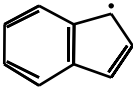
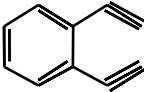
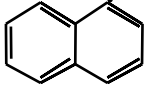
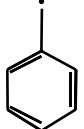
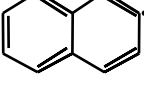
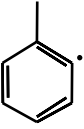
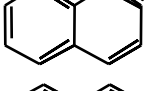
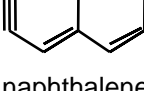
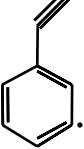
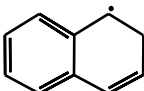
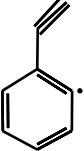
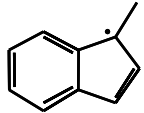
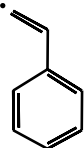
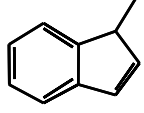
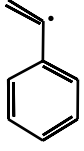
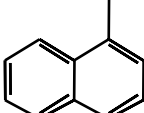
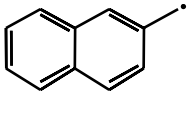
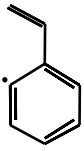


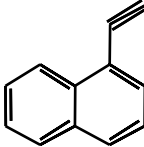
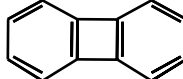
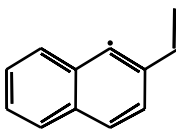
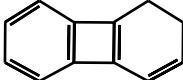
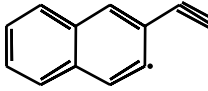
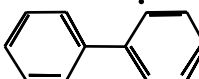
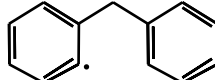
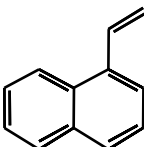
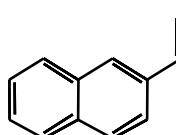
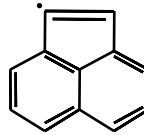
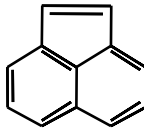
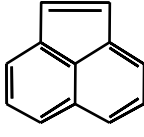
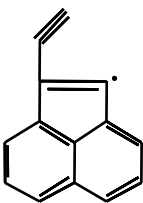
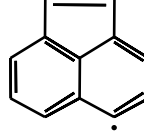
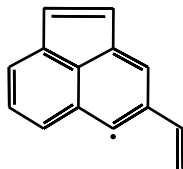
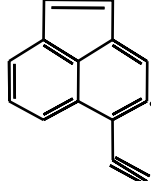
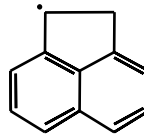
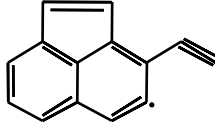
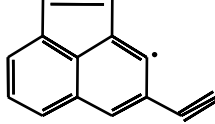
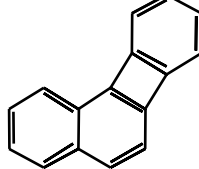
# Appendix C

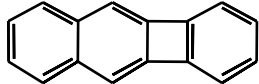
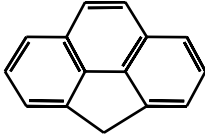
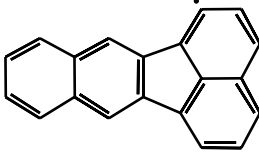
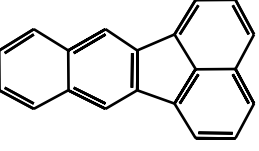
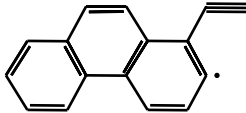
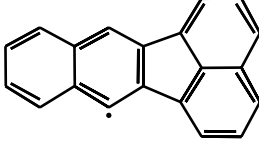
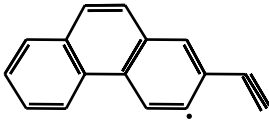
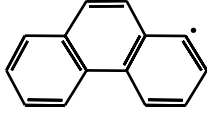
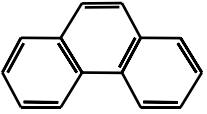
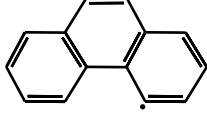
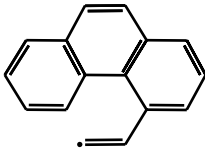
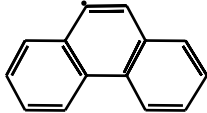
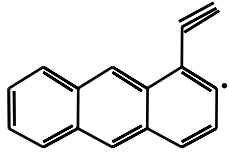
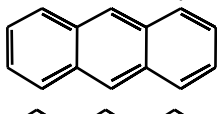
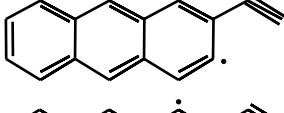
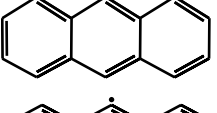
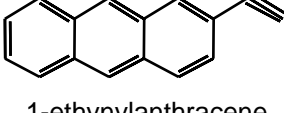
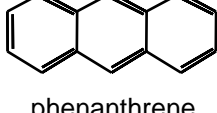
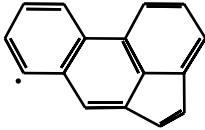
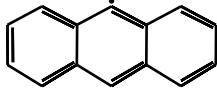
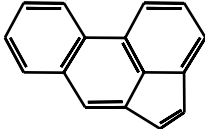
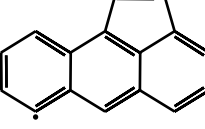
## List of Species and Detailed Reaction Mechanism

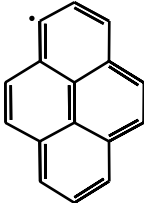
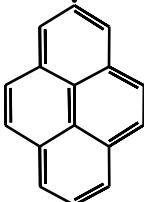
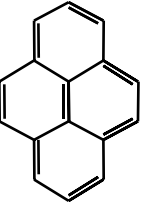
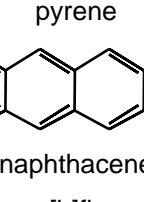
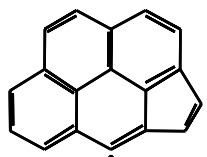
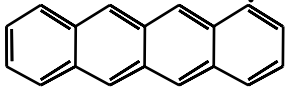
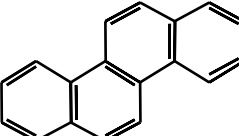
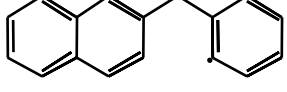
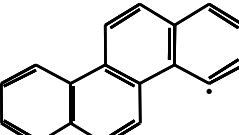
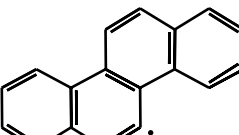
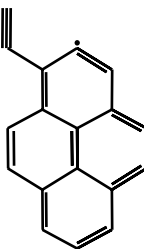
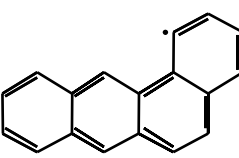
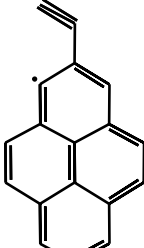
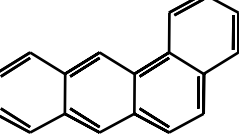
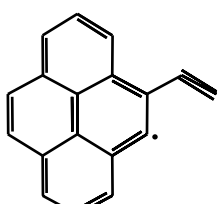
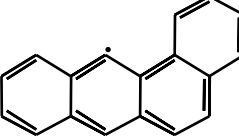
## Species included in the detailed mechanism [75]

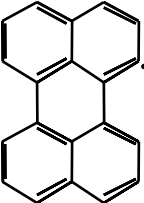
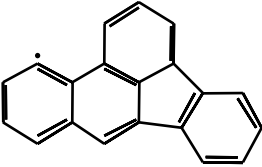
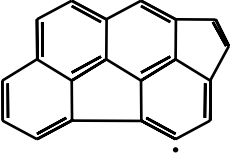
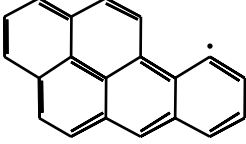
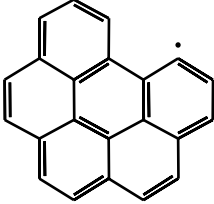
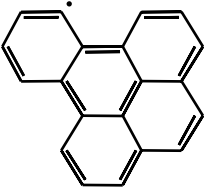
Abbreviation	Formula or name	Abbreviation	Formula or name
H	hydrogen radical	C4H52	
H2	hydrogen	C4H6	1,3-butadiene
C	carbon	C4H612	1,2-butadiene
CH	methylidyne	C4H61	1-butyne
1CH2	methylene (singlet)	C4H62	2-butyne
3CH2	methylene (triplet)	I-C4H7	
CH3	methyl radical	N-C4H7	
CH4	methane	C4H8	1-butene
C2	dicarbon	C5H4	cyclopentatriene
C2H	ethynyl radical	L-C5H4	1,2-pentadiene-4-yne
C2H2	acetylene	C5H5	
C2H3	vinyl radical	L-C5H5	
C2H4	ethylene	C5H4H	
C2H5	ethyl radical	C5H6	cyclopentadiene
C2H6	ethane	C5H7	
C3H2	propadienylidene	L-C5H7	
C3H3		C5H8	cyclopentene
AC3H4	allene	L-C5H8	1,4-pentadiene
PC3H4	propyne	C6H	
CYC3H4	cyclopropene	C6H2	triacetylene
AC3H5		C6H3	
TC3H5		C-C6H4	benzyne
SC3H5		L-C6H4	
C3H6	propene	C6H5	
N-C3H7		N-C6H5	
I-C3H7		I-C6H5	
C3H8	propane	C6H6	benzene
C4H		L-C6H6	1,3-hexadiene-5-yne
C4H2	diacetylene	N-C6H7	
N-C4H3		C-C6H7	
I-C4H3			
C4H4	vinylacetylene		
N-C4H5			
I-C4H5			
C4H512			
N-C4H51			
I-C4H51			

I-C6H7		A1C2H3	styrene
C5H4CH3		A1C2H5	ethylbenzene
L-C6H8	hexatriene	ACH3CH2	
C6H813	1,3-cyclohexadiene	ACH3CH3	xylene
C6H814	1,4-cyclohexadiene	C8H12	4-Vinylcyclohexene
C5H5CH3		C9H7	
1-C6H12	1-hexene	C9H8	indene
C-C6H12	cyclohexane	A1C2H)2	
4m1pent	4-methyl-1-pentene	A2-1	
C7H7		A2-2	
C6H4CH3		A2T1	
C7H8	toluene	A2T2	
C8H2	tetraacetylene	A2	naphthalene
A1C2H-		C10H9	
A1C2H*		indylCH3	
A1C2H	phenylacetylene	C10H10	1,2-dihydronaphthalene
N-A1C2H2		indeneCH3	
I-A1C2H2		A2CH2-1	
C8H8	1,3,5,7-Cyclooctatetraene	A2CH2-2	
A1C2H3*		A2CH3-1	1-methylnaphthalene
		A2CH3-2	2-methylnaphthalene

A2C2H-1*		BIPHEN	
A2C2H-2*		BIPHENH	
A2C2H-23		P2-	
A2C2H-1	1-ethynylindole	P2	biphenyl
A2C2H-2	2-ethynylindole	BENZYL*	
A2C2H2-1		BENZYL	benzylbenzene
A2C2H2-2		fluorene	fluorene
A2C2H3-2	2-vinylindole	A2R5E-1	1-ethynylacenaphthylene
A2C2H5	ethynylindole	A2R5E-3	3-ethynylacenaphthylene
A2R5-1		A2R5E-4	4-ethynylacenaphthylene
A2R5-3		A2R5E-5	5-ethynylacenaphthylene
A2R5-4		A2R5E12	
A2R5-5		A2R5E45	
A2R5	acenaphthylene	A2R5E54	
HA2R5		A2R5E34	
A2R5H2	acenaphthene	A2R5E43	
A2C2H)2	1,2-diethynylindole	A2C6H4-1	

A2C6H4-2			
A2C6H5-2	2-phenylnaphthalene		
FLTHN-1		A3CH3	4-methylphenanthrene
FLTHN-3		A3C2H-1*	
FLTHN-7		A3C2H-1	1-ethynylphenanthrene
FLTHN	fluoranthene	A3C2H-2*	
A3-1		A3C2H-2	2-ethynylphenanthrene
A3-2		A3C2H-4	4-ethynylphenanthrene
A3-4		A3C2H2-4	
A3-9		A3LE-1P	
A3L-1		A3LE-2P	
A3L-2		A3LE-2S	
A3L-9		A3LE-1	1-ethynylanthracene
A3	phenanthrene	A3LE-2	2-ethynylanthracene
A3L	anthracene	A3R5-7	
A3CH2		A3R5-10	
A3CH2R	cyclopenta[def]phenanthrene	A3R5	acephenanthlyrene
		A3LR5*	
		A3LR5	not distinguished radical positions aceanthrylene

A4-1		A4C2H-1 A4C2H-2 A4C2H-4	1-ethynylpyrene 2-ethynylpyrene 4-ethynylpyrene
A4-2		BGHIF- BGHIF	benzo[ghi]fluoranthene
A4-4		CPCDFL* CPCDFL	cyclopenta[cd]fluoranthene
A4	pyrene 	CPCDA4*	
A4L*		CPCDA4	cyclopenta[cd]pyrene
A4L C17H12	naphthacene benzo[b]fluorene	CRYSN-1	
BENZNAP*		CRYSN-4	
BENZNAP	2-benzyl-naphthalene	CRYSN-5	
A4C2H-1*		CRYSN BAA3L-1	chrysene 
A4C2H-2*		BAA3L-12	
A4C2H-4*		BAA3L-4 BAA3L	benzo[a]anthracene 

PERYLN*		BBFLTHN*	
PERYLN	perylene	BBFLTHN	benzo[b]fluoranthene
CPBFL*		BKFLTHN	benzo[k]fluoranthene
CPBFL	cyclopenta[cd]benzo[ghi]fluoranthene	ANTHAN	anthanthracene
DCPA4	dicyclopenta[cd,fg]pyrene	INA4	indeno[1,2,3-cd]pyrene
BAPYR*		BGHIPE*	
BAPYR	benzo[a]pyrene	BGHIPE	benzo[ghi]perylene
BEPYR*		CORONEN	coronene
BEPYR	benzo[e]pyrene	CH3COCH3	acetone
		CH3CO	
		CH3COCH2	
		CH2CO	
		CO	Carbon Monoxide

**Detailed Reaction Mechanism [75]**  
 $k = A T^n \exp(-E_a/RT)$  A: cm<sup>3</sup> mole<sup>-1</sup>s<sup>-1</sup> E<sub>a</sub>: kJ/mol

\*\*\*\* 1. H2 REACTIONS

```
*****
1.  H      +H      +M(1)    =H2      +M(1)    0.100E+19 -1.0      0.0      !Miller&Melius1992
2.  H2     +H      +H      =H2      +H2      9.200E+16 -0.6      0.0      !Miller&Melius1992
*****
```

\*\*\*\* 2. C1 REACTIONS

```
*****
3.  CH      +H      =C       +H2      1.500E+14  0.0      0.000    !Miller&Melius1992
4.  CH      +H2     =3CH2    +H      1.107E+08  1.79     6.990    !Wang&Frenklach1997
5.  CH      +H2     =CH3     +H      3.190E+25 -4.99    11.34    !Richter&Howard2002
6.  3CH2    +H      +M(2)    =CH3     +M(2)    2.500E+16 -0.8      0.000    !Wang&Frenklach1997
LOW      3.200E+27 -3.140    5.150
TROE     0.6800   78.0   1995.0  5590.0
7.  3CH2    +H2     =CH3     +H      0.500E+06  2.0      30.250   !Wang&Frenklach1997
8.  3CH2    +C      =C2H     +H      0.500E+14  0.0      0.000    !Wang&Frenklach1997
9.  3CH2    +CH     =C2H2    +H      0.400E+14  0.0      0.000    !Wang&Frenklach1997
10. 3CH2    +CH     =C2H     +H      +H      5.490E+22 -2.41    48.20    !Westmoreland1986
11. 3CH2    +CH     =C2H3    +H      3.090E+14 -1.98    2.59     !Westmoreland1986
12. 3CH2    +3CH2   =C2H3    +H      7.120E+21 -3.9     10.29    !Westmoreland1986
13. 3CH2    +3CH2   =C2H4    +H      1.110E+20 -3.43    8.66     !Westmoreland1986
14. 3CH2    +3CH2   =C2H2    +H2     3.200E+13  0.0      0.000    !Wang&Frenklach1997
15. 1CH2    +H      =CH      +H2     0.300E+14  0.0      0.000    !Wang&Frenklach1997
16. 1CH2    +H      =3CH2    +H      2.000E+14  0.0      0.0      !Miller&Melius1992
17. 1CH2    +H2     =CH3     +H      0.700E+14  0.0      0.000    !Wang&Frenklach1997
18. 1CH2    +1CH2   =C2H2    +H2     3.010E+13  0.0      0.0      !Zhang&Mckinnon1995
19. 1CH2    +1CH2   =C2H3    +H      2.000E+13  0.0      0.0      !Frank&Just1984
20. CH3     +H      +M(2)    =CH4     +M(2)    1.270E+16 -0.630   1.60     !Wang&Frenklach1997
LOW      2.477E+33 -4.760    10.21
TROE     0.7830   74.0   2941.0  6964.0
21. CH3     +C      =C2H2    +H      0.500E+14  0.0      0.000    !Wang&Frenklach1997
22. CH3     +CH     =C2H3    +H      0.300E+14  0.0      0.000    !Wang&Frenklach1997
23. CH3     +3CH2   =C2H4    +H      0.400E+14  0.0      0.000    !Wang&Frenklach1997
24. CH3     +3CH2   =C2H5    +H      2.530E+20 -3.49    8.49     !Westmoreland1986
25. CH3     +1CH2   =C2H4    +H      0.120E+14  0.0      -2.380   !Wang&Frenklach1997
26. CH3     +1CH2   =C2H5    +H      1.111E+19 -3.20    7.45     !Westmoreland1986
27. CH3     +CH3    +M(2)    =C2H6    +M(2)    2.120E+16 -0.97    2.59     !Wang&Frenklach1997
LOW      1.770E+50 -9.670    26.03
TROE     0.5325   151.0  1038.0  4970.0
28. CH3     +CH3    =C2H4    +H2     1.000E+16  0.0      134.02   !Warnatz1984
29. CH3     +CH3    =C2H5    +H      4.990E+12  0.1      44.350   !Wang&Frenklach1997
30. CH4     +H      =CH3     +H2     0.660E+09  1.62     45.360   !Wang&Frenklach1997
31. CH4     +CH     =C2H4    +H      0.600E+14  0.0      0.000    !Wang&Frenklach1997
32. CH4     +3CH2   =CH3     +CH3    0.246E+07  2.0      34.600   !Wang&Frenklach1997
33. CH4     +1CH2   =CH3     +CH3    0.160E+14  0.0      -2.380   !Wang&Frenklach1997
34. CH4     +CH3    =C2H6    +H      8.000E+13  0.0      167.37   !Tabayashi&Bauer1979
35. CH4     +CH3    =C2H5    +H2     1.000E+13  0.0      96.24    !Tabayashi&Bauer1979
*****
**** 3. C2 REACTIONS
*****
36. C2      +H2     =C2H     +H      4.000E+05  2.4      4.18     !Miller&Melius1992
37. C2H     +M(1)  =C2      +H      +M(1)    4.680E+16  0.0      518.84   !Colket1986
38. C2H     +H      +M(2)    =C2H2    +M(2)    1.000E+17 -1.0      0.000    !Wang&Frenklach1997
LOW      3.750E+33 -4.800    7.95
TROE     0.6464   132.0  1315.0  5566.0
39. C2H     +H2     =C2H2    +H      4.900E+05  2.5      2.34     !Wang&Frenklach1997
40. C2H     +1CH2   =CH      +C2H2    1.810E+13  0.0      0.0      !Tsang1986
41. C2H     +3CH2   =CH      +C2H2    1.810E+13  0.0      0.0      !Zhang&Mckinnon1995
42. C2H     +CH3    =C3H3    +H      2.410E+13  0.0      0.0      !Tsang1986
43. C2H     +CH3    =PC3H4   8.070E+49 -11.305  183.27   !Richter&Howard2002
44. C2H     +CH4     =C2H2    +CH3    1.810E+12  0.0      2.09     !Tsang1986
45. C2H     +C2H     =C4H2    1.800E+13  0.0      0.0      !Fournet1999
46. C2H     +C2H     =C2H2    +C2      1.810E+12  0.0      0.0      !Tsang1986
47. C2H2    +H      +M(2)    =C2H3    +M(2)    0.560E+13  0.0      10.04    !Wang&Frenklach1997
LOW      3.800E+40 -7.270    30.21
TROE     0.7507   98.5   1302.0  4167.0
48. C2H2    +H2     =C2H4    1.410E+41 -9.06    213.945  !Richter&Howard2002
49. C2H2    +CH     =C3H2    +H      3.000E+13  0.0      0.0      !Warnatz1983
50. C2H2    +3CH2   =C3H3    +H      1.200E+13  0.0      27.70    !Böhlund1986
51. C2H2    +1CH2   =C3H3    +H      2.000E+13  0.0      0.0      !Wang&Frenklach1997
52. C2H2    +1CH2   =3CH2    +C2H2    4.000E+13  0.0      0.0      !Miller&Melius1992
53. C2H2    +1CH2   =CYC3H4  1.660E+38 -8.65    25.48    !Richter&Howard2002
54. C2H2    +1CH2   =AC3H4   7.460E+39 -8.78    26.57    !Richter&Howard2002
55. C2H2    +1CH2   =PC3H4   2.620E+40 -8.86    26.82    !Richter&Howard2002
56. C2H2    +CH3    =AC3H4   +H      2.870E+21 -2.74    103.77   !Dean&Westmoreland1987
57. C2H2    +CH3    =PC3H4   +H      1.000E+13 -0.53    56.07    !Dean&Westmoreland1987
58. C2H2    +CH3    =AC3H5   1.400E+04  2.21    69.04    !Diau1994
59. C2H2    +C2H     =C4H2    +H      9.600E+13  0.0      0.0      !Wang&Frenklach1997
```



60.	C2H2	+C2H	=N-C4H3		1.300E+30	-6.12	10.5	!Wang&Frenklach1997
61.	C2H2	+C2H	=I-C4H3		1.600E+34	-7.28	20.21	!Wang&Frenklach1997
62.	C2H2	+C2H2	=C4H2	+H2	1.500E+13	0.0	178.67	!Fournet1999
63.	C2H2	+C2H2	=C4H4		5.500E+12	0.0	154.65	!Duran1989
64.	C2H3	+H	+M(2)	=C2H4	0.608E+13	0.27	1.170	!Wang&Frenklach1997
LOW	1.400E+30	-3.860		13.89				
TROE	0.782	207.5	2663.0	6095.0				
65.	C2H3	+H	=C2H2	+H2	3.000E+13	0.0	0.000	!Wang&Frenklach1997
66.	C2H3	+CH	=3CH2	+C2H2	5.000E+13	0.0	0.0	!Miller&Melius1992
67.	C2H3	+1CH2	=CH3	+C2H2	1.810E+13	0.0	0.0	!Tsang1986
68.	C2H3	+3CH2	=C2H2	+CH3	1.810E+13	0.0	0.0	!Zhang&Mckinnon1995
69.	C2H3	+3CH2	=AC3H4	+H	3.000E+13	0.0	0.0	!Miller&Melius1992
70.	C2H3	+CH3	=AC3H5	+H	7.200E+13	0.0	0.0	!Fahr1999
71.	C2H3	+CH3	=C2H2	+CH4	3.920E+11	0.0	0.0	!Tsang1986
72.	C2H3	+CH3	=C3H6		2.500E+13	0.0	0.0	!Tsang1986
73.	C2H3	+C2H	=C2H2	+C2H2	3.000E+13	0.0	0.0	!Miller&Melius1992
74.	C2H3	+C2H	=C4H4		2.120E+60	-13.45	115.27	!Richter&Howard2002
75.	C2H3	+C2H	=N-C4H3	+H	1.800E+13	0.0	0.0	!Tsang1986
76.	C2H3	+C2H2	=C4H4	+H	4.600E+16	-1.25	35.15	!Wang&Frenklach1994
77.	C2H3	+C2H2	=N-C4H5		2.400E+31	-6.95	23.43	!Wang&Frenklach1994
78.	C2H3	+C2H2	=I-C4H5		1.000E+37	-8.77	41.01	!Wang&Frenklach1994
79.	C2H3	+C2H3	=C2H2	+C2H4	1.440E+13	0.0	0.0	!Fahr1991
80.	C2H3	+C2H3	=C4H6		1.500E+52	-11.97	67.37	!Wang&Frenklach1997
81.	C2H3	+C2H3	=I-C4H5	+H	7.200E+28	-4.49	59.83	!Wang&Frenklach1997
82.	C2H3	+C2H3	=N-C4H5	+H	4.600E+24	-3.38	61.51	!Wang&Frenklach1997
83.	C2H4	+M(2)	=C2H2	+H2	0.800E+13	0.44	371.43	!Wang&Frenklach1997
LOW	7.000E+50	-9.310		417.83				
TROE	0.7345	180.0	1035.0	5417.0				
84.	C2H4	+H	+M(2)	=C2H5	1.080E+12	0.454	7.62	!Wang&Frenklach1997
LOW	1.200E+42	-7.620		29.16				
TROE	0.9753	210.0	987.0	4374.0				
85.	C2H4	+H	=C2H3	+H2	1.330E+06	2.53	51.21	!Wang&Frenklach1997
86.	C2H4	+CH	=AC3H4	+H	1.750E+15	-0.38	0.42	!Richter&Howard2002
87.	C2H4	+CH	=AC3H5		1.670E+34	-7.60	15.44	!Richter&Howard2002
88.	C2H4	+1CH2	=C3H6		9.030E+13	0.0	0.0	!Zhang&Mckinnon1995
89.	C2H4	+3CH2	=AC3H5	+H	3.190E+12	0.0	22.11	!Zhang&Mckinnon1995
90.	C2H4	+CH3	=C2H3	+CH4	0.227E+06	2.0	38.49	!Wang&Frenklach1997
91.	C2H4	+C2H	=C4H4	+H	1.200E+13	0.0	0.0	!Tsang1986
92.	C2H4	+C2H3	=C4H6	+H	7.400E+14	-0.66	35.23	!Wang&Frenklach1997
93.	C2H4	+C2H3	=I-C4H7		2.110E+22	-4.70	4.980	!Richter&Howard2002
94.	C2H4	+C2H4	=C2H3	+C2H5	4.820E+14	0.0	299.33	!Tsang1986
95.	C2H5	+H	+M(2)	=C2H6	0.521E+18	-0.99	6.610	!Wang&Frenklach1997
LOW	1.990E+41	-7.08		27.97				
TROE	0.8422	125.0	2219.0	6882.0				
96.	C2H5	+H	=C2H4	+H2	0.200E+13	0.0	0.00	!Wang&Frenklach1997
97.	C2H5	+1CH2	=C2H4	+CH3	9.030E+12	0.0	0.0	!Zhang&Mckinnon1995
98.	C2H5	+1CH2	=C3H6	+H	9.030E+12	0.0	0.0	!Zhang&Mckinnon1995
99.	C2H5	+3CH2	=C2H4	+CH3	1.810E+13	0.0	0.0	!Zhang&Mckinnon1995
100.	C2H5	+CH3	=C2H4	+CH4	1.950E+13	-0.5	0.0	!Tsang1986
101.	C2H5	+CH3	=C3H8		3.370E+13	0.0	0.0	!Baulch1994
102.	C2H5	+C2H	=C3H3	+CH3	1.810E+13	0.0	0.0	!Tsang1986
103.	C2H5	+C2H	=C2H4	+C2H2	1.810E+12	0.0	0.0	!Tsang1986
104.	C2H5	+C2H3	=C2H6	+C2H2	4.820E+11	0.0	0.0	!Zhang&Mckinnon1995
105.	C2H5	+C2H3	=C4H8		1.500E+13	0.0	0.0	!Tsang1986
106.	C2H5	+C2H5	=C2H6	+C2H4	1.390E+12	0.0	0.0	!Zhang&Mckinnon1995
107.	C2H6	+H	=C2H5	+H2	1.150E+08	1.9	31.51	!Wang&Frenklach1997
108.	C2H6	+1CH2	=C2H5	+CH3	0.400E+14	0.0	-2.30	!Wang&Frenklach1997
109.	C2H6	+CH3	=C2H5	+CH4	0.614E+07	1.74	43.72	!Wang&Frenklach1997
110.	C2H6	+C2H	=C2H5	+C2H2	3.600E+12	0.0	0.0	!Tsang1986
111.	C2H6	+C2H3	=C2H5	+C2H4	1.500E+13	0.0	41.8	!Hidaka1985
*****								
**** 4. C3 REACTIONS								
*****								
112.	C3H2	+CH	=C4H2	+H	5.000E+13	0.0	0.0	!Wang&Frenklach1997
113.	C3H2	+3CH2	=N-C4H3	+H	5.000E+13	0.0	0.0	!Wang&Frenklach1997
114.	C3H2	+CH3	=C4H4	+H	5.000E+12	0.0	0.0	!Wang&Frenklach1997
115.	C3H2	+C3H2	=C4H2	+C2H2	2.000E+13	0.0	355.66	!Kern1991
116.	C3H2	+C3H2	=C6H2	+H2	2.000E+13	0.0	355.66	!Kern1991
117.	C3H3	=C3H2	+H		5.200E+12	0.0	328.24	!Scherer2000
118.	C3H3	+H	+M(2)	=AC3H4	3.000E+13	0.0	0.0	!Wang&Frenklach1997
LOW	1.400E+31	-5.0		-25.11				
TROE	0.500	2000.0	10.0	10000.0				
119.	C3H3	+H	+M(2)	=PC3H4	3.000E+13	0.0	0.0	!Wang&Frenklach1997
LOW	1.400E+31	-5.0		-25.11				
TROE	0.500	2000.0	10.0	10000.0				
120.	C3H3	+H	=C3H2	+H2	5.000E+13	0.0	4.18	!Miller&Melius1992
121.	C3H3	+CH	=N-C4H3	+H	7.000E+13	0.0	0.0	!Miller&Melius1992
122.	C3H3	+CH	=I-C4H3	+H	7.000E+13	0.0	0.0	!Miller&Melius1992
123.	C3H3	+3CH2	=C4H4	+H	2.000E+13	0.0	0.0	!Wang&Frenklach1997
124.	C3H3	+CH3	+M(2)	=C4H612	1.500E+13	0.0	0.0	!Wang&Frenklach1997

LOW	2.600E+58	-11.94	40.88				
TROE	0.175	1340.0	60000.0				9769.0
125.	C3H3	+C2H3	=C5H5	+H	9.630E+40	-7.8	120.59 !Marinov1996
126.	C3H3	+C3H3	=C6H5	+H	3.000E+12	0.0	0.0 !Marinov1996
127.	AC3H4	=PC3H4			2.500E+12	0.0	246.87 !Hidaka1989
128.	AC3H4	+H	=C3H3	+H2	1.150E+08	1.9	31.51 !Wang&Frenklach1997
129.	AC3H4	+CH3	=C3H3	+CH4	1.000E+12	0.0	33.47 !Hidaka1992
130.	AC3H4	+C2H	=C2H2	+C3H3	1.000E+13	0.0	0.0 !Wang&Frenklach1997
131.	AC3H4	+C3H3	=C6H6	+H	1.400E+12	0.0	41.84 !Hidaka1989
132.	AC3H4	+AC3H4	=AC3H5	+C3H3	5.000E+14	0.0	270.9 !Dagaut1990
133.	PC3H4	+H	=C3H3	+H2	1.150E+08	1.9	31.51 !Wang&Frenklach1997
134.	PC3H4	+H	+M(2)	=TC3H5 +M(2)	6.500E+12	0.0	8.37 !Wagner1972
LOW	8.450E+39	-7.27	27.52				!Marinov1996
TROE	0.5	1E+30	1E+30				
135.	PC3H4	+CH3	=C3H3	+CH4	1.000E+12	0.0	33.47 !Hidaka1992
136.	PC3H4	+C2H	=C2H2	+C3H3	1.000E+13	0.0	0.0 !Wang&Frenklach1997
137.	PC3H4	+C2H3	=C3H3	+C2H4	2.200E+00	3.5	19.6 !Ziegler2005
138.	PC3H4	+C2H5	=C3H3	+C2H6	2.200E+00	3.5	27.6 !Ziegler2005
139.	CYC3H4	=AC3H4			1.510E+14	0.0	210.88 !Karnil1988
140.	CYC3H4	=PC3H4			7.080E+13	0.0	182.85 !Karnil1988
141.	AC3H4	+H	+M(2)	=AC3H5 +M(2)	1.200E+11	0.69	12.58 !Tsang1991
LOW	5.560E+33	-5.0	18.61				!Marinov1996
TROE	0.5	1E+30	1E+30				
142.	AC3H4	+H	+M(2)	=TC3H5 +M(2)	8.490E+12	0.0	8.37 !Wagner1972
LOW	1.110E+34	-5.0	18.61				!Marinov1996
TROE	0.5	1E+30	1E+30				
143.	AC3H5	+H	=AC3H4	+H2	1.000E+13	0.0	0.0 !Westbrook&Pitz1984
144.	AC3H5	+1CH2	=C4H6	+H	3.010E+13	0.0	0.0 !Tsang1991
145.	AC3H5	+CH3	=AC3H4	+CH4	3.010E+12	-0.32	0.55 !Tsang1991
146.	AC3H5	+C2H	=C3H3	+C2H3	2.000E+01	0.0	0.0 !Tsang1991
147.	AC3H5	+C2H	=AC3H4	+C2H2	1.500E-01	0.0	0.0 !Tsang1991
148.	AC3H5	+C2H	=C5H6		4.820E+13	0.0	0.0 !Tsang1991
149.	AC3H5	+C2H2	=L-C5H7		3.190E+10	0.0	29.10 !Tsang1991
150.	AC3H5	+C2H3	=AC3H4	+C2H4	2.410E+12	0.0	0.0 !Tsang1991
151.	AC3H5	+C2H3	=C3H6	+C2H2	4.820E+12	0.0	0.0 !Tsang1991
152.	AC3H5	+C2H3	=C5H6	+H +H	1.590E+65	-14.00	256.34 !Marinov1996
153.	AC3H5	+C2H4	=C5H8	+H	6.030E+09	0.0	48.06 !Tsang1991
154.	AC3H5	+C2H5	=AC3H4	+C2H6	9.640E+11	0.0	-0.55 !Tsang1991
155.	AC3H5	+C2H5	=C3H6	+C2H4	2.590E+12	0.0	-0.55 !Tsang1991
156.	AC3H5	+AC3H5	=AC3H4	+C3H6	8.430E+10	0.0	-1.10 !Tsang1991
157.	AC3H5	+C3H3	=C6H6	+H +H	5.600E+20	-2.54	7.1 !Ziegler2005
158.	SC3H5	=PC3H4	+H		1.400E+13	0.0	146.3 !Heyberger2002
159.	SC3H5	=AC3H5			5.000E+13	0.0	154.7 !Weissman1989
160.	SC3H5	+H	=C3H6		1.000E+14	0.0	0.0 !Allara1980
161.	SC3H5	+CH3	=AC3H4	+CH4	1.000E+11	0.0	0.0 !Ziegler2005
162.	SC3H5	+C2H3	=AC3H4	+C2H4	1.000E+11	0.0	0.0 !Ziegler2005
163.	SC3H5	+C2H5	=AC3H4	+C2H6	1.000E+11	0.0	0.0 !Ziegler2005
164.	SC3H5	=C2H2	+CH3		1.300E+13	0.0	139.75 !Dean1985
165.	SC3H5	+H	=PC3H4	+H2	2.000E+13	0.0	0.0 !Marinov1996
166.	SC3H5	+H	=AC3H5	+H	1.000E+14	0.0	0.0 !Marinov1996
167.	TC3H5	+H	=PC3H4	+H2	4.000E+13	0.0	0.0 !Marinov1996
168.	TC3H5	+H	=AC3H5	+H	1.000E+14	0.0	0.0 !Marinov1996
169.	AC3H5	+H	=C3H6		2.000E+14	0.0	0.0 !Tsang1991
170.	TC3H5	+H	=C3H6		1.000E+14	0.0	0.0 !Allara1980
171.	TC3H5	+H	=AC3H4	+H2	3.300E+12	0.0	0.0 !Dagaut1991
172.	TC3H5	+CH3	=AC3H4	+CH4	1.000E+11	0.0	0.0 !Dagaut1991
173.	TC3H5	+C2H3	=AC3H4	+C2H4	1.000E+12	0.0	0.0 !Leung&Lindstedt1995
174.	TC3H5	+C2H5	=AC3H4	+C2H6	1.000E+12	0.0	0.0 !Leung&Lindstedt1995
175.	C3H6	=C2H2	+CH4		1.800E+12	0.0	292.7 !Hidaka1992
176.	C3H6	=PC3H4	+H2		2.000E+13	0.0	334.74 !Hidaka1992
177.	C3H6	+H	+M(2)	=I-C3H7 +M(2)	5.700E+09	1.16	3.66 !Seakins1993
LOW	1.640E+54	-11.1	39.18				
TROE	1.000	1E-15	260.0				3000.0
178.	C3H6	+H	=CH3	+C2H4	3.400E+13	0.0	14.64 !Hidaka1992
179.	C3H6	+H	=AC3H5	+H2	6.000E+12	0.0	6.28 !Rao&Skinner1989
180.	C3H6	+H	=TC3H5	+H2	1.300E+15	0.0	95.40 !Hidaka1992
181.	C3H6	+H	=SC3H5	+H2	2.500E+15	0.0	95.40 !Hidaka1992
182.	C3H6	+1CH2	=AC3H5	+CH3	7.230E+11	0.0	25.91 !Tsang1991
183.	C3H6	+CH3	=AC3H5	+CH4	2.210E+00	3.5	23.75 !Tsang1991
184.	C3H6	+CH3	=TC3H5	+CH4	1.100E+11	0.0	46.44 !Hidaka1992
185.	C3H6	+CH3	=SC3H5	+CH4	2.100E+11	0.0	46.44 !Hidaka1992
186.	C3H6	+C2H	=PC3H4	+C2H3	1.210E+13	0.0	0.0 !Tsang1991
187.	C3H6	+C2H3	=SC3H5	+C2H4	1.300E+00	3.5	45.6 !Tsang1991
188.	C3H6	+C2H3	=AC3H5	+C2H4	2.200E+00	3.5	19.6 !Tsang1991
189.	C3H6	+C2H3	=TC3H5	+C2H4	0.800E+00	3.5	40.5 !Tsang1991
190.	C3H6	+C2H3	=C4H6	+CH3	7.230E+11	0.0	20.96 !Tsang1991
191.	C3H6	+C2H5	=AC3H5	+C2H6	2.230E+00	3.5	27.77 !Tsang1991
192.	C3H6	+C3H6	=AC3H5	+I-C3H7	2.530E+14	0.0	231.0 !Tsang1991
193.	C3H6	+C3H6	=AC3H5	+N-C3H7	4.880E+13	0.0	219.0 !Tsang1991
194.	C3H6	+C3H6	=1-C6H12		1.270E+02	2.5	154.0 !Tsang1991

195.	C3H6	+C3H6	=4mlpent		1.686E+03	2.1	150.0	!Tsang1991	
196.	N-C3H7	=I-C3H7			2.000E+10	1.0	161.3	!Ziegler2005	
197.	N-C3H7	=C3H6	+H		1.260E+13	0.0	161.0	!Dean1985	
198.	N-C3H7	=C2H4	+CH3		1.210E+13	0.0	126.0	!Tsang1988	
199.	N-C3H7	+H	=C2H5	+CH3	1.000E+14	0.0	0.0	!Tsang1988	
200.	N-C3H7	+H	=C3H6	+H2	1.810E+12	0.0	0.0	!Tsang1988	
201.	N-C3H7	+H	=C3H8		1.000E+14	0.0	0.0	!Allara1980	
202.	N-C3H7	+3CH2	=C2H5	+C2H4	1.810E+13	0.0	0.0	!Tsang19880	
203.	N-C3H7	+3CH2	=C3H6	+CH3	1.810E+12	0.0	0.0	!Tsang1988	
204.	N-C3H7	+CH3	=C3H6	+CH4	1.140E+13	-0.32	0.0	!Tsang1988	
205.	N-C3H7	+C2H	=C3H6	+C2H2	6.030E+12	0.0	0.0	!Tsang1988	
206.	N-C3H7	+C2H	=C3H3	+C2H5	1.210E+13	0.0	0.0	!Tsang1988	
207.	N-C3H7	+C2H3	=C3H6	+C2H4	1.210E+12	0.0	0.0	!Tsang1988	
208.	N-C3H7	+C2H3	=C3H8	+C2H2	1.210E+12	0.0	0.0	!Tsang1988	
209.	N-C3H7	+C2H5	=C3H8	+C2H4	1.150E+12	0.0	0.0	!Tsang1988	
210.	N-C3H7	+C2H5	=C3H6	+C2H6	1.450E+12	0.0	0.0	!Tsang1988	
211.	N-C3H7	+C2H6	=C3H8	+C2H5	2.530E-01	3.82	37.83	!Tsang1988	
212.	N-C3H7	+AC3H5	=AC3H4	+C3H8	7.230E+11	0.0	-0.55	!Tsang1991	
213.	N-C3H7	+C3H6	=C3H8	+AC3H5	2.230E+00	3.5	27.77	!Tsang1991	
214.	N-C3H7	+N-C3H7	=C3H8	+C3H6	1.690E+12	0.0	0.0	!Tsang1988	
215.	I-C3H7	=C2H4	+CH3		1.000E+12	0.0	145.0	!Konar1968	
216.	I-C3H7	+H	=C3H6	+H2	3.610E+12	0.0	0.0	!Tsang1988	
217.	I-C3H7	+H	=C3H8		2.000E+13	0.0	0.0	!Warnatz1984	
218.	I-C3H7	+H	=C2H5	+CH3	5.000E+13	0.0	0.0	!Tsang1988	
219.	I-C3H7	+CH3	=C3H6	+CH4	9.410E+10	0.68	0.0	!Tsang1988	
220.	I-C3H7	+C2H	=C3H6	+C2H2	3.610E+12	0.0	0.0	!Tsang1988	
221.	I-C3H7	+C2H2	=C4H6	+CH3	2.770E+10	0.0	27.21	!Tsang1988	
222.	I-C3H7	+C2H3	=C3H6	+C2H4	1.520E+14	-0.7	0.0	!Tsang1988	
223.	I-C3H7	+C2H3	=C3H8	+C2H2	1.520E+14	-0.70	0.0	!Tsang1988	
224.	I-C3H7	+C2H5	=C3H6	+C2H6	2.300E+13	-0.35	0.0	!Tsang1988	
225.	I-C3H7	+C2H5	=C3H8	+C2H4	1.840E+13	-0.35	0.0	!Tsang1988	
226.	I-C3H7	+C2H6	=C3H8	+C2H5	8.440E-01	4.2	36.47	!Tsang1988	
227.	I-C3H7	+AC3H5	=C3H8	+AC3H4	4.580E+12	-0.35	-0.55	!Tsang1991	
228.	I-C3H7	+C3H6	=C3H8	+AC3H5	6.620E-02	4.00	33.77	!Tsang1991	
229.	I-C3H7	+N-C3H7	=C3H8	+C3H6	5.130E+13	-0.35	0.0	!Tsang1988	
230.	I-C3H7	+I-C3H7	=C3H8	+C3H6	2.110E+14	-0.70	0.0	!Tsang1988	
231.	C3H8	+H	=N-C3H7	+H2	1.330E+06	2.54	28.27	!Tsang1988	
232.	C3H8	+H	=I-C3H7	+H2	1.300E+06	2.40	18.71	!Tsang1988	
233.	C3H8	+CH3	=N-C3H7	+CH4	9.040E-01	3.65	29.93	!Tsang1988	
234.	C3H8	+CH3	=I-C3H7	+CH4	1.510E+00	3.46	22.93	!Tsang1988	
235.	C3H8	+N-C3H7	=C3H8	+I-C3H7	8.440E-04	4.00	19.77	!Tsang1988	
*****									
**** 5. C4 REACTIONS									
*****									
236.	C4H	+H	+M(2)	=C4H2	+M(2)	1.000E+17	-1.0	0.0	!Wang&Frenklach1997
LOW		3.750E+33	-4.80	7.95					
TROE	0.6464	132.0	1315.0	5566.0					
237.	C4H	+H2	=C4H2	+H	4.900E+05	2.5	2.34	!Wang&Frenklach1997	
238.	C4H	+C2H2	=C6H2	+H	9.600E+13	0.0	0.0	!Wang&Frenklach1997	
239.	C4H2	+C2H	=C4H	+C2H2	2.000E+13	0.0	0.0	!Frenklach&Warnatz1987	
240.	C4H2	+C2H	=C6H2	+H	9.600E+13	0.0	0.0	!Wang&Frenklach1997	
241.	C4H2	+C2H	=C6H3		1.300E+30	-6.12	10.5	!Wang&Frenklach1997	
242.	C4H2	+C4H	=C8H2	+H	1.200E+14	0.0	0.0	!Kern1991	
243.	C4H2	+C4H2	=C8H2	+H2	1.510E+13	0.0	178.67	!Kern1991	
244.	N-C4H3	=I-C4H3			1.000E+51	-12.45	213.39	!Wang&Frenklach1997	
245.	N-C4H3	+M(2)	=C4H2	+H	+M(2)	1.000E+14	0.0	150.63	!Miller&Melius1992
LOW		1.000E+14	0.0	125.53					
TROE	0.5	1E+30	1E+30						
246.	N-C4H3	+H	=I-C4H3	+H	9.200E+11	0.63	12.51	!Wang&Frenklach1997	
247.	N-C4H3	+H	=C2H2	+C2H2	1.300E+20	-1.85	12.39	!Wang&Frenklach1997	
248.	N-C4H3	+H	=C4H4		1.100E+42	-9.65	29.29	!Wang&Frenklach1997	
249.	N-C4H3	+H	=C4H2	+H2	1.500E+13	0.0	0.0	!Wang&Frenklach1997	
250.	N-C4H3	+C2H2	=L-C6H4	+H	1.800E+19	-1.95	55.23	!Wang&Frenklach1997	
251.	N-C4H3	+C2H2	=N-C6H5		4.100E+33	-7.12	57.32	!Wang&Frenklach1997	
252.	N-C4H3	+C2H2	=C6H5		9.800E+68	-17.58	110.88	!Wang&Frenklach1997	
253.	N-C4H3	+C2H2	=C-C6H4	+H	3.500E+41	-8.63	96.24	!Wang&Frenklach1997	
254.	N-C4H3	+C4H2	=A1C2H-		9.800E+68	-17.58	110.88	!Wang&Frenklach1997	
255.	I-C4H3	+M(2)	=C4H2	+H	+M(2)	1.000E+14	0.0	230.13	!Miller&Melius1992
LOW		2.000E+15	0.0	200.84					
TROE	0.5	1E+30	1E+30						
256.	I-C4H3	+H	=C2H2	+C2H2	3.700E+22	-2.50	21.51	!Wang&Frenklach1997	
257.	I-C4H3	+H	=C4H4		5.300E+46	-10.68	38.79	!Wang&Frenklach1997	
258.	I-C4H3	+H	=C4H2	+H2	3.000E+13	0.0	0.0	!Wang&Frenklach1997	
259.	I-C4H3	+H2	=C2H2	+C2H3	5.010E+10	0.0	83.68	!Colket1986	
260.	I-C4H3	+3CH2	=AC3H4	+C2H	2.000E+13	0.0	0.0	!Miller&Melius1992	
261.	I-C4H3	+CH3	=C5H6		1.000E+12	0.0	0.0	!Ziegler2005	
262.	I-C4H3	+C2H3	=C6H5	+H	6.000E+12	0.0	0.0	!Pope&Miller2000	
263.	C4H4	=C4H2	+H2		1.260E+15	0.0	396.24	!Braun-Unkhoff1989	
264.	C4H4	+H	=N-C4H5		1.100E+50	-11.94	56.07	!Wang&Frenklach1997	
265.	C4H4	+H	=I-C4H5		2.100E+52	-12.44	64.86	!Wang&Frenklach1997	

266.	C4H4	+H	=N-C4H3	+H2	6.650E+05	2.53	51.21	!Wang&Frenklach1997
267.	C4H4	+H	=I-C4H3	+H2	3.330E+05	2.53	38.66	!Wang&Frenklach1997
268.	C4H4	+CH3	=I-C4H3	+CH4	6.300E+11	0.0	66.9	!Ziegler2005
269.	C4H4	+CH3	=N-C4H3	+CH4	6.300E+11	0.0	77.3	!Ziegler2005
270.	C4H4	+C2H	=I-C4H3	+C2H2	4.000E+13	0.0	0.0	!Fournet1999
271.	C4H4	+C2H	=N-C4H3	+C2H2	4.000E+13	0.0	0.0	!Kiefer1985
272.	C4H4	+C2H	=C4H2	+C2H3	1.000E+13	0.0	0.0	!Kiefer1985
273.	C4H4	+C2H2	=C6H5	+H	1.000E+09	0.0	126.00	!Benson1992
274.	C4H4	+C2H2	=C6H6		4.470E+11	0.0	126.00	!Chanmugathas1986
275.	C4H4	+C2H3	=L-C6H6	+H	1.900E+17	-1.32	44.35	!Wang&Frenklach1997
276.	C4H4	+C2H3	=N-C4H3	+C2H4	5.000E+11	0.0	68.20	!Colket1986
277.	C4H4	+C2H3	=I-C4H3	+C2H4	5.000E+11	0.0	68.20	!Colket1986
278.	C4H4	+C3H3	=N-C4H3	+AC3H4	1.000E+13	0.0	94.1	!Ziegler2005
279.	C4H4	+C3H3	=I-C4H3	+AC3H4	1.000E+13	0.0	81.5	!Ziegler2005
280.	C4H4	+AC3H5	=I-C4H3	+C3H6	1.000E+13	0.00	81.5	!Ziegler2005
281.	C4H4	+C4H4	=A1C2H3		0.750E+14	0.0		
	159.00		!estimated/Lundgard&Heicklen1984					
282.	C4H4	+C4H4	=C8H8		4.370E+10	0.0	76.99	!Lundgard&Heicklen1984
283.	N-C4H5	=I-C4H5			4.900E+66	-17.26	231.80	!Wang&Frenklach1994
284.	N-C4H5	+H	=I-C4H5	+H	1.000E+34	-5.61	77.41	!Wang&Frenklach1997
285.	N-C4H5	+H	=C4H4	+H2	1.500E+13	0.0	0.0	!Wang&Frenklach1997
286.	N-C4H5	+C2H2	=N-C6H7		1.100E+14	-1.27	12.13	!Wang&Frenklach1994
287.	N-C4H5	+C2H2	=C-C6H7		5.000E+24	-5.46	19.25	!Wang&Frenklach1994
288.	N-C4H5	+C2H2	=L-C6H6	+H	5.800E+08	1.02	45.61	!Wang&Frenklach1994
289.	N-C4H5	+C2H2	=C6H6	+H	2.100E+15	-1.07	20.08	!Wang&Frenklach1994
290.	N-C4H5	+C2H3	=C6H6	+H2	2.800E-07	5.63	-7.91	!Westmoreland1989
291.	N-C4H5	+C2H3	=C6H813		5.500E+15	-1.67	6.15	!Westmoreland1989
292.	N-C4H5	+C2H3	=N-C6H7	+H	8.300E-28	11.89	20.9	!Westmoreland1989
293.	N-C4H5	+C2H3	=L-C6H8		2.900E+15	-0.78	4.2	!Westmoreland1989
294.	N-C4H5	+AC3H4	=C7H8	+H	2.000E+11	0.0	15.48	!Kern1988
295.	N-C4H5	+PC3H4	=C7H8	+H	3.160E+11	0.0	15.48	!Cole1984
296.	N-C4H5	+C4H2	=A1C2H	+H	3.160E+11	0.0	7.53	!Cole1984
297.	N-C4H5	+C4H4	=A1C2H3	+H	3.160E+11	0.0	2.51	!Cole1984
298.	I-C4H5	+H	=C4H4	+H2	3.000E+13	0.0	0.0	!Wang&Frenklach1997
299.	I-C4H5	+H	=C3H3	+CH3	2.000E+13	0.0	8.37	!Wang&Frenklach1997
300.	I-C4H5	+H	=C4H52	+H	3.000E+13	0.0	0.0	!Marinov1996
301.	C4H52	+H	=C3H3	+CH3	1.000E+14	0.0	0.0	!Marinov1996
302.	C4H52	+C3H3	=C7H7	+H	3.000E+12	0.0	0.0	!Marinov1996
303.	C4H52	+C4H52	=ACH3CH2	+H	3.000E+12	0.0	0.0	!Marinov1996
304.	C4H512	=C4H4	+H		3.000E+13	0.0	188.29	!Hidaka1993
305.	N-C4H51	=I-C4H51			5.000E+12	0.0	156.3	!Belmekki2002
306.	N-C4H51	=C4H4	+H		3.000E+13	0.0	188.29	!Hidaka1993
307.	N-C4H51	=C2H	+C2H4		2.000E+14	0.0	238.50	!Hidaka1993
308.	I-C4H51	+M(2)	=C4H4	+H	1.000E+13	0.0	204.8	!Marinov1996
LOW		2.000E+14	0.0	41.0				
TROE	0.5	1E+30	1E+30					
309.	I-C4H51	+H	=C3H3	+CH3	1.000E+14	0.0	0.0	!Marinov1996
310.	I-C4H51	+H	=C4H4	+H2	2.000E+13	0.0	0.0	!Miller&Melius1992
311.	I-C4H51	+C3H3	=C7H7	+H	3.000E+12	0.0	0.0	!Marinov1996
312.	I-C4H51	+I-C4H51	=ACH3CH2	+H	3.000E+12	0.0	0.0	!Marinov1996
313.	C4H6	=I-C4H5	+H		3.300E+45	-8.95	484.95	!Wang&Frenklach1997
314.	C4H6	=N-C4H5	+H		8.500E+54	-11.78	533.49	!Wang&Frenklach1997
315.	C4H6	=C2H4	+C2H2		6.400E+13	0.0	322.60	!Hidaka1996
316.	C4H6	=C4H4	+H2		2.520E+15	0.0	396.24	!Hidaka1996
317.	C4H6	+H	=N-C4H5	+H2	1.330E+06	2.53	51.21	!Wang&Frenklach1997
318.	C4H6	+H	=I-C4H5	+H2	6.650E+05	2.53	38.66	!Wang&Frenklach1997
319.	C4H6	+CH3	=N-C4H5	+CH4	4.000E+14	0.0	95.40	!Hidaka1993
320.	C4H6	+CH3	=I-C4H5	+CH4	2.000E+14	0.0	95.40	!Hidaka1993
321.	C4H6	+C2H2	=C6H814		2.300E+12	0.0	146.45	!Westmoreland1989
322.	C4H6	+C2H3	=N-C4H5	+C2H4	5.000E+14	0.0	95.40	!Hidaka1993
323.	C4H6	+C2H3	=I-C4H5	+C2H4	5.000E+14	0.0	82.8	!Ziegler2005
324.	C4H6	+C2H3	=L-C6H8	+H	1.000E+10	1.05	58.5	!Westmoreland1989
325.	C4H6	+C3H3	=N-C4H5	+AC3H4	1.000E+13	0.0	94.14	!Kern1988
326.	C4H6	+C3H3	=I-C4H5	+AC3H4	1.000E+13	0.0	94.14	!Kern1988
327.	C4H6	+AC3H5	=I-C4H5	+C3H6	1.000E+13	0.0	81.5	!Ziegler2005
328.	C4H6	+AC3H5	=N-C4H5	+C3H6	1.000E+13	0.0	94.1	!Ziegler2005
329.	C4H6	+C4H6	=C8H12		1.380E+11	0.0	112.26	!Rowley&Steiner1951
330.	C4H612	=C4H6			2.500E+13	0.0	263.60	!Hidaka1995
331.	C4H612	+H	=AC3H4	+CH3	6.000E+12	0.0	8.79	!Hidaka1993
332.	C4H612	+H	=C4H512	+H2	6.500E+13	0.0	39.33	!Hidaka1993
333.	C4H612	+H	=C4H6	+H	2.000E+13	0.0	16.74	!Wang&Frenklach1997
334.	C4H612	+H	=I-C4H5	+H2	1.700E+05	2.5	10.42	!Wang&Frenklach1997
335.	C4H612	+H	=C4H52	+H2	1.500E+07	2.0	25.1	!Marinov1996
336.	C4H612	+H	=I-C4H51	+H2	3.000E+07	2.0	27.2	!Marinov1996
337.	C4H612	+CH3	=I-C4H5	+CH4	2.200E+00	3.5	23.8	!Ziegler2005
338.	C4H612	+CH3	=C4H512	+CH4	1.000E+14	0.0	81.59	!Hidaka1993
339.	C4H612	+C2H3	=C4H512	+C2H4	7.500E+12	0.0	41.84	!Hidaka1993
340.	C4H612	+C2H5	=I-C4H5	+C2H6	2.200E+00	3.5	27.6	!Ziegler2005
341.	C4H612	+C3H3	=C4H512	+AC3H4	5.000E+12	0.0	81.59	!Hidaka1993
342.	C4H61	=C3H3	+CH3		3.000E+15	0.0	317.16	!Hidaka1996

343.	C4H61	=C4H612			2.500E+13	0.0	271.97	!Hidaka1996
344.	C4H61	=I-C4H51	+H		7.700E+14	0.0	367.4	!Belmekki2002
345.	C4H61	=N-C4H51	+H		9.100E+14	0.0	416.3	!Belmekki2002
346.	C4H61	+H	=AC3H4	+CH3	1.300E+05	2.5	4.18	!Hidaka1993
347.	C4H61	+H	=C2H5	+C2H2	6.500E+04	2.5	4.18	!Hidaka1993
348.	C4H61	+H	=I-C4H51	+H2	6.500E+13	0.0	39.33	!Hidaka1993
349.	C4H61	+H	=N-C4H51	+H2	6.500E+13	0.0	39.33	!Hidaka1993
350.	C4H61	+CH3	=I-C4H51	+CH4	1.000E+14	0.0	81.59	!Hidaka1993
351.	C4H61	+CH3	=N-C4H51	+CH4	1.000E+14	0.0	81.59	!Hidaka1993
352.	C4H61	+C2H3	=N-C4H51	+C2H4	1.500E+13	0.0	41.8	!Hidaka1993
353.	C4H61	+C3H3	=N-C4H51	+AC3H4	1.000E+13	0.0	81.59	!Hidaka1993
354.	C4H61	+C3H3	=I-C4H51	+PC3H4	4.000E+12	0.0	5.4	!Belmekki2002
355.	C4H61	+I-C4H3	=I-C4H51	+C4H4	2.000E+12	0.0	54.3	!Belmekki2002
356.	C4H62	=C4H6			3.000E+13	0.0	271.97	!Hidaka1993
357.	C4H62	=C4H612			3.000E+13	0.0	280.34	!Hidaka1993
358.	C4H62	=C4H52	+H		5.000E+14	0.0	365.28	!Dean1985
359.	C4H62	+H	=PC3H4	+CH3	2.600E+05	2.5	4.18	!Hidaka1993
360.	C4H62	+H	=C4H52	+H2	3.400E+05	2.5	10.5	!Belmekki2002
361.	C4H62	+CH3	=C4H52	+CH4	2.000E+14	0.0	81.59	!Hidaka1993
362.	C4H62	+C2H3	=C4H52	+C2H4	1.500E+13	0.0	41.8	!Hidaka1993
363.	C4H62	+C3H3	=C4H52	+AC3H4	1.000E+13	0.0	81.59	!Hidaka1993
364.	C4H62	+C3H3	=C4H52	+PC3H4	1.000E+13	0.0	58.5	!Belmekki2002
365.	C4H62	+I-C4H3	=C4H52	+C4H4	5.000E+12	0.0	58.5	!Belmekki2002
366.	N-C4H7	>C4H6	+H		1.800E+13	0.0	139.2	!Heyberger2002
367.	I-C4H7	=N-C4H7			2.500E+13	0.0	204.8	!Dente1983
368.	I-C4H7	>C4H6	+H		3.200E+13	0.0	200.6	!Weissman1989
369.	I-C4H7	+H	=C4H6	+H2	1.810E+12	0.0	0.0	!Richter&Howard2002
370.	I-C4H7	+H	=C4H8		1.000E+14	0.0	0.0	!Richter&Howard2002
371.	C4H8	=AC3H5	+CH3		1.100E+16	0.0	325.08	!Knyazev&Slagle2001
372.	C4H8	+H	=N-C4H7	+H2	1.300E+07	2.0	10.0	!Chevalier1990
373.	C4H8	+H	=I-C4H7	+H2	5.400E+04	2.5	-7.9	!Ziegler2005
374.	C4H8	+CH3	=N-C4H7	+CH4	3.000E+11	0.0	33.0	!Chevalier1990
375.	C4H8	+CH3	=I-C4H7	+CH4	1.000E+11	0.0	30.5	!Ziegler2005
376.	C4H8	+C2H3	=N-C4H7	+C2H4	3.000E+11	0.0	38.5	!Ziegler2005
377.	C4H8	+C2H3	=I-C4H7	+C2H4	4.400E+00	3.5	17.1	!Ziegler2005
378.	C4H8	+C2H5	=N-C4H7	+C2H6	4.000E+12	0.0	58.5	!Ziegler2005
379.	C4H8	+C2H5	=I-C4H7	+C2H6	4.400E+00	3.5	17.1	!Ziegler2005
380.	C4H8	+AC3H5	=N-C4H7	+C3H6	1.300E+13	0.0	98.2	!Dente1983
381.	C4H8	+AC3H5	=I-C4H7	+C3H6	8.000E+12	0.0	98.2	!Dente1983
382.	C4H8	+SC3H5	=N-C4H7	+C3H6	3.000E+11	0.0	38.5	!Ziegler2005
383.	C4H8	+SC3H5	=I-C4H7	+C3H6	4.400E+00	3.5	17.1	!Ziegler2005

\*\*\*\*\*

\*\*\*\* 6. C5 REACTIONS

\*\*\*\*\*

384.	C5H4	=L-C5H4			1.000E+13	0.0	25.11	!Richter&Howard2002
385.	L-C5H5	+H	=L-C5H4	+H2	1.810E+12	0.0	0.0	!Richter&Howard2002
386.	L-C5H5	+H	=C5H6		1.000E+14	0.0	0.0	!Ziegler2005
387.	L-C5H5	+CH3	=L-C5H4	+CH4	1.950E+13	-0.5	0.0	!Richter&Howard2002
388.	C5H5	=C3H3	+C2H2		2.790E+79	-18.30	547.44	!Moskaleva&Lin2000
389.	C5H5	=L-C5H5			1.640E+96	-23.50	574.95	!Moskaleva&Lin2000
390.	C5H5	=C5H4H			5.170E+80	-20.40	402.46	!Moskaleva&Lin2000
391.	C5H5	+H	=C5H6		2.000E+14	0.0	0.0	!Marinov1996
392.	C5H5	+CH3	=C-C6H7	+H	2.440E+41	-7.989	164.27	!Dean1990
393.	C5H5	+CH3	=C5H5CH3		1.000E+13	0.0	0.0	!Ziegler2005
394.	C5H5	+AC3H5	=C5H6	+AC3H4	1.000E+12	0.0	0.0	!Dean1990
395.	C5H5	+C5H5	>A2	+H	1.000E+11	0.0	33.47	!estimated
396.	C5H4H	=C3H3	+C2H2		3.400E+80	-19.20	427.90	!Moskaleva&Lin2000
397.	C5H4H	+H	=C5H4	+H2	2.800E+13	0.0	9.45	!Richter&Howard2002
398.	C5H6	+H	=C5H5	+H2	2.190E+08	1.77	12.55	!Emdeel1992
399.	C5H6	+H	=C5H4H	+H2	2.800E+13	0.0	147.03	!Richter&Howard2002
400.	C5H6	+H	=AC3H5	+C2H2	6.600E+14	0.0	51.65	!Roy1998
401.	C5H6	+CH3	=C5H5	+CH4	3.110E+11	0.0	23.01	!Marinov1996
402.	C5H6	+CH3	=C5H4H	+CH4	1.800E-01	4.0	137.58	!Richter&Howard2002
403.	C5H6	+C2H3	=C5H5	+C2H4	6.000E+12	0.0	0.0	!Emdeel1992
404.	C5H6	+AC3H5	=C5H5	+C3H6	2.000E-01	4.0	0.0	!Zhong&Bozzelli1998
405.	C5H6	+N-C4H5	=C5H5	+C4H6	1.200E-01	4.0	0.0	!Zhong&Bozzelli1998
406.	C5H6	+I-C4H5	=C5H5	+C4H6	6.000E+12	0.0	0.0	!Emdeel1992
407.	L-C5H7	+H	=L-C5H8		1.000E+14	0.0	0.0	!Marinov1996
408.	C5H7	=C5H6	+H		3.160E+15	0.0	150.63	!Arends1993
409.	C5H7	=L-C5H7			3.160E+15	0.0	165.28	!Arends1993
410.	C5H7	+H	=C5H8		1.000E+14	0.0	0.0	!Ziegler2005
411.	C5H7	+H	=C5H6	+H2	3.600E+12	0.0	0.0	!Ziegler2005
412.	C5H8	=C5H6	+H2		1.100E+13	0.0	246.0	!RickbornSF1986
413.	L-C5H8	+H	=L-C5H7	+H2	7.000E+06	2.0	20.92	!Marinov1996
414.	L-C5H8	+H	=AC3H5	+C2H4	3.350E+08	1.5	8.37	!Marinov1996
415.	C5H8	+H	=C5H7	+H2	1.700E+05	2.5	10.5	!Ziegler2005
416.	C5H8	+CH3	=C5H7	+CH4	2.200E+00	3.5	23.8	!Ziegler2005

\*\*\*\*\*

\*\*\*\* 7. C6 REACTIONS

\*\*\*\*\*

417.	C6H	+H	+M(2)	=C6H2	+M(2)	1.000E+17	-1.0	0.0	!Wang&Frenklach1997
LOW		3.750E+33	-4.80	7.95					
TROE	0.6464	132.0	1315.0	5566.0					
418.	C6H	+H2	=H	+C6H2		4.900E+05	2.5	2.34	!Wang&Frenklach1997
419.	C6H2	+H	=C6H3			2.600E+46	-10.15	64.86	!Wang&Frenklach1997
420.	C6H3	+H	=C4H2	+C2H2		3.700E+22	-2.5	21.51	!Wang&Frenklach1997
421.	C6H3	+H	=L-C6H4			5.300E+46	-10.68	38.79	!Wang&Frenklach1997
422.	C6H3	+H	=C6H2	+H2		3.000E+13	0.0	0.0	!Wang&Frenklach1997
423.	L-C6H4	+H	=N-C6H5			2.600E+43	-9.53	75.73	!Wang&Frenklach1994
424.	L-C6H4	+H	=C6H5			4.700E+78	-20.10	123.43	!Wang&Frenklach1994
425.	L-C6H4	+H	=C-C6H4	+H		9.700E+48	-10.37	112.97	!Wang&Frenklach1994
426.	L-C6H4	+H	=C6H3	+H2		6.650E+06	2.53	38.66	!Wang&Frenklach1997
427.	L-C6H4	+C2H	=C6H3	+C2H2		2.000E+13	0.0	0.0	!Frenklach&Warnatz1987
428.	C-C6H4	+H	=C6H5			1.000E+71	-16.88	143.10	!Wang&Frenklach1994
429.	C-C6H4	+C-C6H4	=BIPHEN			4.600E+12	0.0	0.0	!Porter&Steinfeld1968
430.	N-C6H5	=C6H5				1.300E+59	-14.78	148.96	!Wang&Frenklach1994
431.	N-C6H5	=C-C6H4	+H			1.500E+64	-15.32	257.33	!Wang&Frenklach1994
432.	N-C6H5	+H	=I-C6H5	+H		9.200E+11	0.63	12.51	!Wang&Frenklach1997
433.	N-C6H5	+H	=C4H4	+C2H2		1.300E+20	-1.85	12.39	!Wang&Frenklach1997
434.	N-C6H5	+H	=L-C6H6			1.100E+42	-9.65	29.27	!Wang&Frenklach1997
435.	N-C6H5	+H	=L-C6H4	+H2		1.500E+13	0.0	0.0	!Wang&Frenklach1997
436.	I-C6H5	+H	=C4H4	+C2H2		3.700E+22	-2.50	21.51	!Wang&Frenklach1997
437.	I-C6H5	+H	=L-C6H6			5.300E+46	-10.68	38.79	!Wang&Frenklach1997
438.	I-C6H5	+H	=L-C6H4	+H2		3.000E+13	0.0	0.0	!Wang&Frenklach1997
439.	C6H5	+H	+M(2)	=C6H6	+M(2)	1.000E+14	0.0	0.0	!Wang&Frenklach1997
LOW		6.600E+75	-16.30	29.29					
TROE	1.0000	0.1	584.9	6113.0					
440.	C6H5	+H	=C-C6H4	+H2		4.400E-13	7.831	38.75	!Mabel2001
441.	C6H5	+CH3	=C7H8			1.070E+65	-15.64	95.06	!Richter&Howard2002
442.	C6H5	+CH3	=C7H7	+H		4.440E+33	-5.45	101.63	!Richter&Howard2002
443.	C6H5	+C2H2	=N-A1C2H2			9.900E+41	-9.26	65.69	!Wang&Frenklach1994
444.	C6H5	+C2H2	=A1C2H	+H		8.320E+22	-2.68	72.81	!Richter&Howard2002
445.	C6H5	+C2H2	=A1C2H3*			7.900E+51	-12.41	74.35	!Richter&Howard2002
446.	C6H5	+C2H	=A1C2H			2.540E+17	-1.489	6.45	!Zhang&Mckinnon1995
447.	C6H5	+C2H3	=A1C2H3			3.900E+38	-7.63	53.98	!Wang&Frenklach1997
448.	C6H5	+C2H3	=I-A1C2H2+H			5.800E+18	-1.00	112.14	!Wang&Frenklach1997
449.	C6H5	+C2H3	=N-A1C2H2+H			5.100E+20	-1.56	131.38	!Wang&Frenklach1997
450.	C6H5	+C2H4	=A1C2H3	+H		2.500E+12	0.0	25.94	!Fahr&Stein1988
451.	C6H5	+C2H5	=A1C2H5			5.000E+12	0.0	0.0	!Ziegler2005
452.	C6H5	+N-C4H3	=A2			1.510E+75	-17.845	165.69	!Richter&Howard2002
453.	C6H5	+N-C4H3	=A2-2	+H		1.840E+72	-16.129	241.14	!Richter&Howard2002
454.	C6H5	+C4H4	=A2	+H		9.900E+30	-5.07	88.29	!Appel2000
455.	C6H5	+C4H4	=A1C2H	+C2H3		3.200E+11	0.0	5.65	!Harris1988
456.	C6H5	+C4H6	=A1C2H3	+C2H3		3.200E+11	0.0	7.95	!Harris1988
457.	C6H5	+C5H6	=C5H5	+C6H6		1.000E-01	4.0	0.0	!Zhong&Bozzelli1998
458.	C6H5	+C6H5	=P2			5.940E+42	-8.83	57.87	!Richter&Howard2002
459.	C6H5	+C6H5	=P2-	+H		8.600E+13	0.50	145.69	!Wang&Frenklach1997
460.	L-C6H6	+H	=N-C6H7			1.500E+16	-1.69	6.69	!Wang&Frenklach1994
461.	L-C6H6	+H	=C-C6H7			4.700E+27	-6.11	15.90	!Wang&Frenklach1994
462.	L-C6H6	+H	=C6H6	+H		8.700E+16	-1.34	14.64	!Wang&Frenklach1994
463.	L-C6H6	+H	=N-C6H5	+H2		6.650E+05	2.53	51.21	!Wang&Frenklach1997
464.	L-C6H6	+H	=I-C6H5	+H2		3.330E+05	2.53	38.66	!Wang&Frenklach1997
465.	C6H6	+H	=C-C6H7			3.200E+13	0.0	13.4	!Mebell1997
466.	C6H6	+H	=C6H5	+H2		6.000E+08	1.8	70.2	!Mebell1997
467.	C6H6	+1CH2	=C7H8			1.200E+14	0.0	0.0	!Böhländ1989
468.	C6H6	+3CH2	=C7H8			5.000E+13	0.0	37.50	!Böhländ1989
469.	C6H6	+CH3	=C6H5	+CH4		2.000E+12	0.0	62.7	!Zhang1989
470.	C6H6	+C2H	=A1C2H	+H		5.000E+13	0.0	0.0	!Wang&Frenklach1997
471.	C6H6	+C2H3	=A1C2H3	+H		0.800E+12	0.0	26.78	!Fahr&Stein1989
472.	C6H6	+C2H3	=C6H5	+C2H4		6.000E+11	0.0	54.3	!Ziegler2005
473.	C6H6	+C2H5	=C6H5	+C2H6		6.000E+11	0.0	62.7	!Zhang1989
474.	C6H6	+C3H3	=C6H5	+PC3H4		6.300E+11	0.0	83.6	!Ziegler2005
475.	C6H6	+I-C4H3	=C6H5	+C4H4		6.300E+11	0.0	83.6	!Ziegler2005
476.	C6H6	+C6H5	=P2	+H		9.500E+75	-18.90	165.15	!0.5 Park1999
477.	N-C6H7	=C-C6H7				3.600E+27	-7.54	24.27	!Wang&Frenklach1994
478.	N-C6H7	=C6H6	+H			8.800E+24	-4.86	56.07	!Wang&Frenklach1994
479.	N-C6H7	+H	=I-C6H7	+H		1.600E+42	-8.18	91.22	!Wang&Frenklach1997
480.	N-C6H7	+H	=L-C6H8			6.700E+65	-15.64	97.07	!Wang&Frenklach1997
481.	N-C6H7	+H	=L-C6H6	+H2		1.500E+13	0.0	0.0	!Wang&Frenklach1997
482.	I-C6H7	+H	=L-C6H8			1.400E+55	-12.32	80.76	!Wang&Frenklach1997
483.	I-C6H7	+H	=L-C6H6	+H2		3.000E+13	0.0	0.0	!Wang&Frenklach1997
484.	C-C6H7	=C5H4CH3				5.500E+10	0.0	117.0	!Ritter1990
485.	C-C6H7	+H	=C6H6	+H2		1.000E+13	0.0	0.0	!Louv&Lucas1973
486.	C-C6H7	+H	=C6H813			6.000E+13	0.0	0.0	!Berho1999
487.	C-C6H7	+H	=C6H814			6.000E+13	0.0	0.0	!Berho1999
488.	C-C6H7	+CH3	=C6H6	+CH4		3.000E+12	-0.32	0.4	!DaCosta2003
489.	C-C6H7	+C6H5	=C6H6	+C6H6		1.000E+12	0.0	0.0	!Louv&Lucas1973
490.	C-C6H7	+C-C6H7	=C6H813	+C6H6		1.940E+15	-1.0	0.0	!Berho1999
491.	C-C6H7	+C-C6H7	=C6H814	+C6H6		1.670E+15	-1.0	0.0	!Berho1999
492.	C5H4CH3	=C6H6	+H			3.000E+13	0.0	215.3	!Ziegler2005

493.	C5H4CH3	+H	=C5H5CH3	1.000E+14	0.0	0.0	!Ziegler2005
494.	C5H4CH3	+H	=C5H5 +CH3	1.000E+14	0.0	0.0	!Ritter1990
495.	C6H814	+H	=C-C6H7 +H2	2.800E+13	0.0	9.45	!Royl998
496.	C6H814	=C6H6	+H2	1.050E+12	0.0	178.62	!Ellis&Frey1966
497.	C6H813	=C6H6	+H2	4.700E+13	0.0	257.75	!Orchard&Thrush1974
498.	C6H813	+H	=C-C6H7 +H2	1.100E+05	2.5	-7.9	!Dayma2003
499.	C6H813	+CH3	=C-C6H7 +CH4	2.000E+11	0.0	30.5	!Dayma2003
500.	L-C6H8	=C6H813		7.900E+14	0.0	125.4	!Weissman1989
501.	L-C6H8	+H	=N-C6H7 +H2	1.600E+06	2.5	41.0	!Ziegler2005
502.	L-C6H8	+CH3	=N-C6H7 +CH4	4.000E+00	3.5	48.9	!Ziegler2005
503.	C5H5CH3	+H	=C5H4CH3 +H2	2.200E+08	1.77	12.5	!Ziegler2005
504.	C5H5CH3	+H	=C5H6 +CH3	1.000E+13	0.0	5.4	!Ritter1990
505.	C5H5CH3	+CH3	=C5H4CH3 +CH4	3.100E+11	0.0	23.0	!Ziegler2005
506.	C-C6H12	=1-C6H12		5.010E+16	0.0	369.0	!Tsang1978
507.	1-C6H12	=AC3H5	+N-C3H7	7.940E+15	0.0	296.0	!Tsang1978

\*\*\*\*\*

\*\*\*\* 8. C7 REACTIONS

\*\*\*\*\*

508.	C7H7	=C5H5	+C2H2	6.000E+13	0.0	293.0	!Colket&Seery1994
509.	C7H7	+H	=C7H8	2.590E+14	0.0	0.0	!Baulch1994
510.	C7H7	+1CH2	=A1C2H3 +H	2.400E+14	0.0	0.0	!Lindstedt1996
511.	C7H7	+3CH2	=A1C2H3 +H	7.000E+13	0.0	37.5	!Lindstedt1996
512.	C7H7	+CH3	=A1C2H5	1.190E+13	0.0	0.92	!Brand&Troe1990
513.	C7H7	+C2H2	=C9H8 +H	1.000E+11	0.0	29.29	!Marinov1996
514.	C7H7	+C3H3	=C10H10	1.000E+10	0.0	0.0	!Marinov1996
515.	C7H7	+C6H5	=BENZYL	1.190E+13	0.0	0.92	!Yu&Lin1993
516.	C7H7	+C6H6	>BENZYL +H	1.200E+12	0.0	66.70	!Richter&Howard2002
517.	C6H4CH3	+CH3	>ACH3CH3	1.070E+65	-15.64	95.06	!estimated
			C6H5+CH3=C7H8/Richter&Howard2002				
518.	C7H8	+H	=C6H6 +CH3	1.200E+13	0.0	21.54	!Emdee1992
519.	C7H8	+H	=C7H7 +H2	1.200E+14	0.0	34.46	!Emdee1992
520.	C7H8	+H	>C6H4CH3 +H2	6.000E+08	1.8	70.2	!estimated
			C6H6+H=C6H5+H2/Mebel1997				
521.	C7H8	+CH3	=C7H7 +CH4	3.160E+11	0.0	39.75	!Emdee1992
522.	C7H8	+C6H5	=C7H7 +C6H6	2.100E+12	0.0	18.41	!Emdee1992
523.	C7H8	+C2H3	=C7H7 +C2H4	3.980E+12	0.0	33.47	!Zhang&Mckinnon1995

\*\*\*\*\*

\*\*\*\* 9. C8 REACTIONS

\*\*\*\*\*

524.	A1C2H-	+H	+M(2)	=A1C2H	+M(2)	1.000E+14	0.0	0.0	!Wang&Frenklach1997
LOW		6.600E+75	-16.30	29.29					
TROE	1.0	0.1	584.9	6113.0					
525.	A1C2H*	+H	+M(2)	=A1C2H	+M(2)	1.000E+14	0.0	0.0	!Wang&Frenklach1997
LOW		6.600E+75	-16.30	29.29					
TROE	1.0	0.1	584.9	6113.0					
526.	A1C2H*	+C2H2	=A2-1	2.000E+72	-17.74	153.14	!Wang&Frenklach1994		
527.	A1C2H*	+C2H2	=A1C2H)2 +H	4.800E+29	-4.59	108.79	!Wang&Frenklach1994		
528.	A1C2H*	+C2H2	=A2T1 +H	5.200E+64	-14.54	218.42	!Wang&Frenklach1994		
529.	A1C2H*	+C6H6	=A3 +H	9.550E+11	0.0	18.03	!Richter&Howard2002		
530.	A1C2H*	+A1C2H	=A4 +H	8.510E+11	0.0	16.68	!Park1999		
531.	A1C2H	+H	=N-A1C2H2	1.200E+51	-11.69	72.39	!Wang&Frenklach1994		
532.	A1C2H	+H	=I-A1C2H2	1.200E+51	-11.69	72.39	!Wang&Frenklach1997		
533.	A1C2H	+H	=A1C2H* +H2	2.500E+14	0.0	66.95	!Wang&Frenklach1997		
534.	A1C2H	+H	=A1C2H- +H2	2.500E+14	0.0	66.95	!Wang&Frenklach1997		
535.	A1C2H	+CH3	=A1C2H* +CH4	1.670E+12	0.0	63.00	!Marinov1996		
536.	A1C2H	+C2H	=A1C2H)2 +H	5.000E+13	0.0	0.0	!Wang&Frenklach1997		
537.	A1C2H	+C6H5	=A3 +H	9.550E+11	0.0	18.03	!Richter&Howard2002		
538.	N-A1C2H2+H		=A1C2H +H2	1.210E+14	0.0	0.0	!Richter&Howard2002		
539.	N-A1C2H2+H		=I-A1C2H2+H	1.200E+25	-2.42	127.62	!Wang&Frenklach1997		
540.	N-A1C2H2+C2H2		=A2 +H	2.100E+15	-1.07	20.08	!Wang&Frenklach1997		
541.	I-A1C2H2+H		=A1C2H +H2	3.000E+13	0.0	0.0	!Wang&Frenklach1997		
542.	A1C2H3* +H		+M(2)	=A1C2H3	+M(2)	1.000E+14	0.0	0.0	!Wang&Frenklach1997
LOW		6.600E+75	-16.30	29.29					
TROE	1.0	0.1	584.9	6113.0					
543.	A1C2H3*	+CH3	>C9H8	+H	+H	5.000E+13	0.0	0.0	!Marinov1996
544.	A1C2H3*	+C2H2	=A2	+H		2.100E+15	-1.07	25.11	!Wang&Frenklach1997
545.	A1C2H3	=I-A1C2H2+H				3.800E+37	-6.55	477.84	!Wang&Frenklach1997
546.	A1C2H3	=N-A1C2H2+H				1.300E+44	-8.36	524.70	!Wang&Frenklach1997
547.	A1C2H3	+H	=N-A1C2H2+H2			6.650E+06	2.53	51.21	!Wang&Frenklach1997
548.	A1C2H3	+H	=I-A1C2H2+H2			3.330E+05	2.53	38.66	!Wang&Frenklach1997
549.	A1C2H3	+H	=A1C2H3* +H2			2.500E+14	0.0	66.95	!Wang&Frenklach1997
550.	A1C2H5	+H	>A1C2H3 +H2	+H		8.000E+13	0.0	34.46	!Emdee1992
551.	A1C2H5	+H	=C6H6 +C2H5			1.200E+13	0.0	21.34	!Zhang&Mckinnon1995
552.	A1C2H5	=A1C2H3	+H2			5.010E+12	0.0	267.79	!Clark&Price1970
553.	ACH3CH2	+H	=ACH3CH3			7.460E+13	0.0	0.33	!Brand&Troe1990
554.	ACH3CH3	+H	=ACH3CH2 +H2			3.980E+02	3.44	13.05	!Marinov1996

\*\*\*\*\*

\*\*\*\* 10. C9 REACTIONS

\*\*\*\*\*

555.	C9H7	+H	=C9H8	2.000E+14	0.0	0.0	!Marinov1996
------	------	----	-------	-----------	-----	-----	--------------

556.	C9H7	+CH3	=indenCH3			5.000E+12	0.0	0.0	!Ziegler2005
557.	C9H7	+C5H5	>A3	+H	+H	5.000E+09	0.0	0.0	!estimated Marinov1996
558.	C9H8	+H	=C9H7	+H2		2.190E+08	1.77	12.55	!Marinov1996
559.	C9H8	+CH3	=C9H7	+CH4		3.100E+11	0.0	23.0	!Ziegler2005
560.	C9H8	+C2H3	=C9H7	+C2H4		4.400E+00	3.5	17.1	!Ziegler2005
561.	C9H8	+C2H5	=C9H7	+C2H6		4.400E+00	3.5	17.1	!Ziegler2005
562.	C9H8	+C3H3	=C9H7	+PC3H4		1.600E+11	0.0	63.1	!Ziegler2005
*****									
**** 11. C10 REACTIONS									
*****									
563.	A1C2H)2	+H	=A2-1			4.000E+75	-18.06	144.35	!Appel2000
564.	A1C2H)2	+H	=A2T1	+H		2.700E+76	-17.32	243.52	!Wang&Frenklach1994
565.	A2T1	+H	=A2-1			5.900E+61	-15.42	152.72	!Wang&Frenklach1994
566.	A2T1	+C-C6H4	=A2C6H4-1			4.580E+41	-8.73	53.31	!Richter&Howard2002
567.	A2T1	+C-C6H4	=FLTHN			6.500E+39	-7.56	114.06	!Richter&Howard2002
568.	A2T1	+C-C6H4	=A3R5			5.120E+60	-13.07	204.94	!Richter&Howard2002
569.	A2T1	+C-C6H4	=A3LR5			7.850E+55	-11.98	183.23	!Richter&Howard2002
570.	A2T2	+C-C6H4	=A2C6H4-2			4.580E+41	-8.73	53.31	!Richter&Howard2002
571.	A2T2	+C-C6H4	=FLTHN			6.500E+39	-7.56	114.06	!Richter&Howard2002
572.	A2T2	+C-C6H4	=A3R5			5.120E+60	-13.07	204.94	!Richter&Howard2002
573.	A2T2	+C-C6H4	=A3LR5			7.850E+55	-11.98	183.23	!Richter&Howard2002
574.	A2	+H	=A2-1	+H2		3.230E+07	2.095	66.29	!Richter&Howard2002
575.	A2	+H	=A2-2	+H2		3.230E+07	2.095	66.29	!Richter&Howard2002
576.	A2	+H	=C10H9			5.000E+14	0.0	20.92	!SauerMC1970
577.	A2	+CH3	=A2-1	+CH4		2.000E+12	0.0	63.01	!Richter&Howard2002
578.	A2	+CH3	=A2-2	+CH4		2.000E+12	0.0	63.01	!Richter&Howard2002
579.	A2	+C2H	=A2C2H-1	+H		5.000E+13	0.0	0.0	!Wang&Frenklach1997
580.	A2	+C2H	=A2C2H-2	+H		5.000E+13	0.0	0.0	!Wang&Frenklach1997
581.	A2	+C2H3	=A2C2H3-2	+H		7.940E+11	0.0	26.77	!Richter&Howard2002
582.	A2	+C6H5	>FLTHN	+H2	+H	8.510E+11	0.0	16.68	!Park1999
583.	A2	+C6H5	=A2C6H5-2	+H		2.220E+83	-20.79	196.20	!Park1999
584.	A2	+C7H7	>BENZNAP	+H		1.200E+12	0.0	66.70	!Robough&Tsang1986
585.	A2	+A1C2H*	=BAA3L	+H		8.510E+11	0.0	16.68	!Park1999
586.	A2	+A1C2H*	=CRYSN	+H		8.510E+11	0.0	16.68	!Park1999
587.	A2	+A2-2	>BKFLTHN	+H2	+H	4.000E+11	0.0	16.74	!estimated Marinov1996
588.	A2	+A2-1	>BKFLTHN	+H2	+H	4.000E+11	0.0	16.74	!estimated Marinov1996
589.	A2-1	+H	+M(2)	=A2	+M(2)	1.000E+14	0.0	0.0	!Wang&Frenklach1997
LOW			3.80E+127-31.434	78.24					
TROE	0.2		122.8	478.4	5411.9				
590.	A2-1	+H	=A2-2	+H		6.500E+45	-7.9	232.22	!Wang&Frenklach1997
591.	A2-1	+H	=A2T1	+H2		4.400E-13	7.831	38.75	!Richter&Howard2002
592.	A2-1	+CH3	=A2CH2-1	+H		1.700E+36	-5.91	144.90	!Richter&Howard2002
593.	A2-1	+CH3	=A2CH3-1			3.050E+52	-11.80	73.89	!Richter&Howard2002
594.	A2-1	+C2H2	=A2R5	+H		1.800E+33	-5.91	82.43	!Appel2000
595.	A2-1	+C2H2	=A2C2H-1	+H		9.600E-09	6.44	36.07	!Richter&Howard2002
596.	A2-1	+C2H2	=HA2R5			7.740E+45	-10.85	56.36	!Richter&Howard2002
597.	A2-1	+C2H4	=A2R5H2	+H		2.510E+12	0.0	25.94	!Richter&Howard2002
598.	A2-1	+C4H4	=A3	+H		9.900E+30	-5.07	88.29	!Appel2000
599.	A2-1	+C5H6	=A2	+C5H5		1.000E-01	4.0	0.0	!Richter&Howard2002
600.	A2-1	+C6H5	>FLTHN	+H	+H	1.390E+13	0.0	0.46	!Park&Lin1997
601.	A2-1	+C6H6	>FLTHN	+H2	+H	8.510E+11	0.0	16.68	!Park1999
602.	A2-1	+A2-1	>PERYLN	+H	+H	1.390E+13	0.0	0.46	!Park&Lin1997
603.	A2-1	+A2	>PERYLN	+H2	+H	8.510E+11	0.0	16.68	!Park1999
604.	A2-2	+H	+M(2)	=A2	+M(2)	1.000E+14	0.0	0.0	!Wang&Frenklach1997
LOW			9.50E+129-32.132	78.66					
TROE	0.87		492.7	117.9	5652.0				
605.	A2-2	+H	=A2T2	+H2		4.400E-13	7.831	38.75	!Richter&Howard2002
606.	A2-2	+CH3	=A2CH2-2	+H		1.700E+36	-5.91	144.90	!Richter&Howard2002
607.	A2-2	+CH3	=A2CH3-2			3.050E+52	-11.80	73.89	!Richter&Howard2002
608.	A2-2	+C2H2	=A2C2H-2	+H		1.010E+26	-3.44	84.65	!Richter&Howard2002
609.	A2-2	+C2H2	=A2C2H2-2			2.770E+46	-10.90	59.46	!Richter&Howard2002
610.	A2-2	+C2H4	=A2C2H3-2	+H		2.510E+12	0.0	25.94	!Richter&Howard2002
611.	A2-2	+C4H2	=A3L-2			4.670E+06	1.787	13.65	!Richter&Howard2002
612.	A2-2	+C4H4	=A3	+H		9.900E+30	-5.07	88.29	!Appel2000
613.	A2-2	+C4H4	=A3L	+H		9.900E+30	-5.07	88.29	!estimated Appel2000
614.	A2-2	+C5H6	=A2	+C5H5		1.000E-01	4.0	0.0	!Richter&Howard2002
615.	A2-2	+C6H5	=A2C6H5-2			4.850E-27	-4.32	29.04	!Richter&Howard2002
616.	A2-2	+C6H6	=A2C6H5-2	+H		2.220E+83	-20.79	196.20	!Park1999
617.	A2-2	+C7H7	=BENZNAP			1.190E+13	0.0	0.92	!Yu&Lin1993
618.	A2-2	+A1C2H	=BAA3L	+H		8.510E+11	0.0	16.68	!Park1999
619.	A2-2	+A1C2H	=CRYSN	+H		8.510E+11	0.0	16.68	!Park1999
620.	A2-2	+A2-1	>BKFLTHN	+H	+H	5.000E+12	0.0	0.0	!estimated Marinov1996
621.	C10H9	+H	=C10H10			1.000E+14	0.0	0.0	!Marinov1996
622.	C10H10	+H	=C10H9	+H2		2.000E+05	2.5	10.46	!Marinov1996
623.	indenCH3	+H	=indylCH3	+H2		2.200E+08	1.77	12.5	!Ziegler2005
624.	indenCH3	+H	=C9H8	+CH3		1.000E+13	0.0	5.4	!Ziegler2005
625.	indenCH3	+CH3	=indylCH3	+CH4		3.100E+11	0.0	23.0	!Ziegler2005
626.	indylCH3	>A2	+H			3.000E+13	0.0	21.3	!Ziegler2005
627.	indylCH3	+H	=indenCH3			3.000E+13	0.0	0.0	!Ziegler2005
628.	indylCH3	+H	=C9H7	+CH3		1.000E+14	0.0	0.0	!Ziegler2005



```

*****
**** 12. C11 REACTIONS
*****
629. A2CH2-1 +H      =A2CH3-1      1.000E+14  0.0      0.0      !Marinov1996
630. A2CH3-1 +H      =A2          +CH3      1.200E+13  0.0      21.54   !Marinov1996
631. A2CH3-1 +H      =A2CH2-1 +H2     3.980E+02  3.44     13.05   !Marinov1996
632. A2CH2-2 +H      =A2CH3-2      1.000E+14  0.0      0.0      !Marinov1996
633. A2CH3-2 +H      =A2          +CH3      1.200E+13  0.0      21.54   !Marinov1996
634. A2CH2-2 +CH3    =A2C2H5       1.190E+13  0.0      0.92    !Marinov1996
635. A2CH3-2 +H      =A2CH2-2 +H2     3.980E+02  3.44     13.05   !Marinov1996
*****
**** 12. C12 REACTIONS
*****
636. A2C2H-1*+H      +M(2)      =A2C2H-1 +M(2)     1.000E+14  0.0      0.0      !Wang&Frenklach1997
LOW      9.50E+129-32.132  78.66
TROE     0.87      492.7      117.9      5652.0
637. A2C2H-1*+C2H2  =A3-4          2.000E+72-17.74  153.14   !Wang&Frenklach1997
638. A2C2H-1*+C2H2  =A2C2H)2 +H    4.800E+29 -4.59  108.79   !Wang&Frenklach1997
639. A2C2H-1*+C6H6  =CRYSN +H      8.510E+11  0.0      16.68   !Park1999
640. A2C2H-1*+A1C2H =BAPYR +H      8.510E+11  0.0      16.68   !Park1999
641. A2C2H-2*+H      +M(2)      =A2C2H-2 +M(2)     1.000E+14  0.0      0.0      !Wang&Frenklach1997
LOW      3.80E+127-31.434  78.24
TROE     0.2      122.8      478.4      5411.9
642. A2C2H-2*+C2H2  =A3-1          2.000E+72-17.74  153.14   !Wang&Frenklach1997
643. A2C2H-2*+C2H2  =A2C2H)2 +H    4.800E+29 -4.59  108.79   !Wang&Frenklach1997
644. A2C2H-1 +H      =A2C2H2-1     3.300E+51-11.72  79.08    !Wang&Frenklach1994
645. A2C2H-1 +H      =A2C2H-1*+H2   2.500E+14  0.0      66.95   !Wang&Frenklach1997
646. A2C2H-1 +H      =A2R5 +H       1.000E+40 -7.79  87.87    !Wang&Frenklach1994
647. A2C2H-1 +C2H    =A2C2H)2 +H    5.000E+13  0.0      0.0      !Wang&Frenklach1997
648. A2C2H-1 +A1C2H* =BAPYR +H      8.510E+11  0.0      16.68   !Park1999
649. A2C2H-2 +H      =A2C2H-2*+H2   2.500E+14  0.0      66.95   !Wang&Frenklach1997
650. A2C2H-2 +H      =A2C2H-23+H2   3.230E+07  2.095    66.29   !Richter&Howard2002
651. A2C2H-2 +C2H    =A2C2H)2 +H    5.000E+13  0.0      0.0      !Wang&Frenklach1997
652. A2C2H2-1=A2R5   +H       2.200E+50-11.80  167.79   !Wang&Frenklach1994
653. A2C2H2-2+H      =A2C2H-2 +H2   1.210E+14  0.0      0.0      !Richter&Howard2002
654. A2C2H2-2=A2C2H-2 +H  2.740E+22 -4.061  154.98   !Richter&Howard2002
655. A2C2H2-2+H      =A2C2H3-2     4.800E+10 -0.74  -31.93   !Richter&Howard2002
656. A2C2H3-2+H      =A2C2H2-2+H2   2.000E+07  2.0      25.11   !Marinov1996
657. A2R5 +H         =A2R5-1 +H2    3.230E+07  2.095    82.85   !Mebell1997
658. A2R5 +H         =A2R5-3 +H2    3.230E+07  2.095    66.29   !Mebell1997
659. A2R5 +H         =A2R5-4 +H2    3.230E+07  2.095    66.29   !Mebell1997
660. A2R5 +H         =A2R5-5 +H2    3.230E+07  2.095    66.29   !Mebell1997
661. A2R5-1 +H       =A2R5          1.240E+33 -5.68  37.28    !Richter&Howard2002
662. A2R5-1 +C2H2    =A2R5E-1 +H    1.120E+26 -3.42  87.32    !Richter&Howard2002
663. A2R5-3 +H       =A2R5          1.150E+32 -5.37  35.40    !Richter&Howard2002
664. A2R5-3 +C2H2    =A2R5E-3 +H    1.120E+26 -3.42  87.32    !Richter&Howard2002
665. A2R5-4 +H       =A2R5          1.150E+32 -5.37  35.40    !Richter&Howard2002
666. A2R5-4 +C2H2    =A2R5E-4 +H    1.120E+26 -3.42  87.32    !Richter&Howard2002
667. A2R5-5 +H       =A2R5          1.150E+32 -5.37  35.40    !Richter&Howard2002
668. A2R5-5 +C2H2    =A2R5E-5 +H    2.500E-09  6.63    37.03    !Richter&Howard2002
669. BIPHENH =BIPHENH +H      1.300E+16  0.0      138.93   !Richter&Howard2002
670. BIPHENH +H      =BIPHEN +H2     6.020E+12  0.0      0.0      !Richter&Howard2002
671. BIPHENH =A2R5 +H      1.000E+13  0.0      83.68    !Richter&Howard2002
672. A2C2H-23+C2H2  =A3L-1         4.670E+06  1.787    13.65    !Richter&Howard2002
673. A2C2H5 +H      >A2C2H3-2+H2 +H    8.000E+13  0.0      34.46    !Marinov1996
674. HA2R5 +H        =A2R5 +H2      1.810E+12  0.0      0.0      !Richter&Howard2002
675. HA2R5 +H        =A2R5H2        1.000E+14  0.0      0.0      !Richter&Howard2002
676. A2R5H2 +H       =HA2R5 +H2     5.400E+02  3.5      21.80    !Richter&Howard2002
677. A2R5H2 =A2R5 +H2     4.700E+13  0.0      257.75   !Richter&Howard2002
678. P2 +H          =P2- +H2       3.230E+07  2.095    66.29    !Richter&Howard2002
679. P2- +H         =P2            1.170E+33 -5.57  36.65    !Richter&Howard2002
680. P2- +C2H2      =A3 +H         4.600E+06  1.97     30.54    !Wang&Frenklach1997
*****
**** 14. C13 REACTIONS
*****
681. BENZYL* =fluorene+H  4.000E+11  0.0      50.21    !Richter&Howard2002
682. BENZYL +H        =BENZYL*+H2     3.230E+07  2.095    66.29    !Mebell1997
*****
**** 15. C14 REACTIONS
*****
683. A2C2H)2 +H      =A3-1          2.000E+75-18.06  144.35   !Wang&Frenklach1997
684. A2C2H)2 +H      =A3-4          2.000E+75-18.06  144.35   !Wang&Frenklach1997
685. A3-1 +H         +M(2)      =A3 +M(2)         1.000E+14  0.0      0.0      !Wang&Frenklach1997
LOW      4.00E+148-37.505  86.19
TROE     1.000      1.0      144.9      5632.8
686. A3-1 +H        =A3-4 +H       9.300E+58-11.45  297.50   !Wang&Frenklach1997
687. A3-1 +C2H2     =A3R5 +H       3.590E+22 -2.498  67.62    !Richter&Howard2002
688. A3-1 +C2H2     =A3C2H-1 +H    1.010E-10  7.06     38.53    !Richter&Howard2002
689. A3-1 +C4H4     =CRYSN +H      9.900E+30 -5.07  88.29    !estimated Appel2000
690. A3-1 +C6H5     >BBFLTHN +H    +H          5.000E+12  0.0      0.0      !estimate Marinov1996

```

691.	A3-1	+C6H6	>BBFLTHN	+H2		+H	4.000E+11	0.0	16.74	!estimate Marinov1996
692.	A3-2	+H	=A3				2.150E+19	-1.55	7.11	!Richter&Howard2002
693.	A3-2	+C2H2	=A3C2H-2	+H			1.030E+26	-3.36	93.09	!Richter&Howard2002
694.	A3-2	+C4H4	=CRYSN	+H			9.900E+30	-5.07	88.29	!estimated Appel2000
695.	A3-4	+H	+M(2)	=A3		+M(2)	1.000E+14	0.0	0.0	!Wang&Frenklach1997
LOW		2.10E+139-34	.803						76.99	
TROE	1.000	1.0	171.4	4992.8						
696.	A3-4	+CH3	=A3CH2	+H			5.000E+13	0.0	0.0	!Marinov1996
697.	A3-4	+C2H2	=A3C2H2-4				6.500E+53	-12.59	112.55	!Wang&Frenklach1994
698.	A3-4	+C2H2	=A3C2H-4	+H			3.400E+12	0.34	82.43	!Wang&Frenklach1994
699.	A3-4	+C2H2	=A4	+H			1.870E+07	1.787	13.65	!Richter2001
700.	A3-4	+C6H6	>BEPYR	+H2		+H	8.510E+11	0.0	16.68	!estimated Park1999
701.	A3-9	+H	=A3				2.150E+19	-1.55	7.11	!Richter&Howard2002
702.	A3-9	+C6H5	>BBFLTHN	+H		+H	5.000E+12	0.0	0.0	!estimate Marinov1996
703.	A3-9	+C6H6	>BBFLTHN	+H2		+H	4.000E+11	0.0	16.74	!estimate Marinov1996
704.	A3	+H	=A3-1	+H2			3.230E+07	2.095	66.29	!Richter&Howard2002
705.	A3	+H	=A3-2	+H2			3.230E+07	2.095	66.29	!Richter&Howard2002
706.	A3	+H	=A3-4	+H2			3.230E+07	2.095	66.29	!Richter&Howard2002
707.	A3	+H	=A3-9	+H2			3.230E+07	2.095	66.29	!Richter&Howard2002
708.	A3	+C2H	=A3C2H-4	+H			5.000E+13	0.00	0.0	!Wang&Frenklach1997
709.	A3	+C6H5	>BEPYR	+H2		+H	8.510E+11	0.0	16.68	!estimated Park1999
710.	A3L	=A3					7.940E+12	0.0	271.97	!Colket&Seery1994
711.	A3L	+H	=A3L-1	+H2			3.230E+07	2.095	66.29	!Richter&Howard2002
712.	A3L	+H	=A3L-2	+H2			3.230E+07	2.095	66.29	!Richter&Howard2002
713.	A3L	+H	=A3L-9	+H2			3.230E+07	2.095	66.29	!Richter&Howard2002
714.	A3L-1	+H	=A3L				2.150E+19	-1.55	7.11	!Richter&Howard2002
715.	A3L-1	+C2H2	=A3LR5	+H			3.590E+22	-2.498	67.62	!Richter&Howard2002
716.	A3L-1	+C2H2	=A3LE-1	+H			1.010E-10	7.06	38.53	!Richter&Howard2002
717.	A3L-1	+C4H4	=BAA3L	+H			9.900E+30	-5.07	88.29	!estimated Appel2000
718.	A3L-2	+H	=A3L				2.150E+19	-1.55	7.11	!Richter&Howard2002
719.	A3L-2	+C2H2	=A3LE-2	+H			1.030E+26	-3.36	93.09	!Richter&Howard2002
720.	A3L-2	+C4H4	=BAA3L	+H			9.900E+30	-5.07	88.29	!estimated Appel2000
721.	A3L-9	+H	=A3L				2.150E+19	-1.55	7.11	!Richter&Howard2002
722.	A3L-9	+C2H2	=A3LR5	+H			1.870E+07	1.787	13.65	!Richter2001
723.	A2R5E-3	+H	=A2R5E34	+H2			3.230E+07	2.095	66.29	!Mebell1997
724.	A2R5E-4	+H	=A2R5E45	+H2			3.230E+07	2.095	66.29	!Mebell1997
725.	A2R5E-4	+H	=A2R5E43	+H2			3.230E+07	2.095	66.29	!Mebell1997
726.	A2R5E-5	+H	=A2R5E54	+H2			3.230E+07	2.095	66.29	!Mebell1997
727.	A2R5E45	+C2H2	=A3R5-7*				1.870E+07	1.787	13.65	!Richter2001
728.	A2R5E54	+C2H2	=A3R5-10*				1.870E+07	1.787	13.65	!Richter2001
729.	A2R5E34	+C2H2	=A3LR5*				1.870E+07	1.787	13.65	!Richter2001
730.	A2R5E43	+C2H2	=A3LR5*				1.870E+07	1.787	13.65	!Richter2001
731.	A2R5E-1	+H	=A2R5E12	+H2			3.230E+07	2.095	66.29	!Mebell1997
732.	A2R5E12	+C2H2	=FLTHN-7				1.870E+07	1.787	13.65	!Richter2001
*****										
**** 16. C15 REACTIONS										
*****										
733.	A3CH2	>A3CH2R	+H				1.000E+13	0.0	50.21	!Richter&Howard2002
734.	A3CH2	+H	=A3CH3				1.000E+14	0.0	0.0	!Richter&Howard2002
735.	A3CH3	+H	=A3CH2	+H2			3.980E+02	3.44	13.05	!Park&Lin1997
736.	A3CH3	+H	=A3	+CH3			5.780E+13	0.0	33.85	!Park&Lin1997
*****										
**** 17. C16 REACTIONS										
*****										
737.	A3C2H-4	+H	=A3C2H2-4				1.400E+56	-13.21	87.87	!Wang&Frenklach1994
738.	A3C2H-4	+H	=A4	+H			4.200E+27	-4.25	45.61	!Wang&Frenklach1994
739.	A3C2H2-4	=A4	+H				6.300E+59	-14.70	154.40	!Wang&Frenklach1994
740.	A3C2H-1	+H	=A3C2H-1*	+H2			3.230E+07	2.095	66.29	!Mebell1997
741.	A3C2H-2	+H	=A3C2H-2*	+H2			3.230E+07	2.095	66.29	!Mebell1997
742.	A3C2H-1*	+C2H2	=CRYSN-4				1.870E+07	1.787	13.65	!Richter2001
743.	A3C2H-2*	+C2H2	=CRYSN-1				5.600E+05	2.282	13.64	!Richter&Howard2002
744.	A3LE-1	+H	=A3LE-1P	+H2			3.230E+07	2.095	66.29	!Mebell1997
745.	A3LE-2	+H	=A3LE-2S	+H2			3.230E+07	2.095	66.29	!Mebell1997
746.	A3LE-2	+H	=A3LE-2P	+H2			3.230E+07	2.095	66.29	!Mebell1997
747.	A3LE-1P	+C2H2	=BAA3L-1				1.870E+07	1.787	13.65	!Richter2001
748.	A3LE-2S	+C2H2	=BAA3L-4				1.870E+07	1.787	13.65	!Richter2001
749.	A3LE-2P	+C2H2	=A4L*				1.870E+07	1.787	13.65	!Richter2001
750.	A4-1	+H	=A4				5.000E+13	0.0	0.0	!Richter&Howard2002
751.	A4-1	+C2H2	=A4C2H-1	+H			1.190E-09	6.78	43.81	!Richter&Howard2002
752.	A4-1	+C2H2	=CPCDA4	+H			3.800E+22	-2.475	70.63	!Richter&Howard2002
753.	A4-1	+C6H5	>INA4	+H		+H	5.000E+12	0.0	0.0	!estimate Marinov1996
754.	A4-1	+C6H6	>INA4	+H2		+H	4.000E+11	0.0	16.74	!estimate Marinov1996
755.	A4-2	+H	=A4				5.000E+13	0.0	0.0	!Richter&Howard2002
756.	A4-2	+C2H2	=A4C2H-2	+H			1.260E+29	-4.17	102.35	!Richter&Howard2002
757.	A4-4	+H	=A4				5.000E+13	0.0	0.0	!Richter&Howard2002
758.	A4-4	+C2H2	=A4C2H-4	+H			1.190E-09	6.78	43.81	!Richter&Howard2002
759.	A4-4	+C2H2	=CPCDA4	+H			3.800E+22	-2.475	70.63	!Richter&Howard2002
760.	FLTHN	+H	=FLTHN-1	+H2			3.230E+07	2.095	66.29	!Mebell1997
761.	FLTHN	+H	=FLTHN-3	+H2			3.230E+07	2.095	66.29	!Mebell1997
762.	FLTHN-1	+H	=FLTHN				5.000E+13	0.0	0.0	!Richter&Howard2002

763.	FLTHN-1 +C2H2	=BGHIF +H	1.870E+07	1.787	13.65	!Richter2001
764.	FLTHN-3 +H	=FLTHN	5.000E+13	0.0	0.0	!Richter&Howard2002
765.	FLTHN-3 +C2H2	=CPCDFL +H	3.800E+22	-2.475	70.63	!Richter&Howard2002
766.	FLTHN-7 +H	=FLTHN	5.000E+13	0.0	0.0	!Richter&Howard2002
767.	FLTHN-7 +C2H2	=BGHIF +H	1.870E+07	1.787	13.65	!Richter2001
768.	A4 +H	=A4-1 +H2	3.230E+07	2.095	66.29	!Mebell1997
769.	A4 +H	=A4-2 +H2	3.230E+07	2.095	66.29	!Mebell1997
770.	A4 +H	=A4-4 +H2	3.230E+07	2.095	66.29	!Mebell1997
771.	A2C6H4-1=FLTHN		8.510E+12	0.0	263.02	!Brouwer&Troel1988
772.	A2C6H4-2=A3LR5		8.510E+12	0.0	263.02	!Brouwer&Troel1988
773.	A3R5 =FLTHN		8.510E+12	0.0	263.02	!Brouwer&Troel1988
774.	A3R5-7* +H	=A3R5	5.000E+13	0.0	0.0	!Richter&Howard2002
775.	A3R5-10*+H	=A3R5	5.000E+13	0.0	0.0	!Richter&Howard2002
776.	A3LR5* +H	=A3LR5	5.000E+13	0.0	0.0	!Richter&Howard2002
777.	A3LR5 =A3R5		8.510E+12	0.0	263.02	!Brouwer&Troel1988
778.	A3LR5 =FLTHN		8.510E+12	0.0	263.02	!Brouwer&Troel1988
*****						
**** 18. C17 REACTIONS						
*****						
779.	BENZNAP*=C17H12 +H		1.000E+13	0.0	50.21	!Richter&Howard2002
780.	BENZNAP +H	=BENZNAP*+H2	3.230E+07	2.095	66.29	!Mebell1997
*****						
**** 19. C18 REACTIONS						
*****						
781.	A4C2H-1*+C2H2	=BAPYR*	1.870E+07	1.787	13.65	!Richter2001
782.	A4C2H-2*+C2H2	=BAPYR*	1.870E+07	1.787	13.65	!Richter2001
783.	A4C2H-4*+C2H2	=BEPYR*	1.870E+07	1.787	13.65	!Richter2001
784.	A4C2H-1 +H	=A4C2H-1*+H2	3.230E+07	2.095	66.29	!Mebell1997
785.	A4C2H-2 +H	=A4C2H-2*+H2	3.230E+07	2.095	66.29	!Mebell1997
786.	A4C2H-4 +H	=A4C2H-4*+H2	3.230E+07	2.095	66.29	!Mebell1997
787.	A4L* +H	=A4L	5.000E+13	0.0	0.0	!Richter&Howard2002
788.	BAA3L +H	=BAA3L-1 +H2	3.230E+07	2.095	66.29	!Mebell1997
789.	BAA3L +H	=BAA3L-12+H2	3.230E+09	2.095	66.29	!Mebell1997
790.	BAA3L +H	=BAA3L-4 +H2	3.230E+07	2.095	66.29	!Mebell1997
791.	BAA3L-1 +H	=BAA3L	5.000E+13	0.0	0.0	!Richter&Howard2002
792.	BAA3L-1 +C2H2	=BAPYR +H	1.870E+07	1.787	13.65	!Richter2001
793.	BAA3L-12+H	=BAA3L	5.000E+13	0.0	0.0	!Richter&Howard2002
794.	BAA3L-12+C2H2	=BAPYR +H	1.870E+07	1.787	13.65	!Richter2001
795.	BAA3L-4 +H	=BAA3L	5.000E+13	0.0	0.0	!Richter&Howard2002
796.	BGHIF +H	=BGHIF- +H2	3.230E+07	2.095	66.29	!Mebell1997
797.	BGHIF- +C2H2	=CPBFL +H	3.800E+22	-2.475	70.63	!Richter&Howard2002
798.	CPCDA4 +H	=CPCDA4* +H2	3.230E+07	2.095	66.29	!Mebell1997
799.	CPCDA4* +C2H2	=DCPA4 +H	3.800E+22	-2.475	70.63	!Richter&Howard2002
800.	CPCDFL +H	=CPCDFL* +H2	3.230E+07	2.095	66.29	!Mebell1997
801.	CPCDFL* +C2H2	=CPBFL +H	1.870E+07	1.787	13.65	!Richter2001
802.	CRYSN-1 +H	=CRYSN	5.000E+13	0.0	0.0	!Richter&Howard2002
803.	CRYSN-4 +H	=CRYSN	5.000E+13	0.0	0.0	!Richter&Howard2002
804.	CRYSN-4 +C2H2	=BAPYR +H	1.870E+07	1.787	13.65	!Richter2001
805.	CRYSN-5 +H	=CRYSN	5.000E+13	0.0	0.0	!Richter&Howard2002
806.	CRYSN-5 +C2H2	=BAPYR +H	1.870E+07	1.787	13.65	!Richter2001
807.	CRYSN +H	=CRYSN-1 +H2	3.230E+07	2.095	66.2	!Mebell1997
808.	CRYSN +H	=CRYSN-4 +H2	3.230E+07	2.095	66.2	!Mebell1997
809.	CRYSN +H	=CRYSN-5 +H2	3.230E+07	2.095	66.2	!Mebell1997
*****						
**** 20. C20 REACTIONS						
*****						
810.	BBFLTHN +H	=BBFLTHN*+H2	3.230E+07	2.095	66.29	!Mebell1997
811.	BBFLTHN*+C2H2	=INA4 +H	1.870E+07	1.787	13.65	!Richter2001
812.	BAPYR +H	=BAPYR* +H2	3.230E+07	2.095	66.29	!Mebell1997
813.	BAPYR* +H	=BAPYR	5.000E+13	0.0	0.0	!Richter&Howard2002
814.	BAPYR* +C2H2	=ANTHAN +H	1.870E+07	1.787	13.65	!Richter2001
815.	BEPYR +H	=BEPYR* +H2	3.230E+07	2.095	66.29	!Mebell1997
816.	BEPYR* +H	=BEPYR	5.000E+13	0.0	0.0	!Richter&Howard2002
817.	BEPYR* +C2H2	=BGHIPE +H	1.870E+07	1.787	13.65	!Richter2001
818.	PERYLN +H	=PERYLN* +H2	3.230E+07	2.095	66.29	!Mebell1997
819.	PERYLN* +C2H2	=BGHIPE +H	1.870E+07	1.787	13.65	!Richter2001
820.	CPBFL +H	=CPBFL* +H2	3.230E+07	2.095	66.29	!Mebell1997
*****						
**** 21. C22 REACTIONS						
*****						
821.	BGHIPE +H	=BGHIPE* +H2	3.230E+07	2.095	66.29	!Mebell1997
822.	BGHIPE* +C2H2	=CORONEN +H	1.870E+07	1.787	13.65	!Richter2001
*****						
**** 22. Acetone chemistry						
*****						
823.	CH3COCH3=CH3CO +CH3		1.130E+16	0.0	341.85	!Sato2000
824.	CH3COCH3+H	=CH3COCH2+H2	2.300E+07	2.0	20.92	!Sato2000
825.	CH3COCH3+CH3	=CH3COCH2+CH4	9.500E+03	2.5	35.15	!Sato2000
826.	CH3COCH2=CH2CO +CH3		1.000E+13	0.0	117.16	!Sato2000
827.	CH3CO =CH3 +CO		8.740E+42	-8.62	93.83	!Tsang1986

```

*****
*** Fitted parameters for Tubular Flow Reactor
*****
  H      +C2H2    >C2H3      7.195E+011  0.0   10.467
C2H3    >H      +C2H2      1.910E+010  0.0   193.00
C2H2    +C2H2    =C4H2      8.900E+15   0.0   299.34
C4H4    +C2H2    =C6H6      4.470E+12   0.0   133.00
C6H6    +H      >C6H5      6.512E+015  0.0   66.989
C6H5    +H2     >C6H6      4.898E+012  0.0   41.031

```